

# Advances

## in Clinical and Experimental Medicine

MONTHLY ISSN 1899-5276 (PRINT) ISSN 2451-2680 (ONLINE)

[www.advances.umed.wroc.pl](http://www.advances.umed.wroc.pl)

2020, Vol. 29, No. 7 (July)

Impact Factor (IF) – 1.514  
Ministry of Science and Higher Education – 40 pts.  
Index Copernicus (ICV) – 155.19 pts.



WROCLAW  
MEDICAL UNIVERSITY

Advances  
in Clinical and Experimental  
Medicine



# Advances in Clinical and Experimental Medicine

ISSN 1899-5276 (PRINT)

ISSN 2451-2680 (ONLINE)

www.advances.umed.wroc.pl

**MONTHLY 2020**  
**Vol. 29, No. 7**  
**(July)**

Advances in Clinical and Experimental Medicine is a peer-reviewed open access journal published by Wrocław Medical University. Its abbreviated title is Adv Clin Exp Med. Journal publishes original papers and reviews encompassing all aspects of medicine, including molecular biology, biochemistry, genetics, biotechnology, and other areas. It is published monthly, one volume per year.

---

## Editorial Office

ul. Marcinkowskiego 2–6  
50-368 Wrocław, Poland  
Tel.: +48 71 784 11 36  
E-mail: redakcja@umed.wroc.pl

## Publisher

Wrocław Medical University  
Wybrzeże L. Pasteura 1  
50-367 Wrocław, Poland

© Copyright by Wrocław Medical University,  
Wrocław 2020

Online edition is the original version of the journal

## Editor-in-Chief

Maciej Bagłaj

## Vice-Editor-in-Chief

Dorota Frydecka

---

## Editorial Board

Piotr Dziągpiel  
Marian Klinger  
Halina Milnerowicz  
Jerzy Mozrzyński

---

## Thematic Editors

Marzena Bartoszewicz (microbiology)  
Marzena Dominiak (dentistry)  
Paweł Domosławski (surgery)  
Maria Ejma (neurology)  
Jacek Gajek (cardiology)  
Mariusz Kuształ  
(nephrology and transplantology)  
Rafał Matkowski (oncology)  
Ewa Milnerowicz-Nabzdyk (gynecology)  
Katarzyna Neubauer (gastroenterology)  
Marcin Ruciński (basic sciences)  
Robert Śmigiel (pediatrics)  
Paweł Tabakow (experimental medicine)  
Anna Wiela-Hojeńska  
(pharmaceutical sciences)  
Dariusz Wołowicz (internal medicine)

---

## International Advisory Board

Reinhard Berner (Germany)  
Vladimir Bobek (Czech Republic)  
Marcin Czyz (UK)  
Buddhadeb Dawn (USA)  
Kishore Kumar Jella (USA)

## Secretary

Katarzyna Neubauer

Piotr Ponikowski  
Marek Sąsiadek  
Leszek Szenborn  
Jacek Szepietowski

---

## Statistical Editors

Dorota Diakowska  
Leszek Noga  
Lesław Rusiecki

## Technical Editorship

Joanna Gudarowska  
Paulina Kunicka  
Marek Misiak

## English Language Copy Editors

Eric Hilton  
Sherill Howard Pocięcha  
Jason Schock  
Marcin Tereszewski

---

Pavel Kopel (Czech Republic)  
Tomasz B. Owczarek (USA)  
Ivan Rychlík (Czech Republic)  
Anton Sculean (Switzerland)  
Andriy B. Zimenkovsky (Ukraine)

## Editorial Policy

Advances in Clinical and Experimental Medicine (Adv Clin Exp Med) is an independent multidisciplinary forum for exchange of scientific and clinical information, publishing original research and news encompassing all aspects of medicine, including molecular biology, biochemistry, genetics, biotechnology and other areas. During the review process, the Editorial Board conforms to the "Uniform Requirements for Manuscripts Submitted to Biomedical Journals: Writing and Editing for Biomedical Publication" approved by the International Committee of Medical Journal Editors ([www.ICMJE.org/](http://www.ICMJE.org/)). The journal publishes (in English only) original papers and reviews. Short works considered original, novel and significant are given priority. Experimental studies must include a statement that the experimental protocol and informed consent procedure were in compliance with the Helsinki Convention and were approved by an ethics committee.

For all subscription-related queries please contact our Editorial Office:  
[redakcja@umed.wroc.pl](mailto:redakcja@umed.wroc.pl)

For more information visit the journal's website:  
[www.advances.umed.wroc.pl](http://www.advances.umed.wroc.pl)

Pursuant to the ordinance No. 134/XV R/2017 of the Rector of Wrocław Medical University (as of December 28, 2017) from January 1, 2018 authors are required to pay a fee amounting to 700 euros for each manuscript accepted for publication in the journal Advances in Clinical and Experimental Medicine.

„Podniesienie poziomu naukowego i poziomu umiędzynarodowienia wydawanych czasopism naukowych oraz upowszechniania informacji o wynikach badań naukowych lub prac rozwojowych – zadanie finansowane w ramach umowy 784/p-DUN/2017 ze środków Ministra Nauki i Szkolnictwa Wyższego przeznaczonych na działalność upowszechniającą naukę”.



Indexed in: MEDLINE, Science Citation Index Expanded, Journal Citation Reports/Science Edition, Scopus, EMBASE/Excerpta Medica, Ulrich's™ International Periodicals Directory, Index Copernicus

Typographic design: Monika Kołęda, Piotr Gil  
DTP: Wydawnictwo UMW  
Cover: Monika Kołęda  
Printing and binding: EXDRUK

## Contents

### Original papers

- 777 Yunyu Wu, Jie Li, Shuying Chen, Zhiwu Yu  
**The effects of miR-140-5p on the biological characteristics of ovarian cancer cells through the Wnt signaling pathway**
- 785 Hui Wang, Zhengdong Zhang, Zhe Yan, Shihong Ma  
**PD-L1, PDK-1 and p-Akt are correlated in patients with papillary thyroid carcinoma**
- 793 Xiaolei Zhang, Xianfeng Li, Bin Li, Chengfeng Sun, Peng Zhang  
**miR-21-5p protects hippocampal neurons of epileptic rats via inhibiting STAT3 expression**
- 803 Chuannan Zhai, Hongliang Cong, Kai Hou, Yuecheng Hu, Jingxia Zhang, Yingyi Zhang, Ying Zhang, Hong Zhang  
**Effects of miR-124-3p regulation of the p38MAPK signaling pathway via MEKK3 on apoptosis and proliferation of macrophages in mice with coronary atherosclerosis**
- 813 Dong Xu, Xang Sun, Yang Zhang, Li Cao  
**Ketamine alleviates HMGB1-induced acute lung injury through TLR4 signaling pathway**
- 819 Hyun Jung Park, Jinpyo Hong, Yibo Piao, Hyo Jung Shin, Se Jeong Lee, Im Joo Rhyu, Min-Hee Yi, Jinhyun Kim, Dong Woon Kim, Jaewon Beom  
**Extracorporeal shockwave therapy enhances peripheral nerve remyelination and gait function in a crush model**
- 825 Yonghui Yang, Xiaoxia Li, Xiaoying An, Ling Zhang, Xingbin Li, Liang Wang, Guiyun Zhu  
**Continuous exposure of PM2.5 exacerbates ovalbumin-induced asthma in mouse lung via a JAK-STAT6 signaling pathway**
- 833 Zhen-Zhou Li, Zi-Wei Zhang, Huan Wang, Yong-Quan Chen, Xiao-Fang Zhou, Li-Shuang Duan, Xiao-Xiao Wang, Feng Xu, Jian-Rong Guo  
**Autologous transfusion of "old" red blood cells-induced M2 macrophage polarization through IL-10-Nrf2-HO-1 signaling complexes**
- 841 Anna Pietrzak, Alicja Kalinowska-Łyszczarz, Krystyna Osztynowicz, Alima Khamidulla, Wojciech Kozubski, Sławomir Michalak  
**A long-term follow-up study on biochemical and clinical biomarkers of response to interferon beta-1b treatment in relapsing-remitting multiple sclerosis**
- 853 Marta Kostrzewa, Ewa Głowacka, Tomasz Stetkiewicz, Mariusz Grzesiak, Krzysztof Szyłło, Grzegorz Stachowiak, Jacek Radosław Wilczyński  
**Is serum anti-Müllerian hormone (AMH) assay a satisfactory measure for ovarian reserve estimation? A comparison of serum and peritoneal fluid AMH levels**
- 857 Kajetan Juszcak, Agata Gastecka, Jan Adamowicz, Przemysław Adamczyk, Marta Pokrywczyńska, Tomasz Drewa  
**Health-related quality of life is not related to laparoscopic or robotic technique in radical cystectomy**
- 865 Katarzyna Ura-Sabat, Joanna Morawska, Wojciech Domka, Marta Gamrot-Wrzoł, Wojciech Scierski, Ewa Niebudek-Bogusz  
**The assessment of phonatory and ventilatory functions in patients after microsurgery for Reinke's edema**
- 873 Jiyang Wang, Yong Cai, Zhaoying Sheng  
**Experimental studies on the protective effects of the overexpression of lentivirus-mediated sirtuin 6 on radiation-induced lung injury**
- 879 Li Zhou, Shao-Bin Wang, Shu-Guang Chen, Qiang Qu, Jing-An Rui  
**The prognostic value and non-invasive predictors of splenomegaly in cirrhotic patients with hepatocellular carcinoma following curative resection**
- 887 Li Zhou, Shao-Bin Wang, Shu-Guang Chen, Qiang Qu, Jing-An Rui  
**Risk factors of recurrence and poor survival in curatively resected hepatocellular carcinoma with microvascular invasion**

### Reviews

- 893 Feifei Pu, Jing Feng, Ping Xia  
**Association between heparin-binding hemagglutinin and tuberculosis**



# The effects of miR-140-5p on the biological characteristics of ovarian cancer cells through the Wnt signaling pathway

Yunyu Wu<sup>1,A,B,E,F</sup>, Jie Li<sup>2,B-F</sup>, Shuying Chen<sup>3,B-D</sup>, Zhiwu Yu<sup>3,A-C</sup>

<sup>1</sup> Department of Gynecology, Affiliated Cancer Hospital & Institute of Guangzhou Medical University, China

<sup>2</sup> Department of Intensive Care Unit, Guangdong Provincial Geriatrics Institute, Guangdong Provincial People's Hospital, Guangdong Academy of Medical Sciences, Guangzhou, China

<sup>3</sup> Department of Clinical Laboratory, Affiliated Cancer Hospital & Institute of Guangzhou Medical University, China

A – research concept and design; B – collection and/or assembly of data; C – data analysis and interpretation;

D – writing the article; E – critical revision of the article; F – final approval of the article

Advances in Clinical and Experimental Medicine, ISSN 1899–5276 (print), ISSN 2451–2680 (online)

Adv Clin Exp Med. 2020;29(7):777–784

## Address for correspondence

Zhiwu Yu

E-mail: yuzhiwu1yzw7@163.com

## Funding sources

This work was supported by the Medical Health Science and Technology Project of Guangzhou City (grant No. 20161A010087).

## Conflict of interest

None declared

Received on January 2, 2020

Reviewed on February 13, 2020

Accepted on May 1, 2020

Published online on August 4, 2020

## Cite as

Wu Y, Li J, Chen S, Yu Z. The effects of miR-140-5p on the biological characteristics of ovarian cancer cells through the Wnt signaling pathway. *Adv Clin Exp Med.* 2020;29(7):777–784. doi:10.17219/acem/121933

## DOI

10.17219/acem/121933

## Copyright

© 2020 by Wrocław Medical University

This is an article distributed under the terms of the Creative Commons Attribution 3.0 Unported (CC BY 3.0) (<https://creativecommons.org/licenses/by/3.0/>)

## Abstract

**Background.** Ovarian cancer is usually not diagnosed until the late stage, and it is resistant to platinum and other standard chemotherapy drugs, resulting in high mortality.

**Objectives.** To investigate the effects of miR-140-5p on cell proliferation, apoptosis, invasion, and migration capability in the SKOV3 and OVCAR3 ovarian cancer cell lines through Wnt signaling pathway.

**Material and methods.** Expression levels of miR-140-5p were checked using quantitative real-time polymerase chain reaction (qRT-PCR). The expression of miR-140-5p was upregulated by transfecting cells with a miR-140-5p mimic or a mimic negative control (NC). Cell proliferation was assessed using a CCK8 assay, and cell cycle distribution and apoptosis percentage were detected with flow cytometry. A transwell invasion assay was employed to evaluate cell migration and invasion ability. The target complementary relationship between miR-140-5p and *WNT1* was verified using a dual-luciferase reporter assay while  $\beta$ -catenin in the nuclei was observed using immunofluorescence. The expression of Wnt signaling pathway-related proteins was examined using western blot and qRT-PCR.

**Results.** The relative expression level of miR-140-5p in SKOV3 and OVCAR3 cells was obviously decreased compared with that in the IOSE80 cells ( $p < 0.05$ ). Besides, upregulated miR-140-5p effectively suppressed cell proliferation and increased the apoptosis ratio of SKOV3 and OVCAR3 cells ( $p < 0.05$ ). In addition, the invasion and migration capability of SKOV3 and OVCAR3 cells in miR-140-5p mimic group was largely suppressed compared with the NC group ( $p < 0.05$ ). What is more, the target complementary relationship between miR-140-5p and the *WNT1* gene was revealed; upregulated miR-140-5p suppressed the expression of Wnt signaling-related genes, and restrained nuclear transfer of  $\beta$ -catenin ( $p < 0.05$ ).

**Conclusions.** The overexpression of miR-140-5p restricted the proliferation, migration and invasion abilities, and accelerated cell apoptosis in ovarian cancer cell lines SKOV3 and OVCAR3 through the Wnt signaling pathway.

**Key words:** apoptosis, ovarian cancer, cell proliferation, Wnt signaling pathway, miR-140-5p

Ovarian cancer has the 7<sup>th</sup> highest incidence and 8<sup>th</sup> highest fatality rate among malignant gynecological diseases in the world, with a five-year survival rate lower than 45%.<sup>1–4</sup> At present, the most common therapy for ovarian cancer is surgical resection of visible lesions, combined with chemotherapy using targeted platinum drugs (such as cisplatin or carboplatin) and paclitaxel.<sup>5</sup> However, long-term use of these chemotherapy regimens carries the risk of drug resistance. Various advances in surgical technology and chemotherapy have been made in recent years. However, instead of early detection, ovarian cancer is usually not diagnosed until the late stages, and it is resistant to platinum and other standard chemotherapy drugs, thus resulting in high mortality.<sup>6,7</sup> Therefore, it is urgent to explore new and effective treatments for ovarian cancer.

Gene therapy, especially microRNA-regulated gene therapy, has attracted extensive attention recently years.<sup>8</sup> MicroRNAs (miRs) are able to regulate cell proliferation, differentiation and apoptosis, as well as the occurrence and development of cancer.<sup>9</sup> Regulation of miR expression has provided important ideas for the prevention and control of a variety of malignant diseases, including papillary thyroid cancer, prostate cancer, breast cancer, non-small cell lung cancer (NSCLC), and so on.<sup>10–13</sup> For example, miR-140-5p overexpression has effectively inhibited the growth, metastasis, invasion, and epithelial-mesenchymal transformation of hepatocellular carcinoma (HCC) and NSCLC.<sup>14,15</sup> However, the effects of miR-140-5p on ovarian cancer have not been clearly illustrated. We learned from a biological information website that complementary binding sites exist between miR-140-5p and the *WNT1* gene, and we know that *WNT1* is an important gene in the Wnt signaling pathway, whose abnormal expression plays a key regulatory function in the onset and progress of many cancers.<sup>16</sup>

The aim of our study was to research the expression of miR-140-5p and the *WNT1* gene in ovarian cancer cells, and the effects of miR-140-5p on the biological characteristics of ovarian cancer cells through the Wnt signaling pathway.

## Material and methods

### Cell culture and transfection

The human epithelial ovarian cancer SKOV3 and OVCAR3 cell lines used here were originally purchased from the ATCC cell bank (Manassas, USA). Human normal ovarian epithelial cells IOSE80 were acquired from the cell bank of the Chinese Academy of Sciences (Shanghai, China). The cells were kept in RPMI 1640 medium with 10% fetal bovine serum (FBS), 100 µg/mL of streptomycin and 100 U/mL of penicillin (Gibco BioSciences, Dublin, Ireland) at 37° in 5% CO<sub>2</sub>, and the cells were not sub-cultured until cell density was up to 80%.

SKOV3 and OVCAR3 cells at the logarithmic growth stage were inoculated into six-well plates (5\*10<sup>5</sup> cells/mL)

and were then co-transfected with miR-140-5p mimic or mimic negative control (NC) (Gemma Biological Co., Ltd., Shanghai, China) using Lipofectamin 2000 (Invitrogen Corp., Carlsbad, USA) following standard instructions.

### Dual-luciferase reporter assay

Binding sites between miR-140-5p and *WNT1* were first predicted on the Bioinformatics & Research Computing website ([www.targetscan.org](http://www.targetscan.org)) and the fragment sequence containing the binding sites was obtained. Synthetic *WNT1*-WT or *WNT1*-MUT was inserted into the 3'UTR of the pMIR-reporter (Thermo Fisher Scientific, Waltham, USA) to package recombinant plasmids pMIR-*WNT1*-WT and pMIR-*WNT1*-MUT, respectively. Correctly identified recombinant plasmids *WNT1*-WT or *WNT1*-MUT were co-transfected into HEK293T cells with miR-140-5p or NC plasmids, respectively. After incubating for 48 h, cells were cleaved in 1 × passive lysate, and luciferase activity was assessed using a luciferase test kit (Promega, Madison, USA) using a dual-luciferase reporter assay system (Promega). The related target effect was shown as relative luciferase activity (the ratio of firefly luciferase intensity to that of renilla). Renilla luciferase activity was used as the internal reference.

### qRT-PCR

Total RNA was first extracted using cold Trizol (Invitrogen). After the RNA concentration was measured, 1 µg of total RNA was transcribed reversely using a cDNA Reverse Transcription Kit (Takara Biomedical Technology, Beijing, China). Quantitative real-time polymerase chain reaction (qRT-PCR) was carried out in an ABI7500 quantitative PCR instrument (Thermo Fisher Scientific) using a Fluorescence Quantitative PCR kit (Takara Biomedical Technology) according to the following procedure: pre-denaturation for 10 min at 95°C and 40 PCR cycles (denaturation for 15 s at 95°C, annealing for 30 s at 56°C, extension for 35 s at 72°C). *U6* and *GAPDH* were the internal references for miRNA and mRNAs, respectively. The results were analyzed with the 2<sup>-ΔΔCt</sup> method. All related primers were provided by the Jima Pharmaceutical Technology Co., Ltd. (Shanghai, China) and the primer sequences are listed in Table 1. The RT-PCR was carried out in strict accordance with the instructions, and all consumables used in the experiment were soaked in diethyl pyrocarbonate (DEPC) (Rongyue Biotechnology Co., Ltd., Shanghai, China) to inactivate the enzymes, and were sterilized at a high temperature.

### Western blot

The protein in the cells was extracted using RIPA lysate (R0010; Solarbio Science & Technology Co. Ltd, Beijing, China) containing phenylmethylsulfonyl fluoride (PMSF), and then incubated on ice for 30 min; the supernatant was

Table 1. Related primer sequences of qRT-PCR

Name	Sequence
<i>WNT1</i>	F: 5'-CGCTCTTCCAGTTCTCAGACAC-3' R: 5'-CAGGATGGCAAAGGGTTCCG-3'
miR-140-5p	F: 5'-GAGTGT-CAGTGGTTACCGT-3' R: 5'-GCATGGTCC-GAGGTATTC-3'
$\beta$ -catenin	F: 5'-GCCACAGGATTACAAGAAGC-3' R: 5'-CCACCAGAGTGAAAAGAACG-3' R: 5'-ATCCAGACTCTGACCTTTT-3'
<i>MMP-7</i>	F: 5'-GGGATTAACCTTCTGTATGC-3' R: 5'-GATCTCCATTTCATAGGTTG-3'
<i>GAPDH</i>	F: 5'-GGGTGTGAACCATGAGAAGTATG-3' R: 5'-GATGGCATGGACTGTGGTCAT-3'
<i>U6</i>	F: 5'-CTCGGACTCAGCCTGCA-3' R: 5'-TCAATATTACCGAGCTGCGT-3'

obtained by centrifuging at  $12,000 \times g$  for 10 min at  $4^{\circ}\text{C}$ . The protein concentration was examined using a Pierce BCA Kit (23225; Thermo Fisher Scientific), and adjusted to equilibrium using deionized water. Forty-microgram protein samples were added to wells on SDS-PAGE gel and the proteins were separated at 80 V using 10% SDS-PAGE gel (P0012A; Biyun Tian Biotechnology Research Institute, Shanghai, China) for 2 h. The wet transfer method was used to transfer the protein to the polyvinylidene difluoride (PVDF) membranes (iseq00010; Merck Millipore, Burlington, USA), then the membranes were blocked for 2 h with tris-buffered saline with Tween 20 (TBST) buffer containing 5% skimmed milk powder. After being washed 3 times using TBST buffer, the membranes were incubated with primary antibodies as listed, respectively:  $\beta$ -catenin rabbit antibody (1:1,000, ab32572; Abcam, Cambridge, UK), WNT1 mouse antibody (1:500, ab15251; Abcam), C-myc rabbit antibody (1:1,000, 5605; Cell Signaling Technology, Leiden, the Netherlands), MMP-7 antibody (1:1,000, 71031; CST), and GAPDH rabbit monoclonal antibody (1:10,000, ab181602; Abcam) at  $4^{\circ}\text{C}$  overnight. After being washed 3 times using TBST buffer, the membranes were conjugated with diluted sheep anti-rabbit second antibody (1:2,000–1:50,000, ab205718; Abcam) and sheep anti-mouse second antibody (1:10,000, Jackson; Jackson ImmunoResearch, USA) at room temperature for 90 min. An electrochemiluminescence (ECL) fluorescence detection kit (Amersham, Little Chalfont, UK) was used. The membranes were treated with enhanced chemiluminescence reagent (Amersham) and imaged with the Bio-Rad image analysis system (Bio-Rad Laboratories Inc., Hercules, USA) in gel imager. The protein content was analyzed using Quantity One v. 4.6.2 software (Bio-Rad Laboratories Inc.) and relative protein content was shown as a grey value of a targeted protein band/gray value of a GAPDH band.

## CCK8 assay

Digested SKOV3 and OVCAR3 cells were seeded into 96-well plates, and the absorbance of cells in the NC group and the miR-140-5p mimic group were each measured 3 times.

After 0 h, 24 h, 48 h, and 72 h of culture, cell absorbance was measured using a commercial CCK8 Kit (Solarbio Science & Technology Co. Ltd.).

## Flow cytometry

Cell apoptosis was evaluated using an Annexin V-FITC/PI Double Staining Kit (CA1050; Solarbio Science & Technology Co. Ltd.) as follows: SKOV3 and OVCAR3 cells were centrifuged, re-suspended and then mixed with  $5 \mu\text{L}$  of Annexin V-FITC. The cell suspension was reacted with the  $5 \mu\text{L}$  of Annexin V-FITC added before in the dark at room temperature for 15 min. Then,  $5 \mu\text{L}$  of propidium iodide (PI) was added 5 min before detection. Subsequently,  $5 \mu\text{L}$  of propidium iodide (PI) was added and reacted on ice in the dark for 5 min, and then cell apoptosis was detected using Cube6 flow cytometry (Sysmex Partec GmbH, Münster, Germany).

The cell cycles of the NC group and the miR-140-5p mimic group were detected using a cell cycle DNA detection kit (Solarbio Science & Technology Co. Ltd.) as follows: The cells were centrifuged and re-suspended after washing, and then centrifuged again to remove the supernatant. After being fixed and washed, the cells were gently and evenly blown and passed through the cell strainer to prevent agglomeration. The cells were re-suspended, bathed in water at  $37^{\circ}\text{C}$  for 30 min, mixed with  $400 \mu\text{L}$  of PI staining solution, incubated in the dark at  $4^{\circ}\text{C}$  for 30 min, and detected using flow cytometry.

## Transwell migration and invasion assay

After being transfected for 48 h, the cells were starved in serum-free medium for another 24 h. After being digested and washed, the cells were re-suspended in RPMI1640 medium with  $10 \text{ g/L}$  of bovine serum albumin (BSA) (Thermo Fisher Scientific).

For the invasion assay, a transwell chamber was put into a 24-well plate. The upper chamber surface of the bottom membrane in the transwell chamber was coated with matrigel diluent (4011es08; Shanghai Yisheng Biotechnology Co., Ltd., Shanghai, China). After air-drying at room temperature, the chamber was cleaned twice using serum-free RPMI1640 medium (Gibco, Waltham, USA). The density of the cell suspension was adjusted to  $1 \times 10^5/\text{mL}$ , and  $200 \mu\text{L}$  of cell suspension was added to the upper chamber. At the same time,  $600 \mu\text{L}$  of complete medium accompanied with 10% FBS was added to the lower chamber. After 24 h, the cells adhering to the upper surface were cleaned with cotton swabs, and the invading cells on the bottom surface were fixed with 4% paraformaldehyde (Leigen Biotechnology Co. Ltd., Beijing, China) for 15 min. After staining for 15 min with 0.5% crystal violet (Solarbio Technology Co. Ltd.), the cells were washed 3 times with PBS and 6 fields of vision were randomly selected to be photographed with an inverted microscope, and the cell number was counted.

The migration assay was the same as the invasion assay, except that matrigel coating was not used on the transwell chambers.

## Immunofluorescence test

The cells were inoculated into 24-well plates in which sterile cell climbing slices had already been placed. After 24 h, the supernatant of the culture medium was discarded and the cells were fixed with 4% paraformaldehyde for 20 min and penetrated for 10 min by 0.1% Triton-100. The cells were then washed 3 times and blocked with 5% BSA before being incubated with 0.1 mL of  $\beta$ -catenin primary antibody (1:250, ab32572; Abcam) for 1 h at room temperature. After being washed 3 times, the cells were incubated with 0.1 mL of a fluorescent second antibody (ab150075; Abcam) in the dark for 30 min. After staining the nuclei with DAPI for 5 min, the slides were carefully taken out after being washed 3 more times. Finally, the slides were sealed and observed under a microscope.

## Statistical analysis

The statistical analysis was performed using SPSS v. 21.0 statistical software (SPSS Inc., Chicago, USA). Related measurement data was shown as means  $\pm$  standard deviation (SD). A t-test was used to compare differences between 2 groups and a one-way analysis of variance (ANOVA) with the Bonferroni correction was used to compare differences among multiple groups. A p-value of  $<0.05$  indicated statistically significant differences.

## Results

### Downregulation of miR-140-5p in human ovarian cancer cells

With the aim of studying the effects of miR-140-5p on human ovarian cancer cells, the expression difference of miR-140-5p in the human epithelial ovarian cancer cell line SKOV3, the ovarian cancer cell line OVCAR3 and the human normal ovarian epithelial cell line IOSE80 was first assessed using qRT-PCR (Fig. 1). The results showed that the expression of miR-140-5p in both SKOV3 and OVCAR3 cells was sharply decreased compared with the expression in IOSE80 cells ( $p < 0.05$ ).

### Effects of miR-140-5p overexpression on the proliferation and apoptosis of human ovarian cancer cells

To verify the impact of miR-140-5p on human ovarian cancer cells, the expression level of miR-140-5p in SKOV3 and OVCAR3 cells was first checked with qRT-PCR, and then cell proliferation was detected using a CCK8 assay

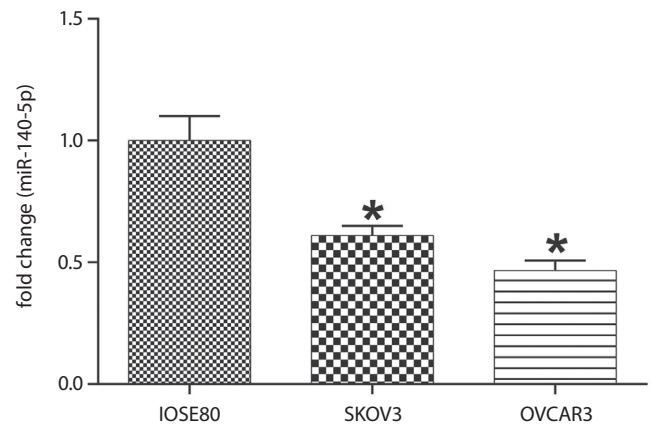


Fig. 1. miR-140-5p expression in human ovarian cancer cells and normal human ovarian epithelial cells compared with the IOSE80 group, \* $p < 0.05$

(Fig. 2A,B). The results showed that expression of miR-140-5p was significantly upregulated in the miR-140-5p mimic group compared with the NC group ( $p < 0.05$ ). Correspondingly, the proliferation of miR-140-5p in the mimic group was significantly decreased compared with the NC group ( $p < 0.05$ ).

The cell cycle was further examined using flow cytometry (Fig. 2C). The cell cycle of the miR-140-5p mimic group was mainly blocked in the G0/G1 phase compared with the NC group ( $p < 0.05$ ). Cell apoptosis detection was conducted using annexin V-FITC/PI staining (Fig. 2D) and the proportion of early apoptotic cells was found to be significantly increased in the miR-140-5p mimic group compared with the NC group ( $p < 0.05$ ). These results made it clear that upregulated miR-140-5p suppressed proliferation and accelerated apoptosis in SKOV3 and OVCAR3 cells.

### Effects of miR-140-5p on migration and invasion of ovarian cancer cells

Effects of miR-140-5p on the migration and invasion capacity of SKOV3 and OVCAR3 cells were evaluated using transwell assays (Fig. 3). The results showed that the migration and invasion capacity of SKOV3 and OVCAR3 cells were both largely inhibited by the miR-140-5p mimic compared with the mimic NC ( $p < 0.05$ ).

### MiR-140-5p mediated the Wnt signal pathway by targeting WNT1

Binding sites between miR-140-5p and *WNT1* were first forecast using a bioinformatics analysis website (Fig. 4A) and then verified with a dual-luciferase reporter assay (Fig. 4B). Luciferase activity was strongly decreased in the co-transfection group of the miR-140-5p mimic and *WNT1*-WT compared with the NC group ( $p < 0.05$ ), but luciferase activity was not obviously affected by the co-transfection of the miR-140-5p mimic and *WNT1*-MUT compared with that in the NC group.

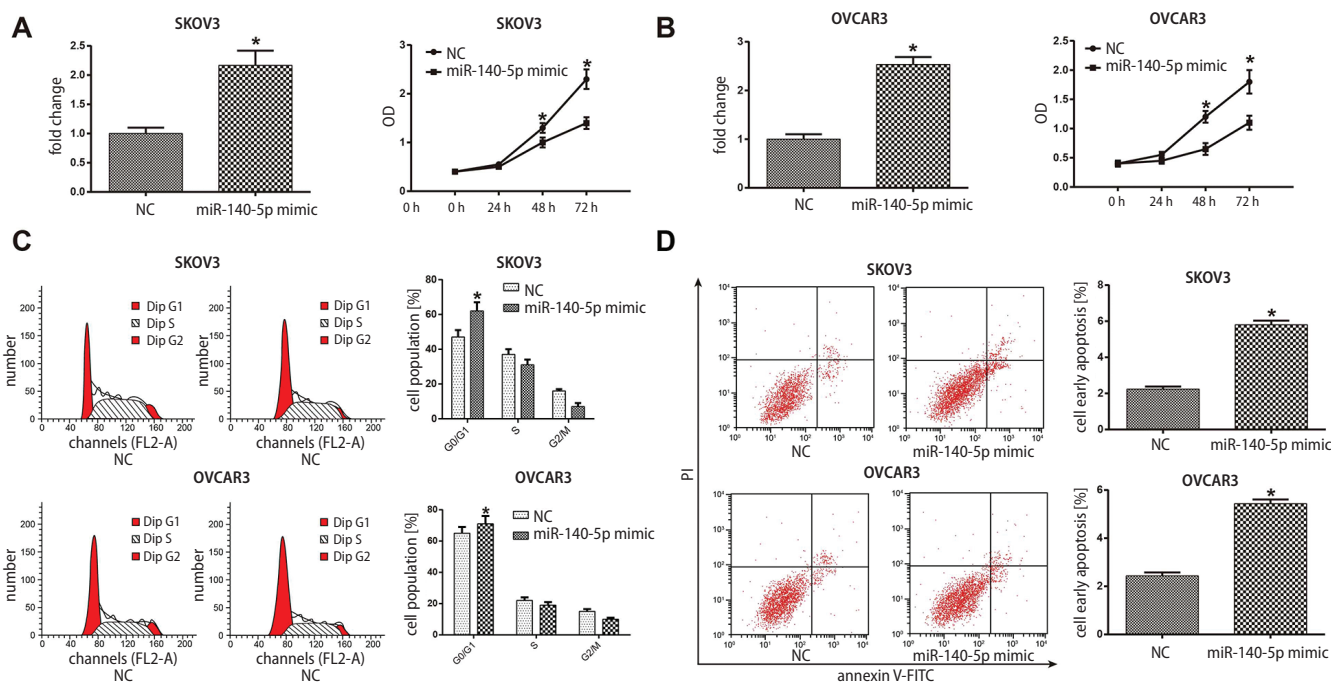


Fig. 2. Proliferation and apoptosis of ovarian cancer cells

A. miR-140-5p expression in SKOV3 cells and cell proliferation detection. B. miR-140-5p expression in OVCAR3 cells and cell proliferation detection. C. Cell cycle detected with flow cytometry and the corresponding column analysis. D. Cell apoptosis detected with flow cytometry and the corresponding column analysis. Compared with the NC group, \* $p < 0.05$ .

To further reveal the association between miR-140-5p and the Wnt signaling pathway, expressions of the Wnt signaling pathway-related  $\beta$ -catenin, *WNT1* and associated downstream factors *C-myc* and *MMP-7*, which are closely related to tumor development, were evaluated using qRT-PCR (Fig. 4C) and western blot (Fig. 4F,G). The results showed that the expressions of  $\beta$ -catenin, *WNT1*, *C-myc*, and *MMP-7* were all decreased in the miR-140-5p mimic group compared to the NC group ( $p < 0.05$ ).

The results of immunofluorescence in Fig. 4D and 4E showed that the number of cells with  $\beta$ -catenin transfer to the nucleus was significantly lower in the miR-140-5p mimic group than in the NC group, indicating that miR-140-5p overexpression effectively suppresses nuclear transfer of  $\beta$ -catenin ( $p < 0.05$ ).

## Discussion

From the perspective of molecular biology, we studied the role and mechanisms of miR-140-5p in ovarian cancer cells. We found that an miR-140-5p mimic largely reduced the expression level of Wnt signaling pathway-related signal molecules, suppressing their activity and thus promoting cell apoptosis and inhibiting the invasion and migration capabilities of ovarian cancer cells.

Our study found that miR-140-5p was weakly expressed in ovarian cancer cell lines. Zheng et al. also found that miR-140-5p was weakly expressed in gastric cancer tissues and cells compared with normal tissues and cells.<sup>17</sup>

Similar situations have also been demonstrated in breast cancer and cervical cancer,<sup>18,19</sup> and downregulated miR-140-5p has always presaged a poor prognosis. Analogously, we demonstrated that the overexpression of miR-140-5p could inhibit the proliferation, metastasis and development of ovarian cancer cell lines. MiR-140-5p has also demonstrated an ability to block the development of multiple cancers, including the proliferation and metastasis of gastric cancer cells.<sup>17</sup> Besides, miR-140-5p has been shown to inhibit tumor metastasis and development by downregulating the expression of ADAM-related genes in hypopharyngeal and colorectal cancer.<sup>20,21</sup> Moreover, miR-140-5p can not only inhibit the proliferation of synovial fibroblasts and inflammatory cytokine secretion by targeting TLR4, but can also inhibit proliferation and migration of glioma cells by targeting the *VEGFA/MMP2* pathway.<sup>22,23</sup> In conclusion, miR-140-5p can regulate the malignant behavior of various kinds of cancers, including ovarian cancer, and prevent further deterioration of ovarian cancer.

For our in-depth study of corresponding mechanisms of miR-140-5p in ovarian cancer, the potential signaling pathways regulated by miR-140-5p were predicted using a bioinformatics website, and it was found that there are binding sites between miR-140-5p and *WNT1*. The expressions of Wnt pathway-related  $\beta$ -catenin, *WNT1*, *C-myc*, and *MMP-7* were found to be significantly reduced in the miR-140-5p mimic group compared to the NC group, and the number of cells with  $\beta$ -catenin transfer to the nucleus in the miR-140-5p mimic group was also decreased significantly compared with the NC group.

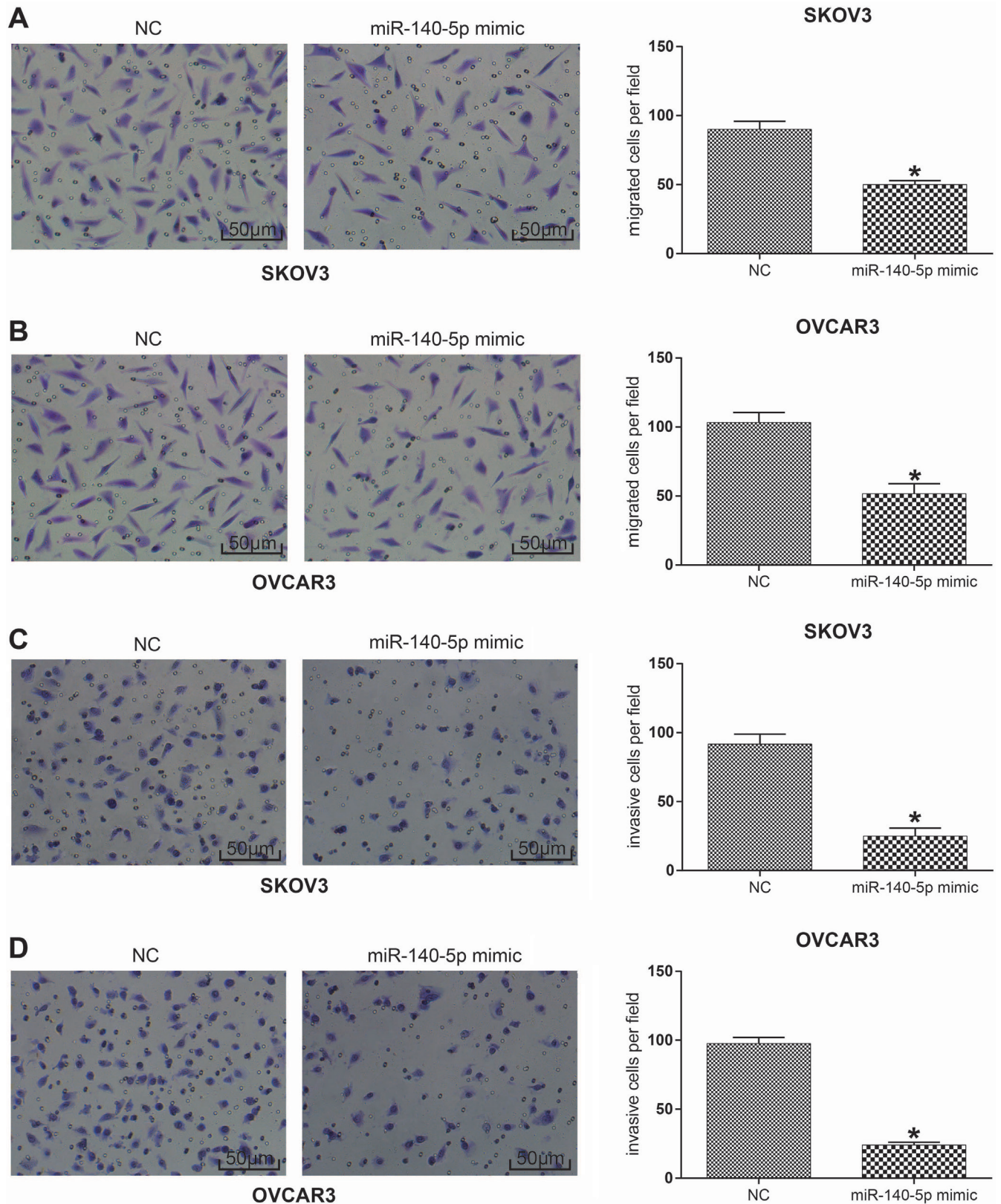
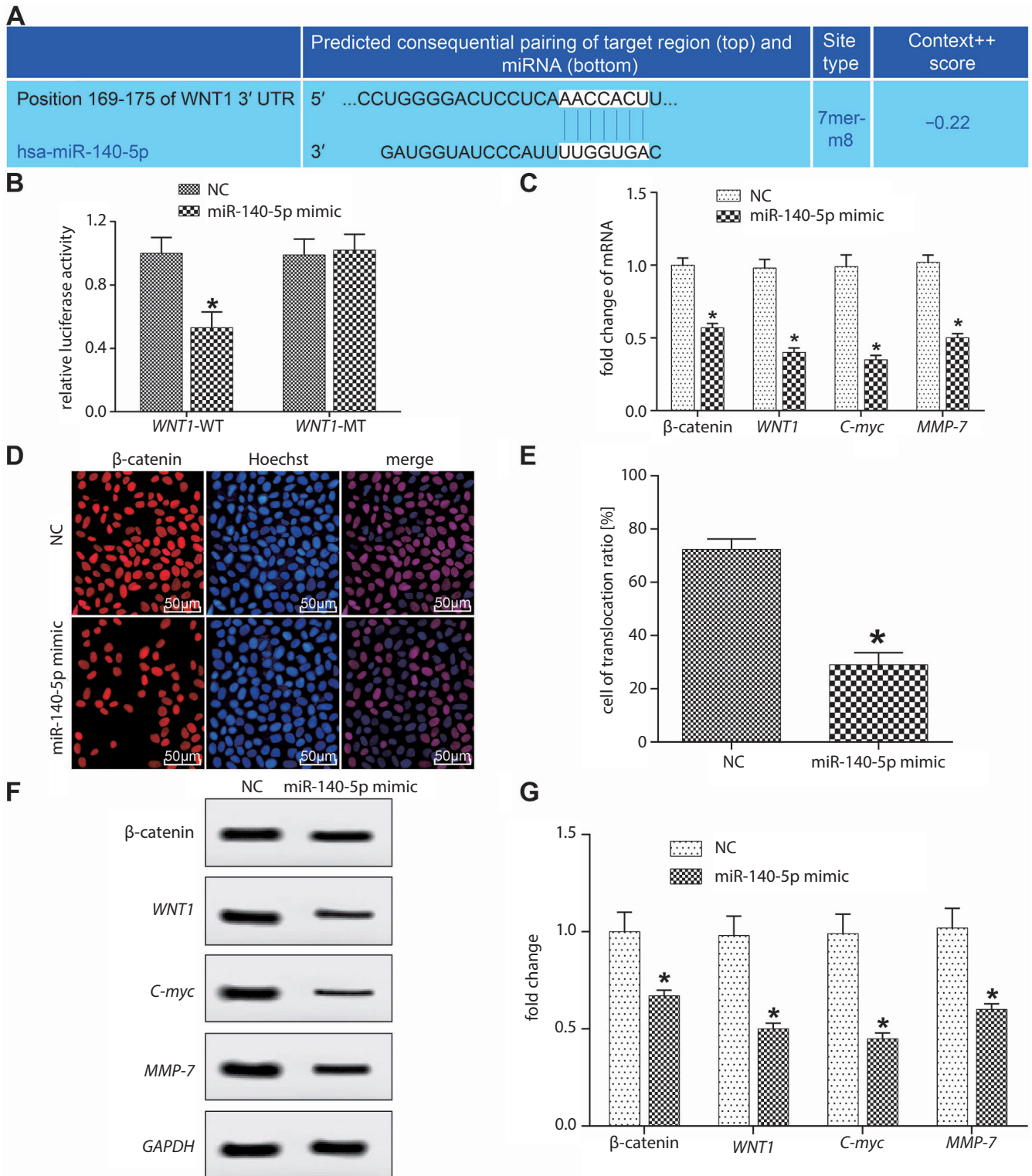


Fig. 3. Cell migration and invasion capacity detection

A. Cell migration detection in SKOV3 cells and the related histogram analysis. B. Cell migration detection in OVCAR3 cells and the related histogram analysis. C. Cell invasion detection in SKOV3 cells and the related histogram analysis. D. Cell invasion detection in OVCAR3 cells and the related histogram analysis. Compared with the NC group, \* $p < 0.05$ .



**Fig. 4.** miR-140-5p mediates the Wnt signaling pathway

A. Binding sites between miR-140-5p and *WNT1* were analyzed using a bioinformatics analysis website. B. The relationship between miR-140-5p and *WNT1* was further verified with a dual-luciferase reporter assay. C. The expression of Wnt signaling pathway-related signal molecules was detected using qRT-PCR. D and E. Nuclear transfer of  $\beta$ -catenin was detected using an immunofluorescence test. The corresponding histogram analysis is also shown. F and G. Expression of Wnt signaling pathway-related signal molecule genes was detected with western blot; the corresponding histogram analysis is also shown. Compared with the NC group, \* $p < 0.05$ .

*WNT1* is an important regulatory gene of the Wnt signaling pathway, and overexpression of *WNT1* has been shown to upregulate the expression of  $\beta$ -catenin, *C-myc*, *MMP-7*, and related other factors, thus accelerating the proliferation and development of lung cancer cells.<sup>24</sup> In most cases, the Wnt pathway activates its target genes by promoting  $\beta$ -catenin transfer into the nucleus.<sup>25</sup> However, abnormal activation of the Wnt signal has the ability to regulate cancer stem cells and plays a key role in the production and deterioration of multiple types of cancer.<sup>26</sup> Similarly, Wu et al. found that miR-140-5p can inhibit the Wnt signaling pathway so as to reduce cell proliferation and strengthen drug efficacy in breast cancer cells.<sup>27</sup>

Although we have shown that miR-140-5p regulates the proliferation, apoptosis, migration, and invasion ability of ovarian cancer cells by regulating *WNT1*, it is still unclear whether miR-140-5p could also regulate the progression of ovarian cancer through other signal factors. Thus, more experiments are needed to further explore the function and molecular mechanisms of miR-140-5p in ovarian cancer, in order to provide a more powerful basis for clinical application.

## Conclusions

We found that miR-140-5p inactivates the Wnt/ $\beta$ -catenin signaling pathway by regulating *WNT1*, and prevents further deterioration of ovarian cancer. MiR-140-5p is expected to provide novel ideas for the treatment of ovarian cancer.

### ORCID iDs

Yunyu Wu  <https://orcid.org/0000-0002-2975-5365>

Jie Li  <https://orcid.org/0000-0002-4734-1940>

Shuying Chen  <https://orcid.org/0000-0002-0148-0048>

Zhiwu Yu  <https://orcid.org/0000-0002-1870-1409>

### References

- Webb PM, Jordan SJ. Epidemiology of epithelial ovarian cancer. *Best Pract Res Clin Obstet Gynaecol*. 2017;41:3–14.
- Heintz APM, Odicino F, Maisonneuve P, et al. Carcinoma of the ovary. FIGO 26<sup>th</sup> Annual Report on the Results of Treatment in Gynecological Cancer. *Int J Gynaecol Obstet*. 2006;95(Suppl 1):S161–S192.
- Reid BM, Permuth JB, Sellers TA. Epidemiology of ovarian cancer: A review. *Cancer Biol Med*. 2017;14(1):9–32.
- Li W, Liu Z, Chen L, Zhou L, Yao Y. MicroRNA-23b is an independent prognostic marker and suppresses ovarian cancer progression by targeting runt-related transcription factor-2. *FEBS Lett*. 2014;588(9):1608–1615.
- Chen W, Huang L, Hao C, et al. MicroRNA-155 promotes apoptosis in SKOV3, A2780, and primary cultured ovarian cancer cells. *Tumour Biol*. 2016;37(7):9289–9299.
- Li X, Chen W, Zeng W, et al. microRNA-137 promotes apoptosis in ovarian cancer cells via the regulation of XIAP. *Br J Cancer*. 2017;116(1):66–76.
- Wang M, He Y, Shi L, Shi C. Multivariate analysis by Cox proportional hazard model on prognosis of patient with epithelial ovarian cancer. *Eur J Gynaecol Oncol*. 2011;32(2):171–177.
- Li Y, Chen Y, Li J, et al. Co-delivery of microRNA-21 antisense oligonucleotides and gemcitabine using nanomedicine for pancreatic cancer therapy. *Cancer Sci*. 2017;108(7):1493–1503.
- Li P, Sun Y, Liu Q. MicroRNA-340 induces apoptosis and inhibits metastasis of ovarian cancer cells by inactivation of NF- $\kappa$ B. *Cell Physiol Biochem*. 2016;38(5):1915–1927.
- Kan Q, Su Y, Yang H. MicroRNA-335 is downregulated in papillary thyroid cancer and suppresses cancer cell growth, migration and invasion by directly targeting ZEB2. *Oncol Lett*. 2017;14(6):7622–7628.
- Liu C, Liu R, Zhang D, et al. MicroRNA-141 suppresses prostate cancer stem cells and metastasis by targeting a cohort of pro-metastasis genes. *Nat Commun*. 2017;8:14270–14270.
- Santos JC, Lima NDS, Sarian LO, et al. Exosome-mediated breast cancer chemoresistance via miR-155 transfer. *Sci Rep*. 2018;8(1):829–829.
- Flamini V, Jiang W, Cui Y. Therapeutic role of MiR-140-5p for the treatment of non-small cell lung cancer. *Anticancer Res*. 2017;37(8):4319–4327.
- Zhai H, Fesler A, Ba Y, Wu S, Ju J. Inhibition of colorectal cancer stem cell survival and invasive potential by hsa-miR-140-5p mediated suppression of Smad2 and autophagy. *Oncotarget*. 2015;6(23):19735–19746.
- Yang P, Xiong J, Zuo L, Liu K, Zhang H. miR-140-5p regulates cell migration and invasion of non-small cell lung cancer cells through targeting VEGFA. *Mol Med Rep*. 2018;18(3):2866–2872.
- Dihlmann S, von Knebel Doeberitz M. Wnt/ $\beta$ -catenin-pathway as a molecular target for future anti-cancer therapeutics. *Int J Cancer*. 2005;113(4):515–524.
- Fang Z, Yin S, Sun R, et al. miR-140-5p suppresses the proliferation, migration and invasion of gastric cancer by regulating YES1. *Mol Cancer*. 2017;16(1):139–139.
- Lu Y, Qin T, Li J, et al. MicroRNA-140-5p inhibits invasion and angiogenesis through targeting VEGF-A in breast cancer. *Cancer Gene Ther*. 2017;24(9):386–392.
- Su Y, Xiong J, Hu J, et al. MicroRNA-140-5p targets insulin like growth factor 2 mRNA binding protein 1 (IGF2BP1) to suppress cervical cancer growth and metastasis. *Oncotarget*. 2016;7(42):68397–68411.
- Jing P, Sa N, Xu W. miR-140-5p affects the migration and invasion of hypopharyngeal carcinoma cells by downregulating ADAM10 expression [in Chinese]. *Zhonghua Er Bi Yan Hou Tou Jing Wai Ke Za Zhi*. 2016;51(3):189–196.
- Yu L, Lu Y, Han X, et al. microRNA-140-5p inhibits colorectal cancer invasion and metastasis by targeting ADAMTS5 and IGFBP5. *Stem Cell Res Ther*. 2016;7(1):180.
- Li H, Guan S, Lu Y, Wang F. MiR-140-5p inhibits synovial fibroblasts proliferation and inflammatory cytokines secretion through targeting TLR4. *Biomed Pharmacother*. 2017;96:208–214.
- Hu Y, Li Y, Wu C, et al. MicroRNA-140-5p inhibits cell proliferation and invasion by regulating VEGFA/MMP2 signaling in glioma. *Tumour Biol*. 2017;39(4):1010428317697558. doi:10.1177/1010428317697558.
- Huang CL, Liu D, Ishikawa S, et al. Wnt1 overexpression promotes tumour progression in non-small cell lung cancer. *Eur J Cancer*. 2008;44(17):2680–2688.
- Lustig B, Behrens J. The Wnt signaling pathway and its role in tumor development. *J Cancer Res Clin Oncol*. 2003;129(4):199–221.
- Duchartre Y, Kim YM, Kahn M. The Wnt signaling pathway in cancer. *Crit Rev Oncol Hematol*. 2016;99:141–149.
- Wu D, Zhang J, Lu Y, et al. miR-140-5p inhibits the proliferation and enhances the efficacy of doxorubicin to breast cancer stem cells by targeting Wnt1. *Cancer Gene Ther*. 2019;26(3–4):74–82.

# PD-L1, PDK-1 and p-Akt are correlated in patients with papillary thyroid carcinoma

Hui Wang<sup>A,B</sup>, Zhengdong Zhang<sup>B,C,F</sup>, Zhe Yan<sup>B,C,F</sup>, Shihong Ma<sup>A,E,F</sup>

Department of General Surgery, Shanghai Xuhui Center Hospital, China

A – research concept and design; B – collection and/or assembly of data; C – data analysis and interpretation; D – writing the article; E – critical revision of the article; F – final approval of the article

Advances in Clinical and Experimental Medicine, ISSN 1899–5276 (print), ISSN 2451–2680 (online)

*Adv Clin Exp Med.* 2020;29(7):785–792

## Address for correspondence

Shihong Ma  
E-mail: msh191203@yeah.net

## Funding sources

The study was funded by the Foundation for Development of Clinical Medical Science and Technology (grant No. JLY20180041) and the Research Foundation of Xuhui Center Hospital (grant No. 2018XHYY-10).

## Conflict of interest

None declared

Received on February 19, 2020  
Reviewed on March 6, 2020  
Accepted on April 30, 2020

Published online on August 4, 2020

## Abstract

**Background.** Papillary thyroid carcinoma (PTC) is the most common type of thyroid carcinoma.

**Objectives.** To investigate the clinical significance of programmed death ligand 1 (PD-L1) and phosphoinositide-dependent protein kinase 1 (PDK1) in PTC.

**Material and methods.** A total of 194 PTC patients were recruited. Contralateral normal thyroid tissues were obtained and used as controls (n = 80). The expression levels of PD-L1, PDK1 and p-Akt were determined using immunohistochemistry.

**Results.** The PD-L1, PDK1 and p-Akt were upregulated in cancer tissues compared to the normal tissues. The mean optical density (MOD) values of PD-L1, PDK1 and p-Akt were significantly higher in the PTC tissues. The expression of PD-L1 positively correlated with the levels of PDK1 and p-Akt. In addition, the expression of PD-L1, PDK1 and p-Akt in PTC patients without chronic lymphocytic thyroiditis (CLT) was significantly higher than the expression of those proteins in the CLT patients. The patients with higher expression levels of PD-L1, PDK1 or p-Akt had remarkably larger tumors and higher rates of TNM III–IV, capsular infiltration, lymph node metastasis, and of recurrence. The Kaplan–Meier curve showed that patients with lower expression of PD-L1, PDK1 or p-Akt had significantly longer recurrence-free time. The logistic regression analysis revealed that only CLT, PD-L and capsular infiltration were risk factors for patients' five-year recurrence.

**Conclusions.** The PD-L1, PDK1 and p-Akt were found to be positively correlated with a poor prognosis in PTC.

**Key words:** prognosis, papillary thyroid carcinoma, p-Akt, sPD-L1, PDK-1

## Cite as

Wang H, Zhang Z, Yan Z, Ma S. PDK-1 and p-Akt are correlated in patients with papillary thyroid carcinoma. *Adv Clin Exp Med.* 2020;29(7):785–792. doi:10.17219/acem/121518

## DOI

10.17219/acem/121518

## Copyright

© 2020 by Wrocław Medical University  
This is an article distributed under the terms of the Creative Commons Attribution 3.0 Unported (CC BY 3.0) (<https://creativecommons.org/licenses/by/3.0/>)

## Introduction

Papillary thyroid carcinoma (PTC) is the most common type of thyroid carcinoma.<sup>1,2</sup> It accounts for about 70–85% of all thyroid carcinoma cases.<sup>3,4</sup> Compared to other types of thyroid carcinomas, such as follicular thyroid carcinoma (FTC) and anaplastic thyroid carcinoma (ATC), PTC has a better prognosis with a five-year survival rate of over 90%.<sup>5,6</sup> However, lymph node metastasis and recurrence are very common in PTC patients.<sup>7</sup> Recurrence has been reported in 15–30% of cases and lymph node metastasis occurs in 5–10% of PTC patients.<sup>8,9</sup> For these patients, the five-year survival rate is only about 50%.<sup>10</sup>

Chronic lymphocytic thyroiditis (CLT), also known as Hashimoto's thyroiditis, is an autoimmune disease characterized by a painless and diffuse goiter, occasionally accompanied by atypical symptoms, such as hyperthyroidism, exophthalmos, hypothyroidism, etc.<sup>11</sup> The relationship between CLT and PTC has been reported in recent years. Previous studies have shown that PTC patients with concurrent CLT had better prognoses than those without CLT.<sup>12,13</sup> However, a deeper understanding of the relationship between PTC and CLT is still needed.

Programmed death ligand 1 (PD-L1), also known as CD274, is a cell surface glycoprotein that belongs to the B7 family.<sup>14</sup> It plays important roles in many cancers, such as non-small-cell lung cancer and pancreatic cancer.<sup>15,16</sup> Recent evidence has revealed that PD-L1 was up-regulated in PTC emerging from CLT and was correlated with metastasis.<sup>17</sup> However, the clinical significance of PD-L1 in PTC remains unclear. In addition, another study found that PD-L1 was correlated with the phosphoinositide/dependent protein kinase 1 (PDK1), the phosphorylation of Akt in ovarian cancer.<sup>18</sup> However, to the best of our knowledge, no study has focused on the relationship between PD-L1, PDK1 and p-Akt in PTC patients with or without CLT.

We aimed to perform an observational study to investigate the clinical significance of PD-L1, PDK1 and p-Akt in PTC patients. Our data showed that PD-L1, PDK1 and p-Akt were upregulated in PTC patients, especially those without CLT, and that the high expression of PD-L1, PDK1 and p-Akt was correlated with a poor prognosis of PTC. These findings might provide clinical evidence for the potential application of PD-L1, PDK1 and p-Akt as biomarkers in PTC diagnosis.

## Material and methods

### Patients

The present study included 194 patients with PTC who went to our hospital between April 2011 and October 2014, and met the inclusion criteria. All patients were first diagnosed with PTC using histological analysis. The exclusion

criteria were as follows: receiving chemotherapy or radiotherapy before the study; other thyroid diseases apart from CLT, such as nodular goiter; other immune diseases; and other cancers or papillary thyroid microcarcinoma. In addition, 80 contralateral normal thyroid tissue samples were obtained from the same patients and all were confirmed to be healthy tissues through histological analysis. The study was approved by the Ethic Committee of Shanghai Xuhui Center Hospital, China.

### Immunohistochemistry

The expression levels of PD-L1, PDK1 and p-Akt were determined using immunohistochemistry (IHC). Briefly, tissues were collected immediately after resection and stored at  $-20^{\circ}\text{C}$  before being used. After the samples were fixed with 10% formalin, embedded in paraffin and sectioned, hematoxylin and eosin (H&E) staining was performed. The samples were then immersed in 3%  $\text{H}_2\text{O}_2$  followed by incubation with primary antibodies – anti-PD-L1 (ab205921; Abcam, Cambridge, UK), anti-PDK1 (ab90444; Abcam), or anti-p-Akt (ab38449; Abcam) – at  $4^{\circ}\text{C}$  overnight. After being incubated with a corresponding second antibody at  $37^{\circ}\text{C}$  for 30 min, the samples were stained with diaminobenzidine (DAB). Some sections were treated with phosphate-buffered saline (PBS) instead of primary antibody and were used as negative controls. Sections with a high expression of PD-L1, PDK1 or p-Akt served as positive controls. The Allred scoring system was used for pathological scoring. The degrees of staining intensity were the following: 0 (no staining); 1 (weak staining); 2 (moderate staining); and 3 (strong staining). Scores for the percentage of stained area were as follows: 0 (none); 1 (<1%); 2 (1–10%); 3 (10–33%); 4 (33–66%); and 5 (>66%). Both were used as the final IHC score: 0–2 (negative); 3–4 (weak); 5–6 (moderate); and 7–8 (strong). To further determine the expression levels of PD-L1, PDK1 and p-Akt, semi-quantitative analysis was conducted by calculating the mean optical density (MOD) using Image Pro Plus v. 6.0 software (Media Cybernetics, Rockville, USA). Briefly, photographs were collected at a magnification of  $\times 400$  under the same exposure conditions. Five random photographs were captured for each slice. The integrated optical density (IOD) was calculated. For pictures with no blank area,  $\text{MOD} = \text{IOD}/\text{picture area}$ ; for pictures with a blank area,  $\text{MOD} = \text{IOD}/(\text{picture area} - \text{blank area})$ . The MOD value of 1 slice was calculated as the mean value of the 5 randomly selected fields in the slice.

### Data collection

The basic characteristics of all patients were collected, including age, sex and body mass index (BMI). The clinical variables – including TNM (tumor–nodule–metastasis) stage, tumor diameter, capsular infiltration, tumor number, and lymph node metastasis – were also recorded.

All patients were followed up for 5 years from admission. To analyze the recurrence rate, the recurrence-free time was calculated during the study period from admission to death or to the end of follow-up.

### Statistical analysis

The measurement data are expressed as means ± standard deviation (SD). Comparisons between 2 groups of continuous data were performed using Student’s t-test. The  $\chi^2$  test was used to compare the categorical variables. Pearson’s correlation analysis was performed to analyze the correlation of PD-L1, PDK1 and p-Akt. For recurrence analysis, Kaplan–Meier curve was used with the log-rank test. For logistic analysis, logistic regression was conducted using the stepwise method. A p-value <0.05 was considered to be statistically significant. All data analysis was performed using SPSS v. 22.0 software (IBM Corp., Armonk, USA).

## Results

### Basic characteristics of all patients

The basic characteristics of the patients are listed in Table 1. Among the 194 PTC patients, 68 had CLT and 126 were without concurrent CLT. The ratio of female patients in the PTC+CLT group was significantly higher and the mean age of the patients was significantly lower than in the patients without CLT ( $p < 0.05$ ; Table 1). The PCT

Table 1. Basic characteristics of all patients

Variables	PTC without CLT, n = 126	PTC+CLT, n = 68	p-value
Age [years]	48.76 ±9.48	42.30 ±10.27	<0.001
Sex, female (%)	86 (68.25)	57 (83.82)	0.008
BMI [kg/m <sup>2</sup> ]	22.92 ±3.00	23.39 ±3.09	0.307
TNM stage, n (%)			
I–II	67 (53.17)	50 (73.53)	0.002
III–IV	59 (46.83)	18 (26.47)	
Mean diameter [cm]	2.21 ±0.69	1.92 ±0.61	<0.001
Capsular infiltration, n (%)			
yes	79 (62.70)	25 (36.76)	<0.001
no	47 (37.30)	43 (63.24)	
Number of tumors, n (%)			
≥6	17 (13.49)	10 (14.71)	0.684
<6	109 (86.51)	58 (85.29)	
Lymph node metastasis, n (%)			
yes	69 (54.76)	27 (39.71)	0.034
no	57 (45.24)	41 (60.29)	

BMI – body mass index; PTC – papillary thyroid carcinoma; CLT – chronic lymphocytic thyroiditis.

patients with CLT showed significantly lower rates of TNM III–IV, capsular infiltration and lymph node metastasis, as well as markedly smaller tumor diameter than those without CLT ( $p < 0.05$ ). However, there was no significant difference in the number of tumors between the 2 groups.

### Expression of PD-L1, PDK1 and p-Akt was upregulated and positively correlated in PTC patients

The expression levels of PD-L1, PDK1 and p-Akt were determined with IHC and the MOD values were assessed. As shown in Fig. 1, the expression levels of PD-L1, PDK1 and p-Akt were upregulated in the cancer tissues and remained low in the normal tissues. Similarly, the MOD values of PD-L1, PDK1 and p-Akt were significantly higher in PTC tissues compared with the controls ( $p < 0.05$ ). Moreover, the expression of PD-L1, PDK1 and p-Akt in PTC patients without CLT was markedly higher than that in patients with CLT ( $p < 0.05$ ). The Pearson’s analysis revealed that the levels of PD-L1 and PDK1, PD-L1 and p-Akt, and PDK1 and p-Akt were positively correlated in all tissues ( $p < 0.05$ ; Table 2).

Table 2. Expression of PD-L1 and PDK1, PD-L1 and p-Akt, and PDK1 and p-Akt were positively correlated

Proteins	Statistical variables	PD-L1	PDK1	p-Akt
PD-L1	Pearson’s correlation	1	0.542	0.585
	p-value	–	0.000	0.000
PDK1	Pearson’s correlation	0.542	1	0.556
	p-value	0.000	–	0.000
p-Akt	Pearson’s correlation	0.585	0.556	1
	p-value	0.000	0.000	–

PD-L1 – programmed death ligand 1; PDK1 – phosphoinositide-dependent protein kinase 1.

### PD-L1, PDK1 and p-Akt levels correlated with patients’ clinical outcomes

To further study the roles of PD-L1, PDK1 and p-Akt in PTC, the clinical characteristics of all patients were analyzed. The PTC patients were divided into high/low PD-L1 groups according to the MOD value of PD-L1 (0.023), as well as high/low PDK1 groups and high/low p-Akt groups according to the MOD values of PDK1 (0.021) and p-Akt (0.022). The results showed that patients with high expression of PD-L1, PDK1 or p-Akt had significantly more cases of TNM III–IV ( $p < 0.05$ ; Tables 3–5). Furthermore, the percentage of patients with capsular infiltration, lymph node metastasis and five-year recurrence

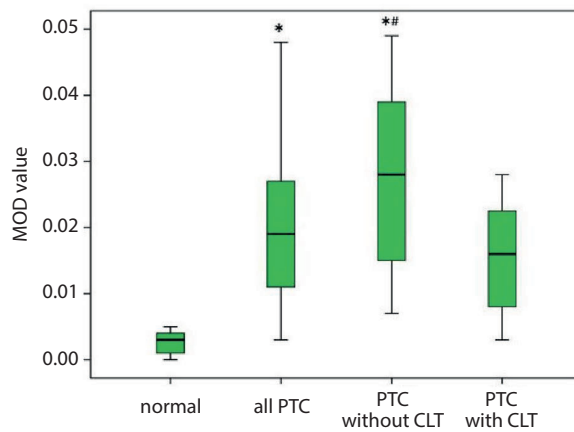
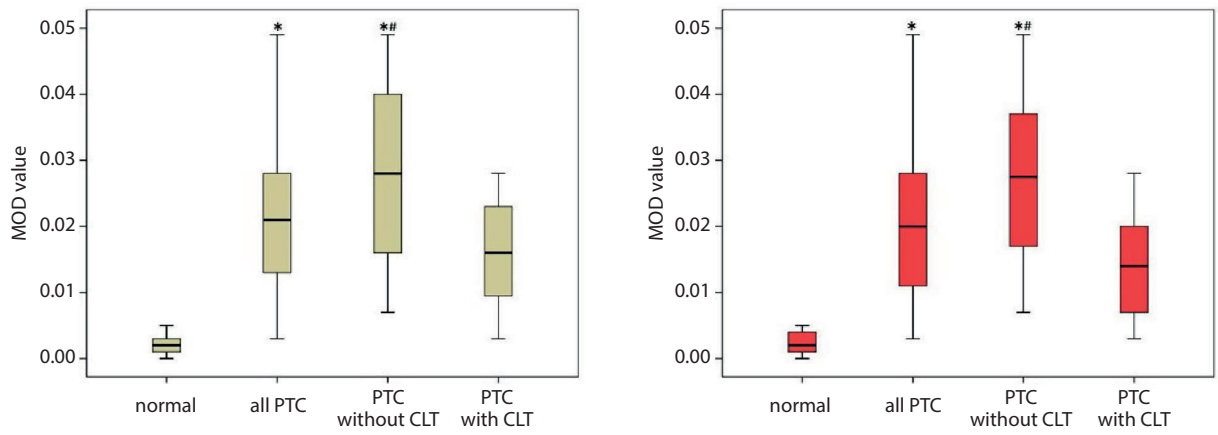
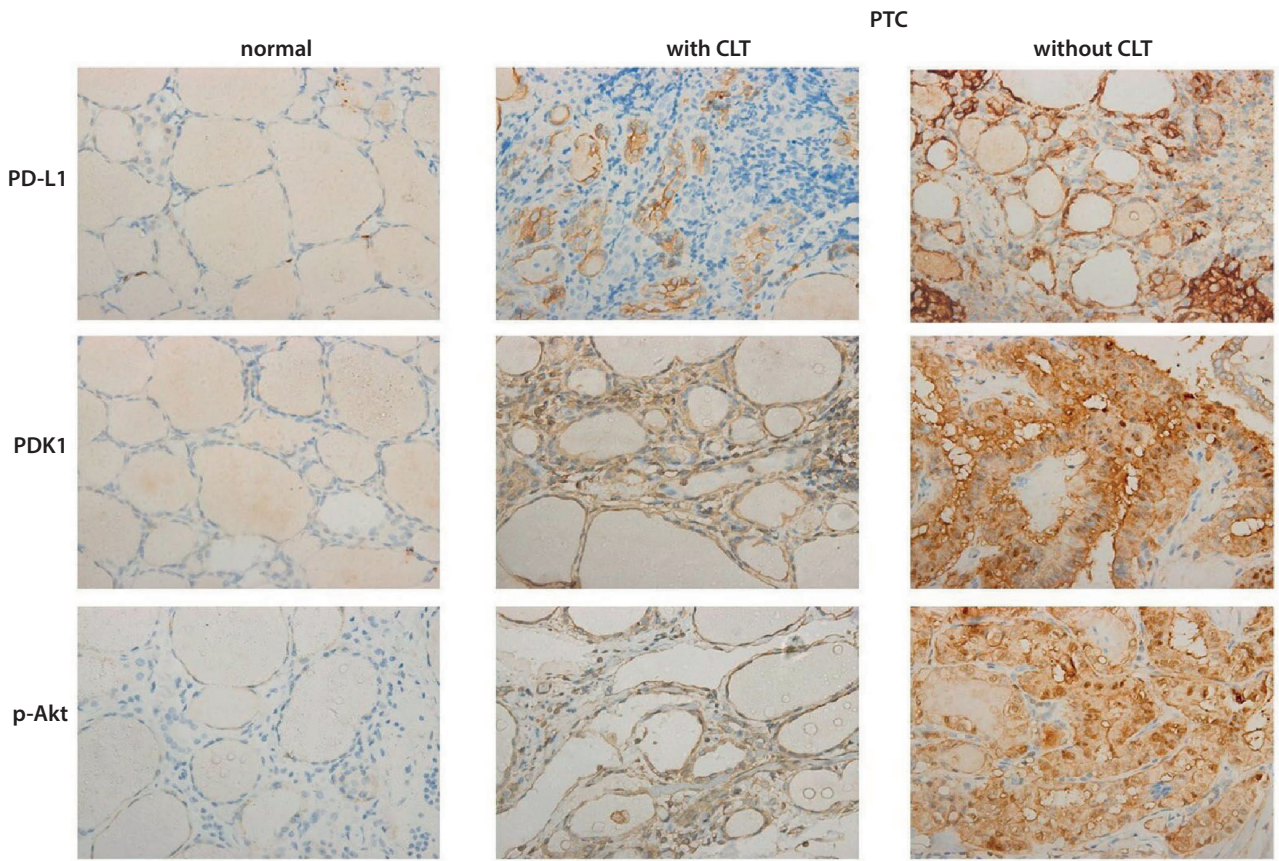


Fig. 1. Expressions of PD-L1, PDK1 and p-Akt were upregulated and positively correlated in PTC patients

**Table 3.** PD-L1 correlated with patients' clinical outcomes

Variables	High PD-L1 (n = 92)	Low PD-L1 (n = 102)	p-value
Age [years]	47.35 ±10.46	45.64 ±9.94	0.247
Sex, female (%)	69 (75.00)	74 (72.55)	0.694
BMI [kg/m <sup>2</sup> ]	23.19 ±2.86	22.98 ±3.22	0.638
TNM stage, n (%)			
I–II	47 (51.09)	70 (68.63)	0.011
III–IV	45 (48.91)	32 (31.37)	
Mean diameter [cm]	2.13 ±0.67	2.09 ±0.69	0.672
Capsular infiltration, n (%)			
yes	59 (64.13)	45 (44.12)	0.005
no	33 (35.87)	57 (55.88)	
Number of tumors, n (%)			
≥6	12 (13.04)	15 (14.71)	0.733
<6	80 (86.95)	87 (85.29)	
Lymph node metastasis, n (%)			
yes	61 (66.30)	35 (34.31)	0.000
no	32 (34.70)	67 (65.69)	
MOD of PDK1	0.023 ±0.011	0.021 ±0.013	0.155
MOD of p-Akt	0.025 ±0.012	0.020 ±0.011	0.005
Five-year recurrence, n (%)	17 (17.53)	7 (6.86)	0.021

BMI – body mass index; MOD – mean optical density; PD-L1 – programmed death ligand 1.

**Table 4.** PDK1 correlated with patients' clinical outcomes

Variables	High PDK1 (n = 97)	Low PDK1 (n = 97)	p-value
Age [years]	47.42 ±10.36	45.57 ±10.04	0.209
Sex, female (%)	69 (71.13)	74 (76.29)	0.407
BMI [kg/m <sup>2</sup> ]	22.93 ±3.14	23.24 ±2.94	0.480
TNM stage, n (%)			
I–II	51 (52.58)	66 (68.04)	0.025
III–IV	46 (47.42)	31 (31.96)	
Mean diameter [cm]	2.24 ±0.72	1.98 ±0.61	0.008
Capsular infiltration, n (%)			
yes	59 (60.82)	45 (46.39)	0.041
no	38 (39.18)	52 (53.61)	
Number of tumors, n (%)			
single	82 (84.54)	85 (87.63)	0.528
multiple	15 (15.46)	12 (12.37)	
Lymph node metastasis, n (%)			
yes	56 (57.73)	39 (40.21)	0.013
no	41 (42.27)	58 (59.79)	
MOD of PD-L1	0.027 ±0.012	0.020 ±0.012	0.001
MOD of p-Akt	0.025 ±0.013	0.021 ±0.011	0.063
Five-year recurrence, n (%)	18 (18.56)	6 (6.19)	0.008

BMI – body mass index; MOD – mean optical density; PDK1 – phosphoinositide-dependent protein kinase 1.

**Table 5.** p-Akt correlated with patients' clinical outcomes

Variables	High p-Akt (n = 96)	Low p-Akt (n = 98)	p-value
Age [years]	48.12 ±10.34	44.90 ±9.89	0.028
Sex, female (%)	68 (70.83)	75 (76.53)	0.360
BMI [kg/m <sup>2</sup> ]	22.75 ±2.94	23.42 ±3.10	0.120
TNM stage, n (%)			
I–II	49 (51.04)	68 (69.39)	0.008
III–IV	47 (48.96)	30 (30.61)	
Mean diameter [cm]	2.20 ±0.70	2.01 ±0.64	0.054
Capsular infiltration, n (%)			
yes	59 (61.46)	45 (45.92)	0.028
no	37 (38.54)	53 (54.08)	
Number of tumors, n (%)			
single	81 (84.38)	86 (88.76)	0.472
multiple	15 (15.63)	12 (12.24)	
Lymph node metastasis, n (%)			
yes	54 (56.25)	41 (41.84)	0.042
no	42 (43.75)	57 (58.16)	
MOD of PD-L1	0.026 ±0.013	0.021 ±0.012	0.003
MOD of PDK1	0.025 ±0.012	0.020 ±0.011	0.008
Five-year recurrence, n (%)	17 (17.71)	7 (7.14)	0.023

BMI – body mass index; MOD – mean optical density.

were significantly higher in patients with high expression levels of PD-L1, PDK1 or p-Akt than the ones with low expression ( $p < 0.05$ ). The mean diameter of PTC tumors in patients with high expression of PDK1 was significantly higher than that in the group with low PDK1 expression, while no significant difference in tumor diameter was observed in the patients with high/low PD-L1 or high/low p-Akt ( $p < 0.05$ ). Additionally, the age of the patients with lower expression of p-Akt was markedly lower than the age of the patients with high p-Akt expression ( $p < 0.05$ ). All of these results indicate that PD-L1, PDK1 and p-Akt expression levels correlate with the clinical outcomes of PTC patients.

### PD-L1, PDK1 and p-Akt expression correlated with patients' recurrence

Finally, we analyzed the correlation between PD-L1, PDK1 and p-Akt expression, and the recurrence of PTC patients. The recurrence-free time was analyzed using the Kaplan–Meier curve (Fig. 2). Patients with lower expression levels of PD-L1, PDK1 or p-Akt had significantly longer recurrence-free time compared to the ones with high expression levels ( $p < 0.05$ ). Then logistic regression showed that only CLT, PD-L1 and capsular infiltration were risk factors for patients' five-year recurrence (Table 6).

**Table 6.** PD-L1 and PDK1 correlated with patients' recurrence

Variable	Wald	OR	95% CI	p-value
Age	2.261	0.039	1.040 (0.988–1.094)	0.133
BMI	1.190	−0.105	0.900 (0.746–1.087)	0.275
Diameter	0.119	0.128	1.137 (0.549–2.355)	0.730
Sex	1.294	0.835	2.306 (0.547–9.727)	0.255
CLT	6.622	1.943	0.143 (0.033–0.629)	0.010
TNM stage	1.066	−0.549	0.578 (0.204–1.637)	0.302
Capsular infiltration	3.926	1.232	3.428 (1.013–11.596)	0.048
Number of tumors	0.476	0.487	1.627 (0.408–6.484)	0.490
Lymph node metastasis	0.327	−0.318	0.728 (0.245–2.162)	0.567
PD-L1	7.808	60.801	12.545 (7.66–8.453)	0.005
PDK1	3.660	43.209	5.829 (0.347–9.794)	0.056
p-Akt	0.658	15.821	1.902 (0.000–2.975)	0.417

BMI – body mass index; CLT – chronic lymphocytic thyroiditis; PD-L1 – programmed death ligand 1; PDK1 – phosphoinositide-dependent protein kinase 1; OR – odds ratio; 95% CI – 95% confidence interval.

## Discussion

With the development of surgical and chemotherapy methods, the five-year survival condition for PTC patients has been greatly improved.<sup>19</sup> However, lymph node metastasis commonly occurs in PTC patients, who often have poor prognosis. Thus, the early diagnosis of PTC is of great significance. In this study, we found that PD-L1, PDK1 and p-Akt were upregulated in PTC tissues, especially in patients without CLT, and that this upregulation correlated with a poor prognosis of the PTC patients.

The involvement of PD-L1 has been reported in many cancers. Tanaka et al. demonstrated that ERO1- $\alpha$  promoted immune escape by elevating PD-L1 in breast cancer.<sup>20</sup> It was also reported that poly(ADP-ribose)polymerase (PARP) inhibitor enhanced cancer-associated immunosuppression by upregulating PD-L1.<sup>21</sup> Chintakuntlawar et al. demonstrated that high PD-L1 expression in anaplastic thyroid cancer trended toward worse progression-free survival and overall survival.<sup>22</sup> In a more recent study, upregulation of PD-L1 was found in PTC patients and the high expression of PD-L1 predicted shorter disease-free time in these patients.<sup>23</sup> In medullary thyroid carcinoma, however, the expression of PD-L1 was low, indicating the controversial role of PD-L1 in human cancers.<sup>24</sup> In this study, we found that PD-L1 was upregulated in PTC patients. Moreover, the expression of PD-L1 was higher in PTC patients without CLT. PD-L1 was also found to be positively correlated with PDK1 expression, and high expression of PD-L1 was related to poor prognosis in PTC patients.

The PDK1 is an important protein in the development of multiple cancers. Zhang et al. reported that dicumarol

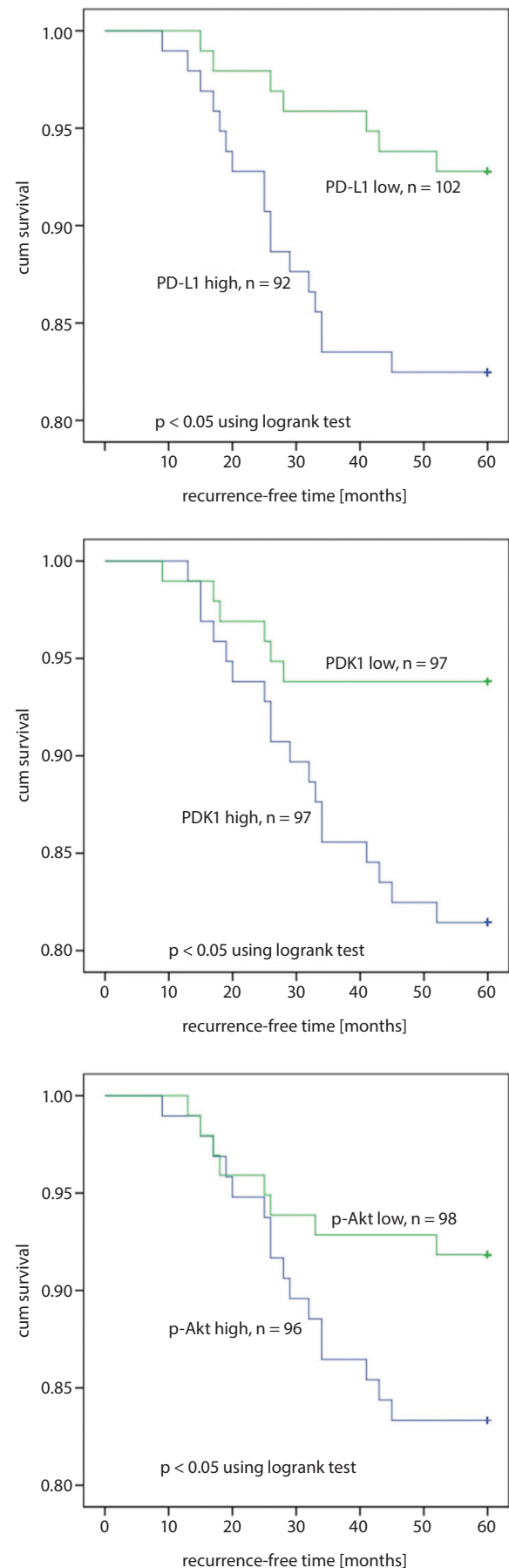


**Fig. 2.** The recurrence-free time in PTC patients was analyzed using Kaplan–Meier curve

facilitated the progression of ovarian cancer by suppressing PDK1.<sup>25</sup> It was found that PDK1 induced the invasion and migration of gallbladder cancer.<sup>26</sup> Fujiwara et al. reported that the inhibition of PDK1 could also be considered as a novel therapeutic target in multiple myeloma.<sup>27</sup> In this study, we demonstrated for the first time that a high expression level of PDK1 correlated with poor prognosis and positively correlated with the expression of PD-L1 in PTC patients.

Additionally, the relationship between PD-L1 and PDK1 was also observed in several previous studies. Recent data showed that aberrant upregulation of PDK1 was correlated with the overexpression of PD-L1,<sup>18</sup> which was consistent with our data. The p-Akt is the downstream protein of PDK1, which is also reported to play important roles in PTC. A recent study found that Akt inhibitor suppressed the proliferation of PTC cells.<sup>28</sup> Also, the activation of the Akt signaling pathway promoted the development of PTC.<sup>29</sup> Consistent with the above in vitro studies, we showed that the expression of p-Akt was upregulated in PTC tissues and that it predicted worse prognosis of PTC. We also found that the expression of p-Akt was higher in patients without CLT. Further investigations are needed to elucidate the molecular mechanism underlying the regulation of PD-L1, PDK1 and p-Akt in PTC progression.

The present study has some limitations. Firstly, the sample size was small. Secondly, only PTC patients were included. Other histological types of thyroid carcinoma were not investigated. Thirdly, the molecular mechanisms of PD-L1, PDK1 and p-Akt in PTC development are not clear yet and their relationship with CLT needs to be clarified.

## Conclusions

This observational study evaluated the clinical significance of PD-L1, PDK1 and p-Akt in PTC. The results show that PD-L1, PDK1 and p-Akt were upregulated in PTC patients, and their expression levels were higher in patients without CLT. The high expression of PD-L1, PDK1 and p-Akt correlated with poor prognosis of PTC. This study provided clinical evidence for the potential use of PD-L1, PDK1 and p-Akt as novel potential biomarkers in PTC diagnosis.

### ORCID iDs

Hui Wang  <https://orcid.org/0000-0002-0045-8797>

Zhengdong Zhang  <https://orcid.org/0000-0002-1033-4763>

Zhe Yan  <https://orcid.org/0000-0002-4823-3327>

Shihong Ma  <https://orcid.org/0000-0002-5548-9777>

### References

1. Abdullah MI, Junit SM, Ng KL, Jayapalan JJ, Karikalan B, Hashim OH. Papillary thyroid cancer: Genetic alterations and molecular biomarker investigations. *Int J Med Sci.* 2019;16(3):450–460.
2. Liang J, Cai W, Feng D, et al. Genetic landscape of papillary thyroid carcinoma in the Chinese population: Somatic mutational profile of PTC in China. *J Pathol.* 2017;244(2):215–226.
3. Lim H, Devesa SS, Sosa JA, Check D, Kitahara CM. Trends in thyroid cancer incidence and mortality in the United States, 1974–2013. *JAMA.* 2017;317(13):1338–1348.
4. Lai X, Xia Y, Zhang B, et al. A meta-analysis of Hashimoto's thyroiditis and papillary thyroid carcinoma risk. *Oncotarget.* 2017;8(37):62414–62424.
5. Chen JP, Bai J, Yang K. Prognostic value of cervical lymph node metastasis ratio in Asian papillary thyroid carcinoma 5-year relapse-free survival: A meta-analysis. *Int J Clin Exp Med.* 2018;11(3):1401–1410.
6. Dincel O, Bayraktar C. Evaluation of platelet indices as a useful marker in papillary thyroid carcinoma. *Bratisl Lek Listy.* 2017;118(3):153–155.
7. Ji WS, Han K, Lee J, et al. Application of metabolomics in prediction of lymph node metastasis in papillary thyroid carcinoma. *PLoS One.* 2018;13(3):e0193883.
8. Haugen BR, Alexander EK, Bible KC, et al. 2015 American Thyroid Association Management Guidelines for Adult Patients with Thyroid Nodules and Differentiated Thyroid Cancer. *Thyroid.* 2016;26(1):1–133.
9. Arianpoor A, Asadi M, Amini E, Ziaemehr A, Ahmadi Simab S, Seyed Zakavi SR. Investigating the prevalence of risk factors of papillary thyroid carcinoma recurrence and disease-free survival after thyroidectomy and central neck dissection in Iranian patients. *Acta Chir Belg.* 2019;120(3):173–178.
10. Liu W, Cheng R, Su Y, et al. Risk factors of central lymph node metastasis of papillary thyroid carcinoma: A single-center retrospective analysis of 3273 cases. *Medicine (Baltimore).* 2017;96(43):e8365.
11. Vita R, Ieni A, Tuccari G, Benvenga S. The increasing prevalence of chronic lymphocytic thyroiditis in papillary microcarcinoma. *Rev Endocr Metab Disord.* 2018;19(4):301–309.
12. Pilli T, Toti P, Occhini R, et al. Chronic lymphocytic thyroiditis (CLT) has a positive prognostic value in papillary thyroid cancer (PTC) patients: The potential key role of Foxp3+ T lymphocytes. *J Endocrinol Invest.* 2018;41(6):703–709.
13. Resende de Paiva C, Grønhoj C, Feldt-Rasmussen U, von Buchwald C. Association between Hashimoto's thyroiditis and thyroid cancer in 64,628 patients. *Front Oncol.* 2017;7:53.
14. Trotter DEG, Meng X, McQuade P, et al. In vivo imaging of the programmed death ligand 1 by 18 F positron emission tomography. *J Nucl Med.* 2017;58(11):1852–1857.
15. Rehman JA, Han G, Carvajal-Hausdorf DE, et al. Quantitative and pathologist-read comparison of the heterogeneity of programmed death-ligand 1 (PD-L1) expression in non-small cell lung cancer. *Mod Pathol.* 2017;30(3):340–349.
16. Nomi T, Sho M, Akahori T, et al. Clinical significance and therapeutic potential of the programmed death-1 ligand/programmed death-1 pathway in human pancreatic cancer. *Clin Cancer Res.* 2007;13(7):2151–2157.
17. Lubin D, Baraban E, Lisby A, Jalali-Farahani S, Zhang P, Livolsi V. Papillary thyroid carcinoma emerging from Hashimoto thyroiditis demonstrates increased PD-L1 expression, which persists with metastasis. *Endocr Pathol.* 2018;29(4):317–323.
18. Wang JJ, Siu MK, Jiang, YX, et al. Aberrant upregulation of PDK1 in ovarian cancer cells impairs CD8+ T cell function and survival through elevation of PD-L1. *Oncoimmunology.* 2019;8(11):e1659092.
19. Boos LA, Schmitt A, Moch H, et al. MiRNAs are involved in tall cell morphology in papillary thyroid carcinoma. *Cancers (Basel).* 2019;11(6):885.
20. Tanaka T, Kutomi G, Kajiwara T, et al. Cancer-associated oxidoreductase ERO1- $\alpha$  promotes immune escape through upregulation of PD-L1 in human breast cancer. *Oncotarget.* 2017;8(15):24706–24718.
21. Jiao S, Xia W, Yamaguchi H, et al. PARP inhibitor upregulates PD-L1 expression and enhances cancer-associated immunosuppression. *Clin Cancer Res.* 2017;23(14):3711–3720.
22. Chintakuntlawar AV, Rumilla KM, Smith CY, et al. Expression of PD-1 and PD-L1 in anaplastic thyroid cancer patients treated with multimodal therapy: Results from a retrospective study. *J Clin Endocrinol Metab.* 2017;102(6):1943–1950.
23. Aghajani M, Roberts T, Yang T, et al. Elevated levels of soluble PD-L1 are associated with reduced recurrence in papillary thyroid cancer. *Endocr Connect.* 2019;8(7):1040–1051.
24. Bongiovanni M, Rebecchini C, Saglietti C, et al. Very low expression of PD-L1 in medullary thyroid carcinoma. *Endocr Relat Cancer.* 2017;24(6):L35–L38.

25. Zhang W, Su J, Xu H, et al. Dicumarol inhibits PDK1 and targets multiple malignant behaviors of ovarian cancer cells. *PLoS One*. 2017;12(6): e0179672.
26. Lian SX, Shao YB, Liu HB, et al. PDK1 induces JunB, EMT, cell migration and invasion in human gallbladder cancer. *Oncotarget*. 2015;6(30): 29076–29086.
27. Fujiwara S, Kawano Y, Yuki H, et al. PDK1 inhibition is a novel therapeutic target in multiple myeloma. *Br J Cancer*. 2013;108(1):170–178.
28. LeBoeuf B, Anderson B, Young M, Franco A, MacDonald L. Evaluating the effectiveness of MAPK, AKT, and mTOR inhibitors in reducing proliferation in cellular models of papillary and follicular thyroid cancer [abstract]. *Cancer Res*. 2018;78(13 Suppl):2887.
29. Xu J, Cai J, Jin X, et al. PIG3 plays an oncogenic role in papillary thyroid cancer by activating the PI3K/AKT/PTEN pathway. *Oncol Rep*. 2015;34(3):1424–1430.

# miR-21-5p protects hippocampal neurons of epileptic rats via inhibiting STAT3 expression

\*Xiaolei Zhang<sup>1,A,D,F</sup>, \*Xianfeng Li<sup>2,A,C,D,F</sup>, Bin Li<sup>3,B,F</sup>, Chengfeng Sun<sup>4,B,F</sup>, Peng Zhang<sup>5,E,F</sup>

<sup>1</sup> Department of Neurology, Jining Combine Traditional Chinese and Western Medicine Hospital, China

<sup>2</sup> Department of Neurosurgery, Penglai People's Hospital, Yantai, China

<sup>3</sup> Second Department of Neurology, The Second People's Hospital of Liaocheng, China

<sup>4</sup> Department of Traditional Chinese Medicine, Linyi County Hospital of Traditional Chinese Medicine, Dezhou, China

<sup>5</sup> Department of Neurology, Gaomi People's Hospital, Weifang, China

A – research concept and design; B – collection and/or assembly of data; C – data analysis and interpretation; D – writing the article; E – critical revision of the article; F – final approval of the article

Advances in Clinical and Experimental Medicine, ISSN 1899–5276 (print), ISSN 2451–2680 (online)

Adv Clin Exp Med. 2020;29(7):793–801

## Address for correspondence

Peng Zhang

E-mail: zhangpeng84kw@163.com

## Funding sources

None declared

## Conflict of interest

None declared

\* Xiaolei Zhang and Xianfeng Li contributed equally to this work.

Received on December 1, 2019

Reviewed on January 30, 2020

Accepted on May 1, 2020

Published online on August 3, 2020

## Cite as

Zhang X, Li X, Li B, Sun C, Zhang P. miR-21-5p protects hippocampal neurons of epileptic rats via inhibiting STAT3 expression. *Adv Clin Exp Med.* 2020;29(7):793–801. doi:10.17219/acem/121929

## DOI

10.17219/acem/121929

## Copyright

© 2020 by Wrocław Medical University

This is an article distributed under the terms of the Creative Commons Attribution 3.0 Unported (CC BY 3.0) (<https://creativecommons.org/licenses/by/3.0/>)

## Abstract

**Background.** Epilepsy is a common chronic neurological disorder worldwide.

**Objectives.** To investigate the effects of miR-21-5p and signal transducer and activator of transcription-3 (STAT3) expressions on the apoptosis of hippocampal neurons in epileptic rats.

**Material and methods.** We created a rat model of epilepsy and examined the relationship between miR-21-5p and STAT3 using a bioinformatics website and dual the luciferase reporter (DLR) assay. Real-time quantitative polymerase chain reaction (RT-qPCR) and western blot were used to detect the expression levels of miR-21-5p and STAT3 in hippocampal neurons as well as the protein expression levels of cleaved caspase-3, Bax and Bcl-2, which were related to apoptosis of hippocampal neuron. The apoptosis and survival of hippocampal neurons were detected using TUNEL and Nissl staining. Expressions of inflammatory factors interleukin (IL)-6 and tumor necrosis factor  $\alpha$  (TNF- $\alpha$ ) in serum were examined with enzyme-linked immunosorbent assay (ELISA).

**Results.** miR-21-5p can bind to STAT3. Compared with the miR-21-5p inhibitor negative control (NC) group, the expression levels of caspase-3 and Bax were higher and the expression level of Bcl-2 was lower in the miR-21-5p inhibitor group, whereas the caspase-3 and Bax levels were lower and Bcl-2 level was higher in the si-STAT3 (interfering STAT3 gene expression by transfecting small interfering RNA) group (all  $p < 0.05$ ). Treatment with miR-21-5p inhibitor can lead to significant loss and apoptosis of hippocampal neurons, while interfering with STAT3 expression can reduce the loss and apoptosis of the neurons (all  $p < 0.05$ ). Compared with the miR-21-5p inhibitor NC group, the level of IL-6 was lower in the si-STAT3 group and higher in the miR-21-5p inhibitor group (both  $p < 0.05$ ).

**Conclusions.** miR-21-5p can inhibit STAT3 expression and reduce apoptosis and loss of hippocampal neurons and IL-6 level, thereby achieving protective effects on hippocampal neurons of epileptic rats.

**Key words:** epilepsy, STAT3, hippocampal neuron, miR-21-5p, epileptic rats

## Introduction

Epilepsy is a common chronic neurological disorder worldwide. It is characterized by recurrent unpredictable seizures and often results from overstimulation of neurons or disorders of metabolism and the nervous system due to brain damage.<sup>1–3</sup> According to the statistics from the World Health Organization (WHO) on the worldwide prevalence rate of diseases in 2010, epilepsy ranked second among neurological diseases.<sup>4</sup> The lifespan of patients with epilepsy is much shorter than of healthy people.<sup>5</sup> Even though the treatment for epilepsy, including medication, neuromodulation, surgical management, and diet control, have been advancing in recent years, nearly 30% of the patients still do not respond to epilepsy medications and experience regular onset after treatment.<sup>6,7</sup> Therefore, it is necessary to develop new drugs or gene therapies for better treatment of this disease.

In recent years, the molecular mechanism of gene regulation by microRNA (miRNA) has been gaining attention. MicroRNA can bind to the 3'untranslated region (3'UTR) of its target gene to inhibit mRNA translation.<sup>8</sup> Some studies have found that miRNA serves a critical role in various biological process, including cell proliferation and growth, inflammation progression, neuronal progenitor synthesis, as well as growth and differentiation of immature neurons.<sup>9</sup> Of all the discovered miRNAs, about 70% are specifically expressed in the brain and take a critical part in the function and development of the nervous system.<sup>10</sup> miR-21-5p, a type of miRNA mainly expressed in brain and neurons, has an essential role in various brain diseases.<sup>11–13</sup> In the present study, we used bioinformatics website and dual luciferase reporter (DLR) assay to determine whether miR-21-5p can target signal transducer and activator of transcription-3 (*STAT3*). Other studies have demonstrated that *STAT3* overexpression can promote neuronal apoptosis, while inhibiting *STAT3* expression can reduce brain damage and neuroinflammation (including the neuroinflammation in patients with cerebral ischemia).<sup>14,15</sup> Therefore, in the present study, we hypothesized that miR-21-5p could protect the hippocampal neurons of epileptic rats through regulating *STAT3* signaling pathway.

## Material and methods

### Transfection of miRNA and model creation

Male Sprague Dawley rats at the age of 6–8 weeks (weight 300 g, purchased from SJA Laboratory Animal, Changsha, China) were kept in separate cages with a constant temperature and humidity. They were fed with a standard diet and sterile water for 1 week and randomized into the following 6 groups with 6 rats in each group: 1) normal group (blank control); 2) model group (epilepsy model); 3) miR-21-5p inhibitor negative control (NC) group (epilepsy model +

miR-21 inhibitor negative control); 4) miR-21-5p inhibitor group (epilepsy model + miR-21-5p inhibition); 5) si-*STAT3* group (epilepsy model + *STAT3* interference); and 6) miR-21-5p inhibitor + si-*STAT3* group (epilepsy model + both miR-21-5p inhibition and *STAT3* interference).

All animal experiments followed the institutional guide for the care and use of laboratory animals, and the study was approved by the Ethics Committee of our hospital.

Rat model of epilepsy was induced through an intraperitoneal injection of 127 mg/kg of lithium chloride, followed by 10 mg/kg of atropine methobromide 18–24 h later and another 30 mg/kg of pilocarpine 30 min later.<sup>16</sup> Rats in the normal group were intraperitoneally injected with an equal volume of normal saline. The behavior of the rats was observed. According to the Racine's scale, if there was no seizure or the seizure did not reach level IV, intraperitoneal injection of 10 mg/kg of pilocarpine would be administered every 15 min until status epilepticus (SE) occurred.<sup>17</sup> Since SE was defined as epilepsy reaching level IV–V and lasting for over 30 min, the SE model was considered to be successfully established if the rats survived and had an epilepsy level over IV. All the reagents used in the model creation were from Sigma-Aldrich (St. Louis, USA).

Lithium chloride-pilocarpine rat model is a common model used in the study on epilepsy. The mechanism of this model creation may be related to the reaction with the acetylcholine receptor. Pilocarpine is an agonist for muscarinic acetylcholine receptors (mAChRs), which can induce a persistent generalized tonic-clonic seizure. The mAChRs can couple with G protein, while G protein can pass the stimulus to phospholipase C, which then hydrolyzes phosphatidylinositol 4,5-bisphosphate (PIP<sub>2</sub>) to generate two-second messengers, inositol triphosphate (IP<sub>3</sub>) and diacylglycerol (DG). Excessive levels of IP<sub>3</sub> and DG can damage the neuron. Lithium chloride can inhibit the decomposition of IP<sub>3</sub>, thereby synergizing with pilocarpine.

The sequences of miR-21-5p inhibitor NC, miR-21-5p inhibitor and si-*STAT3* (interfering *STAT3* gene expression by transfecting small interfering RNA) were synthesized and provided by Ribobio (Guangzhou, China; 5 nmol in each tube). They were diluted with 50  $\mu$ L nuclease-free water to make 5 nmol/50  $\mu$ L solution and were divided into 5 tubes of 10  $\mu$ L each, followed by storage at  $-20^{\circ}\text{C}$ . Before use, the solution of the sequences was diluted to 1 nmol/50  $\mu$ L with 40  $\mu$ L pre-cooled normal saline. Five hours after successful modeling, the stereotaxic technique was conducted for administering miR-21-5p inhibitor NC, miR-21-5p inhibitor and si-*STAT3*.<sup>18</sup> The rats were fixed onto an animal brain solid positioner after anesthesia. After preoperative skin preparation and disinfection, the skin and muscle were separated to expose the skull bone. The anterior fontanelle was regarded as the origin of coordinate and the right cerebral ventricle was located for drug administration. A microsyringe was inserted for slow administration (1 nmol/50  $\mu$ L within 30 min) and

Table 1. RT-qPCR primer sequence

Gene	Forward primer (5'-3')	Reverse primer (5'-3')
mir-21-5p	GTC AATAGCTTATCAGACTGA	GTTGGCTCTGGTGCAGGGTCCGAGGTATTTCGCA
Bax	CTGAGCTGACCTTGGAGC	GACTCCAGCCACAAAGATG
Bcl-2	CTGGTGGACAACATCGCTCTG	GGTCTGCTGACCTCACTTGTG
Caspase-3	ATGGACAACAACGAAACCTC	TTAGTGATAAAAGTACAGTTCTT
U6	TGCGGGTGCTCGCTTCGGCAGC	CCAGTGCAGGGTCCGAGGT
GADPH	TGGTGAAGGTCCGGAGTGAAC	GGAAGATGGTATGGCCCTTTC

Bax – BCL2-associated X protein; Bcl-2 – B-cell lymphoma-2; GAPDH – glyceraldehyde-3-phosphate dehydrogenase.

then slowly removed, followed by suture and disinfection. Afterward, the rats were normally kept for 48 h.

Sodium pentobarbital (30 mg/kg, 2%) was intraperitoneally injected to the rats for deep anesthesia. The chest was opened and a 50 mL syringe was inserted into the left cardiac ventricle. The cardiac apex was cut for perfusion with about 150 mL of normal saline and the blood was removed. Next, a craniotomy was performed to take out the brain tissue, and the hippocampus was located and stored in a labeled freezing tube in liquid-nitrogen for RNA and protein analysis; meanwhile, some samples were fixed with 4% paraformaldehyde and kept at 4°C for subsequent experiments.

## Dual-luciferase reporter assay

We analyzed the pairing of miR-21-5p with *STAT3* using a bioinformatics website ([www.targetscan.org](http://www.targetscan.org)), followed by DLR assay to verify the targeting of miR-21-tp toward *STAT3*. The synthesized 3'UTR fragments of *STAT3*, *STAT3*-WT (wild) and *STAT3*-Mut (mutant) were inserted into the downstream of the firefly gene in pMIR-reporter DLR vector (Huayueyang, Beijing, China) to construct recombinant vectors pMIR-*STAT3*-WT and pMIR-*STAT3*-Mut, respectively. The correctly sequenced DLR plasmid *STAT3*-WT or *STAT3*-Mut were then transfected into HEK293T (the Cell Bank of the Chinese Academy of Sciences, Beijing, China) along with miR-21-5p mimic or miR-21-5p NC. The renilla luciferase (Promega, Madison, USA) was used as an internal control, and the cells were collected and lysed after 48 h of transfection. The firefly luciferase activity and renilla luciferase activity were measured with a DLR kit (E1910; Promega) according to the manufacturer's instruction. The value of firefly luciferase activity divided by renilla luciferase activity was calculated for statistical analysis.

## RT-qPCR

The hippocampus tissue was taken out from the liquid nitrogen and weighed. The tissue (0.1 g) was grounded to fine powder and 1 mL of Trizol was added (15596026; Invitrogen, Carlsbad, USA). The total RNA was extracted using the single-step method according to the manufacturer's instructions, and the concentration was measured with Eppendorf BioPhotometer (Takara, Kyoto, Japan)

before reverse transcription of the total RNAs (1 µg) into cDNAs. In accordance with the manufacturer's protocol, the samples were first treated with 5 Xg DNA eraser buffer, gDNA eraser and total RNA for 2 min at 42°C to erase DNA, and then reversely transcribed into cDNAs (37°C for 15 min and 85°C for 5 s). The real-time quantitative polymerase chain reaction (RT-qPCR) was conducted using SYBR® Premix Ex Taq™ kit (Tli RNaseH Plus; Takara) and a RT-qPCR device (ABI 7500; Thermo Fisher Scientific, Waltham, USA) with the running parameters were as follows: 95°C for 10 min (pre-denaturation) and 40 PCR cycles (pre-denaturation 95°C for 30 s, denaturation 95°C for 30 s, annealing for 20 s, and extension 72°C for 30 s). miR-21-5p was applied as an internal control for U6, and *GADPH* was applied as an internal control for other genes. The primers (GenePharma, Shanghai, China) are listed in Table 1.

## Western blot

The hippocampus tissue was taken from the liquid nitrogen and weighed. The tissue (0.1 g) was added into an EP tube containing RIPA lysis buffer and protease inhibitor. The homogenate was prepared using an electric pestle. After an ice-bath for 30 min, the samples were centrifuged in order to collect the supernatant, and the protein concentration was measured using a bicinchoninic acid (BCA) kit. Next, the protein samples (30 µg) were separated using SDS-PAGE and then transferred to a polyvinyl difluoride (PVDF) membrane (Merck Millipore, Burlington, USA). The membrane was blocked with 5% bovine serum albumin (BSA) for 90 min at room temperature, followed by discarding the blocking solution and washing in phosphate-buffered saline with Tween (PBST). Next, the membrane was incubated at 4°C overnight with the following antibodies: anti-*STAT3* mouse monoclonal antibody (1:1,000, 9139; Cell Signaling Technology, Leiden, the Netherlands), anti-cleaved caspase-3 rabbit polyclonal antibody (1:1,000, 9664, Cell Signaling Technology), anti-Bax rabbit monoclonal antibody (1:1,000, 14796; Cell Signaling Technology), anti Bcl-2 mouse monoclonal antibody (1:2,000, ab117115; Abcam, Cambridge, UK), and anti-GAPDH rabbit monoclonal antibody (1:10,000, ab181602; Abcam). The membrane was washed in TBST (PBS buffer containing 0.1% Tween-20) 3 times (10 min per wash) and incubated with horseradish

peroxidase (HRP)-conjugated goat anti-rabbit and goat anti-mouse antibody (1:10,000; Jackson ImmunoResearch, West Grove, USA) at room temperature for 1 h. Next, the samples were washed in TBST 3 times (10 min per wash) and then immersed in Pierce enhanced chemiluminescence (ECL) solution (Thermo Fischer Scientific) at room temperature for 1 min. Afterward, the solution was removed and the membrane was covered with plastic wrap and placed in the dark for X-ray film exposure and developing to capture the image. The grayscale of the protein bands was analyzed using ImageJ software (National Institutes of Health, Bethesda, USA) and the results in each experimental group were compared to the internal control for statistical analysis.

## TUNEL staining

The TUNEL staining was conducted using a test kit (MK1020; Boster, Pleasanton, USA). The hippocampus tissue was fixed with 4% paraformaldehyde and sectioned in 5- $\mu$ m thick slices after paraffin embedding. The samples were dried for 2 h at 60°C, followed by dewaxing and hydration with xylene and a gradient of alcohol (concentration from high to low). Subsequently, the samples were incubated with 3% hydrogen peroxide at room temperature for 10 min to remove endogenous peroxide and washed with distilled water 3 times. Proteinase K diluted with 0.01 M Tris-buffered saline (TBS) was then added to the sample and digested at 37°C for 10 min followed by 3 washes in 0.01 M TBS. Next, 20  $\mu$ L of labeling buffer was added to keep the section moist (1  $\mu$ L of terminal deoxynucleotidyl transferase (TdT) + 1  $\mu$ L of digoxigenin with deoxyuridine triphosphate (DIG-d-UTP) + 18  $\mu$ L of labeling buffer for each section). After mixing, the samples were placed in a humidified box for labeling for 2 h at 37°C and washed in 0.01 M TBS 3 times. The samples were then treated with blocking solution for 30 min at room temperature and with no wash, reacted with anti-digoxigenin biotinylated antibody (1:100, diluted with antibody diluent) at 37°C for 30 min and washed with TBS 3 times, followed by reaction with streptavidin conjugate (SABC) (1:100, diluted with antibody diluent) for 30 min at 37°C and 4 washes in TBS. The samples were then stained with 3,3'-diaminobenzidine (DAB), mildly counterstained with hematoxylin, and washed once in TBS and distilled water. Subsequently, the sections were dehydrated, cleared, sealed, and observed under a microscope. Samples taken from each rat had 3 sections and 6 fields were randomly picked in each section. The number of apoptotic cells was calculated using the averaging method. Cell death rate was counted as number of dead neuron/total cell count  $\times$  100 %.

## Nissl staining

The samples were fixed, embedded, dewaxed, and hydrated in the same way as described above. After rinsing with water, 0.1% of cresyl violet was added for staining

at room temperature for 10 min, and the excess liquid was washed away with running water. Dehydration was performed through a gradient of alcohol. The samples were then cleared in dimethylbenzene, mounted with neutral balsam, and observed under a microscope. Live cells were identified as having an intact shape and a purple-blue nucleus. Six fields were randomly picked from each section, and the live neuron and total cell were counted. Cell survival rate was counted as the number of live neuron/total cell count  $\times$  100%.

## ELISA

Blood (0.5 mL) was collected from the tail vein and the serum was separated. The levels of inflammatory factors, interleukin 6 (IL-6) and tumor necrosis factor  $\alpha$  (TNF- $\alpha$ ), were measured according to the instructions of the enzyme-linked immunosorbent assay (ELISA) kit (R&D Systems, Minneapolis, USA).

## Statistical analysis

The SPSS 21.0 v. software (IBM Corp., Armonk, USA) was used for statistical analysis. Measurement data are expressed as mean  $\pm$  standard deviation (SD); comparison between 2 groups was conducted with one-way analysis of variance (ANOVA) and Bonferroni post hoc test. P-value <0.05 was considered to indicate a statistically significant difference.

## Results

### miR-21-5p can target *STAT3*

The bioinformatics website TargetScan ([www.targetscan.org](http://www.targetscan.org)) predicted that miR-21-5p can target *STAT3* (Fig. 1A). The DLR assay was conducted and it was found that, compared with the miR-21-5p inhibitor NC group,

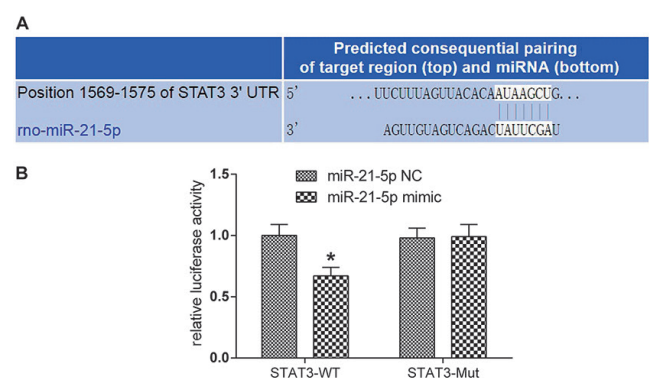


Fig. 1. miR-21-5p can target *STAT3*. A. The pairing of miR-21-5p and *STAT3* as predicted using TargetScan website. B. Dual luciferase reporter verified that miR-21-5p can target *STAT3*

\*p < 0.05 vs the miR-21-5p inhibitor NC group.

the luciferase activity in the group with co-transfection of miR-21-5p mimic and STAT3-WT was much lower ( $p < 0.05$ ), whereas the luciferase activity in the group with co-transfection of STAT3-Mut was similar (Fig. 1B), indicating that miR-21-5p can target *STAT3* and regulate its expression.

### Expressions of miR-21-5p and STAT3 in rats after transfection

The RT-qPCR was performed to measure the miR-21-5p expression level in each group (Fig. 2A). The results showed that, compared with the normal group, the expression level of miR-21-5p in the other groups was lower (all  $p < 0.05$ ). Moreover, the expression levels of miR-21-5p in the miR-21-5p inhibitor and miR-21-5p inhibitor + si-STAT3 groups were lower than those in the model and miR-21-5p inhibitor NC groups (all  $p < 0.05$ ). No intergroup differences were observed among the model, miR-21-5p inhibitor NC and si-STAT3 in this marker (all  $p > 0.05$ ). The si-STAT3 group had a higher level of miR-21-5p than the miR-21-5p inhibitor and miR-21-5p inhibitor + si-STAT3 groups (both  $p < 0.05$ ).

Western blot was performed to detect the protein level of *STAT3* in each group (Fig. 2B,C). The results showed that, compared with the normal group, the protein level of *STAT3* was higher in the other groups, except for the si-STAT3 group (all  $p < 0.05$ ). Compared with the model and miR-21-5p inhibitor NC groups, the protein expression level of *STAT3* was higher in the miR-21-5p inhibitor group and lower in the si-STAT3 group (both  $p < 0.05$ ). The si-STAT3 group had a lower level of *STAT3* than the miR-21-5p inhibitor and miR-21-5p inhibitor + si-STAT3 groups (both  $p < 0.05$ ). No intergroup differences were observed among the model, miR-21-5p inhibitor NC and miR-21-5p inhibitor + si-STAT3 groups in this marker (all  $p > 0.05$ ).

The results revealed a good transfection rate in each group and showed that suppressing miR-21-5p expression can promote the gene and protein expressions of *STAT3*, which further verified that miR-21-5p can target *STAT3* and negatively regulate its expression.

### Protein expressions levels of caspase-3, Bax and Bcl-2 in hippocampal neurons

Both RT-qPCR and western blot were performed to measure the expression levels of apoptosis-associated proteins, caspase-3, *Bax*, and *Bcl-2*, in hippocampus tissues (Fig. 3). The results displayed that, compared with the normal group, the other groups had higher expression levels of caspase-3 and *Bax* and a lower expression level of *Bcl-2* (all  $p < 0.05$ ). Compared with the model and miR-21-5p inhibitor NC groups, the miR-21-5p inhibitor group had higher expression levels of caspase-3 and *Bax* and a lower expression level of *Bcl-2*, whereas the si-STAT3 group had lower expression levels of caspase-3 and *Bax* and a higher expression level of *Bcl-2* (all  $p < 0.05$ ). Of the miR-21-5p inhibitor, miR-21-5p inhibitor + si-STAT3 and si-STAT3 groups, the si-STAT3 group had the lowest expression levels of caspase-3 and *Bax* and the highest level of *Bcl*, and the miR-21-5p inhibitor group had the highest expression levels of caspase-3 and *Bax* and the lowest level of *Bcl* expression (all  $p < 0.05$ ). The results demonstrated that apoptosis of hippocampal neurons can be promoted by inhibiting miR-21-5p expression and restrained by interfering with *STAT3* expression.

### Neuronal apoptosis in rat hippocampus

The TUNEL staining was conducted to detect the neuronal apoptosis in the CA1 region of rat hippocampus

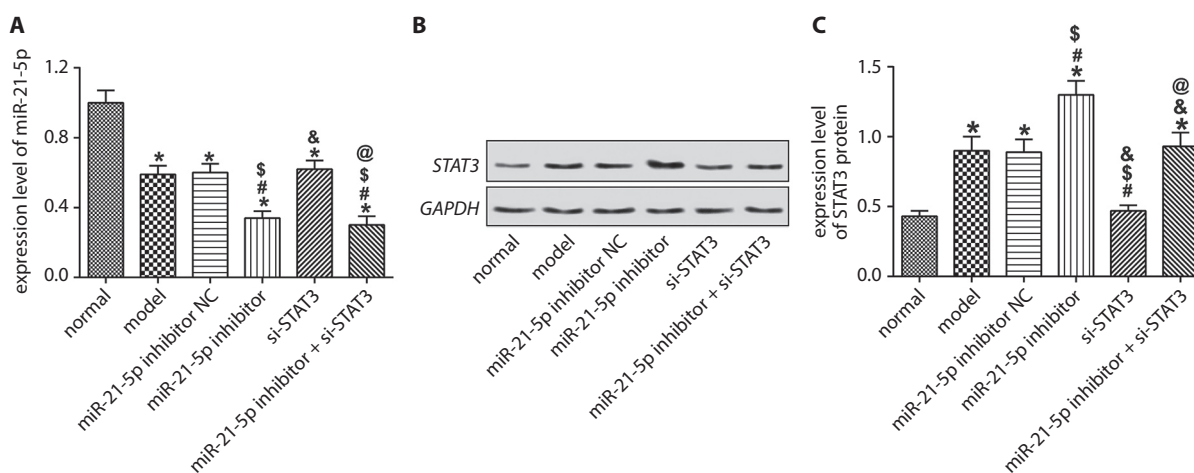
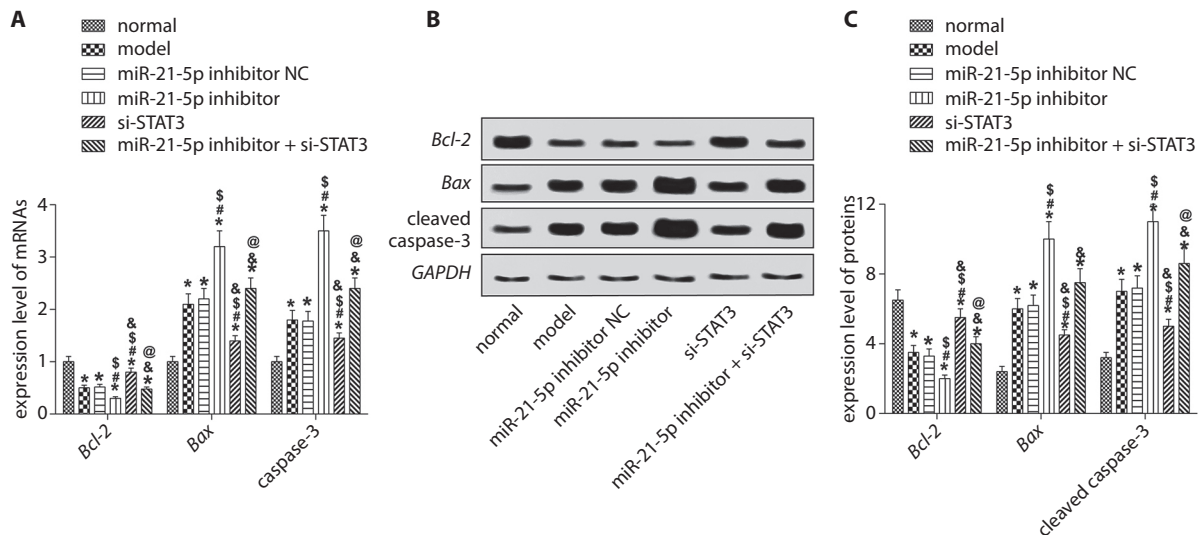


Fig. 2. Expressions of miR-21-5p and STAT3 in epileptic rats. A. miR-21-5p expression level measured using RT-qPCR. B and C. STAT3 expression level measured with western blot and its statistical graph

\* $p < 0.05$  vs the normal group; # $p < 0.05$  vs the model group; \$ $p < 0.05$  vs miR-21-5p inhibitor NC group; & $p < 0.05$  vs miR-21-5p inhibitor group; @ $p < 0.05$  vs the si-STAT3 group.



**Fig. 3.** Expressions of Bcl-2, Bax and caspase-3 in epileptic rats. A. Expression levels of the apoptosis-associated proteins measured with RT-qPCR. B and C. Expression levels of the proteins measured with western blot and its statistical graph

\* $p < 0.05$  vs the normal group; # $p < 0.05$  vs the model group; § $p < 0.05$  vs miR-21-5p inhibitor NC group; & $p < 0.05$  vs miR-21-5p inhibitor group; @ $p < 0.05$  vs the si-STAT3 group.

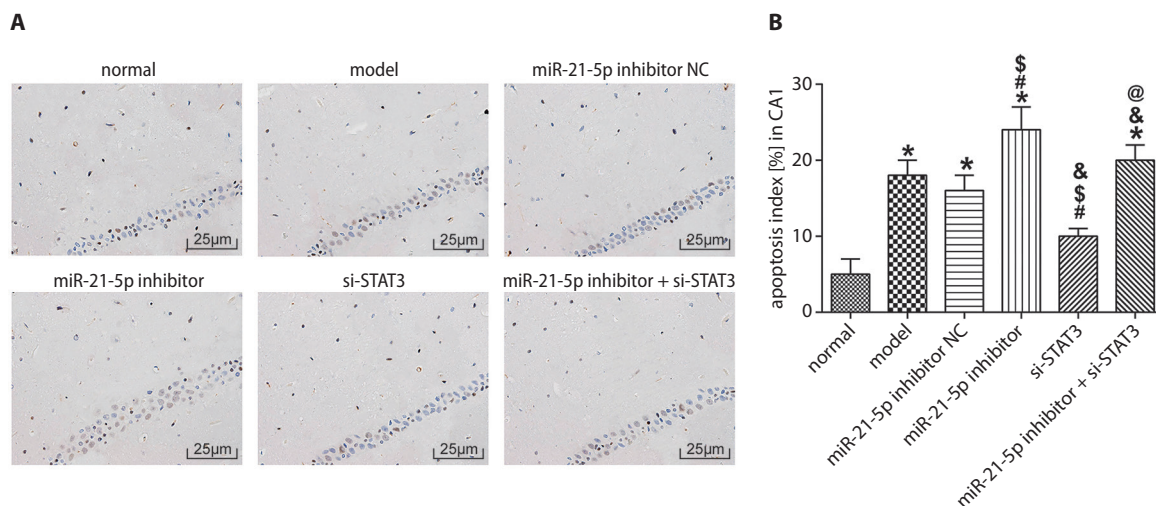


**Fig. 4.** Neuronal apoptosis in rat hippocampus. A. Neuronal apoptosis in rat hippocampus measured using TUNEL assay. B. Statistical graph of the neuronal apoptosis

\* $p < 0.05$  vs the normal group; # $p < 0.05$  vs the model group; § $p < 0.05$  vs miR-21-5p inhibitor NC group; & $p < 0.05$  vs miR-21-5p inhibitor group; @ $p < 0.05$  vs the si-STAT3 group.

(Fig. 4). The apoptotic cells had an irregular shape, pyknosis and a reduced size of cytoplasm. The results showed that, compared with the normal group, the number of apoptotic cells was higher in the model, miR-21-5p inhibitor NC, miR-21-5p inhibitor, and miR-21-5p inhibitor + si-STAT3 groups (all  $p < 0.05$ ). Compared with the model and miR-21-5p inhibitor NC groups, the number of apoptotic cells was higher in the miR-21-5p inhibitor group and lower in the si-STAT3 group (both  $p < 0.05$ ). Of the miR-21-5p inhibitor, si-STAT3 and miR-21-5p inhibitor + si-STAT3 groups, the number of apoptotic cells was highest in the miR-21-5p inhibitor group and lowest in the si-STAT3 group (all  $p < 0.05$ ).

## Loss and survival of hippocampal neurons

Nissl staining was performed to detect the loss and survival of hippocampal neurons in the CA1 region in epileptic rats (Fig. 5). Live neurons are those with an intact shape, clear structure, big nucleus, and a high level of Nissl bodies. The results showed that, compared with the normal group, the number of live neurons in the model, miR-21-5p inhibitor NC, miR-21-5p inhibitor, and miR-21-5p inhibitor + si-STAT3 groups was lower (all  $p < 0.05$ ). Compared with the model and miR-21-5p inhibitor NC groups, the number of live cells was lower in the miR-21-5p inhibitor

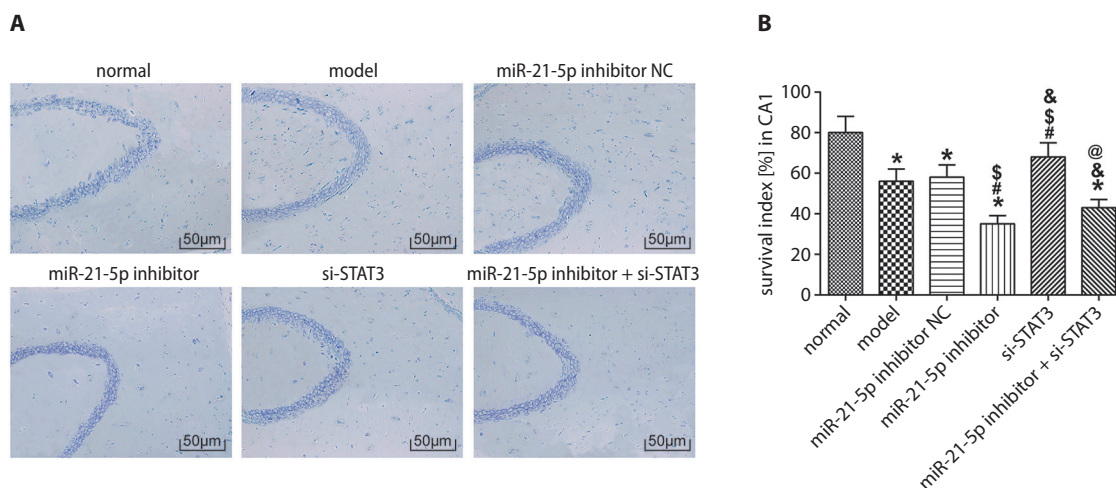


Fig. 5. Survival of hippocampal neurons. A. Survival of hippocampal neurons detected using Nissl staining. B. Statistical graph of the live neurons

\*p < 0.05 vs the normal group; #p < 0.05 vs the model group; \$p < 0.05 vs miR-21-5p inhibitor NC group; &p < 0.05 vs miR-21-5p inhibitor group; @p < 0.05 vs the si-STAT3 group.

group and higher in the si-STAT3 group (all p < 0.05). Of the miR-21-5p inhibitor, si-STAT3, and miR-21-5p inhibitor + si-STAT3 groups, the number of live cells was the lowest in the miR-21-5p inhibitor group and the highest in the si-STAT3 group (all p < 0.05).

### Expression levels of IL-6 and TNF-α in serum

The ELISA was performed to measure the expression levels of inflammatory factors IL-6 and TNF-α in each group (Fig. 6). The results showed that, compared with the normal group, the IL-6 levels in the other groups were much higher (all p < 0.05). No intergroup differences were observed among the model, miR-21-5p inhibitor NC and miR-21-5p

inhibitor + si-STAT3 groups. Compared with the model and miR-21-5p inhibitor NC groups, the expression level of IL-6 was higher in the miR-21-5p inhibitor group and lower in the si-STAT3 group (all p < 0.05). Of the miR-21-5p inhibitor, si-STAT3 and miR-21-5p inhibitor + si-STAT3 groups, the level of IL-6 was highest in the miR-21-5p inhibitor group and lowest in the si-STAT3 group (all p < 0.05). Compared with the normal group, the expression level of TNF-α in the other groups was higher (all p < 0.05). Moreover, the expression level of TNF-α was similar among the groups, except for the normal group. These findings showed that miR-21-5p can inhibit *STAT3* expression, thus decreasing the expression of IL-6, which suggests that the signal transduction of IL-6 in epileptic rats requires the participation of *STAT3*.

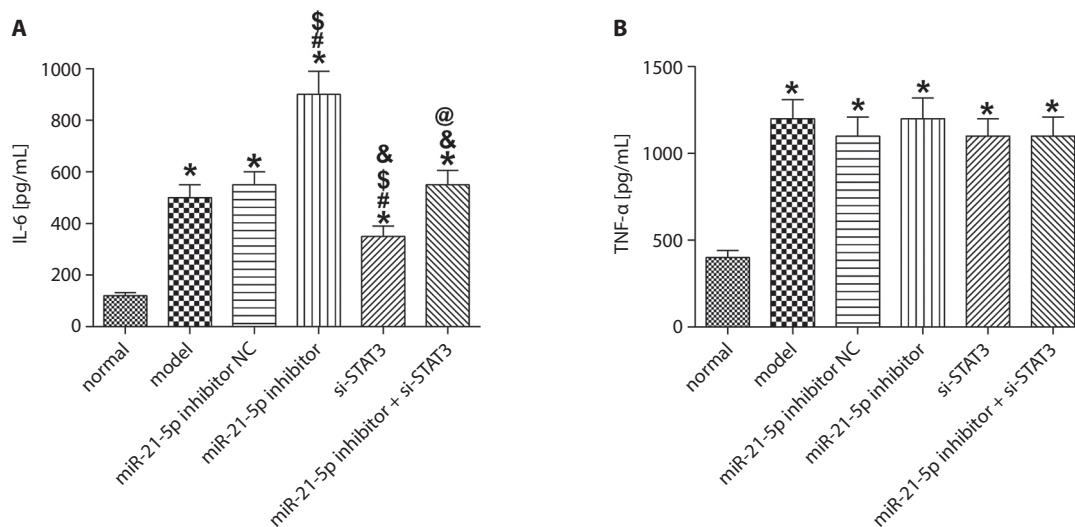


Fig. 6. A. Expression level of IL-6 measured with ELISA. B. Expression level of TNF-α measured with ELISA

\*p < 0.05 vs the normal group; #p < 0.05 vs the model group; \$p < 0.05 vs miR-21-5p inhibitor NC group; &p < 0.05 vs miR-21-5p inhibitor group; @p < 0.05 vs the si-STAT3 group.

## Discussion

Our results showed that in the hippocampus of epileptic rats, the expression level of miR-21-5p was low, while the level of *STAT3* was high. miR-21 can exert cerebral protective effects in various diseases, alleviate the secondary blood–brain barrier damage after traumatic brain injury in rats, inhibit the neuron death mediated by microglia after hypoxia and ischemia, and prevent hypoxia and low glucose-induced apoptosis of human neural stem cell through suppressing JNK and p38 MAPK signaling pathways.<sup>19–23</sup> The overexpression of *STAT3* gene can lead to neuroinflammation, induce schizophrenia, and is involved in the neurotoxicity caused by arsenic.<sup>24–26</sup> In our study, we found that miR-21-5p can target *STAT3* and regulate its expression after conducting an analysis using a website on bioinformatics and a DLR assay. Compared with the model and miR-21-5p inhibitor NC groups, the miR-21-5p inhibitor group had a higher *STAT3* protein expression level, whereas the si-*STAT3* group had a lower *STAT3* protein expression level, revealing that inhibiting miR-21-5p expression can promote the expression level of *STAT3*. This finding further demonstrates that miR-21-5p can target *STAT3* and negatively regulate its expression.

To further understand the mechanism of miR-21-5p in regulating the gene expression of *STAT3* in epilepsy, we measured the levels of apoptosis-associated proteins in rat hippocampus and found that the expression levels of caspase-3 and *Bax* were higher and expression level of *Bcl-2* was lower in the hippocampus of epileptic rats. Moreover, when the miR-21-5p expression was inhibited, the expression levels of caspase-3 and *Bax* were further increased and the expression level of *Bcl-2* was further reduced, whereas silencing *STAT3* reversed these changes. Some studies have demonstrated that miR-21 can suppress apoptosis of many types of cells, including neurons.<sup>22,27,28</sup> In a study by Shi et al., miR-21 was found to be able to inhibit the protein activity of caspase-3 and downregulate the ratio of *Bax* to *Bcl-2*.<sup>29</sup> Caspase-3 and *Bax* are known to be common apoptosis-associated factors and can promote cell apoptosis when highly expressed.<sup>30,31</sup> *Bcl-2* is an anti-apoptotic protein, which can regulate the permeability of the mitochondrial membrane; however, *Bax* can damage mitochondrial membrane, thereby promoting cell apoptosis.<sup>32</sup> Mao et al. have documented that the activation of *STAT3* can participate in the induction of neurotoxicity and promote neuronal apoptosis.<sup>25</sup> Based on these findings and our study results, we concluded that miR-21-5p can reduce the expression of *STAT3*, thereby inhibiting the neuronal apoptosis in the hippocampus.

Some studies have revealed that neuron activity in the hippocampus can be reduced by a low expression of miR-21-5p and increased by silencing *STAT3*. Our results showed that in the rat model of epilepsy, the levels of IL-6 and TNF- $\alpha$  rose significantly. Both IL-6 and TNF- $\alpha$  are common inflammatory factors, serving critical roles

in the development of many diseases.<sup>33,34</sup> In our study, IL-6 level was increased by silencing miR-21-5p, while TNF- $\alpha$  level remained unchanged after silencing miR-21-5p or inhibiting *STAT3* expression. These results showed that miR-21-5p can inhibit *STAT3* expression, thus lowering the expression level of IL-6, which indicated that the signal transduction of IL-6 in epileptic rats requires the participation of *STAT3*.

## Conclusions

miR-21-5p can target *STAT3* and negatively regulate its expression, increase the neuronal activity in the hippocampus and inhibit the expression of apoptosis-related factors, thereby suppressing neuronal apoptosis. Meanwhile, miR-21-5p can alleviate neuroinflammation in epileptic rats by reducing the inflammatory factor IL-6 in serum. The understanding of this miRNA may provide some new insights into the treatment of epilepsy. However, the present study only analyzed the mechanism of miR-21-5p in regulating *STAT3* and did not investigate the signaling pathways or other molecules that were involved. Therefore, more studies need to be conducted in the future to provide a strong basis for the clinical application of miR-21-5p.

### ORCID iDs

Xiaolei Zhang  <https://orcid.org/0000-0001-5075-0780>

Xianfeng Li  <https://orcid.org/0000-0002-3364-4051>

Bin Li  <https://orcid.org/0000-0002-0461-7759>

Chengfeng Sun  <https://orcid.org/0000-0001-6540-2164>

Peng Zhang  <https://orcid.org/0000-0003-1937-6860>

### References

1. Vezzani A, Fujinami RS, White HS, et al. Infections, inflammation and epilepsy. *Acta Neuropathol.* 2016;131(2):211–234.
2. Herzberg JL, Fenwick PB. The aetiology of aggression in temporal-lobe epilepsy. *Br J Psychiatry.* 1988;153:50–55.
3. Orsini A, Zara F, Striano P. Recent advances in epilepsy genetics. *Neurosci Lett.* 2018;667:4–9.
4. Zack M, Kobau R. Letter re: Prevalence and incidence of epilepsy: A systematic review and meta-analysis of international studies. *Neurology.* 2017;89(6):641.
5. Devinsky O, Hesdorffer DC, Thurman DJ, Lhatoo S, Richerson G. Sudden unexpected death in epilepsy: Epidemiology, mechanisms, and prevention. *Neurology.* 2016;15(10):1075–1088.
6. Jacobs J, Staba R, Asano E, et al. High-frequency oscillations (HFOs) in clinical epilepsy. *Prog Neurobiol.* 2012;98(3):302–315.
7. O'Connell BK, Gloss D, Devinsky O. Cannabinoids in treatment-resistant epilepsy: A review. *Epilepsy Behav.* 2017;70(Pt B):341–348.
8. Shioya M, Obayashi S, Tabunoki H, et al. Aberrant microRNA expression in the brains of neurodegenerative diseases: miR-29a decreased in Alzheimer disease brains targets neuron navigator 3. *Neuropathol Appl Neurobiol.* 2010;36(4):320–330.
9. Dong RF, Zhang B, Tai LW, Liu HM, Shi FK, Liu NN. The neuroprotective role of miR-124-3p in a 6-hydroxydopamine-induced cell model of Parkinson's disease via the regulation of ANAX5. *J Cell Biochem.* 2018;119(1):269–277.
10. Sun ZZ, Lv ZY, Tian WJ, Yang Y. MicroRNA-132 protects hippocampal neurons against oxygen-glucose deprivation-induced apoptosis. *Int J Immunopathol Pharmacol.* 2017;30(3):253–263.
11. Ge X, Huang S, Gao H, et al. miR-21-5p alleviates leakage of injured brain microvascular endothelial barrier in vitro through suppressing inflammation and apoptosis. *Brain Res.* 2016;1650:31–40.

12. Yao X, Wang Y, Zhang D. microRNA-21 confers neuroprotection against cerebral ischemia-reperfusion injury and alleviates blood–brain barrier disruption in rats via the MAPK signaling pathway. *J Mol Neurosci*. 2018;65(1):43–53.
13. Buller B, Liu X, Wang X, et al. MicroRNA-21 protects neurons from ischemic death. *FEBS J*. 2010;277(20):4299–4307.
14. Wan J, Fu AK, Ip FC, et al. Tyk2/STAT3 signaling mediates beta-amyloid-induced neuronal cell death: Implications in Alzheimer's disease. *J Neurosci*. 2010;30(20):6873–6881.
15. Hu GQ, Du X, Li YJ, Gao XQ, Chen BQ, Yu L. Inhibition of cerebral ischemia/reperfusion injury-induced apoptosis: Nicotiflorin and JAK2/STAT3 pathway. *Neural Regen Res*. 2017;12(1):96–102.
16. Curia G, Longo D, Biagini G, Jones RS, Avoli M. The pilocarpine model of temporal lobe epilepsy. *J Neurosci Methods*. 2008;172(2–4):143–157.
17. Racine RJ. Modification of seizure activity by electrical stimulation. I. After-discharge threshold. *Electroencephalogr Clin Neurophysiol*. 1972;32(3):269–279.
18. Aronica E, Fluiter K, Iyer A, et al. Expression pattern of miR-146a, an inflammation-associated microRNA, in experimental and human temporal lobe epilepsy. *Eur J Neurosci*. 2010;31(6):1100–1107.
19. Peng J, Omran A, Ashhab MU, et al. Expression patterns of miR-124, miR-134, miR-132, and miR-21 in an immature rat model and children with mesial temporal lobe epilepsy. *J Mol Neurosci*. 2013;50(2):291–297.
20. Zhang H, Wang Y, Lv Q, Gao J, Hu L, He Z. MicroRNA-21 overexpression promotes the neuroprotective efficacy of mesenchymal stem cells for treatment of intracerebral hemorrhage. *Front Neurol*. 2018;9:931.
21. Ge X, Han Z, Chen F, et al. MiR-21 alleviates secondary blood–brain barrier damage after traumatic brain injury in rats. *Brain Res*. 2015;1603:150–157.
22. Zhang L, Dong LY, Li YJ, Hong Z, Wei WS. miR-21 represses FasL in microglia and protects against microglia-mediated neuronal cell death following hypoxia/ischemia. *Glia*. 2012;60:1888–1895.
23. Chen R, Tai Y, Zhang Y, et al. MicroRNA-21 attenuates oxygen and glucose deprivation induced apoptotic death in human neural stem cells with inhibition of JNK and p38 MAPK signaling. *Neurosci Lett*. 2019;690:11–16.
24. Wang LC, Liao LX, Zhao MB, Dong X, Zeng KW, Tu PF. Protosapannin A exerts anti-neuroinflammatory effect by inhibiting JAK2-STAT3 pathway in lipopolysaccharide-induced BV2 microglia. *Chin J Nat Med*. 2017;15(9):674–679.
25. Mao J, Yang J, Zhang Y, et al. Arsenic trioxide mediates HAPI microglia inflammatory response and subsequent neuron apoptosis through p38/JNK MAPK/STAT3 pathway. *Toxicol Appl Pharmacol*. 2016;303:79–89.
26. Ma X, Zhou Y, Chai Y, Wang X, Huang X. STAT3 controls maturation and terminal differentiation in mouse hippocampal neurons. *J Mol Neurosci*. 2017;61(1):88–95.
27. Han Z, Chen F, Ge X, Tan J, Lei P, Zhang J. miR-21 alleviated apoptosis of cortical neurons through promoting PTEN-Akt signaling pathway in vitro after experimental traumatic brain injury. *Brain Res*. 2014;1582:12–20.
28. Zhou S, Zhang S, Wang Y, et al. MiR-21 and miR-222 inhibit apoptosis of adult dorsal root ganglion neurons by repressing TIMP3 following sciatic nerve injury. *Neurosci Lett*. 2015;586:43–49.
29. Shi L, Chen J, Yang J, Pan T, Zhang S, Wang Z. MiR-21 protected human glioblastoma U87MG cells from chemotherapeutic drug temozolomide induced apoptosis by decreasing Bax/Bcl-2 ratio and caspase-3 activity. *Brain Res*. 2010;1352:255–264.
30. Szobi A, Rajtik T, Carnicka S, Ravingerova T, Adameova A. Mitigation of postischemic cardiac contractile dysfunction by CaMKII inhibition: Effects on programmed necrotic and apoptotic cell death. *Mol Cell Biochem*. 2014;388(1–2):269–276.
31. Fan Y, Lu H, An L, et al. Effect of active fraction of *Eriocaulon sieboldianum* on human leukemia K562 cells via proliferation inhibition, cell cycle arrest and apoptosis induction. *Environ Toxicol Pharmacol*. 2016;43:13–20.
32. Lv J, Liang Y, Tu Y, Chen J, Xie Y. Hypoxic preconditioning reduces propofol-induced neuroapoptosis via regulation of Bcl-2 and Bax and downregulation of activated caspase-3 in the hippocampus of neonatal rats. *Neurol Res*. 2018;40(9):767–773.
33. Zhang C, Chen Z, Meng X, Li M, Zhang L, Huang A. The involvement and possible mechanism of pro-inflammatory tumor necrosis factor alpha (TNF-alpha) in thoracic ossification of the ligamentum flavum. *PLoS One*. 2017;12(6):e0178986.
34. Cosenza S, Ruiz M, Maumus M, Jorgensen C, Noel D. Pathogenic or therapeutic extracellular vesicles in rheumatic diseases: Role of mesenchymal stem cell-derived vesicles. *Int J Mol Sci*. 2017;18(4):889.



# Effects of miR-124-3p regulation of the p38MAPK signaling pathway via MEKK3 on apoptosis and proliferation of macrophages in mice with coronary atherosclerosis

Chuannan Zhai<sup>1,2,A-E</sup>, Hongliang Cong<sup>1,2,E,F</sup>, Kai Hou<sup>1,2,A-C</sup>, Yuecheng Hu<sup>2,A,B</sup>,  
Jingxia Zhang<sup>2,A,B</sup>, Yingyi Zhang<sup>2,A,B</sup>, Ying Zhang<sup>2,A,B</sup>, Hong Zhang<sup>2,A,B</sup>

<sup>1</sup> School of Medicine, Nankai University, Tianjin, China

<sup>2</sup> Department of Cardiology, Tianjin Chest Hospital, China

A – research concept and design; B – collection and/or assembly of data; C – data analysis and interpretation;  
D – writing the article; E – critical revision of the article; F – final approval of the article

Advances in Clinical and Experimental Medicine, ISSN 1899–5276 (print), ISSN 2451–2680 (online)

*Adv Clin Exp Med.* 2020;29(7):803–812

## Address for correspondence

Hongliang Cong  
E-mail: hl\_cong56uj@163.com

## Funding sources

None declared

## Conflict of interest

None declared

Received on January 12, 2020

Reviewed on February 19, 2020

Accepted on May 1, 2020

Published online on August 4, 2020

## Cite as

Zhai C, Cong H, Hou K, et al. Effects of miR-124-3p regulation of the p38MAPK signaling pathway via MEKK3 on apoptosis and proliferation of macrophages in mice with coronary atherosclerosis. *Adv Clin Exp Med.* 2020;29(7):803–812. doi:10.17219/acem/121926

## DOI

10.17219/acem/121926

## Copyright

© 2020 by Wrocław Medical University

This is an article distributed under the terms of the Creative Commons Attribution 3.0 Unported (CC BY 3.0) (<https://creativecommons.org/licenses/by/3.0/>)

## Abstract

**Background.** Atherosclerosis (AS) is the main cause of myocardial infarction and stroke. Macrophage apoptosis in the early stages can attenuate lesions, while in the late stage it is associated with AS plaque rupture.

**Objectives.** To explore the effects of miR-124-3p regulation of the p38MAPK signaling pathway via the *MEKK3* gene on the apoptosis and proliferation of macrophages in mice with coronary AS.

**Material and methods.** Fifty male apolipoprotein E (ApoE)  $-/-$  mice were equally assigned to a normal group and a coronary AS group. In the AS group, the mice were given a high-fat diet to establish a coronary AS model. The macrophages of the mice were isolated for culture and divided into 7 groups: normal, negative control (NC), control, miR-124-3p mimic, miR-124-3p inhibitor, si-MEKK3, and miR-124-3p inhibitor+si-MEKK3.

**Results.** Compared with the normal group, the AS group had lower expression levels of miR-124-3p and higher expression levels of MEKK3 and p-p38MAPK in the coronary artery tissue and peritoneal macrophages (all  $p < 0.050$ ). We found that miR-124-3p could negatively regulate MEKK3 expression. Compared with the control group, the miR-124-3p mimic group and si-MEKK3 group had greater cell apoptosis rates and Bax levels, weaker cell proliferation and invasion abilities, slower cell cycle progression, and lower PCNA and Bcl-2 levels (all  $p < 0.050$ ). This trend was also displayed in the miR-124-3p inhibitor+si-MEKK3 group when compared with the miR-124-3p inhibitor group, and in the si-MEKK3 group when compared with the miR-124-3p inhibitor+si-MEKK3 group (all  $p < 0.050$ ).

**Conclusions.** miR-124-3p overexpression can downregulate MEKK3 expression and inhibit the expression of the p38MAPK signaling pathway, thereby inhibiting macrophage proliferation and promoting macrophage apoptosis in mice with coronary AS.

**Key words:** MiR-124-3p, macrophage, coronary atherosclerosis

## Introduction

Atherosclerosis (AS) is the main cause of myocardial infarction and stroke.<sup>1</sup> It is believed that both macrophages and monocytes play critical roles in AS. The occurrence of AS is associated with unstable plaque in which macrophages are among the main components.<sup>2</sup> Recent studies have demonstrated that macrophages in the arterial plaque can proliferate, while differences exist in macrophage apoptosis between the early and late stages of AS.<sup>3</sup> Macrophage apoptosis in early stages can attenuate lesions, whereas apoptosis in the late stage is associated with AS plaque rupture.<sup>4,5</sup>

The mammalian genome contains hundreds of microRNAs (miRNAs), a type of non-coding RNA molecule of about 18–25 nucleotides regulating the expression of 30% of human genes.<sup>6</sup> MiRNAs can inhibit the transcription and translation of target proteins, thereby affecting cell apoptosis, development and growth.<sup>7</sup> Some studies have found that miRNA plays an essential part in the pathogenesis of AS through regulating multi-targets or signaling pathways.<sup>8,9</sup> Recent studies have documented that homocysteine can downregulate the expression of miR-124-3p in AS, and its mechanism may be related to a change in hypermethylation in the promoter region of miR-124-3p.<sup>10</sup> However, the role of miR-124-3p in AS is yet to be clarified.

As a mitogen-activated protein kinase (MAPK), MEKK3 has a vital role in cardiovascular development and can induce nuclear factor kappa-B activation. All eukaryotes have various MAPK pathways that control gene expression and cellular physiological activities.<sup>11</sup> Normal MAPKs include extracellular signal-regulated kinase (ERK) 1/2, JNK 1/2/3, p38 ( $\alpha$ ,  $\beta$ ,  $\gamma$ ,  $\delta$ ), and big MAPK (ERK5).<sup>12</sup> So far, there has been little research on the role of MEKK3 in AS. The p38MAPK pathway, a member of the MAPK superfamily, is a key pathway in regulating cell proliferation and death, and can participate in many physiological processes. Meanwhile, the correlation between p38MAPK and MEKK3, another MAPK, cannot be neglected, as MEKK3 and MEKK4 are upstream regulators of p38 in many cells.<sup>13</sup> Previous studies have documented that the MAPK pathway participates in cardiomegaly.<sup>14,15</sup> However, the role of the MAPK pathway in the apoptosis and proliferation of macrophages in mice with coronary AS is unclear. The Targetscan bioinformatics website ([www.targetscan.org](http://www.targetscan.org)) predicted that miR-124-3p can target MEKK3, and that miR-124-3p expression is downregulated in AS. Therefore, we infer that miR-124-3p may suppress the p38MAPK signaling pathway through downregulating MEKK3 expression, thereby inhibiting coronary AS and promoting the apoptosis of mouse macrophages.

In the present study, we established the AS model in apolipoprotein E (ApoE) knockout (ApoE  $-/-$ ) mice and cultured mouse macrophages, which were then transfected with a miR-124-3p mimic, a miR-124-3p inhibitor,

si-MEKK3, and miR-124-3p inhibitor+si-MEKK3, respectively. RAW2647 cell apoptosis, cycle, proliferation, and invasion were examined in each group to investigate whether miR-124-3p can suppress phosphorylation of the p38MAPK signaling pathway by downregulating MEKK3 expression and finally affect the apoptosis and proliferation of macrophages in mice with AS.

## Material and methods

### Animal subjects

The study was approved by the Ethics Committee of Nankai University.

Fifty male ApoE  $-/-$  mice at 5 weeks of age were included as subjects and were assigned to a normal group and a coronary AS group (AS group),  $n = 25$  mice each. In the AS group, the mice were given a high-fat diet including 1% cholesterol and 15% lard to establish a coronary AS model<sup>16</sup>; the mice in the normal group were given a normal diet. The feeding lasted 4 weeks and all the mice had access to water ad libitum. After 3 weeks, the coronary artery tissue from the AS and normal mice were collected for examination.

The mice were sacrificed and 3 mL of phosphate-buffered saline (PBS) was injected into the abdominal cavities. A gentle abdominal massage was applied to obtain the buffer from the abdomen. These steps were repeated 3 times. Afterward, the buffer was centrifuged ( $300 \times g$  for 15 min), the supernatant was removed and the peritoneal macrophages in the precipitation were harvested. The cells were cultured in RPMI 1640 (Gibco, Thermo Fisher Scientific, Waltham, USA) which contained 10% fetal bovine serum (FBS), 50 U/mL of penicillin and 100  $\mu\text{g}/\text{mL}$  of streptomycin (all from Gibco) at 37°C in an atmosphere of 5% CO<sub>2</sub> (incubator model: Thermo3111; Jinan Beisheng Medical Instruments Co. Ltd, Jinan, China). The medium was renewed after 2 days, and the cells were sub-cultured every 3–4 days. The cells in good condition and at the logarithmic phase were selected for transfection.

### Cell grouping and transfection

The macrophages at the logarithmic phase from the AS mice were harvested and planted in a six-well culture plate ( $1 \times 10^5$ /well). Serum-free RPMI 1640 medium without penicillin-streptomycin was used 1 day before transfection. The cells were assigned to 6 groups: the control group (macrophages from the AS mice), the negative control (NC) group (macrophages from the AS mice transfected with NC plasmid), the miR-124-3p mimic group (macrophage from the AS mice transfected with 4  $\mu\text{g}$  miR-124-3p mimic plasmid), the miR-124-3p inhibitor group (macrophages from the AS mice transfected with 4  $\mu\text{g}$  miR-124-3p inhibitor plasmid), the si-MEKK3 group (macrophages from

NC:	5'-AGCTTTGCGGGAGTCAACCCAGCTTTTTTCAAGAGAAAAGCTGGGTTGACTCCCGCACCGC-3';
miRNA-124 mimic:	5'-CCGUAAGUGGCGCACGGAAU-3';
miR-124 inhibitor:	5'-GGCAUUCACCGCGUGCCUUA-3';
siRNA:	5'-GGAGAGACGAAUUAUAGCATT-3', 5'-UGCUAUAAUUCGUCUCUCC-3'.

the AS mice transfected with 4 µg of si-MEKK3 plasmid), and miR-124-3p inhibitor+si-MEKK3 group (macrophages from the AS mice co-transfected with 2 µg miR-124-3p inhibitor plasmid and 2 µg si-MEKK3 plasmid). The cells from the normal non-AS mice were cultured in a routine way without any other treatment.

The vectors used were constructed by Tianjin Saier Biotechnology Inc. (Tianjin, China) (see above).

Transfection was performed with Lipofectamine 2000 transfection reagent (Invitrogen, Carlsbad, USA) in accordance with the manufacturer's protocol. After 6 h of transfection, RPMI 1640 with 10% FBS (Gibco) was used as the medium. The cells were harvested for subsequent experiments 48 h after transfection.

## Dual luciferase reporter assay

The miR-124-3p binding site on MEKK3 was first analyzed on the [www.targetscan.org](http://www.targetscan.org) bioinformatics website, followed by a dual luciferase reporter test to validate this relationship. MEKK3 dual luciferase reporter gene vectors with and without mutant miR-124-3p binding sites were constructed and named MEKK3mut and MEKK3wt, respectively. These 2 reporter plasmids were co-transfected with the NC mimic or miR-124-3p mimic into HEK 293T cells. Renilla luciferase was used as a control. After 24 h of transfection, we performed a dual luciferase reporter assay. Cells from each group were lysed and then centrifuged (4800 × g for 1 min), and the supernatant was collected. A commercial dual luciferase reporter assay kit (Promega Biotech Co. Ltd., Beijing, China) was used in accordance with the manufacturer's instruction for measuring the activity of luciferase. The lysed cells were pipetted into Eppendorf tubes and 100 µL of firefly luciferase solution was added to each 10 µL sample. The activity of firefly luciferase was then measured, followed by the addition of 100 µL of renilla luciferase solution to detect the activity of renilla luciferase. The formula is as follows: relative luciferase activity = firefly luciferase activity/renilla luciferase activity.<sup>8</sup>

## qRT-PCR

After 48 h of transfection, cells were harvested from each group. Total RNAs were extracted using Trizol (16096020 from Thermo Fisher Scientific; and B1802 from HaiGene Bio, Quezon City, Philippines) followed by reverse transcription into cDNAs using TaqMan MicroRNA Assays Reverse Transcription Primer (Thermo Fisher Scientific). Next, SYBR<sup>®</sup> Premix ExTaq<sup>™</sup> II kit (Xingzhi Biotech,

Table 1. qRT-PCR primer sequence

Gene	Primer	Sequence
<i>miR-124-3p</i>	forward	5'-GCGAGGATCTGTGAATGCCAAA-3'
	reverse	5'-AGGGGCTGCTTGAGTTGTAGTA-3'
<i>MEKK3</i>	forward	5'-TGTACCTGAGCGACAACAGC-3'
	reverse	5'-CACTGCTGAGGGGATCTAGC-3'
<i>p38MAPK</i>	forward	5'-CCCGAACGATACCAGAACC-3'
	reverse	5'-GCGTGAATGATGGACTGAAA-3'
<i>PCNA</i>	forward	5'-TCACGCCTGTGGTGGTTAC-3'
	reverse	5'-GGTCGGCTTCTGAGTTTCC-3'
<i>Bcl-2</i>	forward	5'-AGTACCTGAACCGGCATCTG-3'
	reverse	5'-GCTGAGCAGGGTCTTCAGAG-3'
<i>Bax</i>	forward	5'-CGAGCTGATCAGAACCATCA-3'
	reverse	5'-GGTCCCGAAGTAGGAGAGGA-3'
<i>U6</i>	forward	5'-GCTTCGGCAGCACATATACTAAAT-3'
	reverse	5'-GCACTCCCGCCACAAAGATG-3'
<i>GAPDH</i>	forward	5'-GGGAAATTCACCGGCACAGT-3'
	reverse	5'-AGATGGTATGGGCTTCCC-3'

MAPK – mitogen-activated protein kinase; GAPDH – glyceraldehyde 3-phosphate dehydrogenase.

Guangzhou, China) was used for quantitative real-time polymerase chain reaction (qRT-PCR). Reagents were added in the following order: SYBR<sup>®</sup> Premix ExTaq<sup>™</sup> II (2×, 25 µL), forward primer (2 µL), reverse primer (2 µL), ROX Reference Dye (50×, 1 µL), DNA template (4 µL), and double distilled H<sub>2</sub>O (16 µL). An ABI Prism<sup>®</sup> 7300 fluorescence quantitative PCR instrument (Shanghai Kunke Instrument & Equipment Co., Shanghai, China) was used to conduct qRT-PCR with the following running parameters: 95°C for 10 min (pre-denaturation), 32 cycles of 95°C for 15 s (denaturation) and 60°C for 30 s (annealing) before extension at 72°C for 1 min.  $\Delta Ct = Ct_{\text{target gene}} - Ct_{\text{GAPDH}}$ ;  $\Delta\Delta Ct = \Delta Ct_{\text{study group}} - \Delta Ct_{\text{control group}}$ . U6 and GAPDH were the internal controls for *miR-124-3p* and other genes, respectively. The relative gene expression of the target gene was calculated using the  $2^{-\Delta\Delta Ct}$  method. The primers are listed in Table 1.

## Western blot

After 48 h of transfection and culture, the cells were washed 3 times in pre-cooled PBS. The total protein was extracted from the cells using RIPA lysis buffer (R0010; Solarbio Science & Technology Co. Ltd., Beijing, China) containing phenylmethylsulfonyl fluoride (PMSF). The protein concentration was measured with a BCA kit (Thermo Fisher Scientific), and the deionized water was used for zeroing.

The sample was then mixed with sample loading buffer and placed in a metal bath at 100°C for 10 min. Afterward, a 50 µg protein sample was loaded for 3 h of electrophoresis at 70 V constant voltage. The samples were then transferred to polyvinylidene difluoride (PVDF) membrane (ISEQ00010; Millipore Sigma, St. Louis, USA) using wet transfer at a constant current of 150 mA. Subsequently, the membrane was blocked in skim milk (5%) in TBST for 2 h at 4°C before the milk was discarded. The samples were washed in tris-buffered saline with Tween 20 (TBST) followed by the addition of polyclonal antibodies of rabbit anti-human MEKK3 (ab26321, 1:5000), anti-p-p38MAPK (ab31828, 1:1000), anti-p38MAPK (ab31828, 1:5000), anti-PCNA (ab92552, 1:5000), anti-Bax (ab8805, 1:1000), anti-Bcl-2 (ab32124, 1:1000), and anti-GAPDH (ab8226, 1:2000, all from Abcam, Cambridge, UK) for incubation at 4°C overnight. Next, the samples were washed 3 times in TBST (6 min per wash) and treated for 2 h with horseradish peroxidase (HRP) labeled goat anti-rabbit IgG antibody (1:5000; Zhongshan Biotech, Beijing, China), followed by 3 more six-minute washes in TBST. Subsequently, the membrane was placed in TBS. Equal volumes of solutions A and B from an Excellent Chemiluminescent Substrate (ECL) kit (BB-3501; BestBio, Shanghai, China) were mixed, and 200 µL was added to the membrane. Images were exposed in a gel-imager, photographed with an imaging analyzer (Bio-Rad Laboratories Inc, Hercules, USA), and analyzed using ImageJ software (National Institutes of Health, Bethesda, USA). The relative protein level = the grayscale value of the protein band/the grayscale value of the GAPDH protein band.

### MTT assay

After 48 h of transfection and culture, the cells were digested routinely and harvested for counting. The cells were planted in a 96-well plate ( $3-6 \times 10^3$ /well, 100 µL/well), and each group had 6 wells. At 24 h, 48 h and 72 h, 20 µL of 5 mg/mL MTT solution (Gibco) was added to each well. The plate was placed in the dark for 4 h, and then 100 µL of DMSO (Sigma-Aldrich, St. Louis, USA) was added into each well. The optical density (OD) value at 495 nm in each well was detected with a microplate reader (NYW-96M; Nuoyawei, Beijing, China). Cell viability curves were plotted with their OD value on the y-axis and time on the x-axis.

### Flow cytometry

After 48 h of transfection, the cells were washed in PBS 3 times followed by centrifugation at  $300 \times g$  for 20 min. Next, the supernatant was discarded and the cell concentration was controlled to  $1 \times 10^5$ /mL using PBS. The sample was then treated with 1 mL of pre-cooled 75% ethanol (Shanghai Coking Co, Shanghai, China) at 4°C for 1 h, before being centrifuged at  $250 \times g$  for 5 min and washed 3 times in PBS. Afterward, 120 µL of RNase A (Thermo Fisher

Scientific) was added in the dark, and the samples were water-bathed at 37°C for 40 min before being stained with 500 µL of propidium iodide (PI; Sigma-Aldrich) in the dark at 4°C for 30 min. The cell cycle was examined with a flow cytometer (Beckman Coulter Inc., Brea, USA) at 488 nm.

After 48 h of transfection, the cells were digested with EDTA-free pancreatin (Thermo Fisher Scientific) and placed in flow cytometry tubes for centrifugation ( $300 \times g$  for 30 min). Next, the supernatant was discarded, and the cells were washed 3 times in pre-cooled PBS before centrifugation ( $300 \times g$  for 20 min). The supernatant was discarded, and annexin V-fluorescein isothiocyanate (FITC)/PI dye was prepared using HEPES buffer (Thermo Fisher Scientific) annexin V-FITC and PI (50:1:2) according to the instructions in a commercial Annexin-V-FITC Cell Apoptosis Detection Kit (Sigma-Aldrich). Subsequently, the samples were mixed with 100 µL of dye and incubated at room temperature for 15 min before being mixed with HEPES buffer (Thermo Fisher Scientific). A flow cytometer was used to detect cell apoptosis. The green fluorescence of annexin V-FITC was examined through the FITC channel (FL1), while the red fluorescence of PI was examined through the PI channel (FL2 or FL3). The excitation and emission wavelengths were 488 nm and 530 nm, respectively.

### Cell invasion

Transwell chambers (Jrdun Biotechnology Co., Shanghai, China) were put in a 96-well plate. The upper chambers were coated with Matrigel (1:8, Sigma-Aldrich) and then dried at room temperature. The cells were digested with pancreatin (Sigma-Aldrich) and washed 3 times in PBS. The cells were then resuspended in RPMI 1640 medium, and the density was adjusted to  $1 \times 10^5$ /mL. Cell suspension (300 µL) was added to the Matrigel-coated upper chambers, and 500 µL of RPMI 1640 medium with 10% FBS (Gibco) was added to the lower chambers. After culturing for 24 h, the transwell chambers were taken, and the non-invaded cells in the upper chamber were gently scraped off using cotton swabs. Subsequently, the samples were fixed with paraformaldehyde (4%) (Beijing Leagene Biotechnology Co. Ltd., Beijing, China) for 20 min, stained with crystal violet (0.5% Solarbio) and then washed 3 times in PBS. Under an inverted microscope, 5 fields were randomly selected for photographing ( $\times 200$  magnification), and the cells passing through the membrane were counted.

### Statistical analysis

The SPSS v. 21.0 software (IBM Corp., Armonk, USA) was used to analyze the data. Measurement data are expressed as means  $\pm$  standard deviation (SD). One-way analysis of variance (ANOVA) was used for multiple group comparisons, and Tukey's post hoc test for pairwise comparisons was used between multiple groups. A value of  $p < 0.050$  indicated a statistically significant difference.

## Results

### Expressions of miR-124-3p, MEKK3 and p-p38MAPK in the coronary arteries of mice

To investigate the expressions of miR-124-3p and MEKK3 and the activation of the p38MAPK signaling pathway in the AS and the normal groups, we measured the expression levels of miR-124-3p and MEKK3 using qRT-PCR, and the phosphorylation of p38MAPK, a factor related to the p38MAPK signaling pathway, using western blot. Compared with the normal group, the miR-124-3p expression level was lower in the coronary arteries in the AS

group ( $p = 0.001$ ), and the phosphorylation levels of MEKK3 and p38MAPK were higher in the AS group ( $p = 0.001$  and  $p = 0.0006$ , respectively). Meanwhile, the basal expression level of the p38MAPK protein was similar in the 2 groups ( $p = 0.340$ ) (Fig. 1).

### Mir-124-3p can negatively regulate the MEKK3 gene

The bioinformatics website [www.microrna.org/microrna/home.do](http://www.microrna.org/microrna/home.do) predicted the existence of a miR-124-3p binding site on MEKK3 (Fig. 2A). Figure 2B shows that compared with the groups transfected with the NC mimic, luciferase activity was much lower in the group

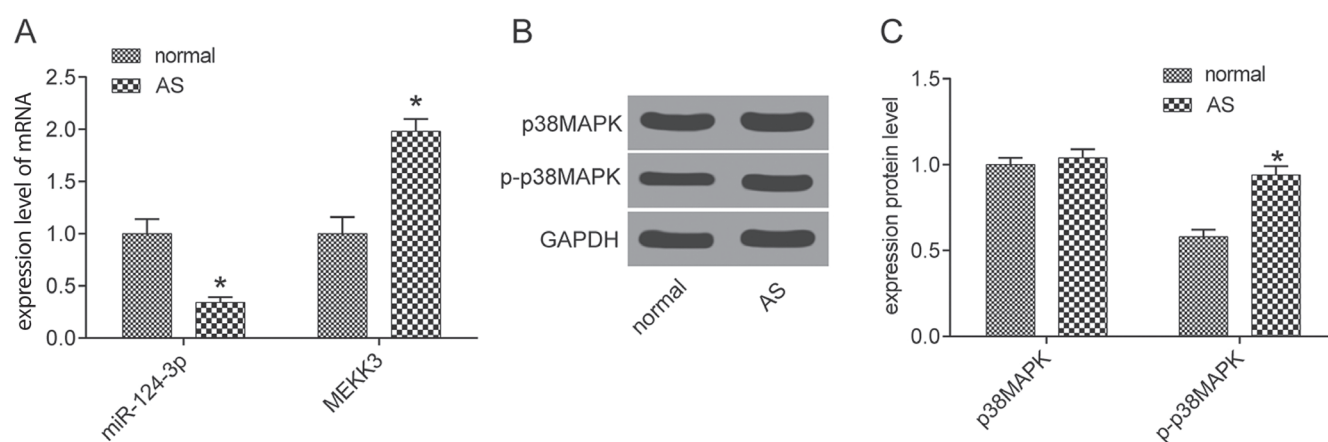


**Fig. 1.** Expressions of miR-124-3p, MEKK3, p38MAPK, and p-p38MAPK in the normal and AS groups. A. Histogram of miR-124-3p and MEKK3 mRNA expression levels in the tissues. B. Protein bands of p38MAPK and p-p38MAPK in the tissues. C. Histogram of protein levels of p38MAPK and p-p38MAPK in the tissues

\* $p < 0.050$  vs the normal group; MAPK – mitogen-activated protein kinase; GAPDH – glyceraldehyde 3-phosphate dehydrogenase.

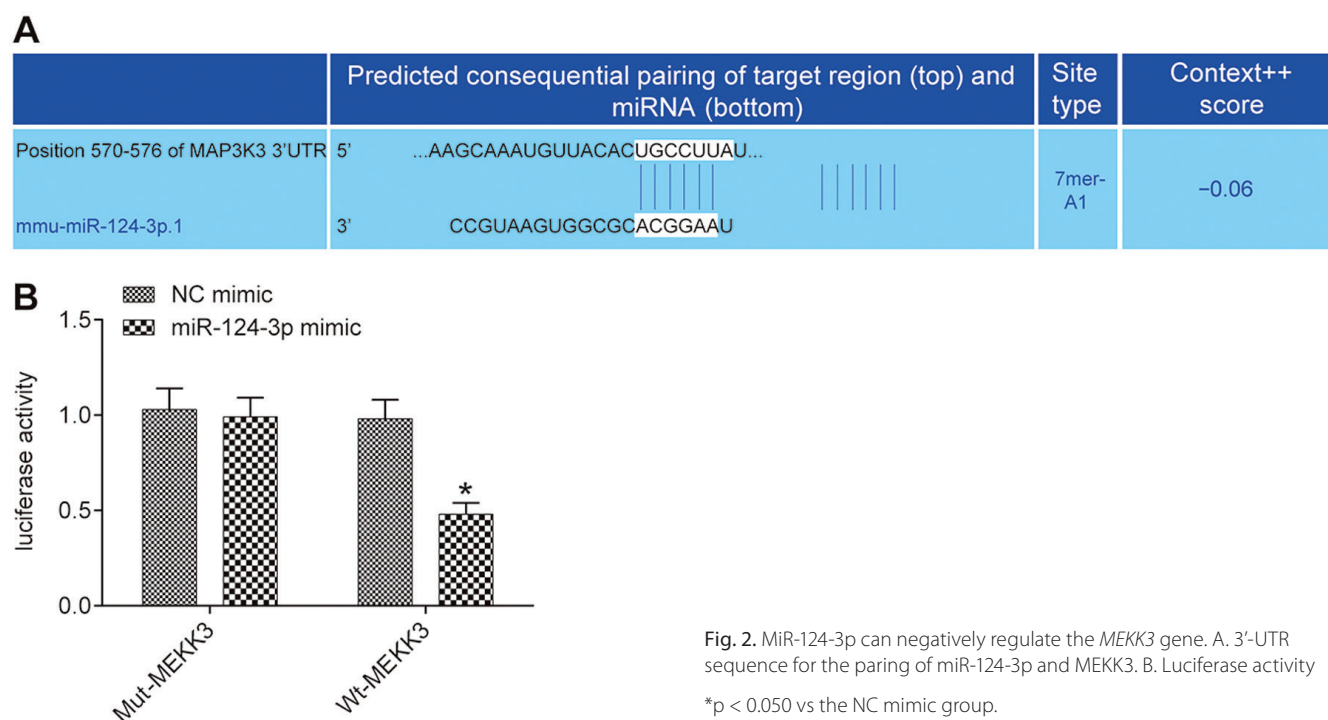


**Fig. 2.** MiR-124-3p can negatively regulate the MEKK3 gene. A. 3'-UTR sequence for the pairing of miR-124-3p and MEKK3. B. Luciferase activity

\* $p < 0.050$  vs the NC mimic group.

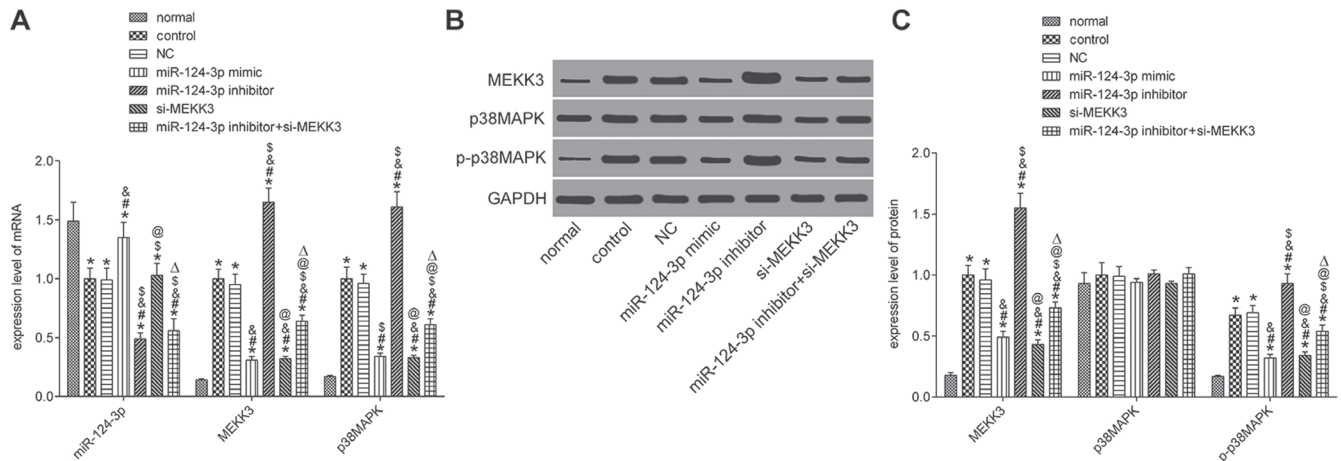


**Fig. 3.** miR-124-3p, MEKK3 and p38MAPK expressions in each group. A. Histogram of miR-124-3p, MEKK3 and p38MAPK mRNA levels. B. Protein bands of MEKK3, p38MAPK and p-p38MAPK. C. Histogram of MEKK3, p38MAPK and p-p38MAPK protein levels

\* $p < 0.050$  vs the normal group; # $p < 0.050$  vs the control group; & $p < 0.050$  vs the NC group; \$ $p < 0.050$  vs the miR-124-3p mimic group; @ $p < 0.050$  vs the miR-124-3p inhibitor group;  $\Delta p < 0.050$  vs the si-MEKK3 group; MAPK – mitogen-activated protein kinase; GAPDH – glyceraldehyde 3-phosphate dehydrogenase.

co-transfected with Wt-MEKK3 and miR-124-3p mimic ( $p = 0.001$ ). At the same time, luciferase activity remained unchanged in the group co-transfected with MEKK3mut ( $p = 0.665$ ). This finding indicates that miR-124-3p can negatively regulate the *MEKK3* gene.

### Mir-124-3p, MEKK3 and p38MAPK expressions in each group

In order to investigate the mechanism of how miR-124-3p mediates the p38MAPK signaling pathway through the *MEKK3* gene and exerts effects on macrophage apoptosis and proliferation in AS mice, we measured the miR-124-3p expression level and mRNA expression levels of MEKK3 and p38MAPK using qRT-PCR, and measured MEKK3 protein expression and the phosphorylation of p38MAPK using western blot. As shown in Fig. 3, compared with the normal group, the other groups had lower levels of miR-124-3p and higher phosphorylation levels of MEKK3 and p38MAPK (all  $p < 0.0001$ ); meanwhile, the basal protein expression level of p38MAPK was similar in the normal group and the other groups ( $p = 0.449$ ). Compared with the control group, the NC group had similar expression levels of each gene; whereas the expression levels of MEKK3 and p-p38MAPK were lower in the miR-124-3p mimic, si-MEKK3 and miR-124-3p inhibitor+si-MEKK3 groups (all  $p < 0.0001$ ); and the expression levels of MEKK3 and p-p38MAPK were higher in the miR-124-3p inhibitor group ( $p = 0.001$ ,  $p = 0.003$ ). The miR-124-3p inhibitor+si-MEKK3 group had higher expression levels of MEKK3 and p-p38MAPK than the si-MEKK3 group ( $p = 0.0005$ ,  $p = 0.0008$ ). Compared with the miR-124-3p inhibitor group, the miR-124-3p inhibitor+si-MEKK3 group had lower expression levels of MEKK3 and p-p38MAPK (both  $p = 0.0002$ ).

### Cell proliferation

The MTT assay results showed that cell growth increased with time. The normal group had lower OD values at 24 h and 48 h than the other groups (all  $p < 0.0001$ ). In comparison with the control group, the NC group had similar OD values at 24 h and 48 h ( $p = 0.818$ ,  $p = 0.744$ ), while the OD values at 48 h and 72 h were lower in the miR-124-3p mimic group, the si-MEKK3 group and the miR-124-3p inhibitor+si-MEKK3 groups ( $p = 0.005$ ,  $p = 0.009$ ), and higher in the miR-124-3p inhibitor group ( $p = 0.018$ ,  $p = 0.032$ ). Meanwhile, the miR-124-3p inhibitor+si-MEKK3 group had higher OD values at 48 h and 72 h than the si-MEKK3 group ( $p = 0.030$ ,  $p = 0.039$ ), and lower OD values at 48 h and 72 h than the miR-124-3p inhibitor group ( $p = 0.030$ ,  $p = 0.039$ ) (Fig. 4).

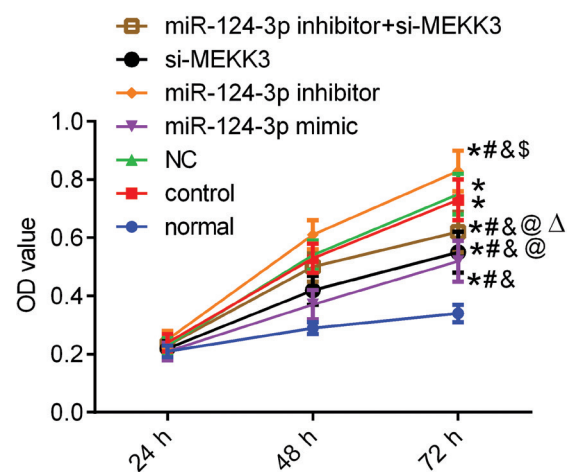


**Fig. 4.** Cell proliferation measured using MTT assay

\* $p < 0.050$  vs the normal group; # $p < 0.050$  vs the control group; & $p < 0.050$  vs the NC group; \$ $p < 0.050$  vs the miR-124-3p mimic group; @ $p < 0.050$  vs the miR-124-3p inhibitor group;  $\Delta p < 0.050$  vs the si-MEKK3 group; OD – optical density.

## Cell cycle

The flow cytometry results displayed that compared to the normal group, the other groups had fewer G1 phase cells and more S phase cells (both  $p < 0.0001$ ). There were no differences between the control and NC groups in terms of the cell ratios at the G1, S and G2 phases ( $p = 0.982$ ,  $p = 0.802$ ,  $p = 0.756$ ). Compared with the control group, the miR-124-3p mimic, si-MEKK3 and miR-124-3p inhibitor+si-MEKK3 groups had more G1 phase cells and fewer S phase cells ( $p = 0.0002$ ,  $p < 0.0001$ ), whereas the miR-124-3p inhibitor group had fewer G1 phase cells and more S phase cells ( $p = 0.003$ ,  $p = 0.008$ ). Meanwhile, the miR-124-3p inhibitor+si-MEKK3 group had fewer G1 cells and more S cells than the si-MEKK3 group ( $p = 0.020$ ,  $p = 0.002$ ), and more G1 phase cells and fewer S phase cells than the miR-124-3p inhibitor group ( $p = 0.001$ ,  $p = 0.0004$ ) (Fig. 5).

## Cell apoptosis

The flow cytometry results showed that compared to the normal group, the other groups had lower cell apoptosis rates ( $p < 0.0001$ ). There was no difference between the control and NC groups in terms of the cell apoptosis rate ( $p = 0.528$ ). Compared with the control group, the miR-124-3p mimic, si-MEKK3 and miR-124-3p inhibitor+si-MEKK3 groups had higher cell apoptosis rates ( $p < 0.0001$ ), and the miR-124-3p inhibitor group had a lower cell apoptosis rate ( $p = 0.0002$ ). The miR-124-3p inhibitor+si-MEKK3 group had a lower cell apoptosis rate than the si-MEKK3 group and a higher apoptosis rate than the miR-124-3p inhibitor group (both  $p < 0.0001$ ) (Fig. 6).

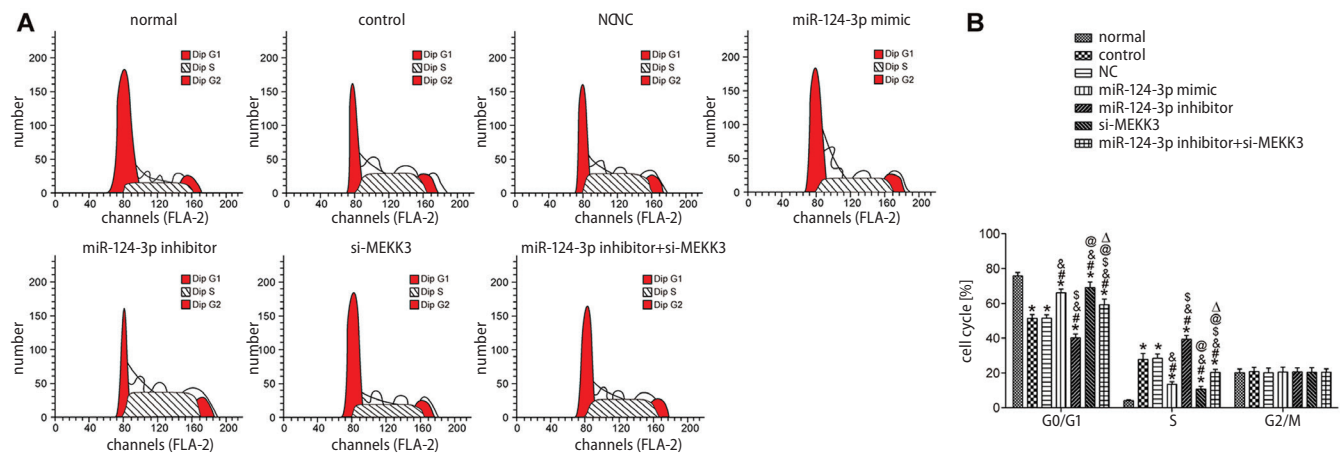


Fig. 5. Cell cycle detected with flow cytometry. A. Cell cycle in each group. B. Histogram of a cell cycle

\* $p < 0.050$  vs the normal group; # $p < 0.050$  vs the control group; & $p < 0.050$  vs the NC group; § $p < 0.050$  vs the miR-124-3p mimic group; @ $p < 0.050$  vs the miR-124-3p inhibitor group; ^ $p < 0.050$  vs the si-MEKK3 group.

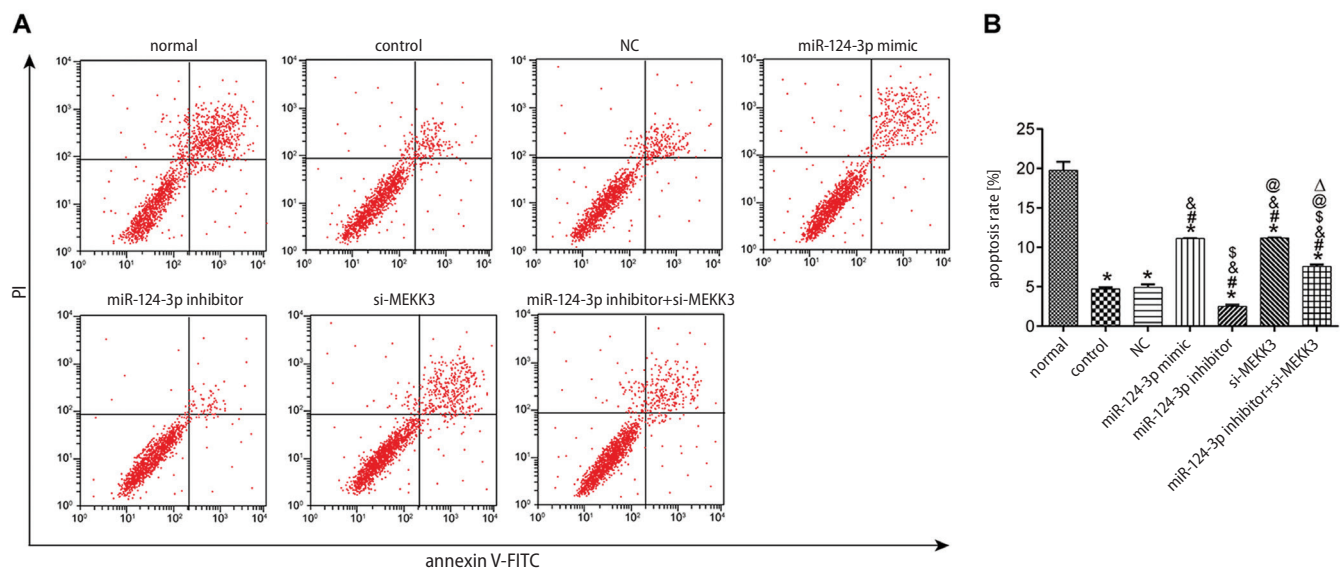


Fig. 6. Cell apoptosis detected using flow cytometry. A. Cell apoptosis rate. B. Histogram of the cell apoptosis rate

\* $p < 0.050$  vs the normal group; # $p < 0.050$  vs the control group; & $p < 0.050$  vs the NC group; § $p < 0.050$  vs the miR-124-3p mimic group; @ $p < 0.050$  vs the miR-124-3p inhibitor group; ^ $p < 0.050$  vs the si-MEKK3 group; FITC – fluorescein isothiocyanate.

## Cell invasion

The transwell assay results showed that compared to the normal group, the other groups had higher numbers of invading cells ( $p < 0.0001$ ). No difference was observed in the number of invading cells between the control and NC groups ( $p = 0.276$ ). Compared with the control group, the miR-124-3p mimic, si-MEKK3 and miR-124-3p inhibitor+si-MEKK3 groups had fewer invading cells ( $p < 0.0001$ ), and the miR-124-3p inhibitor group had more invading cells ( $p = 0.039$ ). Moreover, the miR-124-3p inhibitor+si-MEKK3 group had a higher cell apoptosis rate than the si-MEKK3 group ( $p = 0.007$ ) and fewer invading cells than the miR-124-3p inhibitor group ( $p = 0.003$ ) (Fig. 7).

## mRNA and protein expression levels of PCNA, Bcl-2 and Bax

To investigate how miR-124-3p affects the apoptosis and proliferation of macrophages in mice with AS by mediating the p38MAPK signaling pathway through the *MEKK3* gene, we measured the mRNA and protein expression levels of proliferation-associated factor PCNA and apoptosis-associated factors Bcl-2 and Bax using qRT-PCR and western blot. The results showed that compared to the normal group, the other groups had higher mRNA and protein expression levels of PCNA and Bcl-2, and lower mRNA and protein expression levels of Bax (all  $p < 0.0001$ ). The expression levels of each gene in the control and NC groups were similar. Compared with the control group, the miR-124-3p mimic, si-MEKK3, miR-124-3p inhibitor+si-MEKK3 groups had lower PCNA and Bcl-2 mRNA and protein expression levels (PCNA mRNA,  $p = 0.0004$ , Bcl-2

mRNA  $p < 0.0001$ , PCNA protein  $p < 0.0001$ , Bcl-2 protein  $p < 0.0001$ ), and higher Bax mRNA and protein expression levels ( $p = 0.0002$ ,  $p < 0.0001$ ), while the miR-124-3p inhibitor group had greater PCNA and Bcl-2 mRNA and protein expression levels (PCNA mRNA  $p = 0.0005$ , Bcl-2 mRNA  $p = 0.004$ , PCNA protein  $p = 0.001$ , Bcl-2 protein  $p = 0.001$ ), and lower Bax mRNA and protein expression levels ( $p = 0.010$ ,  $p = 0.002$ ). The miR-124-3p inhibitor+si-MEKK3 group had higher PCNA and Bcl-2 mRNA and protein expression levels (PCNA mRNA  $p = 0.035$ , Bcl-2 mRNA  $p = 0.004$ , PCNA protein  $p = 0.0005$ , Bcl-2 protein  $p = 0.003$ ), and lower Bax mRNA and protein expression levels ( $p = 0.011$ ,  $p < 0.0001$ ) than the si-MEKK3 group, and lower PCNA and Bcl-2 mRNA and protein expression levels (PCNA mRNA  $p = 0.0002$ , Bcl-2 mRNA  $p = 0.001$ , PCNA protein  $p < 0.0001$ , Bcl-2 protein  $p < 0.0001$ ), and higher Bax mRNA and protein expression levels ( $p = 0.0008$ ,  $p = 0.003$ ) than the miR-124-3p inhibitor group (Fig. 8).

## Discussion

Macrophage apoptosis takes part in the whole process of AS and serves a critical role in the pathogenesis of this disease. Macrophage cells are a major component of AS plaque. The plaque is likely to be ruptured if it is unstable, and once the plaque is ruptured, a thrombus can easily form.<sup>17</sup> Macrophages play an essential part in all stages of AS, including lesion occurrence and expansion, necrosis that leads to rupture, the clinical manifestation of AS, and even the subsidence of AS.<sup>18,19</sup> Different phenotypes can be exhibited in macrophages based on the environment and the activation of intracellular signaling pathways. As researchers are gaining more understanding about the role

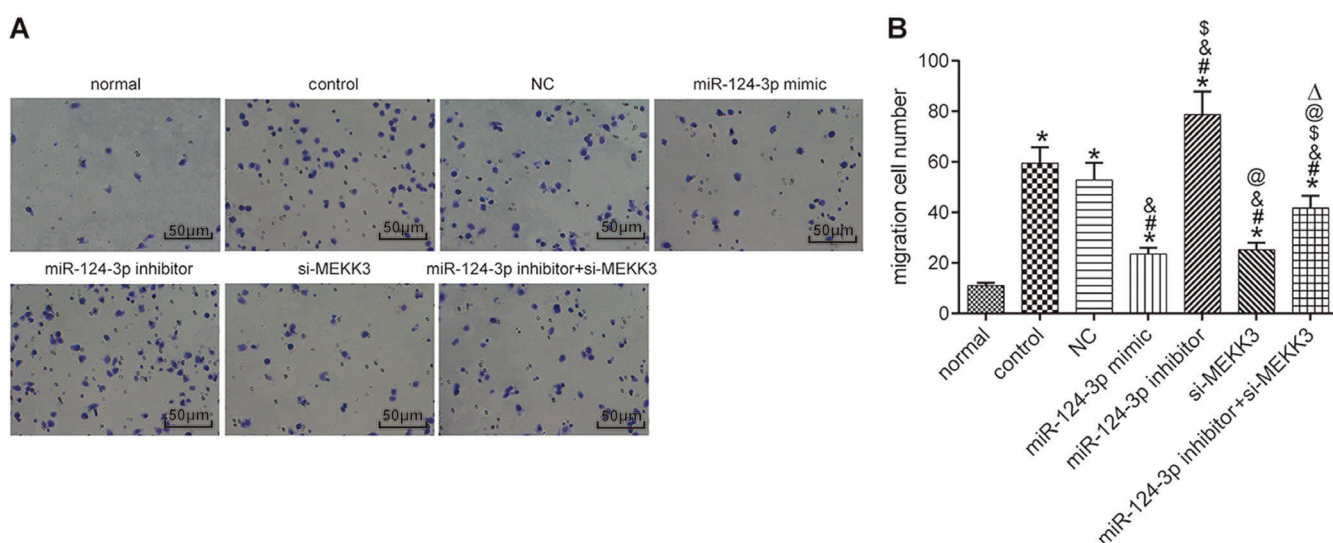
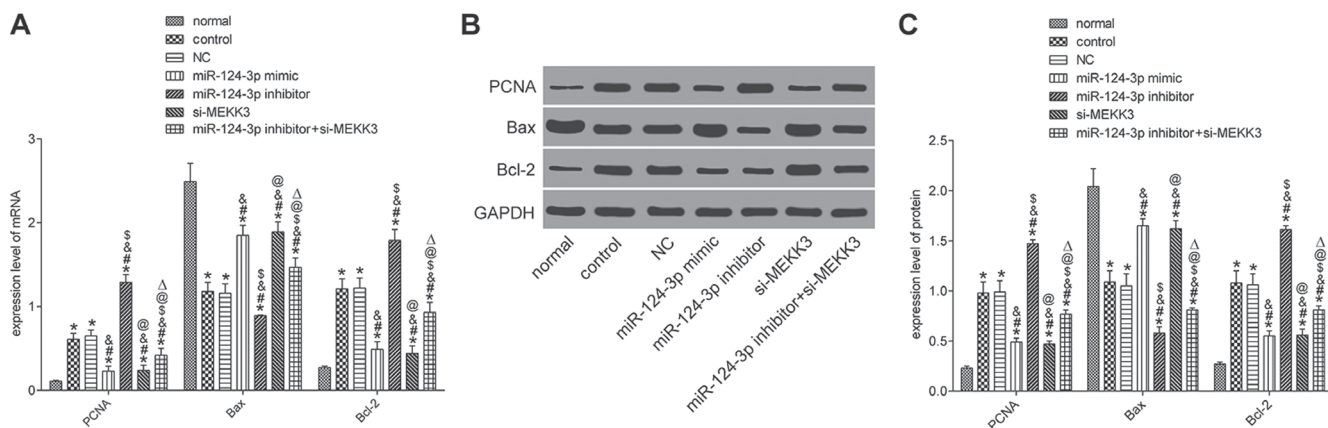


Fig. 7. Cell invasion measured using transwell assay. A. Image of cell invasion (x200 magnification). B. Histogram of the number of invading cells in each group

\* $p < 0.050$  vs the normal group; # $p < 0.050$  vs the control group; \$ $p < 0.050$  vs the NC group; ^ $p < 0.050$  vs the miR-124-3p mimic group; @ $p < 0.050$  vs the miR-124-3p inhibitor group; ^ $p < 0.050$  vs the si-MEKK3 group.



**Fig. 8.** RNA and protein expression levels of PCNA, Bax and Bcl-2. A. Histogram of PCNA, Bax and Bcl-2 mRNA levels. B. Protein bands of PCNA, Bax and Bcl-2. C. Histogram of protein levels of PCNA, Bax and Bcl-2 in each group

\*p < 0.050 vs the normal group; #p < 0.050 vs the control group; &p < 0.050 vs the NC group; §p < 0.050 vs the miR-124-3p mimic group; @p < 0.050 vs the miR-124-3p inhibitor group; ^p < 0.050 vs the si-MEKK3 group.

of inflammatory macrophages, molecular therapy is now emerging.<sup>19,20</sup>

In recent years, miR-124-3p downregulation has been observed in various types of human diseases, including Parkinson’s disease, AS, and nerve damage.<sup>21–23</sup> Activation of the MAPK pathway is a major intracellular event in cellular responses to environmental stress. Some studies have revealed that MEKK3, a MAP3K family member, can be strongly expressed in human and mice platelets, and the lack of platelet-specific MEKK3 can hinder arterial thrombus formation; moreover, MEKK3 can activate ERK1/2 and JNK2 in platelets and cause microthrombus.<sup>24</sup> p38MAPK signaling serves a critical role in regulating cell apoptosis and proliferation. Some studies have demonstrated that suppressing p38MAPK phosphorylation in cardiomyocyte can reduce oxidative injury, whereas p38MAPK phosphorylation in bladder cancer cells can promote the occurrence of tumors.<sup>25,26</sup> Meanwhile, it has also been reported that p38MAPK phosphorylation can aggravate inflammation in fibroblasts and increase inflammatory activity in the retina.<sup>27,28</sup> However, the effect of the p38MAPK signaling pathway in AS remains unclear.

Studies have indicated that the expression level of MEKK3 is elevated in thrombi and that high MEKK3 expression can promote phosphorylation of the p38MAPK signaling pathway via activation of the MAPK pathway, thereby affecting chondriosome and cell nuclei.<sup>29</sup> In the present study, we found that miR-124-3p expression was downregulated in macrophages and in the tissues of AS mice, while MEKK3 and the phosphorylation of p38MAPK signaling pathway were upregulated. In this study, the MEKK3 interference sequence was transfected into the macrophages, and this interference caused marked decreases in p38MAPK phosphorylation, expressions of the proliferation-associated factor PCNA and the antiproliferative factor Bcl-2, cell proliferation and invasion abilities, cell cycle progression, and the interference increased the expression of the pro-apoptotic factor Bax and

the cell apoptosis rate. The results indicated that MEKK3 interference can suppress the phosphorylation of p38MAPK signaling pathway, thereby inhibiting macrophage proliferation and invasion, and promoting macrophage apoptosis in mice, which aligned with previous studies.<sup>13,29</sup>

To further investigate MEKK3 upstream regulation, we checked the [www.microrna.org/microrna/home.do](http://www.microrna.org/microrna/home.do) bioinformatics website and found that miR-124-3p can target MEKK3. It has also been documented that miR-124-3p has inhibitory effects on various diseases.<sup>30</sup> Our dual luciferase reporter assay suggested that miR-124-3p can negatively regulate MEKK3. We performed transfections of miR-124-3p mimic, miR-124-3p inhibitor and miR-124-3p inhibitor+si-MEKK3 into mice macrophages and found that miR-124-3p overexpression can inhibit the proliferation and invasion of macrophages and promote their apoptosis, whereas miR-124-3p silencing can achieve the opposite effect. Compared with the miR-124-3p inhibitor group, macrophages in the miR-124-3p inhibitor+si-MEKK3 group had weaker proliferation and invasion abilities, higher apoptosis rates and lower p38MAPK phosphorylation, suggesting that inhibiting MEKK3 expression can partially counteract the effect of miR-124-3p silencing on macrophage growth, thereby inhibiting the phosphorylation of the p38MAPK signaling pathway. These results demonstrated that miR-124-3p overexpression can inhibit MEKK3 gene expression and the phosphorylation of the p38MAPK signaling pathway in the AS mouse model, thereby inhibiting macrophage proliferation and invasion, and promoting microphage apoptosis.

## Conclusions

MiR-124-3p can mediate the p38MAPK signaling pathway by targeting the MEKK3 gene, thereby inhibiting macrophage growth. The pathogenesis of AS was further

elucidated in this study, which can contribute to the theoretical basis for treating AS. However, more clinical data needs to be included, and the way in which how MEKK3 participates in the p38MAPK signaling pathway needs to be investigated in future studies in order to verify our results and further clarify the relationship between miR-124-3p and AS, the inhibitory effect of miR-124-3p on MEKK3 and the effect of miR-124-3p in AS.

### ORCID iDs

Chuannan Zhai  <https://orcid.org/0000-0003-3504-5957>  
 Hongliang Cong  <https://orcid.org/0000-0001-6525-064X>  
 Kai Hou  <https://orcid.org/0000-0002-0341-8117>  
 Yuecheng Hu  <https://orcid.org/0000-0001-7292-3996>  
 Jingxia Zhang  <https://orcid.org/0000-0002-4936-7554>  
 Yingyi Zhang  <https://orcid.org/0000-0002-9134-7055>  
 Ying Zhang  <https://orcid.org/0000-0003-2639-504X>  
 Hong Zhang  <https://orcid.org/0000-0002-0650-0482>

### References

- Babaev VR, Huang J, Ding L, Zhang Y, May JM, Linton MF. Loss of ricor in monocyte/macrophages suppresses their proliferation and viability reducing atherosclerosis in LDLR null mice. *Front Immunol.* 2018;9:215.
- Kruth HS. Fluid-phase pinocytosis of LDL by macrophages: A novel target to reduce macrophage cholesterol accumulation in atherosclerotic lesions. *Curr Pharm Des.* 2013;19(33):5865–5872.
- McCurdy S, Baumer Y, Toulmin E, Lee BH, Boisvert WA. Macrophage-specific expression of IL-37 in hyperlipidemic mice attenuates atherosclerosis. *J Immunol.* 2017;199(10):3604–3613.
- Xiao Y, He M, Liang X, et al. Pu-erh tea ameliorates atherosclerosis associated with promoting macrophage apoptosis by reducing NF-kappaB activation in ApoE knockout mice. *Oxid Med Cell Longev.* 2018;2018:3197829.
- Gonzalez L, Qian AS, Tahir U, Yu P, Trigatti BL. Sphingosine-1-phosphate receptor 1, expressed in myeloid cells, slows diet-induced atherosclerosis and protects against macrophage apoptosis in Ldlr KO mice. *Int J Mol Sci.* 2017;18(12):2721.
- Zhang YL, Li XB, Hou YX, Fang NZ, You JC, Zhou QH. The lncRNA XIST exhibits oncogenic properties via regulation of miR-449a and Bcl-2 in human non-small cell lung cancer. *Acta Pharmacol Sin.* 2017;38(3):371–381 [Erratum in: The lncRNA XIST exhibits oncogenic properties via regulation of miR-449a and Bcl-2 in human non-small cell lung cancer. *Acta Pharmacol Sin.* 2017;38(3):443.
- O'Connell RM, Rao DS, Chaudhuri AA, Baltimore D. Physiological and pathological roles for microRNAs in the immune system. *Nat Rev Immunol.* 2010;10(2):111–122.
- Song K, Li L, Sun G, Wei Y. MicroRNA-381 regulates the occurrence and immune responses of coronary atherosclerosis via cyclooxygenase-2. *Exp Ther Med.* 2018;15(5):4557–4563.
- Ahmad R, Heidarian E, Fadaei R, Moradi N, Malek M, Fallah S. miR-342-5p expression levels in coronary artery disease patients and its association with inflammatory cytokines. *Clin Lab.* 2018;64(4):603–609.
- Wang X, Lian Y, Wen X, et al. Expression of miR-126 and its potential function in coronary artery disease. *Afr Health Sci.* 2017;17(2):474–480.
- Zhao L, Jiao Y, Yang AN, et al. The effect of miR-124 on homocysteine-induced atherosclerosis via promoter region DNA methylation in ApoE(-/-) mice [in Chinese]. *Sheng Li Xue Bao.* 2015;67(2):207–213.
- Yang J, Lin Y, Guo Z, et al. The essential role of MEKK3 in TNF-induced NF-kappaB activation. *Nat Immunol.* 2001;2(7):620–624.
- Padda R, Wamsley-Davis A, Gustin MC, Ross R, Yu C, Sheikh-Hamad D. MEKK3-mediated signaling to p38 kinase and TonE in hypertonically stressed kidney cells. *Am J Physiol Renal Physiol.* 2006;291(4):F874–F881.
- Feng H, Cao J, Zhang G, Wang Y. Kaempferol attenuates cardiac hypertrophy via regulation of ASK1/MAPK signaling pathway and oxidative stress. *Planta Med.* 2017;83(10):837–845.
- Ren R, Chen SD, Fan J, Zhang G, Li JB. miRNA-138 regulates MLK3/JNK/MAPK pathway to protect BV-2 cells from H2O2-induced apoptosis. *Bratisl Lek Listy.* 2018;119(5):284–288.
- Li Q, Park K, Xia Y, et al. Regulation of macrophage apoptosis and atherosclerosis by lipid-induced PKCdelta isoform activation. *Circ Res.* 2017;121(10):1153–1167.
- van Diepen JA, Berbee JF, Havekes LM, Rensen PC. Interactions between inflammation and lipid metabolism: Relevance for efficacy of anti-inflammatory drugs in the treatment of atherosclerosis. *Atherosclerosis.* 2013;228(2):306–315.
- Tabas I, Bornfeldt KE. Macrophage phenotype and function in different stages of atherosclerosis. *Circ Res.* 2016;118(4):653–667.
- Zhang Q, Lenardo MJ, Baltimore D. 30 years of NF-kappaB: A blossoming of relevance to human pathobiology. *Cell.* 2017;168(1–2):37–57.
- Liu Z, Gan L, Xu Y, et al. Melatonin alleviates inflammasome-induced pyroptosis through inhibiting NF-kappaB/GSDMD signal in mice adipose tissue. *J Pineal Res.* 2017;63(1). doi:10.1111/jpi.12414
- Dong RF, Zhang B, Tai LW, Liu HM, Shi FK, Liu NN. The neuroprotective role of miR-124-3p in a 6-hydroxydopamine-induced cell model of Parkinson's disease via the regulation of ANAX5. *J Cell Biochem.* 2018;119(1):269–277.
- de Ronde MWJ, Kok MGM, Moerland PD, et al. High miR-124-3p expression identifies smoking individuals susceptible to atherosclerosis. *Atherosclerosis.* 2017;263:377–384.
- Geng L, Liu W, Chen Y. miR-124-3p attenuates MPP(+)-induced neuronal injury by targeting STAT3 in SH-SY5Y cells. *Exp Biol Med (Maywood).* 2017;242(18):1757–1764.
- Fan X, Wang C, Shi P, et al. Platelet MEKK3 regulates arterial thrombosis and myocardial infarct expansion in mice. *Blood Adv.* 2018;2(12):1439–1448.
- Ding SK, Wang LX, Guo LS, et al. Syringic acid inhibits apoptosis pathways via downregulation of p38MAPK and JNK signaling pathways in H9c2 cardiomyocytes following hypoxia/reoxygenation injury. *Mol Med Rep.* 2017;16(2):2290–2294.
- He H, Chang R, Zhang T, Yang C, Kong Z. ATM mediates DAB2IP-deficient bladder cancer cell resistance to ionizing radiation through the p38MAPK and NF-kappaB signaling pathway. *Mol Med Rep.* 2017;16(2):1216–1222.
- Menon MB, Gropengieser J, Fischer J, et al. p38(MAPK)/MK2-dependent phosphorylation controls cytotoxic RIPK1 signalling in inflammation and infection. *Nat Cell Biol.* 2017;19(10):1248–1259.
- Cai Y, Li W, Tu H, et al. Curcuminolide reduces diabetic retinal vascular leukostasis and leakage partly via inhibition of the p38MAPK/NF-kappa B signaling. *Bioorg Med Chem Lett.* 2017;27(8):1835–1839.
- Xu J, Tang S, Yin B, Sun J, Bao E. Co-enzyme Q10 upregulates Hsp70 and protects chicken primary myocardial cells under in vitro heat stress via PKC/MAPK. *Mol Cell Biochem.* 2018;449(1–2):195–206.
- Cui M, Wang J, Li Q, Zhang J, Jia J, Zhan X. Long non-coding RNA HOXA11-AS functions as a competing endogenous RNA to regulate ROCK1 expression by sponging miR-124-3p in osteosarcoma. *Biomed Pharmacother.* 2017;92:437–444.

# Ketamine alleviates HMGB1-induced acute lung injury through TLR4 signaling pathway

Dong Xu<sup>1,B,C</sup>, Xang Sun<sup>2,A,B</sup>, Yang Zhang<sup>3,E,F</sup>, Li Cao<sup>1,C,D</sup>

<sup>1</sup> Department of Anesthesiology, Jinan Central Hospital Affiliated to Shandong University, China

<sup>2</sup> Department of Intensive Care Unit, Jinan Central Hospital Affiliated to Shandong University, China

<sup>3</sup> Department of Anesthesiology, Binzhou People's Hospital, China

A – research concept and design; B – collection and/or assembly of data; C – data analysis and interpretation;

D – writing the article; E – critical revision of the article; F – final approval of the article

Advances in Clinical and Experimental Medicine, ISSN 1899–5276 (print), ISSN 2451–2680 (online)

*Adv Clin Exp Med.* 2020;29(7):813–817

## Address for correspondence

Lei Chao

E-mail: qiechengjing58@163.com

## Funding sources

None declared

## Conflict of interest

None declared

Received on June 1, 2018

Reviewed on September 8, 2019

Accepted on May 1, 2020

Published online on July 28, 2020

## Abstract

**Background.** Acute lung injury (ALI) is a common critical respiratory disease that seriously threatens human health. Ketamine has good anti-inflammatory and immune-regulating properties that can delay the lung injury process.

**Objectives.** High mobility group box protein 1 (HMGB1) plays an important role in the occurrence, development and treatment of ALI. Toll-like receptor 4 (TLR4) is the receptor for HMGB1. The aim of this study was to determine the role of the HMGB1 TLR4 signaling pathway in the treatment of ALI using ketamine.

**Material and methods.** A total of 30 healthy, male, 8-week-old Sprague-Dawley rats were randomly, equally divided into a control group, an lipopolysaccharide (LPS) group and a ketamine group. In order to establish a rat ALI model, 15 mg/kg of LPS was injected into the femoral veins. Ketamine was intravenously injected (10 mg/kg) into the experimental group rats. The rats were euthanized 24 h after modeling and lung tissue samples were collected. Western blot was used to test TLR4, MyD88, TRAF-6, LOX-1, and HMGB1 protein expression in the lung tissue. Real-time polymerase chain reaction (RT-PCR) was performed to detect TLR4, MyD88, TRAF-6, LOX-1, and HMGB1 mRNA levels.

**Results.** Compared with the controls, the LPS group had significantly higher TLR4, MyD88, TRAF-6, LOX-1, and HMGB1 mRNA and protein levels ( $p < 0.05$ ). These levels were significantly lower after ketamine intervention in comparison with the LPS group ( $p < 0.05$ ). A positive correlation was found between TLR4 and HMGB1 expression in the LPS and ketamine groups ( $r = 0.952, p < 0.001$ ;  $r = 0.941, p < 0.001$ ).

**Conclusions.** Ketamine attenuates HMGB1-induced ALI, possibly by regulating the TLR4 signaling pathway.

**Key words:** ketamine, acute lung injury, TLR4, HMGB1

## Cite as

Xu D, Sun X, Zhang Y, Chao L. Ketamine alleviates HMGB1-induced acute lung injury through TLR4 signaling pathway.

*Adv Clin Exp Med.* 2020;29(7):813–817.

doi:10.17219/acem/121936

## DOI

10.17219/acem/121936

## Copyright

© 2020 by Wrocław Medical University

This is an article distributed under the terms of the Creative Commons Attribution 3.0 Unported (CC BY 3.0)

(<https://creativecommons.org/licenses/by/3.0/>)

## Introduction

Acute lung injury (ALI) is a type of pulmonary inflammatory reaction which is caused by severe trauma, shock, severe infections, acidosis, and injuries of capillary endothelial cells and alveolar epithelial cells triggered by inflammatory cell cascade.<sup>1</sup> It may lead to diffuse pulmonary interstitial and alveolar edema, resulting in hypoxia and causing tissue necrosis and dysfunction. Acute lung injury may advance to acute respiratory distress syndrome. It is a common critical disease featuring rapid onset, quick development, poor prognosis, and high mortality.<sup>2</sup> In recent years, although ALI treatment has achieved certain progress, the mortality of ALI is still higher than 40%.<sup>3</sup>

Ketamine is widely used in clinical intravenous anesthesia. It has anti-inflammatory and immune-regulating functions, and presents a great inhibitory effect which prevents the production of a variety of inflammatory cytokines, the function of neutrophils and the expression of adhesion molecule.<sup>4–6</sup> Studies have shown that small doses of ketamine can alleviate the symptom of pulmonary edema,<sup>7</sup> indicating that ketamine has a therapeutic effect on ALI.<sup>6,8</sup> In addition, a previous study demonstrated that ketamine can improve the blood gas and pulmonary function index of patients with ALI caused by mechanical ventilation.<sup>9</sup> However, its mechanism has not been fully elucidated. Therefore, this study investigated the mechanism of ketamine in treating ALI in a rat model.

High mobility group box protein 1 (HMGB1) is widely distributed in the nucleus and cytoplasm of all types of cells. The HMGB1 in immune cells translocates from the nucleus to the cytoplasm and is secreted extracellularly under stimulus.<sup>10</sup> Wang et al. first found in 1999 that HMGB1 was an important inflammatory mediator in sepsis.<sup>11</sup> It was reported that HMGB1 was also involved in ALI as an important inflammatory factor.<sup>12,13</sup> Timely blocking the secretion of inflammatory factors is the key to ALI treatment.<sup>14,15</sup> Thus, inhibiting HMGB1 secretion can delay the lung injury process. Toll-like receptor 4 (TLR4) also plays a critical role in the inflammatory response. As the receptor of HMGB1, the TLR4 signaling pathway plays pro-inflammatory roles.<sup>16,17</sup> It was revealed that knockdown of the TLR4 gene can alleviate HMGB1-induced inflammatory response.<sup>18</sup> Therefore, this study tested whether molecules related to the TLR4 signaling pathway and HMGB1 expression are involved in the effects of ketamine on treating ALI, aiming to provide a theoretical basis for using ketamine in the clinical treatment of ALI.

## Material and methods

### Main instruments and reagents

Lipopolysaccharide (LPS) was purchased from Sigma-Aldrich (St. Louis, USA). Ketamine hydrochloride was obtained from Fujian Gutian Pharmaceutical Co., Ltd.

(Ningde, China). A rat HMGB1 ELISA kit was sourced from Shanghai Yaji Biological Technology Co., Ltd. (Shanghai, China), while a rat TLR4 enzyme-linked immunosorbent assay (ELISA) kit was purchased from Shanghai Ricky Biological Technology Co., Ltd. (Shanghai, China). A total protein extraction kit came from BestBio Technologies (Shanghai, China). A Coomassie Brilliant Blue protein detection kit was purchased from MajorBio Technology, Ltd. (Shanghai, China). The SDS-PAGE system, phosphate-buffered saline-Tween (PBST) solution, electrophoresis apparatus, and a GIS-2020D gel image analysis system were obtained from Sigma-Aldrich. HMGB1, TLR4 and GAPDH antibodies came from Abcam (Cambridge, UK). Horseradish peroxidase (HRP)-tagged goat anti-rabbit IgG obtained from Dycen Biotech (Shanghai, China).

### Animal modeling

A total of 30 healthy, male, 8-week-old Sprague Dawley rats (180–220 g) were purchased from the Chinese Academy of Medical Sciences Animal Experiment Center (Beijing, China), and randomly, equally divided into a control group (n = 10) an LPS group (n = 10), and a ketamine group (n = 10). Following the study by Gokcinar et al., 15 mg/kg of LPS was intravenously injected to establish an ALI model.<sup>19</sup> Ketamine was intravenously injected (10 mg/kg) into the ketamine intervention group. An equal amount of normal saline was administered to the controls. The rats were euthanized using CO<sub>2</sub> 24 h after modeling, and lung tissue samples were collected and stored at –80°C.

Rats were used for all experiments, and all procedures were approved by the Animal Ethics Committee of China Meitan General Hospital (Beijing, China).

### PaO<sub>2</sub> to FiO<sub>2</sub> ratio

The arterial blood gases were analyzed using a Bayer Rapidlab 348 Analyzer (Bayer Diagnostics, Leverkusen, Germany) to calculate the ratio of partial pressure of arterial oxygen (PaO<sub>2</sub>) to the percentage of inspired oxygen (FiO<sub>2</sub>).

### Real-time PCR

Tissue RNA was extracted using TRIzol reagent, and the integrity of the RNA was identified using 1% agarose gel electrophoresis. A total of 1 µg of RNA was reverse-transcribed to cDNA with a kit (Takara, Kyoto, Japan). The real-time polymerase chain reaction (RT-PCR) reaction system contained 5 µL of 2 × SYBR Green Mixture, 0.5 µL of cDNA, 0.5 µL of Primer (10 µM), and 4 µL of ddH<sub>2</sub>O. The reaction conditions consisted of 10 min at 95°C, followed by 40 cycles of 95°C for 15 s and 60°C for 60 s. The RT-PCR reaction was performed on a ViiA™ 7 Real-Time PCR System (Thermo Fisher Scientific, Waltham, USA). Each sample was set in 3 parallel trials. β-actin was selected as the internal reference.

## Western blot

Total protein was extracted from the lung tissue and separated using SDS-PAGE. Next, it was transferred to a nitrocellulose (NC) membrane and blocked in 5% skim milk at room temperature for 2 h. After being washed in PBST 3 times, the membrane was incubated with the primary antibody at 4°C overnight. Then, the membrane was incubated with the secondary antibody in 2.5% skim milk for 60 min. After the chemiluminescence reagent was added, the membrane was developed and analyzed with the GIS-2020D gel image system (Ningbo Sija Lab Equipment Co., Ltd, Ningbo, China). The *GAPDH* gene was selected as the internal reference.

## Statistical analysis

The SPSS v. 19.0 software (IBM Corp., Armonk, USA) was used for the data analysis. Data are presented as means  $\pm$  standard deviation (SD). Comparison of the mean values was performed using Student's t-test. Correlation analysis was applied using Pearson analysis. A p-value  $<0.05$  was considered statistically significant.

## Results

### PaO<sub>2</sub>:FiO<sub>2</sub> ratio

To confirm the success of the ALI model, we performed a gas test to measure the PaO<sub>2</sub>:FiO<sub>2</sub> ratio and

found a significantly lower PaO<sub>2</sub>:FiO<sub>2</sub> ratio in the LPS group (156.1  $\pm$  21.3) than in the control group (475.6  $\pm$  39.5) ( $p < 0.05$ ), indicating the successful establishment of an ALI model, which was consistent with the pathological changes of lung as demonstrated by H&E staining (Fig. 1).

### TLR4, MyD88, TRAF-6, LOX-1, and HMGB1 mRNA expression in rat lung tissue

Real-time PCR was performed to test TLR4, MyD88, TRAF-6, LOX-1, and HMGB1 mRNA expression in the study groups (Table 1). Compared with the control group, the LPS group showed significantly higher TLR4, MyD88, TRAF-6, LOX-1, and HMGB1 mRNA expression ( $p < 0.05$ ). These levels were notably lower following ketamine intervention in comparison with the LPS group ( $p < 0.05$ ), but were still higher than those in the control group ( $p < 0.05$ ).

### TLR4, MyD88, TRAF-6, LOX-1, and HMGB1 protein levels in rat lung tissue

Western blot analysis was performed to detect TLR4, MyD88, TRAF-6, LOX-1, and HMGB1 protein levels, and the findings demonstrate a similar tendency as with mRNA (Table 2 and Fig. 2). The LPS group showed markedly up-regulated TLR4, MyD88, TRAF-6, LOX-1, and HMGB1 protein levels compared with the controls ( $p < 0.05$ ). Ketamine intervention significantly reduced the protein levels, but they were still higher than those in the controls ( $p < 0.05$ ).

**Table 1.** mRNA expression levels of TLR4, MyD88, TRAF-6, LOX-1, and HMGB1 in rat lung tissue

Group	n	TLR4	MyD88	TRAF-6	LOX-1	HMGB1
Control	1	1.00 $\pm$ 0.21	1.00 $\pm$ 0.22	1.00 $\pm$ 0.18	1.00 $\pm$ 0.19	1.00 $\pm$ 0.20
LPS	10	3.89 $\pm$ 0.31 <sup>a</sup>	2.96 $\pm$ 0.28 <sup>a</sup>	2.45 $\pm$ 0.42 <sup>a</sup>	1.87 $\pm$ 0.25 <sup>a</sup>	3.24 $\pm$ 0.34 <sup>a</sup>
Ketamine + LPS	10	1.58 $\pm$ 0.27 <sup>ab</sup>	2.02 $\pm$ 0.25 <sup>ab</sup>	1.85 $\pm$ 0.32 <sup>ab</sup>	1.37 $\pm$ 0.36 <sup>ab</sup>	1.64 $\pm$ 0.23 <sup>ab</sup>

<sup>a</sup> $p < 0.05$ , compared with the controls; <sup>b</sup> $p < 0.05$ , compared with the LPS group; LPS – lipopolysaccharide; n – number.

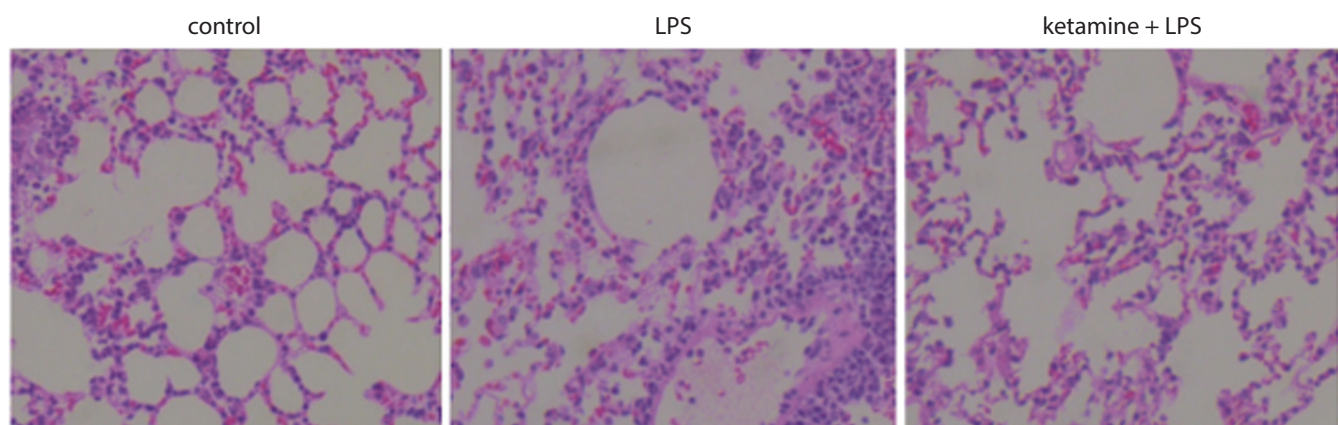


**Fig. 1.** Histological changes of acute lung injury. In the control group, the pulmonary alveolar, interstitial and bronchial vessels were normal. However, the lung tissues in rats treated with LPS were damaged, with obvious pulmonary edema, positive cell infiltration and visible focal necrosis. Rats receiving ketamine displayed a thick alveolar wall, alleviated hyperemia, reduced exudation in the pulmonary alveolar cavity, and relieved infiltration of inflammatory cells

**Table 2.** Protein levels of TLR4, MyD88, TRAF-6, LOX-1, and HMGB1 in rat lung tissue

Group	n	TLR4	MyD88	TRAF-6	LOX-1	HMGB1
Control	10	0.81 ± 0.14	0.58 ± 0.12	0.71 ± 0.14	0.51 ± 0.09	0.78 ± 0.15
LPS	10	1.20 ± 0.10 <sup>a</sup>	0.72 ± 0.11 <sup>a</sup>	0.97 ± 0.13 <sup>a</sup>	1.00 ± 0.11 <sup>a</sup>	1.38 ± 0.13 <sup>a</sup>
Ketamine + LPS	10	0.95 ± 0.12 <sup>a,b</sup>	0.62 ± 0.10 <sup>a,b</sup>	0.81 ± 0.10 <sup>a,b</sup>	0.72 ± 0.12 <sup>a,b</sup>	1.04 ± 0.13 <sup>a,b</sup>

<sup>a</sup> $p < 0.05$ , compared with the controls; <sup>b</sup> $p < 0.05$ , compared with the LPS group; LPS – lipopolysaccharide; n – number.

## TLR4 and HMGB1 protein level correlation analysis in rat lung tissue

Pearson analysis was performed to test TLR4 and HMGB1 protein correlation in the rat lung tissue (Fig. 3). The results show that there was a positive correlation between TLR4 and HMGB1 expression in the LPS and ketamine groups ( $r = 0.952$ ,  $p < 0.001$ ;  $r = 0.941$ ,  $p < 0.001$ ).

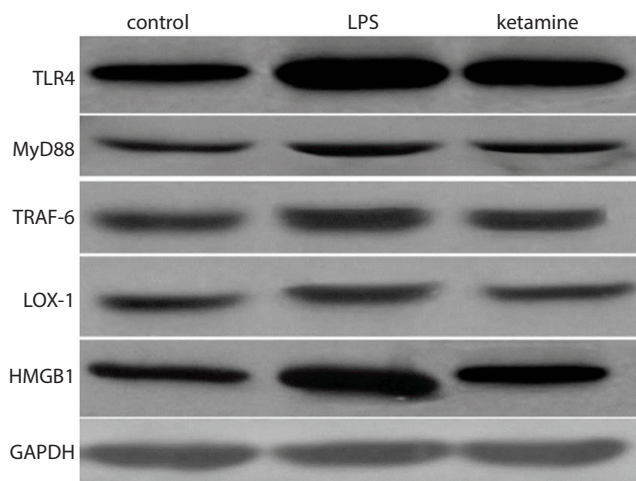


**Fig. 2.** Western blot analysis of protein levels in lung tissue among the 3 groups. The LPS group showed markedly upregulated protein levels of TLR4, MyD88, TRAF-6, LOX-1, and HMGB1 compared with the controls; ketamine intervention obviously reduced these levels, but they were still higher than in the controls

## Discussion

Ketamine, a derivative of phencyclidine, is a noncompetitive N-methyl-D-aspartic acid (NMDA) receptor antagonist and is usually used in anesthesia. Ketamine

can suppress the release of inflammatory factors, such as tumor necrosis factor  $\alpha$  (TNF- $\alpha$ ), interleukin (IL)-6 and IL-8.<sup>20</sup> It was found that ketamine also can inhibit the TLR4 signaling pathway.<sup>21,22</sup> It was reported that ketamine can delay the progress of ALI. In addition, HMGB1 expression is associated with the occurrence of ALI, and inhibiting HMGB1 expression can ameliorate ALI. TLR4 is the receptor for HMGB1, so suppressing the TLR/NF- $\kappa$ B signaling pathway can restrain ALI inflammation.<sup>23</sup> Therefore, we have reasons to believe that ketamine may attenuate HMGB1-induced ALI by regulating the TLR4 signaling pathway.

This study used LPS to establish a rat ALI model and tested molecules related to HMGB1 and the TLR4 signaling pathway in lung tissue. The results showed that the TLR4, MyD88, TRAF-6, LOX-1, and HMGB1 mRNA and protein levels were significantly higher in the LPS group than in the control group. This suggests that both HMGB1 and the TLR4 signaling pathway are involved in ALI. Wang et al. demonstrated that HMGB1 was clearly upregulated in ALI, further proving that HMGB1 plays an important role in this disease.<sup>24</sup> Abdelmageed et al. reported that the TLR4 signaling pathway was involved in the occurrence of ALI, further confirming the critical role of the TLR4 signaling pathway in ALI.<sup>25</sup>

As TLR4 siRNA can alleviate HMGB1-induced inflammation,<sup>17</sup> it appears that ketamine may attenuate HMGB1-induced ALI by regulating the TLR4 signaling pathway. This also demonstrates that clinical drug therapy can inhibit inflammation and delay the ALI process by regulating the TLR4 signaling pathway. Similarly, Qin et al. also discovered that ketamine can downregulate HMGB1 and TLR4 protein levels in bronchoalveolar lavage fluid and lung tissue.<sup>26</sup> In the present study, we found that ketamine intervention significantly decreased TLR4,

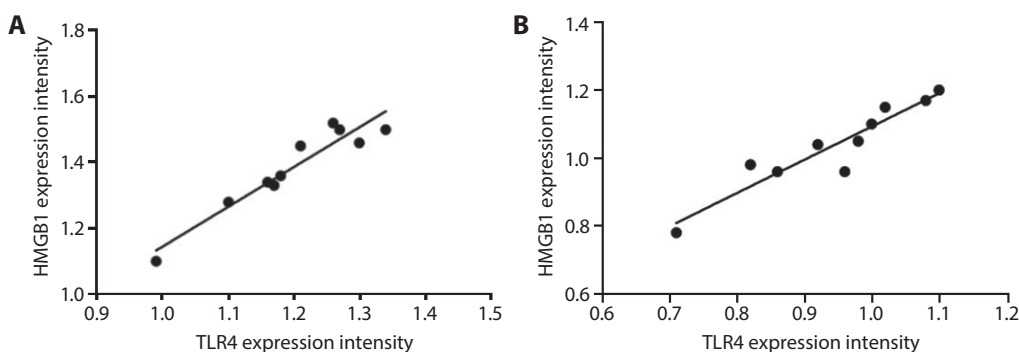


**Fig. 3.** Correlative analysis of TLR4 and HMGB1 level in rat lung tissue. There was a positive correlation between TLR4 and HMGB1 expression in the LPS (A) and ketamine + LPS (B) groups ( $r = 0.952$ ,  $p < 0.001$ ;  $r = 0.941$ ,  $p < 0.001$ )

MyD88, TRAF-6, and LOX-1 mRNA and protein expression in comparison with the LPS group. In addition, TLR4 and HMGB1 expression displayed a positive correlation. Our study suggests that ketamine ameliorates ALI, possibly by regulating the TLR4/HMGB1 signaling pathway, thus exerting anti-inflammatory effects. However, future studies are required to confirm this finding.

The mechanism of ALI is complicated, while ketamine may also have an intricate network in treating ALI. This study only found that ketamine may attenuate HMGB1-induced ALI by regulating the TLR4 signaling pathway. Further investigation is needed in order to clarify its specific mechanism.

### ORCID iDs

Lei Chao  <https://orcid.org/0000-0001-8247-897X>  
 Dong Xu  <https://orcid.org/0000-0002-5199-1110>  
 Xang Sun  <https://orcid.org/0000-0002-3338-5432>  
 Yang Zhang  <https://orcid.org/0000-0002-4141-6630>

### References

- Kao RL, Xu X, Xenocostas A, et al. Induction of acute lung inflammation in mice with hemorrhagic shock and resuscitation: Role of HMGB1. *J Inflamm (Lond)*. 2014;11(1):30.
- Luh SP, Chiang CH. Acute lung injury/acute respiratory distress syndrome (ALI/ARDS): The mechanism, present strategies and future perspectives of therapies. *J Zhejiang Univ Sci B*. 2007;8(1):60–69.
- Villar J, Sulemanji D, Kacmarek RM. The acute respiratory distress syndrome: Incidence and mortality, has it changed? *Curr Opin Crit Care*. 2014;20(1):3–9.
- Berger MM, Pitzer B, Zugel S, et al. Alveolar but not intravenous S-ketamine inhibits alveolar sodium transport and lung fluid clearance in rats. *Anesth Analg*. 2010;111(1):164–170.
- Yang CL, Chen CH, Tsai PS, Wang TY, Huang CJ. Protective effects of dexmedetomidine-ketamine combination against ventilator-induced lung injury in endotoxemia rats. *J Surg Res*. 2011;167(2):e273–e281.
- Yang CH, Tsai PS, Wang TY, Huang CJ. Dexmedetomidine-ketamine combination mitigates acute lung injury in haemorrhagic shock rats. *Resuscitation*. 2009;80(10):1204–1210.
- Shen H, Jin L, Zhuang X, Zhou Y. A single small dose of ketamine prevents lung injury following hepatic ischemia-reperfusion in rabbits. *J Chin Med Assoc*. 2011;74(8):350–356.
- Erdem MK, Yurdakan G, Yilmaz-Sipahi E. The effects of ketamine, midazolam and ketamine/xylazine on acute lung injury induced by alpha-naphthylthiourea in rats. *Adv Clin Exp Med*. 2014;23(3):343–351.
- Wang WF, Liu S, Xu B. A study of the protective effect and mechanism of ketamine on acute lung injury induced by mechanical ventilation. *Eur Rev Med Pharmacol Sci*. 2017;21(6):1362–1367.
- Dange RB, Agarwal D, Teruyama R, Francis J. Toll-like receptor 4 inhibition within the paraventricular nucleus attenuates blood pressure and inflammatory response in a genetic model of hypertension. *J Neuroinflammation*. 2015;12:31.
- Wang H, Bloom O, Zhang M, et al. HMG-1 as a late mediator of endotoxin lethality in mice. *Science*. 1999;285(5425):248–251.
- Zhou M, Zhang Y, Chen X, et al. PTEN-Foxo1 signaling triggers HMGB1-mediated innate immune responses in acute lung injury. *Immunol Res*. 2015;62(1):95–105.
- Entezari M, Javdan M, Antoine DJ, et al. Inhibition of extracellular HMGB1 attenuates hyperoxia-induced inflammatory acute lung injury. *Redox Biol*. 2014;2:314–322.
- Haitisma JJ, Lachmann B, Papadakis PJ. Additives in intravenous anesthesia modulate pulmonary inflammation in a model of LPS-induced respiratory distress. *Acta Anaesthesiol Scand*. 2009;53(2):176–182.
- Liu XX, Yu DD, Chen MJ, et al. Hesperidin ameliorates lipopolysaccharide-induced acute lung injury in mice by inhibiting HMGB1 release. *Int Immunopharmacol*. 2015;25(2):370–376.
- Chen Y, Huang XJ, Yu N, et al. HMGB1 contributes to the expression of P-glycoprotein in mouse epileptic brain through toll-like receptor 4 and receptor for advanced glycation end products. *PLoS One*. 2015;10(10):e0140918.
- Li G, Wu X, Yang L, et al. TLR4-mediated NF-kappaB signaling pathway mediates HMGB1-induced pancreatic injury in mice with severe acute pancreatitis. *Int J Mol Med*. 2016;37(1):99–107.
- Lai CH, Wang KC, Lee FT, et al. Toll-like receptor 4 is essential in the development of abdominal aortic aneurysm. *PLoS One*. 2016;11(1):e0146565.
- Gokcinar D, Ergin V, Cumaoglu A, Menevse A, Aricioglu A. Effects of ketamine, propofol, and ketofol on pro-inflammatory cytokines and markers of oxidative stress in a rat model of endotoxemia-induced acute lung injury. *Acta Biochim Pol*. 2013;60(3):451–456.
- Lange M, Broking K, van Aken H, Hucklenbruch C, Bone HG, Westphal M. Role of ketamine in sepsis and systemic inflammatory response syndrome [in German]. *Anaesthesist*. 2006;55(8):883–891.
- Wu Y, Li W, Zhou C, et al. Ketamine inhibits lipopolysaccharide-induced astrocytes activation by suppressing TLR4/NF-kB pathway. *Cell Physiol Biochem*. 2012;30(3):609–617.
- Yu M, Shao D, Yang R, Feng X, Zhu S, Xu J. Effects of ketamine on pulmonary inflammatory responses and survival in rats exposed to polymicrobial sepsis. *J Pharm Pharm Sci*. 2007;10(4):434–442.
- Tianzhu Z, Shumin W. Esculin inhibits the inflammation of LPS-induced acute lung injury in mice via regulation of TLR/NF-kappaB pathways. *Inflammation*. 2015;38(4):1529–1536.
- Wang SY, Li ZJ, Wang X, Li WF, Lin ZF. Effect of ulinastatin on HMGB1 expression in rats with acute lung injury induced by sepsis. *Genet Mol Res*. 2015;14(2):4344–4353.
- Abdelmageed ME, El-Awady MS, Suddek GM. Apocynin ameliorates endotoxin-induced acute lung injury in rats. *Int Immunopharmacol*. 2016;30:163–170.
- Qin MZ, Gu QH, Tao J, et al. Ketamine effect on HMGB1 and TLR4 expression in rats with acute lung injury. *Int J Clin Exp Pathol*. 2015;8(10):12943–12948.



# Extracorporeal shockwave therapy enhances peripheral nerve remyelination and gait function in a crush model

Hyun Jung Park<sup>1,B,C</sup>, Jinpyo Hong<sup>1,B</sup>, Yibo Piao<sup>1,B</sup>, Hyo Jung Shin<sup>1,2,B</sup>, Se Jeong Lee<sup>3,B</sup>,  
Im Joo Rhyu<sup>3,B</sup>, Min-Hee Yi<sup>4,A,B</sup>, Jinhyun Kim<sup>5,A</sup>, Dong Woon Kim<sup>1,2,A,E</sup>, Jaewon Beom<sup>6,A,C,D,F</sup>

<sup>1</sup> Department of Anatomy, Brain Research Institute, Chungnam National University School of Medicine, Daejeon, South Korea

<sup>2</sup> Department of Medical Science, Chungnam National University School of Medicine, Daejeon, South Korea

<sup>3</sup> Department of Anatomy, Korea University College of Medicine, Seoul, South Korea

<sup>4</sup> Department of Neurology, Mayo Clinic, Rochester, USA

<sup>5</sup> Department of Internal Medicine, Chungnam National University Hospital, Chungnam National University School of Medicine, Daejeon, South Korea

<sup>6</sup> Department of Rehabilitation Medicine, Seoul National University Bundang Hospital, Seongnam, South Korea

A – research concept and design; B – collection and/or assembly of data; C – data analysis and interpretation;

D – writing the article; E – critical revision of the article; F – final approval of the article

Advances in Clinical and Experimental Medicine, ISSN 1899–5276 (print), ISSN 2451–2680 (online)

*Adv Clin Exp Med.* 2020;29(7):819–824

## Address for correspondence

Jaewon Beom

E-mail: powe5@snubh.org

## Funding sources

The Basic Science Research Program through the National Research Foundation of Korea (NRF) (grants No. 2016R1D1A1B03933919 and No. 2016R1A2B4009409) funded this research.

## Conflict of interest

None declared

Received on April 8, 2019

Accepted on May 8, 2020

Published online on July 31, 2020

## Cite as

Park HJ, Hong J, Piao Y, et al. Extracorporeal shockwave therapy enhances peripheral nerve remyelination and gait function in a crush model. *Adv Clin Exp Med.* 2020;29(7):819–824. doi:10.17219/acem/122177

## DOI

10.17219/acem/122177

## Copyright

© 2020 by Wrocław Medical University

This is an article distributed under the terms of the Creative Commons Attribution 3.0 Unported (CC BY 3.0) (<https://creativecommons.org/licenses/by/3.0/>)

## Abstract

**Background.** Conservative treatment, such as electrical stimulation and steroid injection, have been employed in an attempt to improve symptoms after peripheral nerve injury, without significant success. Although non-invasive and safe extracorporeal shockwave therapy (ESWT) can be a practical alternative, the therapeutic effects of ESWT on peripheral nerve remyelination has not been established.

**Objectives.** To investigate the effects of ESWT on peripheral nerve remyelination and gait function for 5 weeks in a sciatic nerve crush model.

**Material and methods.** In total, we divided 97 rats into 5 groups: group 1 – a healthy negative control group; group 2 – 3 weeks after sciatic nerve crush and 3 sessions of ESWT; group 3 – 5 weeks after crush injury with 3 sessions of ESWT; group 4 – 3 weeks after crush injury with no ESWT; and group 5 – 5 weeks after crush injury with no ESWT. The focused ESWT was applied to the unilateral sciatic nerve injury site. One session consisted of 1,500 stimuli, and the session were performed at intervals of 1 week.

**Results.** The degree of myelination and expression of myelin basic protein at the distal part of the injured sciatic nerve tended to increase in the ESWT groups compared with the no-ESWT groups 3 and 5 weeks after crush injury. Regarding the functional gait recovery, the print width and area of the injured leg in the ESWT groups was significantly larger than that in the no-ESWT groups 3 and 5 weeks after crush injury.

**Conclusions.** The ESWT may enhance peripheral nerve remyelination and gait function in a nerve crush model. Long-term follow-up after ESWT and investigation of molecular mechanisms will be needed to confirm these therapeutic effects.

**Key words:** peripheral nerve injuries, extracorporeal shockwave therapy, myelin basic protein, remyelination, gait

## Introduction

Trauma or entrapment, herniated intervertebral discs, and cancer metastasis can cause damage to the peripheral nervous system, resulting in various neuromuscular disorders, depending on the location and extent of the lesion. These conditions present focal neuropathy, plexopathy and radiculopathy, all of which are associated with neuropathic pain and muscle paralysis. The clinical importance of peripheral neuropathy is increasing because of the rising number of neuromuscular diseases due to aging of the society. The aim of treatment is to improve the function and quality of life, in patients with peripheral neuropathy.

Inflammatory reactions occur as macrophages invade the tissue surrounding damaged peripheral nerves. Next, Wallerian degeneration, demyelination and axon regeneration processes are initiated, with various signaling pathways involved. During this process, Schwann cells play a key role in orchestrating repair.<sup>1–3</sup> Extracorporeal shockwave therapy (ESWT) has long been used in urinary stone lithotripsy treatment. In the musculoskeletal field, it has been widely used and researched in lateral and medial epicondylitis, plantar fasciitis, calcific tendinitis of the shoulder, and bony union after fracture. Recently, it has been suggested that these indications should be expanded to include muscle rigidity, muscular pain, knee degenerative arthritis, and lymphedema.<sup>4</sup>

Peripheral nerves regenerate slowly in the human tissues. Various conservative treatments such as electrical stimulation and steroid injection have been used in an attempt to alleviate symptoms after peripheral nerve injury, but without significant results. Recently, stem cell injection has been proven to be effective in animal studies of peripheral nerve injury, but its safety has not been established for long-term follow-up in clinical practice. Thus, non-invasive ESWT may be a realistic alternative. However, the effects of ESWT on angiogenesis, metabolic activation and inflammation response have been suggested but remain to be established. In addition, stimulation parameters such as optimized stimulation intensity (mJ/mm<sup>2</sup>), and number and duration of treatment sessions are also different and remain controversial between studies. Although the efficacy and safety of ESWT have been established, studies on the mechanism of effect are essential in order to expand clinical applications.

The ESWT is thought to cause molecular and biological changes, in addition to mechanical and physical stimulation by shockwave, but it is difficult to determine which among various signaling pathways is involved. It has previously been shown that adipose-derived stem cells maintain pluripotency when ESWT is applied and promote differentiation into Schwann-like cells.<sup>5</sup> It has also been shown that ESWT induces the proliferation of bone marrow stromal cells and their differentiation into osteoprogenitors via induction

of TGF- $\beta$ 1.<sup>6</sup> Recent animal studies have also shown that ESWT stimulates peripheral nerve regeneration.<sup>7–8</sup>

Although ESWT is actively used to treat various diseases other than peripheral nerve damage, its therapeutic effects need to be investigated through animal experiments to validate clinical use and study. We investigated the effects of ESWT on peripheral nerve remyelination and gait function for 5 weeks in a sciatic nerve crush model.

## Material and methods

### Animal model

Nine-week old male Sprague Dawley rats were anesthetized with isoflurane inhalation, and were subject to right sciatic nerve crush proximal to the bisection area with forceps for 40 s. After the crushed nerve was released, the sciatic nerve remained compressed and became pale (Fig. 1). A single endoneurial suture was conducted using 8-0 nylon in order to identify the site of injury when collecting tissue. After the rat recovered from general anesthesia, acetaminophen syrup was administered orally to relieve postoperative pain. Ninety-seven rats were divided into 5 groups: group 1 – healthy group as a negative control; group 2 – 3 weeks after crush injury with 3 sessions of ESWT; group 3 – 5 weeks after crush injury with 3 sessions of ESWT; group 4 – 3 weeks after crush injury with no ESWT applied; and group 5 – 5 weeks after crush injury with no ESWT. The study protocol was reviewed and approved by the Institutional Animal Care and Use Committee of Chungnam National University Hospital, Daejeon, South Korea.

### Extracorporeal shockwave therapy

The focused ESWT device (Dornier MedTech, Weßling, Germany), which is widely used in clinical fields, was applied only to the unilateral sciatic nerve injury site. One session consisted of 1,500 stimuli, and the sessions were performed at intervals of 1 week. Peripheral nerves and surrounding tissues were collected from different animals at 1 week and 3 weeks after the 3 sessions of ESWT were completed.

### Immunostaining

Immunofluorescence was performed on tissue collected 3 or 5 weeks after crush injury. The rats were anesthetized with sodium pentobarbital (50 mg/kg, intraperitoneal) and perfused transcardially with heparinized phosphate-buffered saline (PBS, pH 7.4), followed by perfusion with 4% paraformaldehyde for 15 min. The sciatic nerve from the injured site was removed immediately. Cryoblocks were sectioned and immunostained with anti-myelin basic protein (MBP) primary antibody (1:400; #MAB386, Merck Millipore, Burlington, USA).

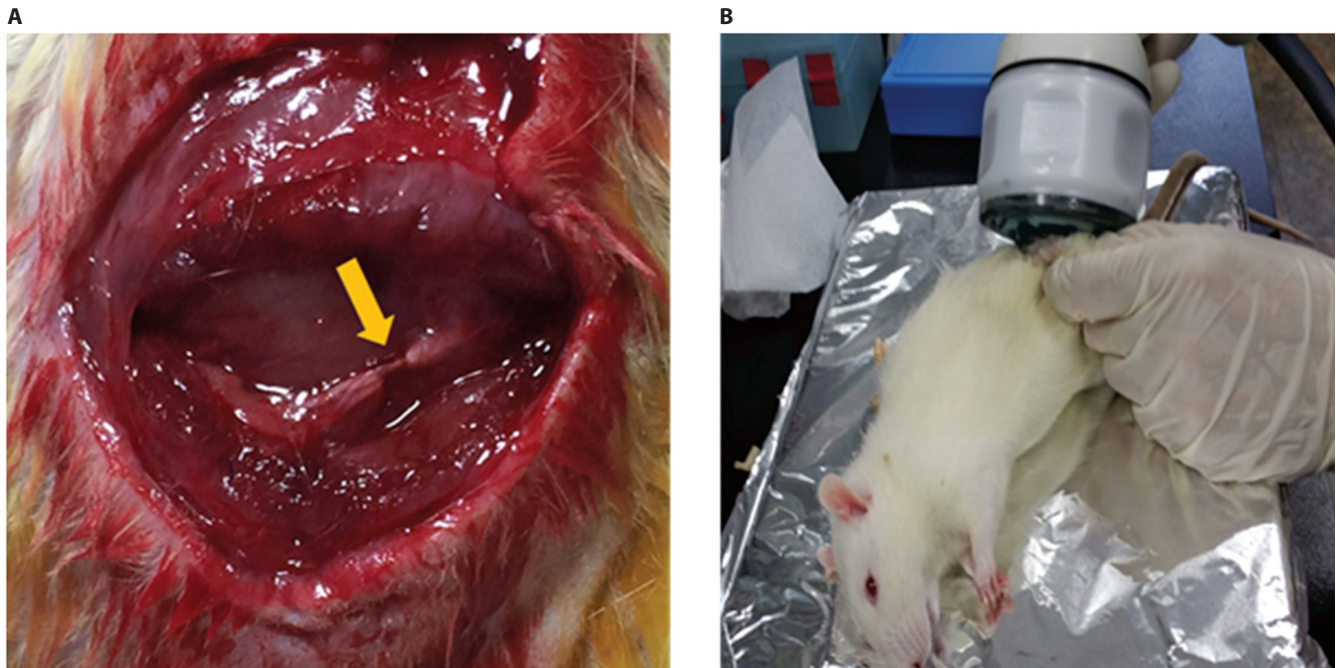


**Fig. 1.** Sciatic nerve crush and application of ESWT. A. When sciatic nerve crush was applied to the proximal portion of the sciatic nerve for 40 s, the nerve became compressed and pale (arrow). B. ESWT was applied to the sciatic nerve injury site

## Electron microscopy

The sciatic nerve was removed and stored in the fresh fixative solution overnight at 4°C. Tissues were washed in 0.1 M phosphate buffer, post-fixed in 1% osmium tetroxide for 2 h and dehydrated through an ascending series of ethanol and propylene oxide, and then embedded in Epon812 mixture (Oken Shoji, Tokyo, Japan). Semi-thin sections (×200 magnification) were made using Leica EM UC7 ultramicrotome (Leica Microsystems, Wetzlar, Germany), mounted on #200 mesh copper grids, stained with 2% uranyl acetate and Reynold's lead citrate for 5 min each, and observed under a Hitachi H-7650 transmission electron microscope (Hitachi, Tokyo, Japan) at the accelerating voltage of 80 kV.

## Quantitative polymerase chain reaction

Since the tissue volume of the rat sciatic nerve is low, right sciatic nerves of 3 rats were harvested and pooled. Total RNA was extracted from the sciatic nerve tissue using TRIzol reagent (Invitrogen, Carlsbad, USA) according to the manufacturer's instructions. After purification with a RNA isolation kit (Hybrid-R; GeneAll Biotechnology, Seoul, South Korea; 305-101) the concentration and purity of RNA were assessed using the NanoDrop spectrophotometer (Thermo Fisher Scientific, Waltham, USA).

Total RNA was used for cDNA synthesis with a TOPscript cDNA synthesis kit (Enzymomics, Daejeon, South Korea; RT 220) in a 20 µL reaction. Subsequently,

quantitative polymerase chain reaction (qPCR) was performed in duplicate in a total volume of 10 µL, including each 5 pM primer, cDNA and TOPreal qPCR SYBR mix (Enzymomics; RT 500). The qPCR conditions were 95°C for 10 min, then 40 amplification cycles of 95°C for 15 s and 60°C for 1 min (AriaMx Realtime PCR System; Agilent Technologies Santa Clara, USA). The primer sequences (Cosmogenetech, Daejeon, South Korea) used for qPCR were as follows: rat *GAPDH*, forward: 5'- CTC ATG ACC ACA GTC CAT GC -3', reverse: 5'- TTC AGC TCT GGG ATG ACC TT -3'; rat *MBP* forward 5'-agagacccctcacagcgacac-3', reverse 5'-agggagccgtagtggtag-3'. The mRNA expression level was normalized to *GAPDH*, and the relative mRNA expression was calculated using the  $2^{-\Delta\Delta C_t}$  method, as previously described.<sup>9</sup>

## CatWalk-automated gait analysis

We performed gait analysis using the CatWalk XT system (Noldus Information Technology, Wageningen, the Netherlands) as a functional evaluation after 1 week of adaptation. Print width (cm) and area (cm<sup>2</sup>) of the right leg were divided by those of the left leg at 3 and 5 weeks respectively after crush injury to derive a ratio of print width and area between both legs.

## Statistics

Statistical analyses were carried out with PASW Statistics v. 18 software (SPSS Inc., Chicago, USA). The Mann-Whitney U test was used to compare differences in qPCR

results. The independent t-test and analysis of variance (ANOVA) were used to compare differences in CatWalk data at 3 and 5 weeks each. Differences were considered significant at a p-value <0.05.

## Results

### Degree of myelination

The distal part of the injured sciatic nerve was prepared and observed. In transmission electron microscopy ( $\times 3,000$  magnification) and immunofluorescence staining, the degree of myelination tended to increase in the ESWT stimulation groups compared to the no-ESWT groups 3 and 5 weeks after crush injury (Fig. 2A,B). In qPCR, expression of MBP tended to be higher in the ESWT groups ( $n = 18$ ) than no-ESWT groups ( $n = 18$ ) when shown using the pooled average method (Fig. 2C).

### Functional gait recovery

In the right sciatic nerve crush model, we performed gait analysis using the CatWalk apparatus as a functional evaluation. Three weeks after crush injury, the print width

and print area (%) of the ESWT groups were significantly larger than in the no-ESWT groups ( $p = 0.030$  for width and  $p = 0.003$  for area). This improvement was maintained 5 weeks after crush injury ( $p = 0.009$  for width and  $p = 0.006$  for area) (Fig. 3). This indicates that gait recovery was achieved when ESWT was applied after sciatic nerve injury.

## Discussion

Microsurgical repair has been performed in cases of traumatic or postoperative peripheral nerve transection, but is not applicable to partial neuronal injury. Electrical stimulation has also been used to prevent muscle atrophy caused by peripheral nerve injury, but is not effective on promoting neural recovery in severe injury.

Stem cell application has recently been suggested as a potential innovative treatment.<sup>10</sup> Stem cells are being tested for amyotrophic lateral sclerosis and serious central nervous system disorders such as stroke and spinal cord injury, and are not commercially available for peripheral neuropathy due to possible long-term adverse effects. The PTEN blockers and microRNA-222 have been studied in animals,<sup>11,12</sup> but they have not been used in the clinical

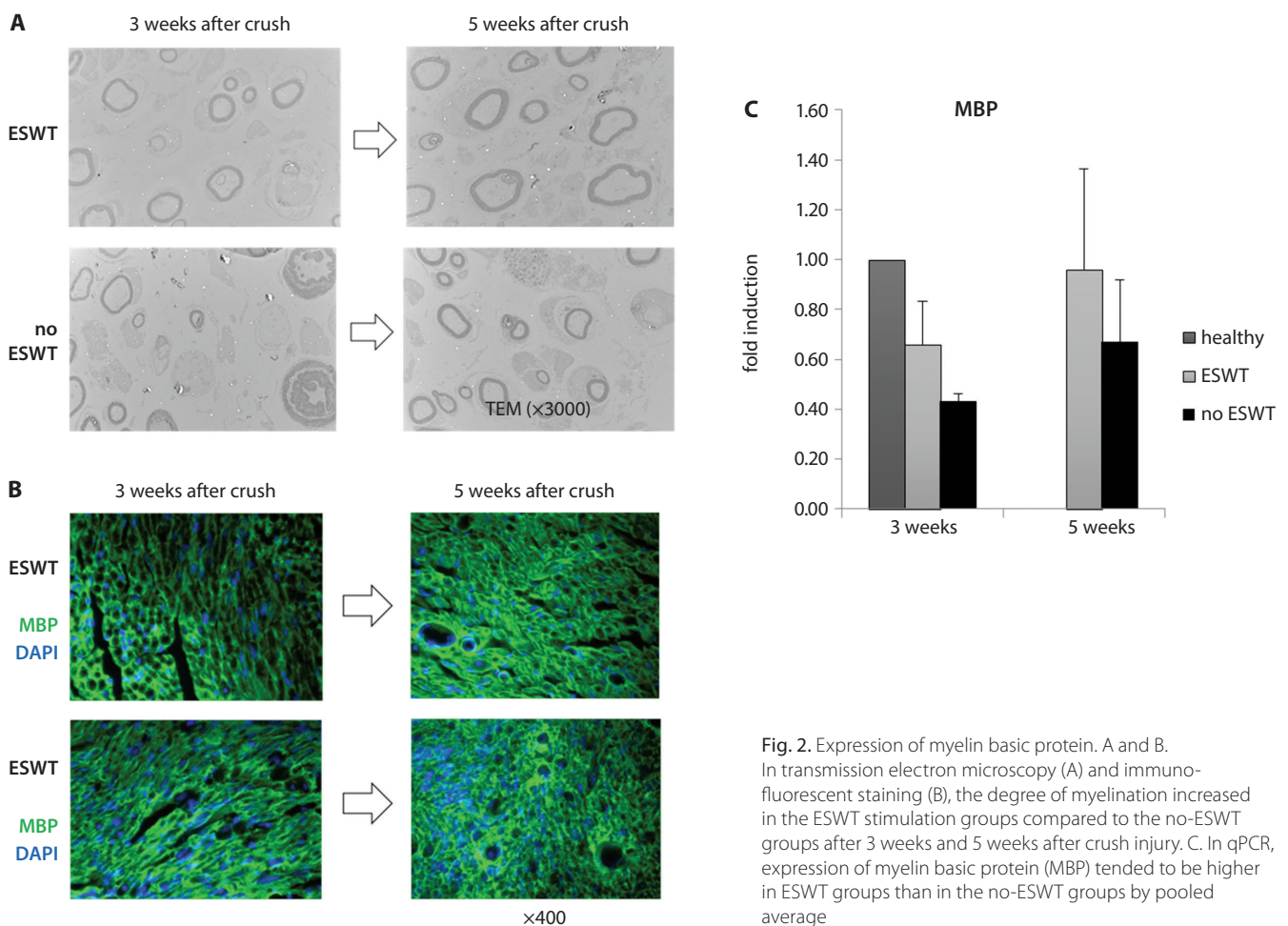


Fig. 2. Expression of myelin basic protein. A and B. In transmission electron microscopy (A) and immunofluorescent staining (B), the degree of myelination increased in the ESWT stimulation groups compared to the no-ESWT groups after 3 weeks and 5 weeks after crush injury. C. In qPCR, expression of myelin basic protein (MBP) tended to be higher in ESWT groups than in the no-ESWT groups by pooled average

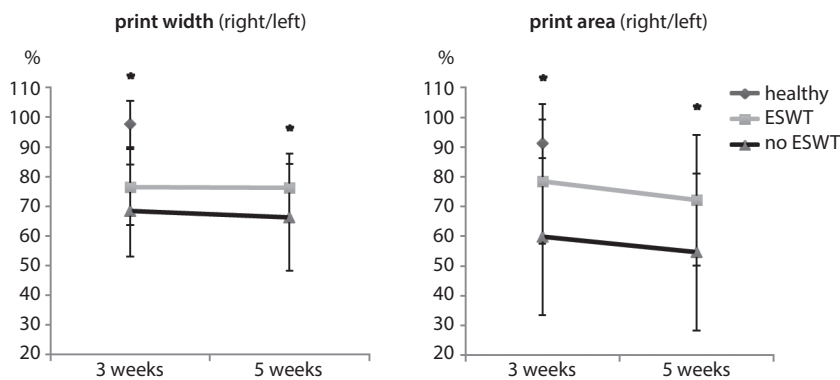


Fig. 3. Gait analysis using CatWalk. Three weeks after crush injury, the ESWT group had significantly larger print width and print area (%) than the no-ESWT group ( $p = 0.030$  for width and  $p = 0.003$  for area). This improvement was maintained 5 weeks after crush injury ( $p = 0.009$  for width and  $p = 0.006$  for area).

field. Therefore, there is a need to develop a realistic and non-adverse treatment modality that can be immediately applied to patients with peripheral nerve damage causing functional decline and poor quality of life.

Recent studies have shown that Schwann cells are the major expression cells of *GDF15*, and may be involved in the regeneration of peripheral nerves through increases in the myelination of injured peripheral nerves or through improving nerve conduction velocity.<sup>13–15</sup> However, in vivo experiments focused on the mechanisms have not been performed. Schwann cells are an important cell type involved in the myelination of peripheral nerves, and Schwann cell plasticity and de-differentiation are newly suggested restoration mechanisms after injury. In normal conditions, Schwann cells are in a resting state that has no other function except for its basic role of nerve conduction. However, when the peripheral nerve is damaged, Schwann cells maintain the function of neuronal cells. This is a substantial phenotypic transformation of Schwann cells, referred to as plasticity or de-differentiation.<sup>16</sup> Schwann cell de-differentiation is largely divided into 2 mechanisms. Firstly, it participates in the demyelination process by activating lysosome or protease proteins. Secondly, it secretes neurotrophic factors involved in peripheral nerve survival or axonal regeneration.

It is also known that the neurotrophic factors secreted during Schwann cell de-differentiation are glial cell-derived neurotrophic factor (GDNF) and extracellular matrix proteins. These factors influence the survival of motor neurons and dorsal root ganglion in the spinal cord, and signal transduction through c-jun is involved in axonal regeneration. These factors and the relationship between GDF15 and Krox20 in the peripheral nerves have not been elucidated. In this study, induction of Schwann cell plasticity could be suggested as a mechanism of peripheral nerve remyelination and functional recovery.

We demonstrated that degree of myelination and expression of MBP tended to increase in the ESWT groups compared to the no-ESWT groups 3 and 5 weeks after crush injury. Regarding functional gait recovery, the print width and areas of the injured leg in the ESWT groups were significantly larger than those in the no-ESWT groups

measured 5 weeks after crush injury. Considering these findings, ESWT may enhance gait function through peripheral nerve remyelination in a crush model.

There could be several limitations in this study. First, toxin-induced demyelination would be more suitable than nerve crush for pure demyelination without axonal loss. However, we selected the crush model that is similar to clinical situation for peripheral nerve injury. Second, the ESWT applicator was relatively large for the lower limb of adult rats. Thus, we tried to focus the center of the applicator on the sciatic nerve crush site. Third, different individuals were analyzed at 3 and 5 weeks after crush injury because rats were sacrificed and tissues harvested at 3 and 5 weeks, respectively. Although longitudinal follow-up in the same individuals would be more reliable to interpret the results, it is not possible in animal studies. Long-term follow-up after ESWT with a small applicator suitable for rats will be needed to confirm the therapeutic effects. Furthermore, molecular mechanisms regarding various signaling pathways are yet to be investigated.

#### ORCID iDs

Hyun Jung Park <https://orcid.org/0000-0002-1982-9172>  
 Jinpyo Hong <https://orcid.org/0000-0002-4776-4396>  
 Yibo Piao <https://orcid.org/0000-0001-9628-4906>  
 Hyo Jung Shin <https://orcid.org/0000-0002-3530-101X>  
 Se Jeong Lee <https://orcid.org/0000-0002-4437-8270>  
 Im Joo Rhyu <https://orcid.org/0000-0002-5558-6278>  
 Min-Hee Yi <https://orcid.org/0000-0003-2066-3584>  
 Jinhyun Kim <https://orcid.org/0000-0001-5235-2612>  
 Dong Woon Kim <https://orcid.org/0000-0001-7691-1394>  
 Jaewon Beom <https://orcid.org/0000-0001-7984-9661>

#### References

- Morton PD, Johnstone JT, Ramos AY, Liebl DJ, Bunge MB, Bethea JR. Nuclear factor-κB activation in Schwann cells regulates regeneration and remyelination. *Glia*. 2012;60(4):639–650.
- Glenn TD, Talbot WS. Signals regulating myelination in peripheral nerves and the Schwann cell response to injury. *Curr Opin Neurobiol*. 2013;23(6):1041–1048.
- Martini R, Fischer S, López-Vales R, David S. Interactions between Schwann cells and macrophages in injury and inherited demyelinating disease. *Glia*. 2008;56(14):1566–1577.
- Bae H, Kim HJ. Clinical outcomes of extracorporeal shock wave therapy in patients with secondary lymphedema: A pilot study. *Ann Rehabil Med*. 2013;37(2):229–234.

5. Schuh CM, Heher P, Weihs AM, et al. In vitro extracorporeal shock wave treatment enhances stemness and preserves multipotency of rat and human adipose-derived stem cells. *Cytotherapy*. 2014;16(12):1666–1678.
6. Hausner T, Pajer K, Halat G, et al. Improved rate of peripheral nerve regeneration induced by extracorporeal shock wave treatment in the rat. *Exp Neurol*. 2012;236(2):363–370.
7. Wu YH, Liang HW, Chen WS, Lai JS, Luh JJ, Chong FC. Electrophysiological and functional effects of shock waves on the sciatic nerve of rats. *Ultrasound Med Biol*. 2008;34(10):1688–1696.
8. Wang FS, Yang KD, Chen RF, Wang CJ, Sheen-Chen SM. Extracorporeal shock wave promotes growth and differentiation of bone-marrow stromal cells towards osteoprogenitors associated with induction of TGF-beta1. *J Bone Joint Surg Br*. 2002;84(3):457–461.
9. Livak KJ, Schmittgen TD. Analysis of relative gene expression data using real-time quantitative PCR and the 2(-delta delta C(T)) method. *Methods*. 2001;25(4):402–408.
10. Lee EJ, Xu L, Kim GH, et al. Regeneration of peripheral nerves by transplanted sphere of human mesenchymal stem cells derived from embryonic stem cells. *Biomaterials*. 2012;33(29):7039–7046.
11. Zhou S, Shen D, Wang Y, et al. microRNA-222 targeting PTEN promotes neurite outgrowth from adult dorsal root ganglion neurons following sciatic nerve transection. *PLoS One*. 2012;7(9):e44768.
12. Wu D, Murashov AK. Molecular mechanisms of peripheral nerve regeneration: Emerging roles of microRNAs. *Front Physiol*. 2013;4:55.
13. Mensching L, Börger AK, Wang X, Charalambous P, Unsicker K, Haastert-Talini K. Local substitution of GDF-15 improves axonal and sensory recovery after peripheral nerve injury. *Cell Tissue Res*. 2012;350(2):225–238.
14. Pereira JA, Lebrun-Julien F, Suter U. Molecular mechanisms regulating myelination in the peripheral nervous system. *Trends Neurosci*. 2012;35(2):123–134.
15. Hung HA, Sun G, Keles S, Svaren J. Dynamic regulation of Schwann cell enhancers after peripheral nerve injury. *J Biol Chem*. 2015;290(11):6937–6950.
16. Jessen KR, Mirsky R. Negative regulation of myelination: Relevance for development, injury, and demyelinating disease. *Glia*. 2008;56(14):1552–1565.

# Continuous exposure of PM2.5 exacerbates ovalbumin-induced asthma in mouse lung via a JAK-STAT6 signaling pathway

Yonghui Yang<sup>1,A–C</sup>, Xiaoxia Li<sup>1,B,C</sup>, Xiaoying An<sup>2,B–D</sup>, Ling Zhang<sup>3,B,C</sup>, Xingbin Li<sup>3,B,C</sup>, Liang Wang<sup>3,B,C</sup>, Guiyun Zhu<sup>1,D–F</sup>

<sup>1</sup> Department of Pathology, Hebei Province Chest Hospital, Lung Cancer Prevention and Control Center of Hebei Province, Shijiazhuang, China

<sup>2</sup> Laboratory of Molecular Biology, Hebei Province Chest Hospital, Lung Cancer Prevention and Control Center of Hebei Province, Shijiazhuang, China

<sup>3</sup> Department of Pneumology, Hebei Province Chest Hospital, Lung Cancer Prevention and Control Center of Hebei Province, Shijiazhuang, China

A – research concept and design; B – collection and/or assembly of data; C – data analysis and interpretation;

D – writing the article; E – critical revision of the article; F – final approval of the article

Advances in Clinical and Experimental Medicine, ISSN 1899–5276 (print), ISSN 2451–2680 (online)

*Adv Clin Exp Med.* 2020;29(7):825–832

## Address for correspondence

Guiyun Zhu

E-mail: zgyblk@163.com

## Funding sources

The China government funds of excellent clinical medical talents and basic research projects.

## Conflict of interest

None declared

Received on September 1, 2019

Reviewed on December 28, 2019

Accepted on April 24, 2020

Published online on June 28, 2020

## Abstract

**Background.** Epidemiological studies and mice models have demonstrated that air pollution containing particulate matter smaller than 2.5  $\mu\text{m}$  (PM2.5) exacerbates acute episodes of asthma in both children and adults.

**Objectives.** To investigate the effect of continuous PM2.5 treatment on asthma regulation mechanism behind this effect.

**Material and methods.** In this study, the effects of continuous exposure to PM2.5 on asthma and eosinophil recruitment was compared to the effect of a single pre-ovalbumin (OVA)-sensitization exposure to PM2.5. Wild-type mice were either challenged once with PM2.5 + OVA before sensitization and asthma induction over a 27-day period, or with 5 times of PM2.5 + OVA treatment and sensitization/asthma induction over the same period.

**Results.** Continuous exposure to PM2.5 significantly increased total plasma immunoglobulin E (IgE), bronchial alveolar lavage fluid (BALF) cell numbers, eosinophils, and macrophages, leading to increased lung injury. This effect was regulated through increased production of chemokines and cytokines, such as interleukin (IL)-1 $\beta$ , monocyte chemoattractant protein 1 (MCP-1), IL-12, IL-5, IL-13, and prostaglandin D2 (PGD<sub>2</sub>). Eosinophil recruitment during continuous PM2.5 treatment was regulated through phosphorylation of the JAK/STAT6 pathway. As this study shows, continuous PM2.5 treatment significantly worsens asthma as compared to single exposure to PM2.5 or OVA exposure alone.

**Conclusions.** Our findings reveal that continuous exposure of PM2.5 exacerbates OVA-induced asthma in mouse lung through JAK-STAT6 signaling pathway.

**Key words:** inflammation, asthma, PM2.5, JAK-STAT6 pathway

## Cite as

Yang Y, Li X, An X, et al. Continuous exposure of PM2.5 exacerbates ovalbumin-induced asthma in mouse lung via a JAK-STAT6 signaling pathway. *Adv Clin Exp Med.* 2020;29(7):825–832. doi:10.17219/acem/121009

## DOI

10.17219/acem/121009

## Copyright

© 2020 by Wrocław Medical University

This is an article distributed under the terms of the Creative Commons Attribution 3.0 Unported (CC BY 3.0) (<https://creativecommons.org/licenses/by/3.0/>)

## Introduction

A combination of enormous population growth, rapid urbanization and industrialization in China has led to a massive increase of air pollution, a phenomenon previously observed in developed countries.<sup>1–3</sup> A detrimental effect from increased air pollution is that the general population is exposed to harmful air pollutants containing particulate matter (PM). Particulate matter contains an extensive variety of toxic substances derived from industrial and vehicular emissions, coal combustions, sea salt, and soil dusts.<sup>3</sup> Depending on the city where the pollutant is collected, PM can contain varying amounts of fossil fuel combustion remains, such as polycyclic aromatic hydrocarbons, sulfates (SO<sub>4</sub><sup>2-</sup>), nitrates (NO<sub>3</sub><sup>-</sup>), microbial material, and chemical elements such as iron, zinc, silica, sodium, and aluminium.<sup>4–6</sup> Furthermore, these PMs can remain in the atmosphere for a lengthy amount of time, transverse great distances and easily trigger lung disease.<sup>7</sup> It has been shown that the smaller the particle size, the greater injury PM causes to the lungs.<sup>8</sup>

Particulate matter has been categorized into 2 grades: PM<sub>10</sub>, whose aerodynamic diameter is less than or equal to 10 µm, and PM<sub>2.5</sub>, whose aerodynamic diameter is less than or equal to 2.5 µm. PM<sub>2.5</sub>, a fine particulate matter, poses the greatest risk, as it induces stronger pulmonary and allergic inflammatory responses as compared to larger counterparts when tested at an equal mass dose.<sup>9,10</sup> This was mainly due to a larger surface area to mass ratio. It must also be noted that, in addition to PM surface area, the chemical composition is also an important determinant of the inflammatory response. Since Asian dust aerosols can spread over a large area, including East Asia, the Korean peninsula and Japan, during spring, anthropogenic pollution has become a major public health concern in Eastern Asia.<sup>11</sup>

Asthma, in both children and adults, is a common respiratory disease worldwide. Asthma is characterized by chronic allergic airway inflammation, with episodes of superimposed acute inflammation.<sup>12</sup> Studies have now shown that PM<sub>2.5</sub> is correlated with the exacerbation of asthma in Europe, the Americas, Korea, Japan, and China,<sup>13–17</sup> where ambient air PM<sub>2.5</sub> increases such incidences as asthma-related emergency department visits, worsened wheezing and dyspnea, and children hospital admissions for asthma.<sup>18–21</sup> Asthma morbidity is also positively associated with daily ambient PM<sub>2.5</sub> levels. In Asia, daily admissions in the clinic for asthma, acute respiratory events in children as well as allergic rhinitis in Taipei, Taiwan coincided with Asian dust storm events containing toxic pollutants.<sup>22–25</sup>

During acute exacerbations of asthma, clinical manifestations include eosinophilic airway inflammation in the distal portion of the lung with symptom exaggeration, such as cough, chest tightness and dyspnea.<sup>26</sup> During presentation of asthma, the typical cytokine profile

is generally observed as a T<sub>H</sub>2-type airway inflammation with increased levels of eosinophils, immunoglobulin E (IgE) and the production of T<sub>H</sub>2-related cytokines such as interleukin (IL)-4, IL-5 and IL-13.<sup>27,28</sup> Interleukin 4 is necessary for the polarization of T helper cells towards a T<sub>H</sub>2-phenotype,<sup>29</sup> IL-5 helps promote proliferation and differentiation of B cells<sup>30</sup> and IL-13 induces the induction of T<sub>H</sub>2 cells.<sup>31</sup> Apart from eosinophil recruitment, macrophages are described to play a role in inflammation during allergic airway inflammation.<sup>32,33</sup> In addition, the TLR2/TLR4/MyD88-signaling pathway has been shown to regulate the exacerbation of murine lung eosinophilia during PM<sub>2.5</sub>/ovalbumin (OVA)-induced asthma.<sup>34</sup>

In this study, urban PM was harvested from the atmosphere in Hebei, China. PM<sub>2.5</sub> was administered to mice, together with OVA, to examine the effects of long-term exposure of pollutants on asthma exacerbation. This effect was compared to a short-term sensitization exposure of PM<sub>2.5</sub> to mice. The study investigated pathological changes of lungs, cellular infiltration in the bronchoalveolar lavage fluid (BALF), inflammatory cytokine changes in BALF, OVA-specific IgE antibodies in serum, as well as the role of the JAK/STAT signaling pathway in the recruitment of eosinophils into the lungs. This study was performed to determine the inflammatory mechanism responsible for asthma exacerbation resulting from long-term exposure to PM<sub>2.5</sub> pollutants.

## Material and methods

### Experimental animals

BALB/c mice were kept in pathogen-free conditions and received sterile OVA-free food and water. The mice were maintained on a 12-hour light/dark cycle, under constant room temperature (24°C) and relative humidity (40–80%). The experimental protocols shown in this study were approved by the Institutional Animal Care and Research Advisory Committee at Chongqing Medical University, China. The use of animals in these experiments was in accordance with the guidelines issued by the Chinese Council on Animal Care.

### PM<sub>2.5</sub> particles preparation

Methods of preparing PM<sub>2.5</sub> were provided by the Hubei Province Center for Disease Control and Prevention, China. First, PM<sub>2.5</sub> was collected on a glass fiber filter using a Thermo Anderson high-volume sampler (Thermo Anderson, San Marcos, USA). The sample membrane was equilibrated at 60°C for 6 h before weighing using an analytical balance. The ambient PM<sub>2.5</sub> concentration was calculated from sample weight and air volume. PM<sub>2.5</sub> was recovered from the membrane using a modification of an aqueous extraction technique: the PM<sub>2.5</sub>-adsorbed

membrane was cut into  $1 \times 3 \text{ cm}^2$  size and immersed in ultrapure water for eluting PM2.5, then 'cold-shocked' for 30 min at low temperature 3 times. Finally, PM2.5 was eluted with gauze filtration, vacuum freeze-dried and stored at  $-20^\circ\text{C}$  for future use or sale.

## Study protocol

Four groups ( $n = 10$  per group) of WT mice were prepared for treatment with particles as shown in Fig. 1: (A) control group ( $n = 10$ ); (B) OVA group ( $n = 10$ ); (C) OVA + PM2.5 pre-treated group; and (D) OVA + PM2.5 long-treatment group. For OVA-induced mouse model of asthma, mice were immunized intraperitoneally with 50 mg of OVA in 1 mg of  $\text{Al}(\text{OH})_3$  in 200 mL saline on days 0, 7 and 14. On days 21, 22 and 23, the mice were nebulized with 300 mg of OVA in 5 mL saline for 25 min per day. For PM2.5 treatment, the mice were treated with 100  $\mu\text{g}$  in sterile phosphate-buffered saline (PBS; 50 mL final volume), where PM2.5 was slowly instilled, followed with 200 mL of clean air. For PM2.5 pre-treatment, the mice were treated with PM2.5 for 7 days from day 0 to day 7. For PM2.5 long-treatment, the mice were treated with PM2.5 for 27 days from day 0 to day 27.

## Lung tissue histology analysis

Lung tissues from the mice were fixed with 10% formalin in saline and embedded in paraffin. The paraffin blocks were serially sectioned at 5- $\mu\text{m}$  thickness and stained with hematoxylin-eosin (H&E) staining for lung histology analysis.

## BALF analysis

Within 24 h after the final challenge, the mice were sacrificed, and the trachea was cannulated. Plasma and BALF were collected from mice at harvest. The BALF was obtained by flushing the lungs 3 times with 1.5 mL of PBS. The BALF cellular typing was determined with cytospin preparation and Wright–Giemsa staining, followed by counting total cell number, macrophages and eosinophils. Plasma IgE (Invitrogen, Carlsbad, USA), BALF IL-1 $\beta$  (eBioscience, Waltham, USA), MCP-1 (eBioscience), IL-12 (eBioscience), IL-5 (eBioscience), IL-13 (PeproTech, Stockholm, Sweden), and prostaglandin D2 (PGD<sub>2</sub>; Caymanchem, Ann Arbor, USA) were determined using enzyme-linked immunosorbent assay (ELISA) kits according to the manufacturers' instructions.

## Western blot

The total proteins from mice lung tissues were isolated, and the protein concentrations were determined using a bicinchoninic acid assay. The proteins from whole-cell lysates were used for western blot. Anti-JAK1, anti-p-JAK1,

anti-JAK2, anti-p-JAK2, anti-STAT6, anti-p-STAT6, and GAPDH (all purchased from Cell Signaling Technology, Leiden, the Netherlands) antibodies were used. Densitometry of bands from western blots was measured using ImageJ software (National Institutes of Health, Bethesda, USA), and the density of the pJAK2 or p-STAT6 proteins relative to total JAK or total STAT6 was calculated.

## Cell culture

Bone marrow-derived eosinophils were cultured in Iscove's modified Dulbecco's medium (IMDM; Invitrogen) with 20% FBS (Invitrogen), 100 IU/mL penicillin and 10 mg/mL streptomycin, 2 mM glutamine, 25 mM HEPES, 1  $\times$  nonessential amino acids, 1 mM sodium pyruvate and 0.006%  $\beta$ -mercaptoethanol (Sigma-Aldrich, St. Louis, USA) supplemented with 100 ng/mL rmSCF (PeproTech) and 100 ng/mL recombinant murine FLT-3 ligand (rm-FLT3-L; PeproTech) from days 0 to 4. On day 4, the medium was replaced with medium containing 10 ng/mL rmIL-5 (PeproTech). The cells were provided with fresh medium supplemented with rmIL-5 every 3 days until to 14 days. A total of  $1 \times 10^6$  bone marrow-derived eosinophils per group were treated with 5.0  $\mu\text{g}/\text{cm}^2$  PM2.5 for 48 h with or without 100 ng/mL ruxolitinib (InvivoGen, San Diego, USA). After 48 h, the cell supernatants were harvested. The concentrations of IL-1 $\beta$ , IL-5 and IL-13 in the supernatants were determined using ELISA.

## Statistical analyses

The data was expressed as the mean and standard error of the mean (SEM). All data was analyzed using SPSS v. 17.0 software (SPSS Inc., Chicago, USA). Comparisons among experimental groups were performed with non-parametric Kruskal–Wallis test (one-way analysis of variance (ANOVA) on ranks) due to multiple group comparisons and abnormal data distribution. Differences with p-values less than 0.05 were considered to be statistically significant.

## Results

### Pathological changes in airways after PM2.5 pre-treatment and long treatment

Mice were either pre-treated with PM2.5 twice a day (day 0 and day 7) followed by OVA administration on day 21 (OVA + PM2.5 pre-treated group) or were subjected to a mix of PM2.5 (day 0, 7, 14, 21, and 27) and OVA administration (day 21 to 27) (OVA + PM2.5 long-treated group) (Fig. 1). Ovalbumin treatment with or without PM2.5 treatment induces asthma.<sup>35</sup> To examine airway changes after OVA and PM2.5 treatment, histopathological analysis on mice lung tissue was conducted. In the control group, mice lung tissue had neatly arranged airway epithelial cells with clear

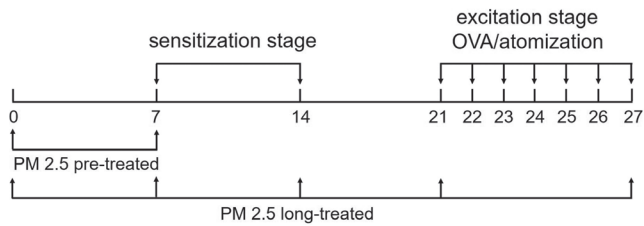


**Fig. 1.** Diagram outlining treatment stages of mice before OVA-induced asthma. Mice from pre-treated group were treated with PM2.5 (7 days) before sensitization for an additional 7 days. The mice were then subjected to OVA on day 21 to induce asthma. In another treatment group (long-treatment group), mice were treated with PM2.5 every 7 days (on day 0, 7, 14, 21, and 27). On day 21 to 27, asthma was induced in mice through OVA treatment

bronchi and alveoli (Fig. 2, control group). Ovalbumin treatment alone resulted in the disruption of the ordered lung tissue structure causing widened alveolar septum, capillary dilation and infiltration of leukocytes (eosinophils shown with arrows) (Fig. 2, OVA group). Combining PM2.5 treatment with OVA caused the further breakdown of the lung tissue with increased alveolar septum widening and capillary dilation (Fig. 2, OVA + PM2.5 pre-treated and long-treated group). Furthermore, increased infiltration of leukocytes was observed with both PM2.5 treatment methods with OVA (pre-treatment and long treatment). However, more eosinophils in PM2.5 long treatment with OVA compared to PM2.5 pre-treatment with OVA were observed (Fig. 2, OVA + PM2.5 long-treated group).

### PM2.5 treatment induces increased eosinophil infiltration into the lungs

High levels of IgE are a typical indicator of asthma. Although OVA treatment alone induced increases in plasma IgE compared to the control, both PM2.5 exposures with

OVA (pre-treatment and long treatment) significantly increased plasma IgE levels compared to OVA treatment alone ( $p < 0.05$ , Fig. 3A).

To analyze cellular infiltration into the lungs in more detail, BALF was used to examine total leukocyte numbers together with eosinophils and macrophages. Ovalbumin-induced asthma alone did increase total cell numbers, eosinophils and macrophages as compared to control group ( $p < 0.001$ , Fig. 3B;  $p < 0.001$ , Fig. 3C; and  $p < 0.01$ , Fig. 3D). However, pre-treatment with PM2.5 and OVA significantly increased total cell numbers as well as eosinophil infiltration compared to OVA treatment alone ( $p < 0.05$ , Fig. 3B; and  $p < 0.05$ , Fig. 3C) but not macrophages. With continuous long treatment of PM2.5 and OVA, total cell numbers, eosinophils and macrophages in the lung were increased as compared to OVA treatment alone ( $p < 0.001$ , Fig. 3B;  $p < 0.001$ , Fig. 3C; and  $p < 0.05$ , Fig. 3D).

### Increased inflammatory cytokines after PM2.5 treatment

Cytokine levels from BALF in control, OVA-treated, and PM2.5 pre- and long-treated mice were examined. The BALF levels of IL-1 $\beta$ , MCP-1, IL-12, IL-5, IL-13, and PGD<sub>2</sub> were increased after OVA treatment ( $p < 0.05$  for IL-1 $\beta$ ;  $p < 0.05$  for MCP-1;  $p < 0.01$  for IL-12;  $p < 0.001$  for IL-5;  $p < 0.05$  for IL-13; and  $p < 0.05$  for PGD<sub>2</sub>; Fig. 4A–F). Pre-treatment with PM2.5 followed by OVA increased BALF MCP-1 and IL-5 ( $p < 0.05$  for MCP-1, Fig. 4B; and  $p < 0.05$  for IL-5, Fig. 4D) but not IL-1, IL-12, IL-13, and PGD<sub>2</sub> (Fig. 4A,C,E,F). Long treatment of PM2.5 with OVA increased IL-1 $\beta$  ( $p < 0.05$ , Fig. 4A), MCP-1 ( $p < 0.05$ , Fig. 4B), IL-12 ( $p < 0.05$ , Fig. 4C), IL-5 ( $p < 0.01$ , Fig. 4D), IL-13 ( $p < 0.01$ , Fig. 4E), and PGD<sub>2</sub> ( $p < 0.01$ , Fig. 4F) in the BALF.

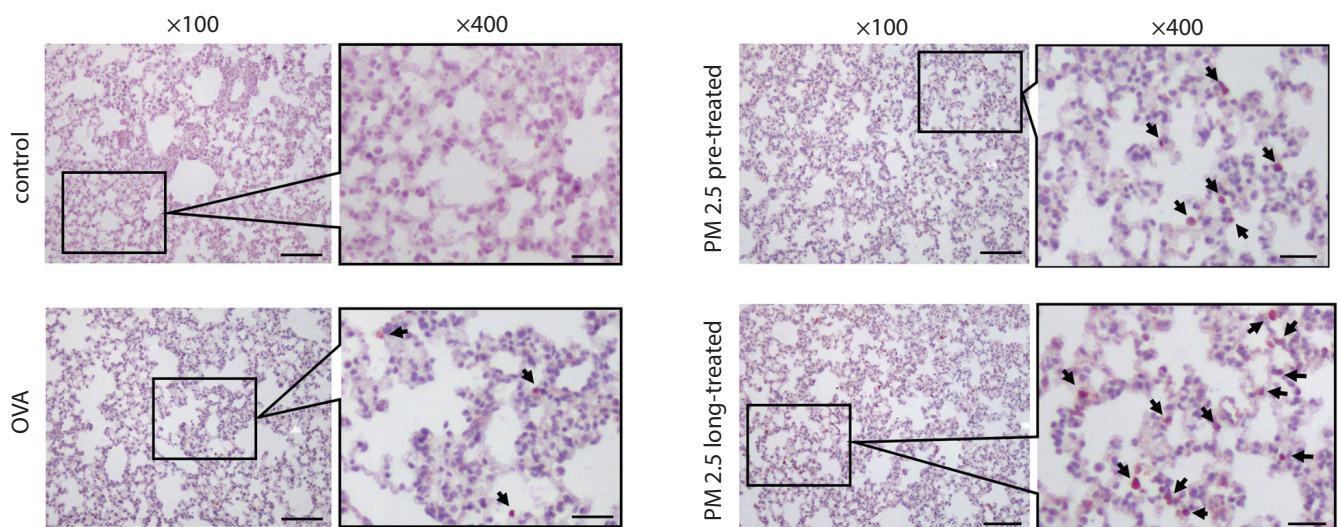


**Fig. 2.** Comparison of eosinophils in lung tissue after treatment with PM2.5. Magnification  $\times 10$  and  $\times 40$  of (A) control group, (B) OVA group, (C) OVA + PM2.5 pre-treated group, and (D) OVA + PM2.5 long-treatment group lung samples H&E-stained for eosinophil infiltration (arrows). Magnification  $\times 10$  scale bar: 100  $\mu\text{m}$ . Magnification  $\times 40$  scale bar: 25  $\mu\text{m}$

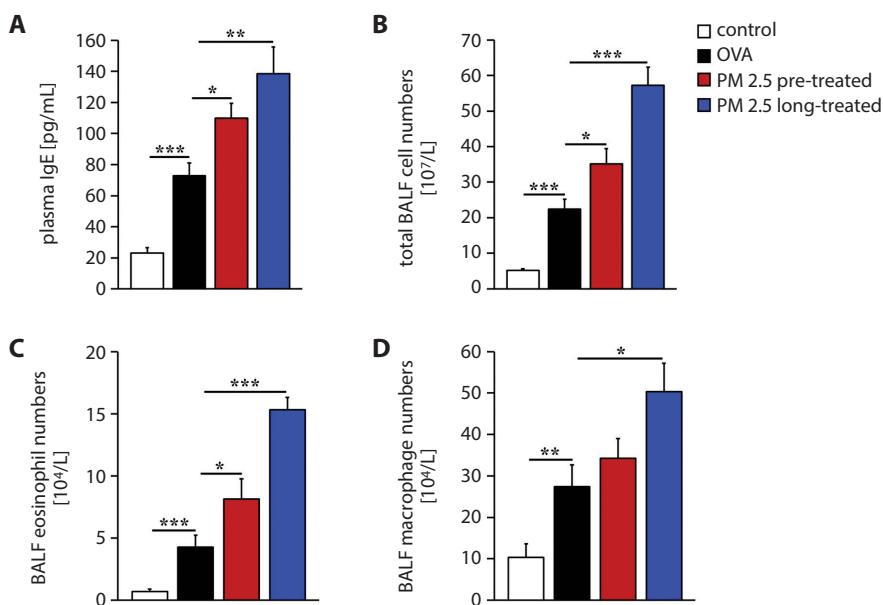


**Fig. 3.** PM2.5 treatment increases plasma IgE and leukocyte infiltration in lung. Measurement of (A) plasma IgE, (B) total cell numbers from the bronchoalveolar lavage fluid (BALF), (C) total BALF eosinophil numbers, and (D) total BALF macrophage numbers in control group (white bars), OVA group (black bars), OVA + PM2.5 pre-treated group (red bars) and OVA + PM2.5 long-treated group (blue bars)

n = 10, p\* < 0.05, p\*\* < 0.01, p\*\*\* < 0.001.

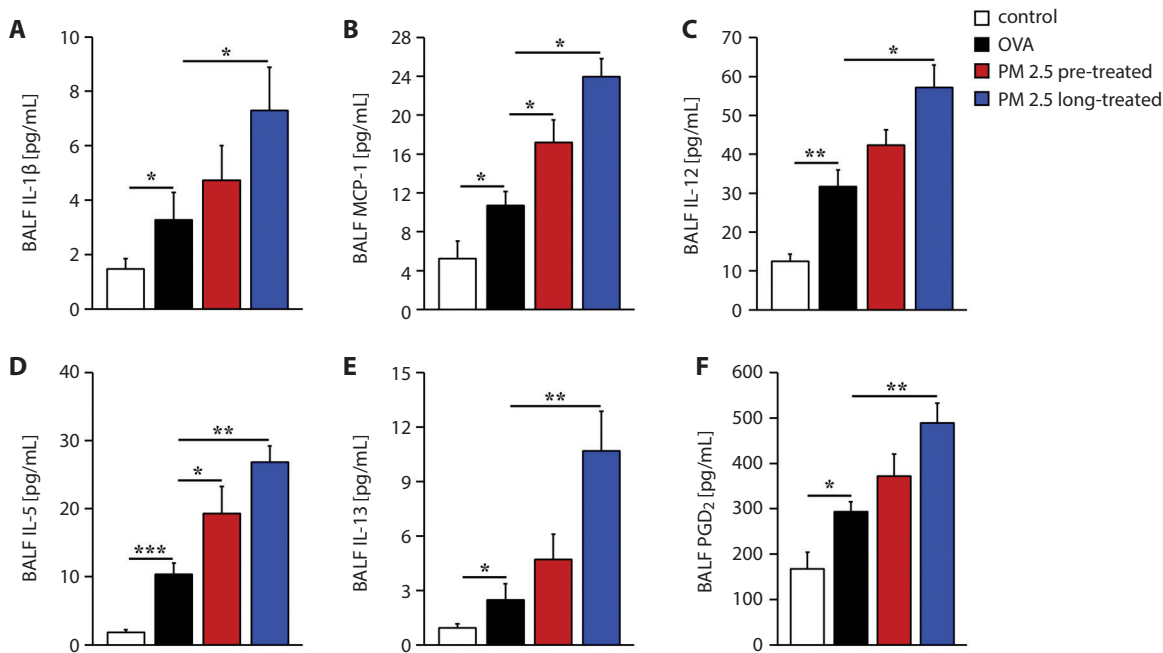


**Fig. 4.** PM2.5 treatment increases inflammatory cytokine levels in lungs. Measurements of BALF (A) IL-1β, (B) MCP-1, (C) IL-12, (D) IL-5, (E) IL-13, and (F) PGD2 in the control group (white bars), OVA group (black bars), OVA + PM2.5 pre-treated group (red bars), and OVA + PM2.5 long-treatment group (blue bars)

n = 10, p\* < 0.05, p\*\* < 0.01, p\*\*\* < 0.001.

### JAK-STAT6 pathway regulates eosinophil infiltration and inflammatory cytokine production in lungs

To determine the signaling pathway that regulated recruitment of eosinophils,<sup>36</sup> protein levels of non-phosphorylated and phosphorylated JAK/STAT6 were examined with western blotting (Fig. 5A) and quantified using densitometry. Ovalbumin increased the phosphorylation of JAK1, JAK2 and STAT6 compared to control group by about

twofold (p < 0.05, Fig. 5B). Long treatment with PM2.5 increased pJAK1 by fourfold compared to the control group and about twofold compared to OVA treatment alone, while pJAK2 was increased by 4-fold compared to the control group and about 1.5-fold compared to OVA treatment alone. Phosphorylation of STAT6 was increased 2-fold after OVA treatment alone while PM2.5 long treatment increased pSTAT6 by 2.5-fold compared to the control group and 1.5-fold compared to OVA treatment alone. No changes in GADPH protein levels were observed (Fig. 5A). Moreover,

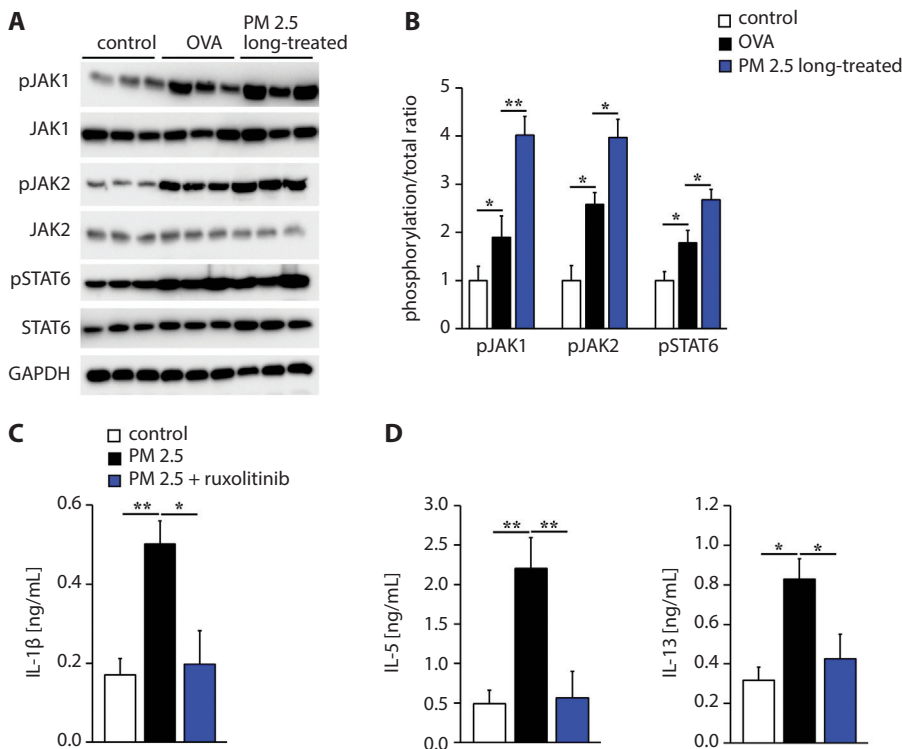


**Fig. 5.** JAK2-STAT6 pathway drives production of inflammatory cytokines and eosinophil infiltration. **A.** Representative western blot showing increase in phosphorylated JAK1, JAK2 and STAT6 after PM2.5 treatment as compared to control group and OVA group.

**B.** Phosphorylation of JAK1, JAK2 and STAT6 as calculated from western blots in control group (white bars), OVA group (black bars) and OVA + PM2.5 long-treatment group (blue bars),  $n = 6$ . Measurements of medium (C) IL-1 $\beta$ , (D) IL-5 and (E) IL-13 in control (white bars), PM2.5-treated (black bars) and PM2.5 + ruxolitinib-treated (blue bars) bone marrow-derived eosinophils,  $n = 4$

$p^* < 0.05$ ,  $p^{**} < 0.01$ .

to confirm that the JAK-STAT6 pathway was involved in PM2.5 and asthma, bone marrow derived eosinophil was treated with PM2.5 with or without JAK1/2 inhibitor, ruxolitinib. PM2.5 increased IL-1 $\beta$  ( $p < 0.01$ , Fig. 5C), IL-5 ( $p < 0.01$ , Fig. 5D) and IL-13 ( $p < 0.05$ , Fig. 5E) production in eosinophil medium; their production was blocked by ruxolitinib treatment ( $p < 0.05$ , Fig. 5C,D).

## Discussion

PM2.5 pollution in developing countries such as China poses a serious public health problem, as exposure to ambient PM2.5 exacerbates allergic diseases. The occurrence of asthma and allergic diseases have been on the rise in both developed and industrializing countries due to exposure to a variety of environmental pollutants in the air.<sup>21,37–39</sup> As such, the effects of PM2.5 have been gaining public attention. We investigated the effects of PM2.5 on eosinophil recruitment in OVA-induced asthma. PM2.5 increased the severity of OVA-induced asthma as indicated increasing in lung injury, alveolar intervals, capillary dilations, and inflammatory leukocytes infiltration. PM2.5 treatment with OVA significantly increased the presence of inflammatory cytokines in the BALF as compared to OVA alone, which increased the number of infiltrating eosinophils and macrophages. The infiltration of eosinophils was regulated through the JAK2 and STAT6 pathway, as increased phosphorylation of both these proteins was observed through western blotting.

The role of eosinophils has been examined in an acute murine PM2.5 OVA-induced asthma model.<sup>40</sup> In that acute

model, mice were first sensitized to OVA, before being exposed to PM2.5 and then challenged with OVA. Under these conditions, the authors observed significant infiltration of eosinophils but not macrophages exposed to 10  $\mu$ g and 100  $\mu$ g of PM2.5 compared to control group after OVA challenge. In agreement with the acute model, our study also observed an increase in eosinophils after PM2.5 pre-treatment. With continuous exposure to PM2.5 (through long treatment), eosinophil infiltration into the lungs was further increased. Although no increase in macrophages was observed in PM2.5 pre-treatment, similar to the acute study, long treatment of PM2.5 did significantly increase macrophage recruitment. As neutrophil recruitment during exposure to concentrated ultrafine airborne particles remains debated,<sup>40,41</sup> neutrophil infiltration was not measured in our study.

During asthma, the presence of T<sub>H</sub>2 cytokines IL-4, IL-5 and IL-13 are typically observed during clinical manifestation of disease.<sup>42</sup> However, particulate matter is known to induce the production of different cytokines due to the activation of diverse cellular and molecular mechanisms. For example, increased levels of IL-17 were observed, but there were no changes in IL-4. In another study, high levels of cytokines (IL-1 $\beta$  and IL-12), not typically associated with T<sub>H</sub>2 responses, were observed.<sup>34</sup> This was in addition to increases in IL-5 and IL-13. Chemokines such as MCP-1 (which recruits monocytes and macrophages) were also detected. In another study, increases in IL-4 and IL-10 with decrease in interferon gamma (IFN $\gamma$ ) were observed.<sup>40</sup> In this study, PM2.5 long treatment increased the levels of IL-1 $\beta$ , IL-12, IL-5, and IL-13. The increased level of IL-12 may have been induced by the macrophage

recruitment in BALF (Fig. 3D). Alveolar macrophages are primed for the production of IL-10 and IL-12 in asthma.<sup>43</sup> However, IL-12 could induce the type I immune response which is antagonistic with type II immune responses. Macrophages appear more as a consequence than as an initiating factor of the T-cell T<sub>H</sub>2 commitment and could be involved in the resolution of the asthmatic inflammation. Together with the chemokine MCP-1, these cytokines were important in the recruitment of macrophages and eosinophils into the lung.

The JAK-STAT pathway is important in the development of asthma.<sup>36</sup> For example, IL-4 induces JAK1/JAK3 resulting in STAT6 activation, which further polarizes the T<sub>H</sub>2 pathway. Another important pathway in asthma development is IL-13-JAK2-STAT6 pathway, which upon activation markedly increases mucous secretion.<sup>44</sup> In this study, eosinophil recruitment was demonstrated to be reliant on the phosphorylation of JAK2 and STAT6. Ovalbumin treatment alone triggers this pathway but co-treatment with PM<sub>2.5</sub> significantly increases the amount of phosphorylation of both JAK2 and STAT6. As a result of JAK2/STAT6 pathway activation, IL-13 was significantly increased and contributed to airway inflammation.

There are several limitations to our study. First, the polycyclic aromatic hydrocarbons, chemicals and metals were not analyzed in our study. Although these components are typically found in PM<sub>2.5</sub>, PM<sub>2.5</sub> from different cities are composed of different compounds, which induces different responses in vivo. In addition, this meant that the component which contributed most to asthma exacerbation in PM<sub>2.5</sub> long, continuous treatment could not be identified. Second, as the data is from a single city, it might be challenging to extend these findings to other cities due to differences in climate and pollution content. Finally, cytokines typically associated with asthma (such as IL-5 and IL-13), pro-inflammatory cytokines (IL-1 $\beta$  and IL-12) and leukocyte chemokines (MCP-1 and PGD<sub>2</sub>) were observed to increase during PM<sub>2.5</sub> long treatment in this study. These factors isolated from the BALF likely contributed to the induction of leukocyte recruitment into the lung and resulted in exacerbating the disease. However, the mechanistic contribution of individual cytokines to eosinophil recruitment was not examined in this study.

## Conclusions

Although the effect of PM<sub>2.5</sub> has been examined by other researchers, their studies have focused on the acute effects of PM<sub>2.5</sub> on aggravating asthma. By providing continuous treatment of PM<sub>2.5</sub> together with OVA treatment, our study demonstrates that prolonged exposure of PM<sub>2.5</sub> increases the severity of asthma through exacerbated inflammation by increasing eosinophil recruitment.

## ORCID iDs

Yonghui Yang  <https://orcid.org/0000-0001-5955-2289>  
 Xiaoxia Li  <https://orcid.org/0000-0001-5401-2398>  
 Xiaoying An  <https://orcid.org/0000-0002-4799-8862>  
 Ling Zhang  <https://orcid.org/0000-0002-9313-4758>  
 Xingbin Li  <https://orcid.org/0000-0003-4411-1303>  
 Liang Wang  <https://orcid.org/0000-0002-5385-3045>  
 Guiyun Zhu  <https://orcid.org/0000-0002-9734-2001>

## References

- Li L, Liu DJ. Study on an air quality evaluation model for Beijing City under haze-fog pollution based on new ambient air quality standards. *Int J Environ Res Public Health*. 2014;11(9):8909–8923.
- Lu S, Wang Y, Teng Y, Yu X. Heavy metal pollution and ecological risk assessment of the paddy soils near a zinc-lead mining area in Hunan. *Environ Monit Assess*. 2015;187(10):627.
- Xie J, Teng J, Fan Y, Xie R, Shen A. The short-term effects of air pollutants on hospitalizations for respiratory disease in Hefei, China. *Int J Biometeorol*. 2019;63(3):315–326.
- Wang Y, Smith JA, Wilmers CC. Residential development alters behavior, movement, and energetics in an apex predator, the puma. *PLoS One*. 2017;12(10):e0184687.
- Maki T, Puspitasari F, Hara K, et al. Variations in the structure of airborne bacterial communities in a downwind area during an Asian dust (Kosa) event. *Sci Total Environ*. 2014;488–489:75–84.
- He M, Ichinose T, Song Y, et al. Effects of two Asian sand dusts transported from the dust source regions of Inner Mongolia and north-east China on murine lung eosinophilia. *Toxicol Appl Pharmacol*. 2013;272(3):647–655.
- Kim KH, Kabir E, Kabir S. A review on the human health impact of air-borne particulate matter. *Environ Int*. 2015;74:136–143.
- Cai Y, Shao Y, Wang C. The association of air pollution with the patients' visits to the department of respiratory diseases. *J Clin Med Res*. 2015;7(7):551–555.
- de Haar C, Hassing I, Bol M, Bleumink R, Pieters R. Ultrafine but not fine particulate matter causes airway inflammation and allergic airway sensitization to co-administered antigen in mice. *Clin Exp Allergy*. 2006;36(11):1469–1479.
- Singh S, Shi T, Duffin R, et al. Endocytosis, oxidative stress and IL-8 expression in human lung epithelial cells upon treatment with fine and ultrafine TiO<sub>2</sub>: Role of the specific surface area and of surface methylation of the particles. *Toxicol Appl Pharmacol*. 2007;222(2):141–151.
- Primbs T, Simonich S, Schmedding D, et al. Atmospheric outflow of anthropogenic semivolatile organic compounds from East Asia in spring 2004. *Environ Sci Technol*. 2007;41(10):3551–3558.
- Shadie AM, Herbert C, Kumar RK. Ambient particulate matter induces an exacerbation of airway inflammation in experimental asthma: Role of interleukin-33. *Clin Exp Immunol*. 2014;177(2):491–499.
- Jacquemin B, Siroux V, Sanchez M, et al. Ambient air pollution and adult asthma incidence in six European cohorts (ESCAPE). *Environ Health Perspect*. 2015;123(6):613–621.
- Baccarelli AA, Zheng Y, Zhang X, et al. Air pollution exposure and lung function in highly exposed subjects in Beijing, China: A repeated-measure study. *Part Fibre Toxicol*. 2014;11:51.
- Hopke PK, Croft D, Zhang W, et al. Changes in the acute response of respiratory diseases to PM<sub>2.5</sub> in New York State from 2005 to 2016. *Sci Total Environ*. 2019;677:328–339.
- Hasunuma H, Yamazaki S, Tamura K, et al. Association between daily ambient air pollution and respiratory symptoms in children with asthma and healthy children in western Japan. *J Asthma*. 2018;55(7):712–719.
- Jo EJ, Lee WS, Jo HY, et al. Effects of particulate matter on respiratory disease and the impact of meteorological factors in Busan, Korea. *Respir Med*. 2017;124:79–87.
- Mar TF, Koenig JQ, Primomo J. Associations between asthma emergency visits and particulate matter sources, including diesel emissions from stationary generators in Tacoma, Washington. *Inhal Toxicol*. 2010;22(6):445–448.
- Vempilly J, Abejie B, Diep V, Gushiken M, Rawat M, Tyner TR. The synergistic effect of ambient PM<sub>2.5</sub> exposure and rhinovirus infection in airway dysfunction in asthma: A pilot observational study from the Central Valley of California. *Exp Lung Res*. 2013;39(10):434–440.

20. Iskandar A, Andersen ZJ, Bonnelykke K, Ellermann T, Andersen KK, Bisgaard H. Coarse and fine particles but not ultrafine particles in urban air trigger hospital admission for asthma in children. *Thorax*. 2012;67(3):252–257.
21. Tecer LH, Alagha O, Karaca F, Tuncel G, Eldes N. Particulate matter (PM<sub>2.5</sub>, PM<sub>10-2.5</sub>, and PM<sub>10</sub>) and children's hospital admissions for asthma and respiratory diseases: A bidirectional case-crossover study. *J Toxicol Environ Health A*. 2008;71(8):512–520.
22. Yang CY, Tsai SS, Chang CC, Ho S-C. Effects of Asian dust storm events on daily admissions for asthma in Taipei, Taiwan. *Inhal Toxicol*. 2005;17(14):817–821.
23. Yoo Y, Choung JT, Yu J, Kim KD, Koh YY. Acute effects of Asian dust events on respiratory symptoms and peak expiratory flow in children with mild asthma. *J Korean Med Sci*. 2008;23(1):66–71.
24. Watanabe M, Yamasaki A, Burioka N, et al. Correlation between Asian dust storms and worsening asthma in Western Japan. *Allergol Int*. 2011;60(3):267–275.
25. Kanatani KT, Ito I, Al-Delaimy WK, et al. Desert dust exposure is associated with increased risk of asthma hospitalization in children. *Am J Respir Crit Care Med*. 2010;182(12):1475–1481.
26. Dougherty RH, Fahy JV. Acute exacerbations of asthma: Epidemiology, biology and the exacerbation-prone phenotype. *Clin Exp Allergy*. 2009;39(2):193–202.
27. Kim HY, DeKruyff RH, Umetsu DT. The many paths to asthma: Phenotype shaped by innate and adaptive immunity. *Nat Immunol*. 2010;11(7):577–584.
28. Miyauchi K. Helper T cell responses to respiratory viruses in the lung: Development, virus suppression, and pathogenesis. *Viral Immunol*. 2017;30(6):421–430.
29. Kirstein F, Nieuwenhuizen NE, Jayakumar J, Horsnell WGC, Brombacher F. Role of IL-4 receptor alpha-positive CD4(+) T cells in chronic airway hyperresponsiveness. *J Allergy Clin Immunol*. 2016;137(6):1852–1862.e9.
30. Horikawa K, Takatsu K. Interleukin-5 regulates genes involved in B-cell terminal maturation. *Immunology*. 2006;118(4):497–508.
31. McKenzie GJ, Bancroft A, Grecis RK, McKenzie AN. A distinct role for interleukin-13 in Th2-cell-mediated immune responses. *Curr Biol*. 1998;8(6):339–342.
32. Lumeng CN. Lung macrophage diversity and asthma. *Ann Am Thorac Soc*. 2016;13(Suppl 1):S31–S34.
33. Fricker M, Gibson PG. Macrophage dysfunction in the pathogenesis and treatment of asthma. *Eur Respir J*. 2017;50(3):1700196.
34. He M, Ichinose T, Yoshida Y, et al. Urban PM<sub>2.5</sub> exacerbates allergic inflammation in the murine lung via a TLR2/TLR4/MyD88-signaling pathway. *Sci Rep*. 2017;7(1):11027.
35. Nials AT, Uddin S. Mouse models of allergic asthma: Acute and chronic allergen challenge. *Dis Model Mech*. 2008;1(4–5):213–220.
36. Pernis AB, Rothman PB. JAK-STAT signaling in asthma. *J Clin Invest*. 2002;109(10):1279–1283.
37. Li S, Batterman S, Wasilevich E, et al. Association of daily asthma emergency department visits and hospital admissions with ambient air pollutants among the pediatric Medicaid population in Detroit: Time-series and time-stratified case-crossover analyses with threshold effects. *Environ Res*. 2011;111(8):1137–1147.
38. Lerchl A. Comments on "Radiofrequency electromagnetic fields (UMTS, 1,950 MHz) induce genotoxic effects in vitro in human fibroblasts but not in lymphocytes" by Schwarz et al. (*Int Arch Occup Environ Health* 2008; doi:10.1007/s00420-008-0305-5). *Int Arch Occup Environ Health*. 2009;82(2):275–278.
39. Nordenhall C, Pourazar J, Ledin MC, Levin JO, Sandström T, Adroth E. Diesel exhaust enhances airway responsiveness in asthmatic subjects. *Eur Respir J*. 2001;17(5):909–915.
40. Zhang X, Zhong W, Meng Q, et al. Ambient PM<sub>2.5</sub> exposure exacerbates severity of allergic asthma in previously sensitized mice. *J Asthma*. 2015;52(8):785–794.
41. Kleinman MT, Sioutas C, Froines JR, et al. Inhalation of concentrated ambient particulate matter near a heavily trafficked road stimulates antigen-induced airway responses in mice. *Inhal Toxicol*. 2007;19(Suppl 1):117–126.
42. Barnes PJ. Targeting cytokines to treat asthma and chronic obstructive pulmonary disease. *Nat Rev Immunol*. 2018;18(7):454–466.
43. Magnan A, van Pee D, Bongrand P, et al. Alveolar macrophage interleukin (IL)-10 and IL-12 production in atopic asthma. *Allergy*. 1998;53:1092–1095.
44. Ding F, Liu B, Zou W, et al. LPS exposure in early life protects against mucus hypersecretion in ovalbumin-induced asthma by downregulation of the IL-13 and JAK-STAT6 pathways. *Cell Physiol Biochem*. 2018;46(3):1263–1274.

# Autologous transfusion of “old” red blood cells-induced M2 macrophage polarization through IL-10-Nrf2-HO-1 signaling complexes

Zhen-Zhou Li<sup>1,2,A–E</sup>, Zi-Wei Zhang<sup>3,A–D</sup>, Huan Wang<sup>2,B,C,E,F</sup>, Yong-Quan Chen<sup>2,B,C,E</sup>,  
Xiao-Fang Zhou<sup>2,B,C</sup>, Li-Shuang Duan<sup>2,C,E</sup>, Xiao-Xiao Wang<sup>2,E</sup>, Feng Xu<sup>4,E</sup>, Jian-Rong Guo<sup>1,2,B,F</sup>

<sup>1</sup> Shanghai Pudong New Area Gongli Hospital Training Base, Ningxia Medical University, China

<sup>2</sup> Department of Anesthesiology, Gongli Hospital, Second Military Medical University, Shanghai, China

<sup>3</sup> Department of Anesthesiology, Yijishan Hospital, Wannan Medical College, Wuhu, China

<sup>4</sup> Department of Anesthesiology, Anhui Province No. 2 People's Hospital, Hefei, China

A – research concept and design; B – collection and/or assembly of data; C – data analysis and interpretation;

D – writing the article; E – critical revision of the article; F – final approval of the article

Advances in Clinical and Experimental Medicine, ISSN 1899–5276 (print), ISSN 2451–2680 (online)

*Adv Clin Exp Med.* 2020;29(7):833–840

## Address for correspondence

Jian-Rong Guo  
E-mail: gjr8259@yeah.net

## Funding sources

Key Disciplines Group Construction Project of Pudong Health Bureau of Shanghai (grant No. PWZxq 2017-10) and National Natural Science Foundation of China (grant No. 81870147).

## Conflict of interest

None declared

Received on September 30, 2019

Reviewed on February 27, 2020

Accepted on May 1, 2020

Published online on August 5, 2020

## Cite as

Li ZZ, Zhang ZW, Wang H, et al. Autologous transfusion of “old” red blood cells-induced M2 macrophage polarization through IL-10-Nrf2-HO-1 signaling complexes. *Adv Clin Exp Med.* 2020;29(7):833–840. doi:10.17219/acem/121924

## DOI

10.17219/acem/121924

## Copyright

© 2020 by Wrocław Medical University

This is an article distributed under the terms of the Creative Commons Attribution 3.0 Unported (CC BY 3.0) (<https://creativecommons.org/licenses/by/3.0/>)

## Abstract

**Background.** Red blood cell (RBC) transfusion is associated with systemic inflammation and immune suppression as adverse outcomes.

**Objectives.** To investigate the immunomodulatory function of the transfused autologous RBC in altering pro-inflammatory and immunosuppressive effects.

**Material and methods.** A total of 24 Sprague Dawley male rats were randomly divided into 3 groups (n = 8 in each group). Group 1 did not receive blood transfusions, while the other 2 groups of rats separately received transfusion of RBC stored for 14 days (group 2) and 35 days (group 3). The rats were treated with HO-1 inhibitor, HO-1 inducer and nuclear factor erythroid 2-related factor 2 (Nrf2) activator after they separately received autologous transfusion of RBC that were cryopreserved for 14 days or 35 days. The blood samples of the rats were collected 12 h after the transfusion, and the macrophage phenotype of M1 and M2 were analyzed with flow cytometry (FCM). Also, the surface protein expression of CD68 and CD200R in macrophages were analyzed and the inflammatory signals in the serum were measured with enzyme-linked immunosorbent assay (ELISA). Moreover, the location and expression of proteins heme oxygenase 1 (HO-1), arginine 1 (Arg-1) and nitric oxide synthase 2 (NOS2) in macrophage were detected with immunofluorescence (IF).

**Results.** Autologous transfusion of long-time stored (“old”) RBC promoted macrophage polarization to M2 phenotype and upregulated the expression of its surface proteins CD68 and CD200R. The pro-inflammatory cytokines tumor necrosis factor  $\alpha$  (TNF- $\alpha$ ), interleukin (IL)-6, IL-1 $\beta$ , and IL-18 were inhibited, and the secretion of NOS isoforms (iNOS) in serum was reduced with blood transfusion; contrarily, the production of IL-10 and CCL22 was increased. Additionally, HO-1, Arg-1 and NOS2 proteins were located in the cytoplasm, and HO-1 and Arg-1 proteins were highly expressed in macrophage, while the expression of protein NOS2 was low. Moreover, Nrf2, HO-1 and Arg-1 proteins were upregulated in macrophage after receiving “old” RBC transfusion.

**Conclusions.** Autologous transfusion of “old” RBC drove the macrophage phenotype toward M2 macrophages and induced immunosuppressive effects through the IL-10-NRF2-HO-1 signals.

**Key words:** immunosuppressive treatment, red blood cell transfusion, M2 macrophage, IL-10-NRF2-HO-1 signals

## Introduction

Blood transfusion is widely used in clinical practice; it is estimated that the transfusion of red blood cells (RBC) is the major type, accounting for nearly 50% of transfusions.<sup>1</sup> The obtained RBC cryopreserved at  $4 \pm 2^\circ\text{C}$  for 35–42 days were recognized as safe<sup>2</sup>; however, in recent years, more adverse effects have occurred after blood transfusions,<sup>3–5</sup> which is why the storage lesions of RBC have attracted more attention. Even though low-temperature storage slows down the metabolism of RBC, studies have revealed that the structure and physiological and immunological characteristics of the long-time stored RBC (also named “old” RBC) have changed. The research of Karon et al. showed that the levels of RBC membrane 2,3-diphosphoglycerate (2,3-DPG) had decreased during storage.<sup>6</sup> The proteomic analysis identified the membrane structural proteins in RBC, such as spectrin, band 3 and band 4.1, which were changed.<sup>7</sup> Moreover, the stored RBC induced hemolysis and the release of free heme, hemoglobin and free iron, which play important roles in immunomodulation.<sup>8</sup> The free heme was not only sequestered by plasma haptoglobin, but also initiated the Fenton reaction to induce the release of iron<sup>9</sup>; then, the accumulation of iron induced the generation of reactive oxygen species (ROS) and radical chains, which thus led to tissue damage and inflammation.<sup>10,11</sup> Additionally, the free heme act as a pro-inflammatory factor engaged in the immune response of monocytes, macrophages, Tregs, and endothelial cells.<sup>12,13</sup> A study showed that free heme mediated macrophage polarization and shaped the expression of M1 and M2 markers.<sup>14</sup> More interestingly, the microvesicles were also found in the stored “old” RBC, which participated in the activity of endothelial activation,<sup>15</sup> blood coagulation<sup>16</sup> and immunomodulation.<sup>17</sup> Hence, the variability of stored RBC is closely associated with systemic pro-inflammatory and immunosuppressive effects in blood post-transfusion.

The “old” RBC transfusion also burdened the phagocytic ability of monocytes and macrophages. A study conducted by Dinkla et al. identified that the storage-induced auto-antibodies in RBC membrane accelerated phagocytosis by macrophages.<sup>18</sup> This correspondingly resulted in heme accumulation in macrophages, which in turn shaped the macrophages toward M2 phenotype through upregulating the heme oxygenase 1 (HO-1) and promoted the secretion of interleukin (IL)-10.<sup>19</sup> Therefore, the stored RBC transfusion induced adverse effects, owing to systemic inflammation and immune suppression. The aim of this study was to investigate the immunomodulation effects on macrophage of the “old” RBC transfusion in animal study and its related mechanism.

## Material and methods

### Material

A total of 24 Sprague Dawley male rats, 6–7 weeks old,  $205.45 \pm 20.55$  g (Shanghai Lab Animal Research Center, Shanghai, China); animal blood-taking needles (G-5mm, Braintree Scientific, USA); uncoated vacutainer tube with sodium citrate (Greiner Bio-One International GmbH, Kremsmünster, Austria); peripherally inserted central catheter (PICC; Bard Access Systems, Inc., Salt Lake City, USA); blood transfusion tube needle (Bard Access Systems, Inc.); plastic storage bag prefilled with mannitol adenine phosphate (MAP) storage solution (Sichuan Nigale Biomedical Co. Ltd., Chengdu, China); HO-1 inducer-cobalt protoporphyrin (CoPP, catalog No. ALX-430-076-M025; Jiangxi Haoran Bio-Pharma Co., Ltd., Nanchang, China); HO-1 inhibitor-zinc protoporphyrin IX (ZnPP IX, catalog No. 282820-50MG; Jiangxi Haoran Bio-Pharma Co., Ltd.); and Nrf2 activator-oltipraz (catalog No. MB2316; Dalian Meilun Biotech Co., Ltd., Dalian, China).

This study conformed to the standards of the animal ethics committee.

### Sample collection

Following transfusion, the fresh whole bloods were collected from the aorta abdominalis after the 10 rats were anesthetized with 2% isoflurane and sacrificed. The obtained blood was leukocyte-depleted with automatic leukocyte filter (catalog No. PXL8Y; Shanghai Jiading Photoelectric Instrument Co., Ltd., Shanghai, China) The left RBC units were then all stored in a plastic storage bag and separately stored at  $4^\circ\text{C}$ .

### Transfusion model

The 24 Sprague Dawley male rats were maintained in adapted cultivation at  $22\text{--}25^\circ\text{C}$ , in a 50–70% relative humidity environment with a 12-hour light/dark cycle for 2 weeks. Then, they were divided into 3 groups: group 1 did not receive blood transfusions, while the other 2 groups of rats separately received transfusion of RBC stored for 14 days (group 2) and 35 days (group 3). The collected RBC samples stored for 14 and 35 days were separately transported in a blood transfusion tube needle connected with a PICC, which was injected into the vein. After a six-hour blood transfusion, the rats were anesthetized with 2% isoflurane and sacrificed; then, the blood samples were collected from the eyeball with an uncoated vacutainer tube with sodium citrate.

### Flow cytometry

The blood samples collected from the eyeball were diluted 1:3 with phosphate-buffered saline (PBS) containing heparin, and 3 mL of Ficoll-Hypaque solution (Tianjin

Haoyang Commercial Co., Ltd., Tianjin, China) was slowly added into the tube, which was then centrifuged twice at  $3,000 \times g$  for 15 min at  $4^{\circ}\text{C}$ . Afterward, the supernatant in the middle class was transferred into a new tube, where its density was adjusted at  $5 \times 10^5 - 3 \times 10^6$  with Dulbecco's modified Eagle's medium (DMEM) containing 10% fetal calf serum (FCS). Later, we firstly analyzed the percentage of macrophages. The steps were as follows: the monocytes were stained with allophycocyanin (APC)-conjugated monoclonal antibody against mouse CD16 (catalog No. 17-0168-41; eBioscience, Thermo Fisher Scientific, Waltham, USA); subsequently, the phycoerythrin (PE)-conjugated monoclonal antibody against mouse CD68 (catalog No. MA5-23572; Invitrogen, Carlsbad, USA) and CD200R (catalog No. 12-9201-42; eBioscience) were separately stained with the monocytes for 1 h at  $4^{\circ}\text{C}$ . Afterward, the cells were washed with PBS and the second antibody – anti-mouse immunoglobulin G (IgG) – was added. Finally, the monocytes were fixed with paraformaldehyde for 30 min and analyzed with FACSCalibur™ (eBioscience). We obtained the monocyte medium and stained the primary conjugated antibody as above. The Fc was blocked and the isotypic antibodies were used as a control; similarly, the surface proteins CD68 and CD200R were analyzed with FACSCalibur.

## ELISA assay

The blood samples collected from the eyeball were centrifuged twice at  $3,000 \times g$  for 15 min at  $4^{\circ}\text{C}$ ; then, the supernatants were transferred into a new tube and analyzed for the inflammatory-associated molecules of tumor necrosis factor  $\alpha$  (TNF- $\alpha$ ; catalog No. 70-ab35884-050; MultiSciences Biotech Co., Ltd., Hangzhou, China), IL-1 $\beta$  (catalog No. 70-ab33591-050; MultiSciences Biotech Co., Ltd.), IL-6 (catalog No. 70-ab36529-050; MultiSciences Biotech Co., Ltd.), IL-10 (catalog No. 70-ab33577-050; MultiSciences Biotech Co., Ltd.), nitric oxide synthase isoform (iNOS; catalog No. 93-E4649-100; BioVision Inc., Milpitas, USA), IL-18 (catalog No. 70-ab33588-050; MultiSciences Biotech Co., Ltd.), and CCL22 (catalog No. 70-ab2243-050; MultiSciences Biotech Co., Ltd.) with enzyme-linked immunosorbent assay (ELISA) kits according to the manufacturer's instructions.

## Immunofluorescence

The blood samples collected from the eyeball were diluted 1:3 with PBS containing heparin, and 3 mL of Ficoll-Hypaque solution (Tianjin Haoyang Commercial Co., Ltd.) was slowly added into the tube, which were then centrifuged twice at  $3000 \times g$  for 15 min at  $4^{\circ}\text{C}$ . Afterward, the supernatants in the middle class were transferred into a new tube, and the monocytes were cultivated with DMEM containing 10% FCS and cell slides were made in each group.

Afterwards, the cell slides were permeabilized with 0.1% TritonX-100 for 5 min, and then they were blocked with 10% bovine serum albumin (BSA) for 1 h at room temperature. After that, the primary antibodies HO-1 (catalog No. ab13248; Abcam, Cambridge, UK), arginine 1 (Arg-1; catalog No. 43933; Cell Signaling Technology, USA) and nitric oxide synthase 2 (NOS2; catalog No. ab15323; Abcam) were separately immunoblotted in the cells for 12 h,  $4^{\circ}\text{C}$ ; then, the cells were incubated with anti-mouse IgG antibody for 1 h at  $37^{\circ}\text{C}$ . Thereafter, the cell slides were washed with PBS 3 times, and then the cell nucleus were dyed with 4',6-diamidino-2-phenylindole (DAPI) and mounted on the cell slide with anti-fade mounting medium; finally, the stained images were examined under confocal microscopy (Leica Camera AG, Wetzlar, Germany).

## Western blot

The 60 rats after adapted cultivation were divided into 3 groups: group 1 ( $n = 20$ ) did not receive a blood transfusion, while the rats in the other 2 groups (group 2:  $n = 20$  and group 3:  $n = 20$ ) separately received a transfusion of RBC stored for 14 days (group 2) and 35 days (group 3). Meanwhile, the rats from each of the 3 parts were divided into 4 subgroups ( $n = 5$  in each subgroup) – control subgroup, HO-1 inhibitor administration (ZnPP IX) subgroup, HO-1 inducer administration (CoPP) subgroup, and Nrf2 activator administration (oltipraz) subgroup. After 12 h, the rats were anesthetized with 2% isoflurane and sacrificed. The blood samples were collected from each rat from the aorta abdominalis and then diluted 1:1 with PBS; subsequently, they were centrifuged and the monocytes were isolated with Ficoll-Hypaque solution. Thereafter, the total proteins of the monocytes were extracted with radioimmunoprecipitation assay (RIPA) buffer containing phenylmethylsulfonyl fluoride (PMSF), and then they were denatured and the protein concentration was evaluated. Afterward, the proteins were isolated with sodium dodecyl sulfate (SDS) polyacrylamide gels and the gels were transferred to polyvinylidene difluoride (PVDF) membranes. They were then blocked with 5% fat-free milk for 1 h; subsequently, the protein membranes were separately incubated with primary antibodies: anti-HO-1 (catalog No. ab13248; Abcam), anti-Arg-1 (catalog No. 43933, Cell Signaling Technology, Danvers, USA) and anti-Nrf2 (catalog No. ab89443; Abcam) for 12 h at  $4^{\circ}\text{C}$ . Afterward, the protein membranes were incubated with anti-mouse IgG antibody for 1 h. The glyceraldehyde-3-phosphate dehydrogenase (GAPDH) protein was used as control. Finally, the electrochemiluminescence (ECL) detection reagents were added into the protein bands, which were visualized with a bandscan instrument (Cytiva, Marlborough, USA), while the gray intensity of the proteins was analyzed with ImageJ software (National Institutes of Health, Bethesda, USA).

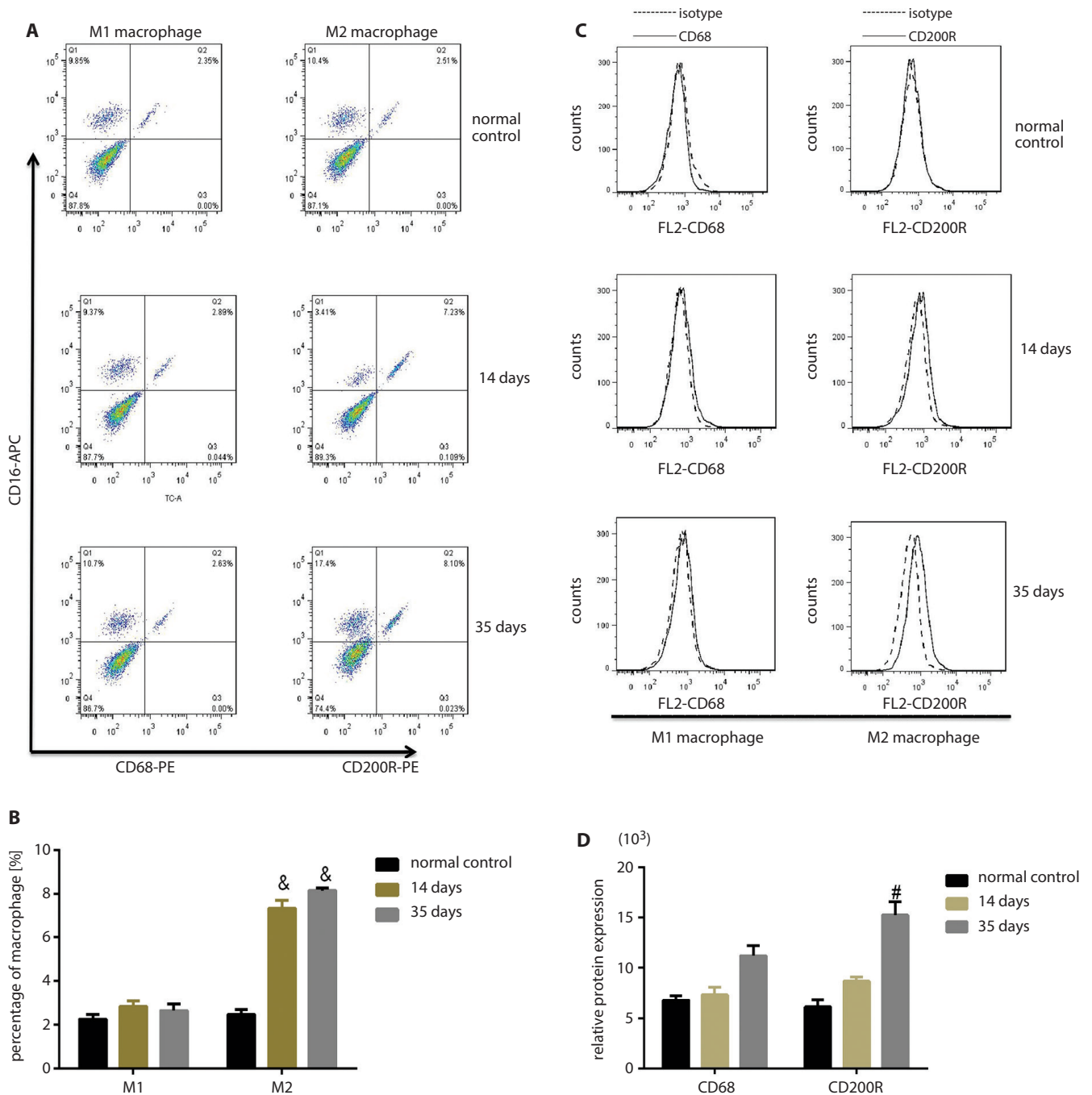


Fig. 1. Flow cytometry (FLC) sorted the macrophage phenotype (A) and detected the surface proteins expression of CD68 and CD200R (C). Blood transfusion shifted the macrophage to M2 phenotype – &#p < 0.05 of M2 percentage with blood transfusion vs without blood transfusion (B). The surface protein CD200R was significantly upregulated – #p < 0.05 with a transfusion of blood stored 35 days vs with a transfusion of blood stored 14 days and without a blood transfusion (D)

## Statistical analysis

The data was analyzed with the IBM SPSS Statistics for Windows software, v. 19.0 (IBM Corp., Armonk, USA), and the one-way analysis of variance (ANOVA) method was

applied for analyzing the group difference. A p-value of <0.05 was considered the statistically significant difference. The graphs were depicted with GraphPad Prism v. 6.0 software (GraphPad Software Inc., San Diego, USA), and presented as means  $\pm$  standard error of means (M  $\pm$  SEM).

## Results

### Autologous transfusion of “old” RBC induced M2 macrophage polarization

After the rats received transfusion of RBC stored for 14 days or 35 days, the flow cytometry (FCM) results showed that the percentage of M2 phenotype macrophage was obviously increased after receiving a blood transfusion (Fig. 1A,B). The surface proteins CD68 in M1 phenotype macrophage and CD200R in M2 phenotype macrophage were also varied. Results revealed that the protein CD200R was highly expressed on M2 macrophage, while the protein CD68 was also upregulated, but the extent was not as evident as in the case of CD200R (Fig. 1C,D); hence, as a whole, the RBC transfusion shifted the macrophage toward to M2 phenotype.

### Autologous transfusion promotes the secretion of pro-inflammatory factors, including IL-6, IL-1β, TNF-α, iNOS, IL-10, IL-18, and CCL22

The pro-inflammatory cytokines TNF-α, IL-6, IL-1β, and IL-18 were decreased with transfusion of blood stored for 35 days, while its amount was increased with a transfusion of RBC stored for 14 days. The variation tendency of iNOS was similar to the pro-inflammatory cytokines, which was consistent with the activity of iNOS involved in inflammation and enhancing the synthesis of pro-inflammatory mediators (Fig. 2). Conversely, the secretion of anti-inflammatory cytokine IL-10 and chemokine CCL22 was increased in blood after transfusion (Fig. 2). The extent of anti-inflammatory cytokine IL-10

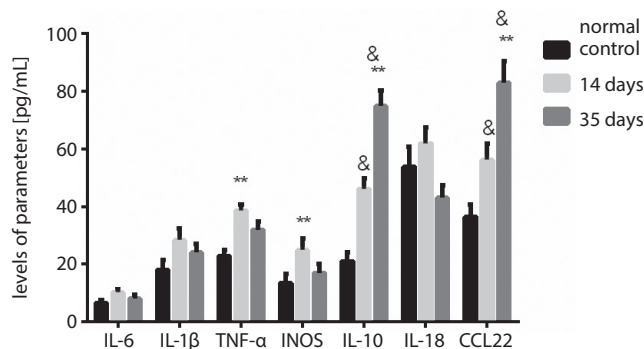


Fig. 2. The ELISA assay detected the amount of inflammatory molecules – \*\*p < 0.05 of TNF-α, iNOS, IL-10, and CCL22 with a transfusion of blood stored 14 days vs without a blood transfusion; &p < 0.05 of IL-10 and CCL22 with a transfusion of blood stored 35 days vs with a transfusion of blood stored 14 days

and chemokine CCL22 secretion was more obvious with a transfusion of RBC stored for 35 days. These results demonstrated that autologous transfusion of blood could increase the inflammatory response.

### Autologous transfusion directs the subcellular distribution of HO-1, Arg-1 and NOS2 to the cytoplasm

A few studies reported that HO-1 could mediate the anti-inflammatory phenotype of macrophage through regulating NRF2.<sup>20</sup> In this study, the proteins HO-1, Arg-1 and NOS2 were found to be located in the cytoplasm of macrophage; HO-1 and Arg-1 had high expression (Fig. 3). Therefore, we proposed that autologous transfusion of blood exerted its function through the redistribution of HO-1, Arg-1 and NOS2.

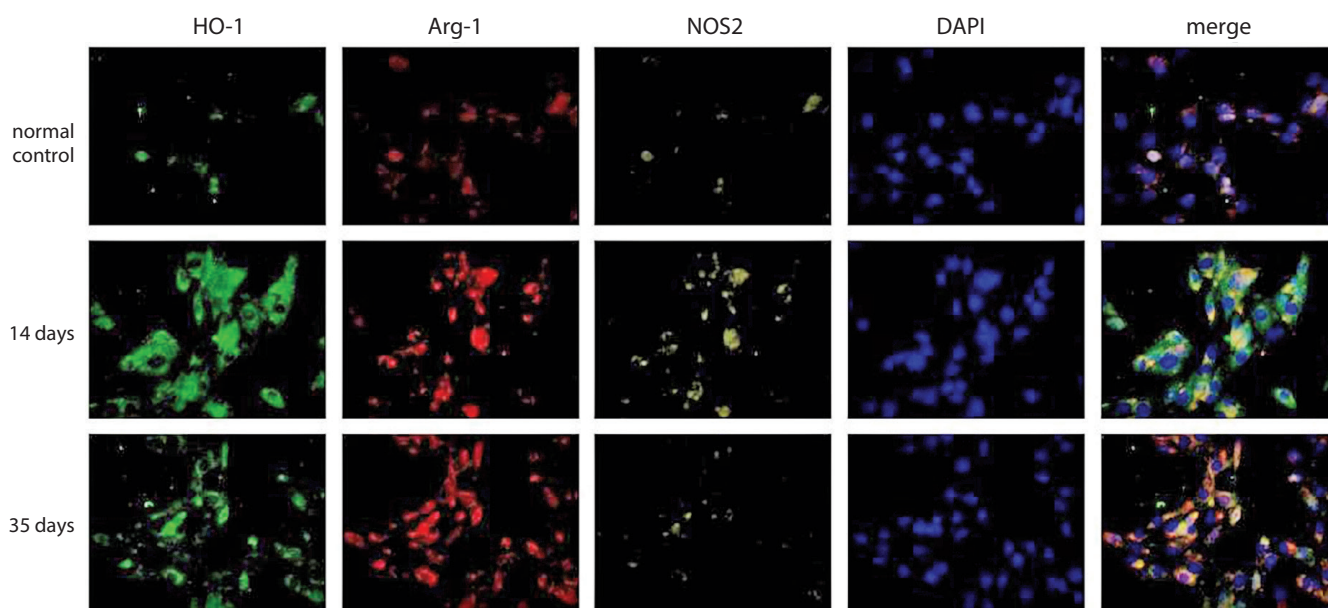
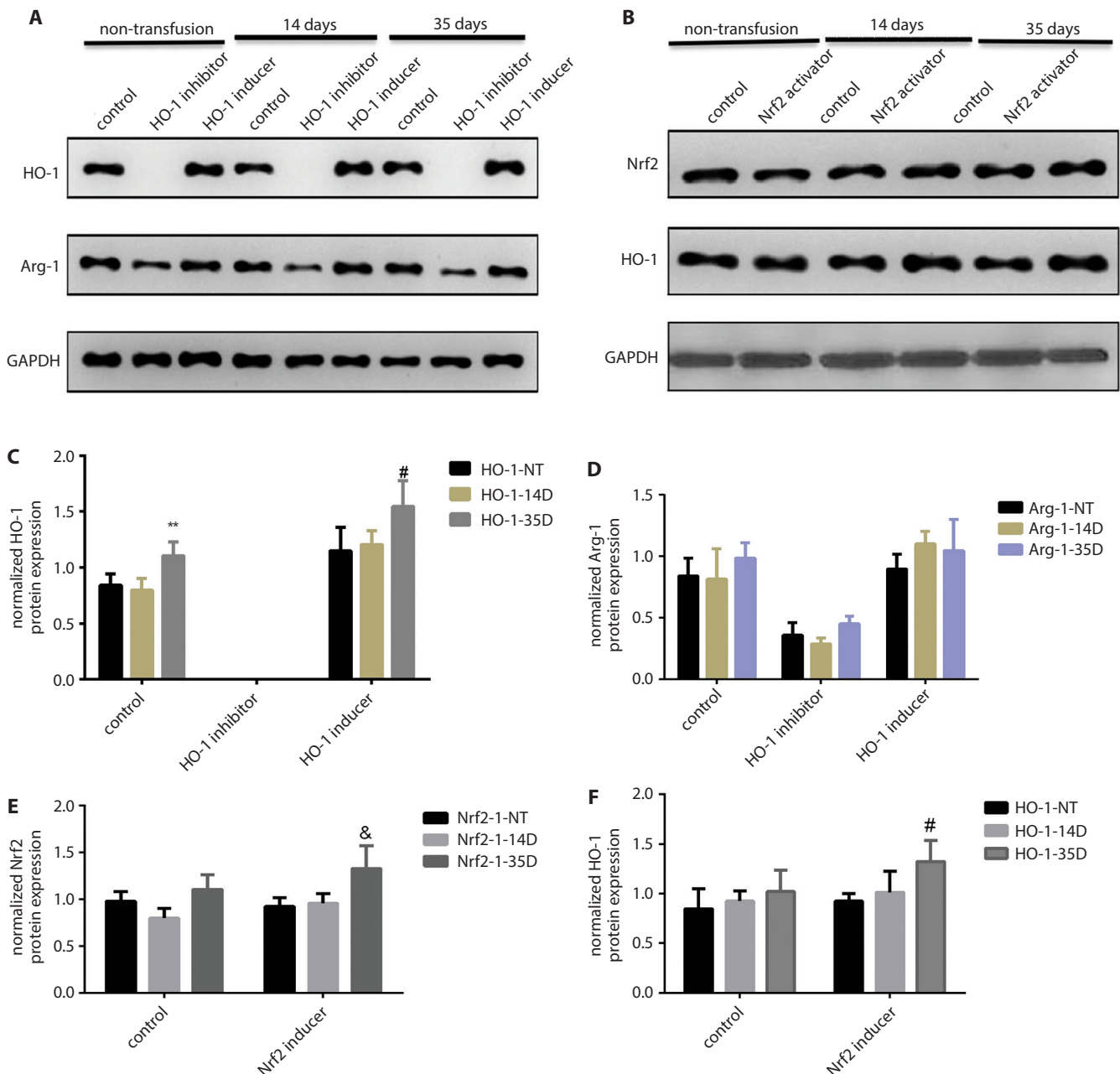


Fig. 3. Immunofluorescence (IF) identified the proteins HO-1, Arg-1 and NOS2. The proteins HO-1, Arg-1 and NOS2 located in the cytoplasm of macrophage and proteins HO-1 and Arg-1 with a high expression, while protein NOS2 did not have a high level of expression



**Fig. 4.** A and B. The expression of proteins Nrf2, HO-1 and Arg-1 in macrophages of rats with or without blood transfusion analyzed with western blot. The HO-1 inhibitor (ZnPP IX), HO-1 inducer (CoPP) and Nrf2 activator (oltipraz) were all administrated in rats with or without blood transfusion. C. The upregulated HO-1 with a transfusion of blood stored 35 days – \*\* $p < 0.05$  vs with a transfusion of blood stored 14 days; # $p < 0.05$  vs without a blood transfusion. D. With HO-1 inhibitor (ZnPP IX) administration, the protein Arg-1 downregulated. E and F. The upregulated Nrf2, HO-1 with a transfusion of blood stored 35 days; &# $p < 0.05$  of proteins Nrf2, HO-1 vs without a blood transfusion

### HO-1 inhibitor significantly repressed the protein expression of HO-1 while promoting the expression of Arg-1, but NRF2 activator has no effects on NRF2 and HO-1 after autologous transfusion

With the HO-1 inhibitor administration (ZnPP IX), HO-1 inducer administration (CoPP) and Nrf2 activator administration (oltipraz), we found that the expression

of proteins Nrf2, HO-1 and Arg-1 was significantly changed with a transfusion of RBC stored for 35 days, compared with the rats who did not receive blood transfusion or received a transfusion of RBC stored for 14 days (Fig. 4A,B). The inhibition of HO-1 affected the expression of protein Arg-1 (Fig. 4C,D), and to some extent, the activation of HO-1 and Nrf2 promoted the expression of proteins Nrf2, HO-1 and Arg-1 with a transfusion of RBC stored for 35 days (Fig. 4E,F). Hence, an autologous transfusion of “old” RBC induced immunosuppressive effects through

the IL-10-Nrf2-HO-1 signals. These results indicated that an autologous transfusion of blood functioned through HO-1 and Arg-1, but not through Nrf2.

## Discussion

The mechanism responsible for the adverse outcomes of systemic inflammation and immune suppression was controversial. In our study, we found that the transfusion of “old” RBC in rats induced the polarization of macrophages to M2 phenotype and upregulated their surface marker CD200R expression. The levels of anti-inflammatory signals IL-10 and CCL22 were also enhanced. More interestingly, the pro-inflammatory signals TNF- $\alpha$ , iNOS, IL-6, IL-1 $\beta$ , and IL-18 were increased after a transfusion of RBC stored for 14 days, while their levels were decreased after a transfusion of RBC stored for 35 days. This feature might be caused by the regulation of both pro-inflammation and anti-inflammation response. However, a RBC transfusion in a human study showed that there was no increase in pro-inflammatory cytokines, except for a small increase in non-transferrin-bound iron (NTBI).<sup>21</sup> However, a rat model with of blood transfusion suggested that a pro-inflammatory cytokine storm and an increase of NTBI occurred.<sup>22</sup> Hence, the debatable results may be caused by species difference and the limitation of study samples. The transfusion of stored blood resulting in increased hemolysis and erythrophagocytosis features were increasingly confirmed, which lead to a significant increase in serum iron, free heme and bilirubin levels.<sup>23–25</sup> The free heme was suggested as a pro-inflammatory signal, involved in the activity of IL-1 and TNF- $\alpha$ , and ROS generation.<sup>26,27</sup> Hence, this may be the reason that the pro-inflammatory signals TNF- $\alpha$ , iNOS, IL-6, IL-1 $\beta$ , and IL-18 were increased with the transfusion blood stored for 14 days. Moreover, HO-1 was suggested as a free heme scavenger, which had anti-inflammatory effects with a reduction of TNF- $\alpha$ , IL-8 and macrophage inflammatory protein (MIP)-1 $\beta$  levels and upregulation of IL-12.<sup>28</sup> This evidence was in line with our study that the pro-inflammatory signals were decreased with a transfusion of blood stored for 35 days. On the other hand, studies also showed that HO-1 was involved in the activity of polarizing M2 phenotype<sup>29,30</sup>; hence, this may be potentially involved in polarizing M2 phenotype.

With further studies, we found that HO-1, Arg-1, NOS2, and Nrf2 proteins were indeed engaged in M2 polarization. The HO-1, Arg-1 and Nrf2 proteins were obviously expressed in macrophages. This finding was consistent with the conclusion of Park et al.<sup>31</sup> that Nrf2 was an essential regulator of HO-1 participating in antioxidative stress-induced inflammatory activity. Moreover, the results of M1 subtype marker molecule – NOS2 and M2 marker – Arg-1<sup>32</sup> further confirmed our finding that “old” RBC transfusion induced M2 phenotype polarization. Hence, the immunomodulation mechanism of our study was closely associated with Nrf2-HO-1 signals. Additionally,

in our study, the secretion of CCL22 was also increased after transfusion. The CCL22 played roles in the trafficking of activated/effector T-lymphocytes. The study also showed that heme could drive the expansion of Tregs by inducing HO-1 expression in non-classical monocytes,<sup>33</sup> so there is a sign that Tregs lymphocytes may also be involved in the immunosuppressive activity.

On the other hand, numerous studies have identified the cluster of differentiation (CD) molecules that are closely associated with the phagocytosis ability. The CD47, an integrin-associated protein of RBC, was proved to be a self-marker in deciding its phagocytosis by binding to the signal regulatory protein  $\alpha$  (SIRP $\alpha$ ) of the macrophage.<sup>34,35</sup> Furthermore, the microvesicles of CD47, PS, CD55, and CD59 also shaped the phagocytosis of RBC.<sup>36,37</sup> Therefore, we should further investigate the changes in RBC, such as the change in membrane proteins, the secretion of microvesicles or spontaneous hemolysis, so as to more clearly reveal the mechanism of “old” RBC transfusion. Our study showed that the transfusion of “old” RBC in rats induced the polarization of macrophages to M2 phenotype through the IL-10-NFR2-HO-1 signals.

## ORCID iDs

Zhen-Zhou Li  <https://orcid.org/0000-0003-3774-7565>  
 Zi-Wei Zhang  <https://orcid.org/0000-0002-2140-4886>  
 Huan Wang  <https://orcid.org/0000-0003-3646-2656>  
 Yong-Quan Chen  <https://orcid.org/0000-0002-3525-1518>  
 Xiao-Fang Zhou  <https://orcid.org/0000-0002-9300-4478>  
 Li-Shuang Duan  <https://orcid.org/0000-0001-8510-7277>  
 Xiao-Xiao Wang  <https://orcid.org/0000-0003-4764-2281>  
 Feng Xu  <https://orcid.org/0000-0002-7750-7809>  
 Jian-Rong Guo  <https://orcid.org/0000-0002-3995-2995>

## References

- Carson JL, Guyatt G, Heddle NM, et al. Clinical practice guidelines from the AABB: Red blood cell transfusion thresholds and storage. *JAMA*. 2016;316(19):2025–2035.
- Dagur PK, McCoy JP. Collection, storage, and preparation of human blood cells. *Curr Protoc Cytom*. 2015;73:5.1.1–5.1.16. doi:10.1002/0471142956.cy0501s73
- Muszynski JA, Spinella PC, Cholette JM, et al; Pediatric Critical Care Blood Research Network (Blood Net). Transfusion-related immunomodulation: Review of the literature and implications for pediatric critical illness. *Transfusion*. 2017;57(1):195–206.
- Hod EA, Godbey EA. The outsider adverse event in transfusion: Inflammation. *Presse Med*. 2016;45(7–8 Pt 2):e325–e329.
- van de Watering L. Red cell storage and prognosis. *Vox Sang*. 2011; 100(1):36–45.
- Karon BS, Hoyer JD, Stubbs JR, Thomas DD. Changes in Band 3 oligomeric state precede cell membrane phospholipid loss during blood bank storage of red blood cells. *Transfusion*. 2009;49(7):1435–1442.
- D’Amici GM, Rinalducci S, Zolla L. Proteomic analysis of RBC membrane protein degradation during blood storage. *J Proteome Res*. 2007;6(8):3242–3255.
- Ozment CP, Mamo LB, Campbell ML, Lokhnygina Y, Ghio AJ, Turi JL. Transfusion-related biologic effects and free hemoglobin, heme, and iron. *Transfusion*. 2013;53(4):732–740.
- Banerjee S. Glyoxal-induced modification enhances stability of hemoglobin and lowers iron-mediated oxidation reactions of the heme protein: An in vitro study. *Int J Biol Macromol*. 2018;107(Pt A): 494–501.
- Spitalnik SL. Stored red blood cell transfusions: Iron, inflammation, immunity, and infection. *Transfusion*. 2014;54(10):2365–2371.

11. Baek JH, Yalamanoglu A, Gao Y, et al. Iron accelerates hemoglobin oxidation increasing mortality in vascular diseased guinea pigs following transfusion of stored blood. *JCI Insight*. 2017;2(9):e93577.
12. Dutra FF, Bozza MT. Heme on innate immunity and inflammation. *Front Pharmacol*. 2014;5:115.
13. Haldar M, Kohyama M, Yick-Lun So A, et al. Heme-mediated SPI-C induction promotes monocyte differentiation into iron-recycling macrophages. *Cell*. 2014;156(6):1223–1234.
14. Vinchi F, Costa da Silva M, Ingoglia G, et al. Hemopexin therapy reverts heme-induced pro-inflammatory phenotypic switching of macrophages in a mouse model of sickle cell disease. *Blood*. 2016;127(4):473–486.
15. Straat M, van Hezel ME, Böing A, et al. Monocyte-mediated activation of endothelial cells occurs only after binding to extracellular vesicles from red blood cell products, a process mediated by  $\beta$ -integrin. *Transfusion*. 2016;56(12):3012–3020.
16. Rubin O, Delobel J, Prudent M, et al. Red blood cell-derived microparticles isolated from blood units initiate and propagate thrombin generation. *Transfusion*. 2013;53(8):1744–1754.
17. Straat M, Böing AN, Tuip-De Boer A, Nieuwland R, Juffermans NP. Extracellular vesicles from red blood cell products induce a strong pro-inflammatory host response, dependent on both numbers and storage duration. *Transfus Med Hemother*. 2016;43(4):302–305.
18. Dinkla S, Novotný VMJ, Joosten I, Bosman GJCGM. Storage-induced changes in erythrocyte membrane proteins promote recognition by autoantibodies. *PLoS One*. 2012;7(8):e42250.
19. Yazdanbakhsh K, Bao W, Zhong H. Immunoregulatory effects of stored red blood cells. *Hematology Am Soc Hematol Educ Program*. 2011;2011:466–469.
20. Hod EA, Brittenham GM, Billote GB, et al. Transfusion of human volunteers with older, stored red blood cells produces extravascular hemolysis and circulating non-transferrin-bound iron. *Blood*. 2011;118(25):6675–6682.
21. Hod EA, Zhang N, Sokol SA, et al. Transfusion of red blood cells after prolonged storage produces harmful effects that are mediated by iron and inflammation. *Blood*. 2010;115(21):4284–4292.
22. Hult A, Malm C, Oldenburg PA. Transfusion of cryopreserved human red blood cells into healthy humans is associated with rapid extravascular hemolysis without a pro-inflammatory cytokine response. *Transfusion*. 2013;53(1):28–33.
23. Knutson MD, Vafa MR, Haile DJ, Wessling-Resnick M. Iron loading and erythrophagocytosis increase ferroportin 1 (FPN1) expression in J774 macrophages. *Blood*. 2003;102(12):4191–4197.
24. Youssef LA, Rebbaa A, Pampou S, et al. Increased erythrophagocytosis induces ferroptosis in red pulp macrophages in a mouse model of transfusion. *Blood*. 2018;131(23):2581–2593.
25. Hao K, Hanawa H, Ding L, et al. Free heme is a danger signal inducing expression of pro-inflammatory proteins in cultured cells derived from normal rat hearts. *Mol Immunol*. 2011;48(9–10):1191–1202.
26. Larsen R, Gouveia Z, Soares MP, Gozzelino R. Heme cytotoxicity and the pathogenesis of immune-mediated inflammatory diseases. *Front Pharmacol*. 2012;3:77.
27. Cherry AD, Piantadosi CA. Regulation of mitochondrial biogenesis and its intersection with inflammatory responses. *Antioxid Redox Signal*. 2015;22(12):965–976.
28. Naito Y, Takagi T, Higashimura Y. Heme oxygenase-1 and anti-inflammatory M2 macrophages. *Arch Biochem Biophys*. 2014;564:83–88.
29. Weis N, Weigert A, von Knethen A, Brüne B, Luo K. Heme oxygenase-1 contributes to an alternative macrophage activation profile induced by apoptotic cell supernatants. *Mol Biol Cell*. 2009;20(5):1280–1288.
30. Park EJ, Kim YM, Park SW, et al. Induction of HO-1 through p38 MAPK/Nrf2 signaling pathway by ethanol extract of *Inula helenium* L. reduces inflammation in LPS-activated RAW 264.7 cells and CLP-induced septic mice. *Food Chem Toxicol*. 2013;55:386–395.
31. Lu S, Li D, Xi L, Calderone R. Interplay of interferon-gamma and macrophage polarization during *Talaromyces marneffei* infection. *Microb Pathogen*. 2019;134:103594.
32. Zhong H, Yazdanbakhsh K. Hemolysis and immune regulation. *Curr Opin Hematol*. 2018;25(3):177–182.
33. Hagmann M. A new way to keep immune cells in check. *Science*. 2000;288(5473):1945–1946.
34. Oldenburg PA. Role of CD47 as a marker of self on red blood cells. *Science*. 2000;288(5473):2051–2054.
35. Stachurska A, Dorman M, Korsak J, et al. Selected CD molecules and the phagocytosis of microvesicles released from erythrocytes ex vivo. *Vox Sang*. 2019;114(6):576–587.
36. van Manen L, Peters AL, van der Sluijs PM, Nieuwland R, van Bruggen R, Juffermans NP. Clearance and phenotype of extracellular vesicles after red blood cell transfusion in a human endotoxemia model. *Transfus Apher Sci*. 2019;58(4):508–511.

# A long-term follow-up study on biochemical and clinical biomarkers of response to interferon beta-1b treatment in relapsing-remitting multiple sclerosis

Anna Pietrzak<sup>1,A–D</sup>, Alicja Kalinowska-Łyszczarz<sup>2,C–E</sup>, Krystyna Osztynowicz<sup>2,B</sup>, Alima Khamidulla<sup>3,B</sup>, Wojciech Kozubski<sup>1,A,E,F</sup>, Sławomir Michalak<sup>2,A,C,E,F</sup>

<sup>1</sup> Department of Neurology, Poznan University of Medical Sciences, Poland

<sup>2</sup> Department of Neurochemistry and Neuropathology, Department of Neurology, Poznan University of Medical Sciences, Poland

<sup>3</sup> Department of Neurology, West Kazakhstan Marat Ospanov Medical University, Aktobe, Kazakhstan

A – research concept and design; B – collection and/or assembly of data; C – data analysis and interpretation;

D – writing the article; E – critical revision of the article; F – final approval of the article

Advances in Clinical and Experimental Medicine, ISSN 1899–5276 (print), ISSN 2451–2680 (online)

*Adv Clin Exp Med.* 2020;29(7):841–851

## Address for correspondence

Anna Pietrzak

E-mail: [apiet@o2.pl](mailto:apiet@o2.pl)

## Funding sources

This research was funded by the Poznan University of Medical Sciences young scientists grant (No. 502-14-01111145-41212).

Anna Pietrzak received travel compensation from Zentiva. Alicja Kalinowska-Łyszczarz received personal compensation for speaking services and/or travel cost compensation and/or research grants from Biogen, Bayer, Merck Serono, Novartis, Teva Pharmaceuticals, CSL Behring, Shire, Sanofi-Genzyme, and Roche. Sławomir Michalak received a travel grant from Bayer.

## Conflict of interest

None declared

Received on November 20, 2019

Reviewed on March 13, 2020

Accepted on April 27, 2020

Published online on June 5, 2020

## Cite as

Pietrzak A, Kalinowska-Łyszczarz A, Osztynowicz K, Khamidulla A, Kozubski W, Michalak S. A long-term follow-up study on biochemical and clinical biomarkers of response to interferon beta-1b treatment in relapsing-remitting multiple sclerosis. *Adv Clin Exp Med.* 2020;29(7):841–851. doi:10.17219/acem/121063

## DOI

10.17219/acem/121063

## Copyright

© 2020 by Wrocław Medical University

This is an article distributed under the terms of the Creative Commons Attribution 3.0 Unported (CC BY 3.0) (<https://creativecommons.org/licenses/by/3.0/>)

## Abstract

**Background.** While interferon beta-1b (IFN- $\beta$ -1b) is still a commonly used disease-modifying drug in the treatment of multiple sclerosis (MS), therapeutic possibilities are expanding, and treatment failure should be identified early. Markers to predict response to IFN- $\beta$ -1b, either clinical or biochemical, are therefore urgently needed. Interferon-induced proteins, including viperin, suppressor of cytokine signaling 3 (SOCS3), ubiquitin specific peptidase-18 (USP18), and myxovirus resistance protein A (MxA), are possible markers of IFN- $\beta$ -1b bioavailability and treatment response.

**Objectives.** To evaluate viperin, SOCS3, USP18 and MxA as markers of treatment response in Polish IFN- $\beta$ -1b-treated patients with MS.

**Material and methods.** In 45 IFN- $\beta$ -1b-treated Polish patients with MS, serum concentrations of viperin, SOCS3, USP18, and MxA were assessed before and after 24 months of IFN- $\beta$ -1b treatment. The patients were followed clinically and with magnetic resonance imaging (MRI) for a median of 6.8 years.

**Results.** Low viperin, USP18 and MxA at baseline and 24 months and high SOCS3 at 24 months correlated with higher disease activity up to the 6<sup>th</sup> year of observation, but only baseline MxA and USP18 were independently related to outcome, with higher concentrations predicting less disease activity in the first 3 years and after the 1<sup>st</sup> year, respectively.

**Conclusions.** We confirm the predictive value of MxA and propose USP18 as a possible new prognostic biomarker in IFN- $\beta$ -1b-treated MS patients.

**Key words:** multiple sclerosis, interferon beta, viperin, suppressor of cytokine signaling 3, ubiquitin specific peptidase 18

## Background

Multiple sclerosis (MS), a chronic inflammatory and degenerative disorder of the central nervous system (CNS), remains a major cause of disability in young adults.<sup>1</sup> With the introduction of new, increasingly effective disease modifying drugs (DMD) for the relapsing-remitting form of MS (RRMS), the therapeutic paradigm has shifted from decreasing to abolishing any detectable disease activity. The concept of no evidence of disease activity (NEDA)<sup>2,3</sup> assumes no detectable activity in 3 domains: 1) no clinical relapses, 2) no disability progression (measured with the Expanded Disability Status Scale (EDSS)) and 3) no magnetic resonance imaging (MRI) activity (no new or enlarging T2/FLAIR lesions and no gadolinium enhancing lesions). As MS etiology and its exact pathomechanism are still uncertain, there is no single biomarker that could be used to measure disease activity. Therefore, combined assessment tools, such as NEDA, are often used as surrogates.

The arrival of new, more effective DMDs has been progressively decreasing the use of interferon beta (IFN- $\beta$ ) over the years, although the new agents are costly and often less safe,<sup>4</sup> and a subset of patients experience an uneventful disease course on IFN- $\beta$  for many years. A marker capable of identifying the patients likely to respond to treatment with IFN- $\beta$  would be of great value.

Prognostic tools to predict treatment response may comprise the patient's initial characteristics, such as gender, age and disease course, including current disability, number of relapses before treatment or features of the first relapses. Alternatively, markers of early response to DMD may be used to predict longer-term outcome: composite scores featuring clinical and imaging features over the 1<sup>st</sup> year of treatment were used, e.g., the Rio<sup>5</sup> and modified Rio score.<sup>6</sup> Unfortunately, neither classic baseline risk factors nor early clinical response scores are specific and sensitive enough to guide treatment decisions; furthermore, the response scales require a year of treatment trial. In an attempt at finding earlier and more reliable prognostic tools, numerous biochemical markers were proposed. Among them are markers of inflammation and neuronal damage as well as drug-specific markers, measured either at baseline or as an early response marker. Biomarkers intended specifically for IFN- $\beta$  response prediction include IFN-inducible proteins, such as viperin and myxovirus resistance protein A (MxA), anti-IFN antibodies,<sup>7–10</sup> cytokines (tumor necrosis factor  $\alpha$ <sup>11</sup>, interleukin 17,<sup>11–13</sup> interleukin 25,<sup>11</sup> interleukin 6<sup>12</sup> and interleukin 10<sup>13</sup>) and certain miRNA profiles.<sup>14,15</sup>

Based on previous research (Table 1), we selected 3 little-explored IFN-inducible particles with distinctive traits and promising reports: viperin (also known as radical s-adenosyl methionine domain-containing protein 2 – RSAD2), suppressor of cytokine signaling 3 (SOCS3) and ubiquitin specific peptidase 18 (USP18) to evaluate and compare with a more acknowledged marker, namely MxA. Specifically,

Table 1. Selected markers of response to IFN- $\beta$  therapy in patients with MS

Name	Function	Clinical findings	Reference
Viperin	multifunctional antiviral	markedly lower expression in the presence of NABs	10
SOCS3	STAT3 inhibitor	decrease in expression during relapse; expression higher in MS than in healthy controls	26, 27
USP18	protease (ubiquitin-like protein ISG15 residuals deconjugation), negative class I IFN receptor regulator	expression lower in untreated MS than in healthy controls; USP18 polymorphism with lower expression associated with more active MS course	7, 20
MxA	antiviral GTP-ase	MxA mRNA at 1 year of treatment predicts relapses and disability progression; low expression before treatment associated with more relapses and MRI activity during IFN treatment; higher mean MxA mRNA independently predicts lower risk of disability progression	9, 32–35

STAT – signal transducer and activator of transcription; ISG15 – interferon-stimulated gene 15; SOCS3 – suppressor of cytokine signaling 3; USP18 – ubiquitin specific peptidase 18; MxA – myxovirus resistance protein A.

the aim of this study was to compare serum levels of viperin, SOCS3, USP18 and MxA in IFN- $\beta$ -1b-treated RRMS patients with and without disease activity during a long-term follow-up.

## Material and methods

### Patients and treatment

Through years 2008–2013, we consecutively recruited 45 patients (31 women and 14 men), diagnosed with RRMS, who were started on IFN- $\beta$ -1b treatment in the setting of national MS treatment program at Heliodor Świącicki University Hospital in Poznań, Poland. Retrospective analysis revealed that all patients fulfilled the revised 2010 McDonald criteria<sup>16</sup> at the time of enrollment. Eligibility criteria included: age  $\geq 18$  years, no prior DMD treatment, qualification for the national MS treatment program (Supplementary Table 1). Exclusion criteria included pregnancy, decompensated liver (aminotransferase levels  $\geq 2$  upper reference limit) or thyroid disease (no euthyrosis), intractable depressive mood disorder, history of suicidal ideation, or epilepsy. The study protocol was approved by the Ethics Board of Poznan University of Medical Sciences. All subjects gave written informed consent for study participation.

The participants were started on subcutaneous IFN- $\beta$ -1b (Betaferon, n = 41, Extavia, n = 4) 250  $\mu$ g (8 MIU) every other day.

## Follow-up

The study cohort was followed through years 2008–2018. Each patient was assessed monthly by a neurologist. Imaging follow-up consisted of initial and then yearly 1.5 Tesla brain MRI (Siemens Avanto, Erlangen, Germany) using a 12-channel head coil with gadolinium contrast administration, including T1, FLAIR, T2, and PD sequences. Spinal MRI was performed in selected cases based on the physician's judgment. For each patient, every year, we determined: the number of relapses, the EDSS score, the presence of new or enhancing lesions in MR, NEDA-3 status and, if relevant, information about treatment termination.

## Definition of NEDA

We used a previously established NEDA (NEDA-3) definition<sup>2</sup>: for a given period of time, NEDA means the absence of relapses, disability progression and MRI activity. A relapse was defined as the appearance of new or the worsening of past symptoms with focal neurological abnormality applicable to MS that persists for  $\geq 24$  h, is not accompanied by fever and was preceded by  $\geq 30$  days of clinical stability. Disability progression was defined as an increase in EDSS by at least 1.5 from the baseline EDSS 0, by 1.0 from baseline 1.0–5.0 and by 0.5 from baseline 5.5 or more, confirmed after 3 months. The activity of MRI denotes new or enlarging T2/FLAIR hyperintense lesions or contrast enhancing lesions.

## Laboratory assays

Serum samples were collected at baseline and after 24 months of treatment and stored in  $-70^{\circ}\text{C}$ . Serum concentrations of MxA, viperin, USP18, and SOCS3 proteins were measured with the use of viperin, SOCS3 and USP18 ELISA kits (product No. MBS2023571, MBS703435 and MBS9338610, MyBiosource, San Diego, USA) and human MxA ELISA kit (product No. RD 194349200R, BioVendor, Brno, Czech Republic), according to the manufacturer's instructions.

## Statistical methods

P-values  $\leq 0.05$  were considered significant. Normalities of distributions were assessed with d'Agostino-Pearson test. Results were accordingly reported as either means  $\pm$  standard deviation (SD) or medians with interquartile range (IQR).

Baseline clinical characteristics (sex, age at first relapse, time from 1<sup>st</sup> to 2<sup>nd</sup> relapse, time to treatment initiation,

number of relapses prior to treatment initiation, EDSS score at treatment start) and baseline concentrations of MxA, viperin, USP18, and SOCS3 were compared between subgroups of patients with and without disease activity, including NEDA-3 and its components, in different time ranges.

Then, MxA, viperin, USP18, and SOCS3 were compared at 24 months. We used t-test and paired t-test for normally distributed interval variables, the Mann–Whitney U test for variables with non-normal data distribution and ordinal variables, and Fisher's exact test for nominal variables.

Stepwise logistic regression models were calculated. Variable sets included baseline characteristics as defined above and markers measured at baseline or at 24 months or their change from baseline at 24 months.

Statistical analyses were performed with the use of STATISTICA v. 13<sup>17</sup> (StatSoft, Inc., Tulsa, USA) and MedCalc for Windows, v. 15.8<sup>18</sup> (MedCalc Software, Ostend, Belgium).

## Results

### Baseline

A total of 45 patients were included. Their baseline characteristics are displayed in Table 2. Women were significantly older than men; otherwise, there were no gender-based differences. Median concentrations of biochemical markers are presented in Table 3. A statistically significant change from baseline to 24 months was noted for SOCS3 (a decrease) and MxA (an increase).

Median follow-up lasted 6.5 years (IQR 4.6 to 8.5). Throughout the observation, a gradual loss of NEDA was observed (Fig. 1).

### Discontinuation statistics

In 29 patients, treatment was terminated during the follow-up. The national treatment program was initially restricted to 3 years. This was the sole discontinuation reason in 2 patients (6.9%). Three patients (10.3%)

Table 2. Baseline characteristics of the study cohort

Parameter	All	Women	Men
Age at first relapse [years], mean $\pm$ SD	29.7 $\pm$ 7.9	31.4 $\pm$ 8.5*	25.8 $\pm$ 5.0*
Time to second relapse [months], median (IQR)	10 (3.3 to 25.0)	9 (3.8 to 25.0)	10 (3 to 36)
Time to treatment initiation [months], median (IQR)	17 (8.8 to 37.0)	22 (9.8 to 36.8)	15.5 (8 to 60)
Relapses before treatment, median (IQR)	2 (2 to 3)	3 (2 to 3)	2.5 (2 to 4)
EDSS at baseline, median (IQR)	1 (0 to 1.5)	1 (0 to 1)	1 (0 to 2)
OCB in CSF, % positive	89.7%	88.9%	91.7%

\*p = 0.008.

**Table 3.** Serum concentrations of different markers of response to IFN- $\beta$ -1b in relapsing-remitting patients with MS

Marker	Baseline		24 months		0–24-month change	
	N	median (IQR)	N	median (IQR)	N	median (IQR)
USP18 [ng/mL]	43	1.294 (0.707 to 2.099)	41	1.283 (0.659 to 2.653)	40	0.168 (–0.637 to 1.132)
SOCS3 [pg/mL]	43	5.703 (2.417 to 13.249)	41	0 (0.000 to 1.592)	40	–2.098* (–9.368 to –0.235)
viperin [ng/mL]	43	0.651 (0.385 to 0.943)	41	0.459 (0.243 to 0.722)	40	–0.204 (–0.505 to 0.145)
MxA [ng/mL]	24	2.612 (0.811 to 8.066)	19	4.747 (2.417 to 13.249)	8	1.498** (0.579 to 9.015)

\* $p < 0.001$ ; \*\* $p = 0.036$ ; SD – standard deviation; IQR – interquartile range.

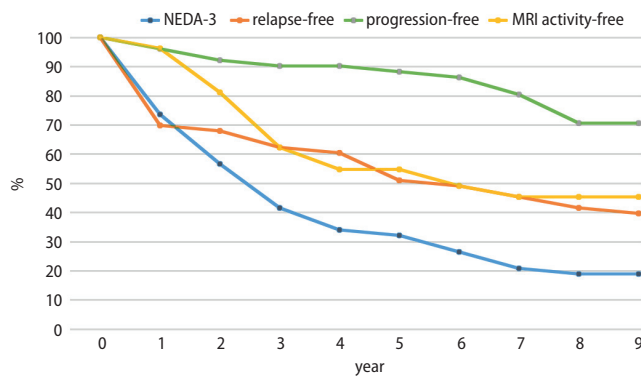


**Fig. 1.** Proportion of patients with no disease activity (according to NEDA-3 criteria), relapses, progression, and MRI activity over time

became pregnant or were planning pregnancy. Adverse reactions were the indication in 9 cases (31.0%) and treatment failure (2 or more severe relapses, >2 new MRI lesions, >1 enhancing lesion or EDSS increase beyond 4.5) in further 11 patients (37.9%). Four patients (13.8%) resigned for personal reasons. Patients who discontinued treatment did not differ in marker concentrations.

## Mutual correlations

There were few correlations between baseline clinical features and biomarkers considered in this study. Among clinical features, there was a weak correlation between older age at 1<sup>st</sup> relapse and shorter time to 2<sup>nd</sup> relapse. More pre-treatment relapses were associated with higher pre-treatment EDSS score.

Baseline USP18, SOCS3, viperin, and MxA had no significant correlations. On the other hand, pre-treatment SOCS3 and USP18 correlated positively with USP18 at 24 months. Baseline viperin and MxA correlated positively with MxA at 24 months.

There was little association between our markers and clinical characteristics. For baseline EDSS, there was a positive correlation with baseline SOCS3 and negative with baseline and 24-month MxA, however, not with MxA change. The interval between 1<sup>st</sup> and 2<sup>nd</sup> relapse was positively correlated with viperin at 24 months.

## Correlations with disease activity

A summary of marker concentration differences in patients with and without disease activity is presented in Table 4. Detailed results concerning USP18 (Supplementary Table 2), SOCS3 (Supplementary Table 3), viperin (Supplementary Table 4), and MxA (Supplementary Table 5) can be found in supplementary materials.

## Baseline molecular biomarkers

Numerous statistically significant differences were found for USP. Higher concentrations were associated with less disease activity in the first 5 years. Baseline SOCS3 had no correlations with disease activity. Baseline viperin levels were generally higher in subjects without disease activity, but they were lower in those without progression after the 7<sup>th</sup> year. Baseline MxA levels were higher in patients with no activity after the 5<sup>th</sup> year. More importantly, baseline MxA was higher in patients without progression during the entire follow-up.

## Molecular biomarkers at 24 months

Higher USP concentrations at 24 months were associated with less disease activity in the first 5 years. Suppressor of cytokine signaling 3 at 24 months was lower in patients with no disease activity, including NEDA in first 4 years and all its individual components in the 2<sup>nd</sup> year. At 24 months, compared to baseline, SOCS3 decreased in subjects with no MRI activity in the first 2 years, while in active cases, it had a tendency to remain unchanged or increase. Viperin levels at 24 months were higher in patients with no relapses after the 4<sup>th</sup> year. Regarding viperin change at 24 months, a decrease was noted in patients with no activity in earlier years, while an increase correlated with no disease activity in late follow-up. A notable exception was the increase in patients with no MRI activity in the first 5 years.

Two-year MxA levels were higher in patients without progression during the entire follow-up. In contrast, MxA at 24 months was lower in patients with no MRI activity until the 6<sup>th</sup> year.

**Table 4.** Marker concentration in relation to disease activity

Observation	p-value
<b>At baseline</b>	
USP18	
higher in pts with NEDA in the first 5 years	0.018
higher in pts without relapses in the first 5 years	0.041
higher in pts without MRI activity in the first 6 years	0.034
higher in pts without MRI activity during the entire follow-up	0.037
SOCS3	
None	
Viperin	
higher in pts with NEDA in year 2	0.031
higher in pts without relapses in year 2	0.010
higher in pts without disability progression in the first 7 years	0.041
lower in pts without disability progression after year 7	0.044
MxA	
higher in pts with NEDA after year 5	0.027
higher in pts without disability progression during the entire follow-up	0.007
Clinical	
Delay to treatment	
longer in pts with relapses after year 1	0.045
shorter in pts with NEDA after year 1	0.016
Baseline EDSS	
higher in pts with progression anytime during the follow-up	0.027
Pre-treatment relapses	
more in pts with progression within 6 years	0.010
Age at first relapse	
older: progression after year 2	0.036
younger: MRI activity within 7 years	0.014
Age at treatment initiation	
older: pts with NEDA after year 5	0.009
Time to second relapse	
shorter in pts with MRI activity in year 1	0.010
<b>At 24 months</b>	
USP18 at 24 months	
higher in pts with NEDA in the first 5 years	0.016
USP18 change	
none	
SOCS3 at 24 months	
lower in pts with NEDA in the first 4 years	0.042
lower in pts without relapses in year 2	0.008
lower in pts without disability progression in year 2	0.021
lower in pts without MRI activity in the first 2 years	0.039
SOCS3 change	
decrease in pts with no MRI activity in the first 2 years	0.016
Viperin at 24 months	
higher in pts without relapses after year 4	0.024
Viperin change	
decrease in pts with NEDA in the first 2 years	0.005
decrease in pts without relapses in year 2	0.008
decrease in pts without disability progression in the first 4 years	0.048
increase in pts with NEDA after year 7	0.010
increase in pts without relapses after year 4	0.018
increase in pts without disability progression after year 7	0.010
increase in pts without MRI activity in the first 5 years	0.033
MxA at 24 months	
lower in pts with no MRI activity until year 2	0.050
MxA change	
none	

pts – patients.

**Table 5.** ROC curve analysis results

Outcome	Criterion	ROC p-value	LR (95% CI)
NEDA in first 3 years	baseline USP >1.44	0.045	3.3 (1.4 to 7.7)
NEDA after year 1	baseline MxA >9.07	0.032	7.5 (1.8 to 31.4)
NEDA in first 4 years	delay to treatment onset	0.848	N/A
Relapse in first 5, 6 or 7 years	age at treatment onset	0.182	N/A

LR – likelihood ratio; CI – confidence interval; N/A – not available.

### Logistic regression and ROC analysis

Overall, the robust associations were not confirmed by stepwise regression. The only statistically significant models were for three-year NEDA, where baseline USP18 remained as the only contributor ( $p = 0.017$ ), NEDA after the 1<sup>st</sup> year with baseline MxA ( $p = 0.034$ ), four-year NEDA with the delay to treatment onset ( $p = 0.001$ ), and relapses in the first 7 years, which were inversely correlated to the age at treatment onset ( $p = 0.002$ ). Receiver operating characteristic (ROC) analysis allowed us to select cutoff values for USP and MxA as shown in Table 5.

### Discussion

This work is a prospective long-term follow-up study on novel biochemical biomarkers of response to IFN- $\beta$ -1b treatment in RRMS patients.

Overall, patients with no disease activity during the follow-up had a tendency to exhibit higher levels of USP18, viperin and MxA levels at baseline and at 24 months of treatment. Conversely, there was no difference in baseline SOCS3, while higher levels at 24 months were observed in patients with active disease.

Ubiquitin specific peptidase-18 is a class-I IFN induced enzyme that opposes IFN activity by enzymatic and non-enzymatic mechanisms.<sup>19</sup> Expression of USP18 is lower in untreated MS patients than in healthy controls, which indicates the possible involvement in disease pathomechanism.<sup>7</sup> In a cross-sectional study comparing USP18 polymorphism prevalence in MS patients and healthy controls, patients with a haplotype associated with lower USP18 expression experienced more active disease.<sup>20</sup> More recent research is scarce. A small (20 cases) retrospective study failed to show an association between baseline USP18 and response to IFN- $\beta$  in MS.<sup>21</sup>

Our results support the association of higher USP18 levels with lower disease activity in MS. Both baseline and 24-month levels were lower in patients with disease activity in subsequent years, indicating a mechanism independent from possible interference with IFN- $\beta$  treatment. In fact, the change in USP18 after 2 years of therapy did not differ between patients with good and poor response. Further

supporting our observation, baseline USP18 remained the only independent variable in stepwise regression model for NEDA in the first 3 years.

The family of suppressors of cytokine signaling (SOCS) contains regulators of intracellular signaling pathways of various cytokines induced predominately by the JAK-STAT cascade.

Suppressor of cytokine signaling 3 is induced by STAT3 and acts as an inhibitor of STAT3, with a complex impact on the immune system. It attenuates responses to class I and II IFNs, inhibits maturation of Th17 cells and directs macrophage polarization towards the M2 phenotype.<sup>22</sup> At the same time, SOCS3 may play a role in neuroprotection, as SOCS3 overexpression promotes neural differentiation and survival *in vitro*.<sup>23</sup>

Animal studies indicate both protective and harmful effects on the CNS in experimental autoimmune encephalitis (EAE).<sup>24</sup> Experimental autoimmune encephalitis in SOCS3-transfected mice develops later, but is more severe.<sup>25</sup>

Little research has been done on SOCS3 in human MS subjects. During relapse, a decrease in leukocyte SOCS3 expression was observed.<sup>26</sup> On the other hand, in a small American study,<sup>27</sup> SOCS3 expression was significantly higher in MS patients than in the healthy controls, with a trend towards more disability in patients with higher expression. This observation was not confirmed in a more recent study.<sup>28</sup>

In our study, baseline SOCS3 levels were not different in patients with and without disease activity. However, the levels rose and were higher at 24 months in those with activity in the 2<sup>nd</sup> year, possibly reflecting a maintained, but unbeneficial drug effect. However, the observation was lost when controlled for other variables.

Viperin is an anti-viral protein induced by class I interferons<sup>29</sup> and a specific marker of IFN- $\beta$  activity.<sup>7</sup> In the INSIGHT trial, viperin and MxA expression were compared among patients with and without anti-IFN antibodies.<sup>10</sup> In patients with NABs, the expression levels of all 3 proteins were lower or absent at NAb titres  $\geq 100$  TRU. The study was not designed to assess correlations between marker expression and disease activity.

In our cohort, baseline viperin concentrations were higher in patients with no disease activity. However, the baseline values were lower in those with no progression later on. At 24 months, viperin levels were higher in those who did not experience relapses in the subsequent years.

While the absolute values were higher in cases with better outcome, viperin change between baseline and 24 months showed a general trend to be more negative in patients with no disease activity in earlier years (up to the 4<sup>th</sup>) and more positive in those stable in later follow-up. This was apparent for NEDA, relapses and progression. For MRI activity, which is considered to be the earliest indicator of disease activity among NEDA components, there was a concordant rise in viperin in stable patients in both earlier and later years, with a similar trend for the entire follow-up.

Overall, no independent association with prognosis was found in regression models. Myxovirus resistance protein A (MxA), a class I IFN-induced GTP-ase with antiviral properties,<sup>29</sup> is considered one of the most reliable markers of IFN- $\beta$  bioavailability.<sup>30</sup> The absence of MxA induction signifies total loss of IFN activity, as no other IFN-induced proteins are detected in this setting.<sup>31</sup> Unsurprisingly, numerous studies reported an association between low MxA mRNA and poor response to IFN. MxA mRNA measured at 1 year of treatment was a better predictor of relapses than NAb titers.<sup>9,32</sup> In another study, MxA induction at 1 year predicted a longer time to a relapse or EDSS progression.<sup>33</sup> More intriguing is that low MxA expression before treatment was also associated with a higher risk of relapses or EDSS worsening while on IFN.<sup>34</sup> Higher mean MxA mRNA, measured over the period from 6 months to 2 years of treatment, predicted a lower risk of disability progression in the first 3 years, independently from relapse activity.<sup>35</sup> On the other hand, in 2 more recent studies<sup>21,36</sup> MxA mRNA levels failed to predict treatment response to IFN- $\beta$  in a two-year observation.

Our results replicated the association of higher MxA levels, both during IFN therapy and in treatment-naive patients, with less disease activity. What is more, baseline MxA was the only independent predictor of disease activity past year 1, with the highest levels  $>9.07$  ng/mL associated with a 7.5 likelihood ratio for no disease activity.

The heterogeneity of immunologic profiles in MS, as well as their associations with treatment response, has been addressed in several recent works.<sup>11–13,37</sup> Our study lends support to the notion that certain alterations convey a higher risk of poor outcome. The study yielded multiple findings. However, only several have potential clinical utility. In logistic regression, higher baseline USP18 remained the only independent prognostic factor for NEDA, and only in the first 3 years of treatment. High baseline MxA, on the other hand, was independently associated with NEDA in the observation after the 1<sup>st</sup> year.

Our study has several limitations. The choice of testing material requires commentary. Previous studies concerning their expression utilized either mRNA (MxA, viperin, USP18, SOCS3) or protein measurement (MxA) in peripheral blood cells. Quantitative real-time polymerase chain reaction (qRT-PCR) for mRNA is more sensitive, but protein detection methods are cheaper; furthermore, the short half-life of mRNA forces strict timing of sample collection in relation to drug administration: For MxA, mRNA levels begin to increase at 3 and peak at 12 h post-injection, decreasing two-fold by 24 h<sup>38</sup>; MxA protein levels remain more stable,<sup>39</sup> allowing more flexible sampling. It is also worth noting that, on the one hand, mRNA detection reflects the earliest expression stage most closely related to gene induction by IFN and, on the other, protein measurement accounts for all post-transcription and post-translation regulatory processes and may, therefore, more accurately correlate with actual biological activity. For MxA, a dose effect of IFN is apparent at protein level, but not at mRNA level.<sup>40</sup>

All the assessed proteins are intracellular. Due to technical limitations, no cellular material was available for this study. We, therefore, performed a number of preliminary measurements on healthy donors (data not published) and found that the aforementioned particles are detectable at various levels in sera. This may reflect either protein release from fragmented cells or the protein contained in nanoparticles.

By detecting associations with disease activity, this study confirms that serum is a valid material for the measurement of USP18, SOCS3, viperin, and MxA. What is more, we provide evidence that the differences in IFN-inducible gene products expression are apparent at the protein stage, not only at mRNA, as shown in previous studies.

A considerable proportion of cases was lost during observation, and other cases were recruited late in the study, resulting in a median follow-up of almost 7 years. The lower number of cases in years 6–9 may have contributed to the fact that most of the significant associations were not present beyond the 5<sup>th</sup> year. Knowing that the baseline marker levels kept their associations until then, the true prognostic value of measurements at 24 months may be underappreciated in our study.

A number of peculiarities concerning treatment decisions in our cohort need to be addressed. The considerable delay between diagnosis and treatment initiation is caused by procedural barriers, including limited access to imaging facilities and long waiting queues at MS treatment centers in Poland. Due to treatment program rules and lack of registered second-line therapies, many patients with ongoing disease activity continued IFN treatment. In addition, 2 patients were excluded from further treatment due to treatment program duration restriction that was in force until 2012.

Unanswered questions leave implications for future research. It would be informative to assess USP18, viperin, SOCS3, and MxA levels in patients on other DMDs and without treatment, in order to separate their natural variance in SM from drug effects and to assess whether they are predictive of response to any particular drug. In addition, it might be prudent to focus on early dynamics of the markers included in this study.

## Conclusions

Low levels of plasma USP-18, viperin and MxA at baseline and at 24 months of treatment and high levels of SOCS3 at 24 months are associated with more disease activity and worse outcome in IFN- $\beta$ -1b-treated MS patients.

However, only baseline USP18 and MxA were independent predictors of disease activity: Baseline USP18 > 1.44 ng/mL was associated with NEDA in the first 3 years with LR of 3.3, while baseline MxA > 9.07 ng/mL was associated with NEDA in the entire observation beyond year 1 with LR of 7.5, identifying infrequent patients with very mild disease and sustained good response to IFN- $\beta$ -1b.

Suppressor of cytokine signaling 3 was the only marker with higher instead of lower concentrations in the cases with more active MS. Moreover, its concentration decreased during two-year IFN treatment and at that time point, higher values were observed in patients currently experiencing relapses, MRI activity or progression. While SOCS3 failed to predict later course, this association appears to reflect an important qualitative variability of response to IFN- $\beta$ -1b.

## ORCID iDs

Anna Pietrzak  <https://orcid.org/0000-0002-3606-7296>  
 Alicja Kalinowska-Lyszczarz  <https://orcid.org/0000-0002-0618-1637>  
 Krystyna Osztynowicz  <https://orcid.org/0000-0003-4782-1474>  
 Alima Khamidulla  <https://orcid.org/0000-0002-5007-8151>  
 Wojciech Kozubski  <https://orcid.org/0000-0003-2777-261X>  
 Sławomir Michalak  <https://orcid.org/0000-0002-5602-4306>

## References

- Dobson R, Giovannoni G. Multiple sclerosis: A review. *Eur J Neurol*. 2019;26(1):27–40. doi:10.1111/ene.13819
- Kappos L, De Stefano N, Freedman MS, et al. Inclusion of brain volume loss in a revised measure of “no evidence of disease activity” (NEDA-4) in relapsing-remitting multiple sclerosis. *Mult Scler*. 2016;22(10):1297–1305. doi:10.1177/1352458515616701
- Mayssam EN, Eid C, Khoury SJ, Hannoun S. “No evidence of disease activity”: Is it an aspirational therapeutic goal in multiple sclerosis? *Mult Scler Relat Disord*. 2020;40:101935. doi:10.1016/j.msard.2020.101935
- Freedman MS, Selchen D, Prat A, Giacomini PS. Managing multiple sclerosis: Treatment initiation, modification, and sequencing. *Can J Neurol Sci*. 2018;45(5):489–503. doi:10.1017/cjn.2018.17
- Río J, Castelló J, Rovira A, et al. Measures in the first year of therapy predict the response to interferon  $\beta$  in MS. *Mult Scler*. 2009;15(7):848–853. doi:10.1177/1352458509104591
- Sormani MP, Río J, Tintorè M, et al. Scoring treatment response in patients with relapsing multiple sclerosis. *Mult Scler J*. 2013;19(5):605–612. doi:10.1177/1352458512460605
- Malhotra S, Bustamante MF, Miralles F, et al. Search for specific biomarkers of IFN $\beta$  bioactivity in patients with multiple sclerosis. *PLoS One*. 2011;6(8). doi:10.1371/journal.pone.0023634
- Malucchi S, Gilli F, Caldano M, et al. One-year evaluation of factors affecting the biological activity of interferon beta in multiple sclerosis patients. *J Neurol*. 2011;258(5):895–903. doi:10.1007/s00415-010-5844-5
- Malucchi S, Gilli F, Caldano M. Predictive markers for response to interferon therapy in patients with multiple sclerosis. *Neurology*. 2008;(70):1119–1127. doi:10.1212/01.wnl.0000304040.29080.7b
- Pachner AR, Warth JD, Pace A, Goelz S. Effect of neutralizing antibodies on biomarker responses to interferon beta: The INSIGHT study. *Neurology*. 2009;73(18):1493–1500. doi:10.1212/WNL.0b013e3181bf98db
- Bărcuțean LI, Romaniuc A, Maier S, et al. Clinical and serological biomarkers of treatment’s response in multiple sclerosis patients treated continuously with interferon  $\beta$ -1b for more than a decade. *CNS Neurol Disord Drug Targets*. 2018;17(10):780–792. doi:10.2174/1871527317666180917095256
- Taheri M, Ghafouri-Fard S, Solgi G, Sayad A, Mazdeh M, Omrani MD. Determination of cytokine levels in multiple sclerosis patients and their relevance with patients’ response to Cinnovex. *Cytokine*. 2017;96:138–143. doi:10.1016/j.cyto.2017.04.007
- Balasa R, Maier S, Voidazan S, et al. Assessment of interleukin-17A, interleukin-10 and transforming growth factor-beta1 serum titers in relapsing remitting multiple sclerosis patients treated with avonex, possible biomarkers for treatment response. *CNS Neurol Disord Drug Targets*. 2017;16(1):93–101. doi:10.2174/1871527315666160615110739
- Manna I, Iaccino E, Dattilo V, et al. Exosome-associated miRNA profile as a prognostic tool for therapy response monitoring in multiple sclerosis patients. *FASEB J*. 2018;32(8):4241–4246. doi:10.1096/fj.201701533R
- Magner WJ, Weinstock-Guttman B, Rho M, et al. Dicer and microRNA expression in multiple sclerosis and response to interferon therapy. *J Neuroimmunol*. 2016;292:68–78. doi:10.1016/j.jneuroim.2016.01.009

16. Polman CH, Reingold SC, Banwell B, et al. Diagnostic criteria for multiple sclerosis: 2010 Revisions to the McDonald criteria. *Ann Neurol*. 2011;69(2):292–302. doi:10.1002/ana.22366
17. TIBCO Software Inc. Statistica (data analysis software system), v. 13. Palo Alto, CA. <http://statistica.io>. Accessed November 15, 2017.
18. MedCalc Software bvba. MedCalc statistical software. Ostend, Belgium. <https://www.medcalc.org/>. Accessed on May 13, 2017.
19. Malakhova OA, Kim K II, Luo JK, et al. UBP43 is a novel regulator of interferon signaling independent of its ISG15 isopeptidase activity. *EMBO J*. 2006;25(11):2358–2367. doi:10.1038/sj.emboj.7601149
20. Malhotra S, Morcillo-Suárez C, Nurtdinov R, et al. Roles of the ubiquitin peptidase USP18 in multiple sclerosis and the response to interferon- $\beta$  treatment. *Eur J Neurol*. 2013;20(10):1390–1397. doi:10.1111/ene.12193
21. Martire S, Navone ND, Montarolo F, Perga S, Bertolotto A. A gene expression study denies the ability of 25 candidate biomarkers to predict the interferon-beta treatment response in multiple sclerosis patients. *J Neuroimmunol*. 2016;292:34–39. doi:10.1016/j.jneuroim.2016.01.010
22. Gao Y, Zhao H, Wang P, Wang J, Zou L. The roles of SOCS3 and STAT3 in bacterial infection and inflammatory diseases. *Scand J Immunol*. 2018;88(6):e12727. doi:10.1111/sji.12727
23. Mishra KK, Gupta S, Banerjee K. SOCS3 induces neurite differentiation and promotes neuronal cell survival. *IUBMB Life*. 2016;68(6):468–476. doi:10.1002/iub.1505
24. Benveniste EN, Liu Y, McFarland BC, Qin H. Involvement of the Janus kinase/signal transducer and activator of transcription signaling pathway in multiple sclerosis and the animal model of experimental autoimmune encephalomyelitis. *J Interf Cytokine Res*. 2014;34(8):577–588. doi:10.1089/jir.2014.0012
25. Tanaka K, Ichiyama K, Hashimoto M, et al. Loss of suppressor of cytokine signaling 1 in helper T cells leads to defective Th17 differentiation by enhancing antagonistic effects of IFN- $\gamma$  on STAT3 and Smads. *J Immunol*. 2008;180(6):3746–3756. doi:10.4049/JIMMUNOL.180.6.3746
26. Frisullo G, Mirabella M, Angelucci F, et al. The effect of disease activity on leptin, leptin receptor and suppressor of cytokine signalling-3 expression in relapsing-remitting multiple sclerosis. *J Neuroimmunol*. 2007;192(1–2):174–183. doi:10.1016/j.jneuroim.2007.08.008
27. Sedeño-Monge V, Arcega-Revilla R, Rojas-Morales E, et al. Quantitative analysis of the suppressors of cytokine signaling 1 and 3 in peripheral blood leukocytes of patients with multiple sclerosis. *J Neuroimmunol*. 2014;273(1–2):117–119. doi:10.1016/j.jneuroim.2014.05.013
28. Toghi M, Taheri M, Arsang-Jang S, et al. SOCS gene family expression profile in the blood of multiple sclerosis patients. *J Neurol Sci*. 2017;375:481–485. doi:10.1016/j.jns.2017.02.015
29. Chemudupati M, Kenney AD, Bonifati S, et al. From APOBEC to ZAP: Diverse mechanisms used by cellular restriction factors to inhibit virus infections. *Biochim Biophys Acta Mol Cell Res*. 2019;1866(3):382–394. doi:10.1016/j.bbamcr.2018.09.012
30. Bertolotto A, Granieri L, Marnetto F, et al. Biological monitoring of IFN- $\beta$  therapy in multiple sclerosis. *Cytokine Growth Factor Rev*. 2015;26(2):241–248. doi:10.1016/j.cytogfr.2014.12.002
31. Hesse D, Sellebjerg F, Sorensen PS. Absence of MxA induction by interferon  $\beta$  in patients with MS reflects complete loss of bioactivity. *Neurology*. 2009;73(5):372–377. doi:10.1212/WNL.0b013e3181b04c98
32. Van Der Voort LF, Visser A, Knol DL, Oudejans CBM, Polman CH, Killestein J. Lack of interferon-beta bioactivity is associated with the occurrence of relapses in multiple sclerosis. *Eur J Neurol*. 2009;16(9):1049–1052. doi:10.1111/j.1468-1331.2009.02649.x
33. Matas E, Bau L, Martínez-Iniesta M, Romero-Pinel L, Mañé-Martínez MA, Martínez-Yélamos S. Absence of MxA induction is related to a poor clinical response to interferon beta treatment in multiple sclerosis patients. *J Neurol*. 2016;263(4):722–729. doi:10.1007/s00415-016-8053-z
34. Matas E, Bau L, Martínez-Iniesta M, et al. Baseline MxA mRNA expression predicts interferon beta response in multiple sclerosis patients. *PLoS One*. 2014;9(11):e112758. doi:10.1371/journal.pone.0112758
35. Serena F, Imberti L, Amato MP, et al. MxA quantification and disability progression in interferon beta-treated multiple sclerosis patients. *PLoS One*. 2014;9(4):e94794. doi:10.1371/journal.pone.0094794
36. Libertinova J, Meluzinova E, Tomek A, et al. Myxovirus resistance protein A mRNA expression kinetics in multiple sclerosis patients treated with IFN $\beta$ . *PLoS One*. 2017;12(1):e0169957. doi:10.1371/journal.pone.0169957
37. Hegen H, Adrianto I, Lessard CJ, et al. Cytokine profiles show heterogeneity of interferon- $\beta$  response in multiple sclerosis patients. *Neurol Neuroimmunol NeuroInflamm*. 2016;3(2):e202. doi:10.1212/NXI.0000000000000202
38. Gilli F, Marnetto F, Caldano M, et al. Biological responsiveness to first injections of interferon-beta in patients with multiple sclerosis. *J Neuroimmunol*. 2005;158(1–2):195–203. doi:10.1016/j.jneuroim.2004.08.006
39. Kracke A, von Wussow P, Al-Masri AN, Dalley G, Windhagen A, Heidenreich F. Mx proteins in blood leukocytes for monitoring interferon beta-1b therapy in patients with MS. *Neurology*. 2000;54(1):193–199. doi:10.1212/WNL.54.1.193
40. Bertolotto A, Gilli F, Sala A, et al. Evaluation of bioavailability of three types of IFN $\beta$  in multiple sclerosis patients by a new quantitative-competitive-PCR method for MxA quantification. *J Immunol Methods*. 2001;256(1–2):141–152. doi:10.1016/S0022-1759(01)00434-3

## Supplementary material

Supplementary Table 1. Polish National MS treatment program eligibility criteria in the years 2008–2013

Criteria	Before 2012	From 2012
Diagnosis	2005 McDonald criteria and contrast-enhanced head MRI consistent with MS	
Disease activity	at least 2 relapses within 2 last years	not specified
Required score	21	15
Scoring system	Age: 16–40 years – 6 pt 40–60 years – 3 pt over 60 years – 1 pt Disease duration: 0–3 years – 6 pt 3–6 years – 3 pt 6–10 years – 2 pt over 10 years – 1 pt RRMS with no deficit – 5 pt Number of relapses in the last year: 3–4 – 5 pt 1–2 – 4 pt 6–7 – 2 pt none (less than 1/year) – 1 pt over 7 – 0 pt EDSS score: 0–2 – 6 pt 2.5 – 4 – 3 pt 4.5 – 5 – 2 pt over 5 – 1 pt	Disease duration: 0–3 years – 6 pt 3–6 years – 4 pt 6–10 years – 2 pt over 10 years – 1 pt RRMS with no deficit – 5 pt Number of relapses in the last year: 3 and more – 5 pt 1–2 – 4 pt none – 1 pt EDSS score: 0–2 – 6 pt 2.5–4 – 5 pt 4.5–5 – 2 pt over 5 – 1 pt
Exclusion criteria	1. hypersensitivity to IFN- $\beta$ ; 2. primarily or secondarily progressive MS; 3. pregnancy; 4. decompensated liver disease (aminotransferase levels $\geq 2$ upper reference limit); 5. thyroid disease (no euthyrosis); 6. intractable depressive mood disorder or history of suicidal ideation; 7. epilepsy.	

MRI – magnetic resonance imaging; MS – multiple sclerosis; RRMS – relapsing-remitting multiple sclerosis; pt – points; EDSS – Expanded Disability Status Score.

**Supplementary Table 2.** Statistically significant differences in USP18 (all values in ng/mL) between patients with and without disease activity

Comparison	Non-active				Active		p-value
	N	mean ±SD or median (IQR)			N	mean ±SD or median (IQR)	
Baseline USP18 vs NEDA							
until 3 years	16	2.142 ±1.5828		>	24	1.195 ±0.6954	0.036
until 4 years	12	2.517 ±1.6506		>	28	1.170 ±0.6694	0.018
until 5 years	12	2.517 ±1.6506		>	28	1.170 ±0.6694	0.018
Baseline USP18 vs relapses							
until 5 years	18	2.037 ±1.5173		>	21	1.188 ±0.7462	0.041
Baseline USP18 vs MRI							
until 3 years	25	1.621 (0.947 to 2.335)		>	12	0.897 (0.484 to 1.217)	0.003
until 4 years	18	2.124 ±1.4866		>	17	0.958 ±0.5297	0.005
until 5 years	18	2.124 ±1.4866		>	17	0.958 ±0.5297	0.005
until 6 years	13	2.253 ±1.7165		>	20	1.092 ±0.5982	0.034
after year 1	19	2.030 ±1.5449		>	22	1.134 ±0.5854	0.026
after year 2	17	2.026 ±1.6095		>	20	1.155 ±0.5947	0.048
entire follow-up	20	1.946 ±1.5496		>	22	1.134 ±0.5854	0.037
USP18 at 24 month vs NEDA							
until 4 years	10	2.586 (1.496 to 4.970)		>	28	0.939 (0.583 to 2.074)	0.040
until 5 years	10	2.462 (1.353 to 3.834)		>	28	0.939 (0.583 to 2.074)	0.016

N – number of cases; SD – standard deviation; IQR – interquartile range; USP18 – ubiquitin specific protease 18; \*small groups.

**Supplementary Table 3.** Statistically significant differences in SOCS3 (all values in pg/mL) between patients with and without disease activity

Comparison	Non-active				Active		p-value
	N	mean ±SD or median (IQR)			N	mean ±SD or median (IQR)	
Baseline SOCS3 vs NEDA, relapses, MRI or progression: no significant differences							
SOCS3 at 24 months vs NEDA							
in year 2	29	0.000 (0.000 to 0.473)		<	11	5.422 (0.101 to 14.834)	0.011
until 4 years	10	0.000 (0.000 to 1.338)		<	28	0.000 (0.000 to 3.889)	0.042
SOCS3 at 24 months vs relapses							
in year 2	31	0.000 (0.000 to 0.534)		<	9	12.086 (0.303 to 44.016)	0.008
SOCS3 at 24 months vs progression							
in year 2*	37	0.000 (0.000 to 0.726)		<	3	12.086 (7.088 to 100.121)	0.021
SOCS3 at 24 months vs MRI							
in year 2	34	0.000 (0.000 to 0.565)		<	5	12.737 (1.766 to 44.016)	0.039
until 2 years	34	0.000 (0.000 to 0.565)		<	5	12.737 (1.766 to 44.016)	0.039
SOCS3 change at 24 months vs MRI							
until 2 years	33	-3.337 (-10.616 to -0.483)		<	5	0.000 (-1.621 to 31.013)	0.016
in year 2	33	-3.337 (-10.616 to -0.483)		<	5	0.000 (-1.621 to 31.013)	0.016

N – number of cases; SD – standard deviation; IQR –interquartile range; SOCS3 – suppressor of cytokine signaling 3.

Supplementary Table 4. Statistically significant differences in viperin (all values in ng/mL) between patients with and without disease activity

Comparison	Non-active			Active			p-value
	N	mean $\pm$ SD or median (IQR)		N	mean $\pm$ SD or median (IQR)		
Baseline viperin vs NEDA							
in year 2	31	0.760 $\pm$ 0.4035	>	11	0.458 $\pm$ 0.3156		0.031
Baseline viperin vs relapses							
in year 2	33	0.763 $\pm$ 0.3915	>	9	0.381 $\pm$ 0.2922		0.010
Baseline viperin vs progression							
until 2 years	38	0.670 (0.447 to 0.970)	>	4	0.193 (0.0474 to 0.385)		0.005
until 3 years	34	0.670 (0.447 to 0.947)	>	5	0.292 (0.0710 to 0.348)		0.003
until 4 years	29	0.776 (0.480 to 0.991)	>	5	0.292 (0.0710 to 0.348)		0.002
until 5 years	28	0.780 (0.469 to 1.012)	>	6	0.298 (0.0947 to 0.478)		0.005
until 6 years	25	0.687 (0.428 to 0.991)	>	7	0.305 (0.144 to 0.510)		0.023
until 7 years	20	0.765 $\pm$ 0.4301	>	10	0.440 $\pm$ 0.2991		0.041
after year 7	14	0.503 (0.312 to 0.653)	<	5	1.054 (0.839 to 1.124)		0.044
Baseline viperin vs MRI: no significant differences							
Viperin at 24 months vs relapses							
after year 4	17	0.570 (0.418 to 0.786)	>	12	0.263 (0.0749 to 0.532)		0.024
after year 5	19	0.570 (0.360 to 0.734)	>	8	0.241 (0.0749 to 0.412)		0.022
after year 6	19	0.570 (0.360 to 0.734)	>	7	0.325 (0.152 to 0.426)		0.048
Viperin change at 24 months vs NEDA							
in year 8	13	0.0133 (-0.188 to 0.187)	>	6	-0.431 (-0.546 to -0.347)		0.005
until 2 years	21	-0.364 (-0.630 to 0.119)	<	18	-0.124 (-0.326 to 0.355)		0.005
after year 7	12	0.0280 (-0.234 to 0.212)	>	7	-0.364 (-0.534 to -0.271)		0.010
Viperin change at 24 months vs relapses							
in year 2	30	-0.337 (-0.525 to 0.117)	<	9	0.0834 (-0.116 to 0.650)		0.008
in year 5	23	-0.107 (-0.360 to 0.236)	>	6	-0.529 (-1.089 to -0.371)		0.023
after year 3	15	0.0427 (-0.306 to 0.332)	>	14	-0.367 (-0.546 to -0.107)		0.046
after year 4	17	0.0427 (-0.361 to 0.383)	>	12	-0.367 (-0.758 to -0.124)		0.018
Viperin change at 24 months vs progression							
in year 8	14	0.0109 (-0.326 to 0.163)	>	5	-0.497 (-0.652 to -0.322)		0.010
until 2 years	35	-0.246 (-0.509 to 0.109)	<	4	0.438 (0.107 to 0.661)		0.031
until 3 years	31	-0.246 (-0.509 to 0.109)	<	5	0.355 (-0.0556 to 0.591)		0.047
until 4 years	26	-0.286 (-0.512 to 0.117)	<	5	0.355 (-0.0556 to 0.591)		0.048
after year 7	14	0.0109 (-0.326 to 0.163)	>	5	-0.497 (-0.652 to -0.322)		0.010
Viperin change at 24 months vs MRI							
until 4 years	15	0.0427 (-0.384 to 0.332)	>	17	-0.364 (-0.530 to -0.202)		0.033
until 5 years	15	0.0427 (-0.384 to 0.332)	>	17	-0.364 (-0.530 to -0.202)		0.033

N – number of cases; SD – standard deviation; IQR – interquartile range; \*small groups.

**Supplementary Table 5.** Statistically significant differences in MxA (all values in ng/mL) between patients with and without disease activity

Comparison	Non-active				Active			p-value
	N	mean ±SD or median (IQR)			N	mean ±SD or median (IQR)		
Baseline MxA vs NEDA								
after year 5	8	8.852 (2.570 to 26.005)		>	9	1.404 (0.294 to 2.543)		0.027
Baseline MxA vs relapses: no significant differences								
Baseline MxA vs progression								
after year 1	16	3.844 (1.853 to 12.141)		>	8	0.983 (0.196 to 2.052)		0.007
after year 2	17	3.829 (1.405 to 11.274)		>	7	1.404 (0.435 to 2.078)		0.040
after year 5	11	3.860 (2.086 to 19.293)		>	6	0.983 (0.393 to 2.001)		0.020
entire follow-up	16	3.844 (1.853 to 12.141)		>	8	0.983 (0.196 to 2.052)		0.007
MxA at 24 months vs NEDA: no significant differences								
MxA at 24 months vs relapses: no significant differences								
MxA at 24 months vs progression								
after year 1	12	8.127 (3.118 to 15.994)		>	7	2.536 (0.000 to 3.404)		0.022
after year 2	12	8.127 (3.118 to 15.994)		>	6	2.536 (0.000 to 3.404)		0.025
after year 3	10	11.269 (3.228 to 17.155)		>	5	2.774 (1.723 to 4.216)		0.040
entire follow-up	13	7.718 (3.173 to 15.414)		>	6	2.536 (0.000 to 3.404)		0.022
MxA at 24 months vs MRI								
until year 6	6	2.891 (0.393 to 3.228)		<	9	7.718 (3.127 to 15.414)		0.050
MxA change at 1 month vs relapses: no significant differences								

N – number of cases; SD – standard deviation; IQR – interquartile range; MxA – myxovirus resistance protein A.



# Is serum anti-Müllerian hormone (AMH) assay a satisfactory measure for ovarian reserve estimation? A comparison of serum and peritoneal fluid AMH levels

Marta Kostrzewa<sup>1,A-E</sup>, Ewa Głowacka<sup>2,B,C</sup>, Tomasz Stetkiewicz<sup>1,C,E,F</sup>, Mariusz Grzesiak<sup>3,C,E</sup>, Krzysztof Szyłło<sup>1,E,F</sup>, Grzegorz Stachowiak<sup>1,A,E,F</sup>, Jacek Radosław Wilczyński<sup>4,A,E,F</sup>

<sup>1</sup> Department of Operative Gynecology and Gynecologic Oncology, Polish Mother's Memorial Hospital Research Institute, Łódź, Poland

<sup>2</sup> Laboratory Diagnostics Center, Polish Mother's Memorial Hospital Research Institute, Łódź, Poland

<sup>3</sup> Department of Perinatology, Obstetrics and Gynecology, Polish Mother's Memorial Hospital Research Institute, Łódź, Poland

<sup>4</sup> Department of Gynecological Surgery and Oncology, Medical University of Lodz, Poland

A – research concept and design; B – collection and/or assembly of data; C – data analysis and interpretation; D – writing the article; E – critical revision of the article; F – final approval of the article

Advances in Clinical and Experimental Medicine, ISSN 1899–5276 (print), ISSN 2451–2680 (online)

*Adv Clin Exp Med.* 2020;29(7):853–856

## Address for correspondence

Marta Kostrzewa  
E-mail: kostrzewa.marta1@gmail.com

## Funding sources

The study had financial support from Young Scientist Grant No. 502-03/5-105-02/502-54-131 from the Medical University of Lodz, Poland.

## Conflict of interest

None declared

Received on November 12, 2019

Reviewed on December 20, 2019

Accepted on April 24, 2020

Published online on July 31, 2020

## Cite as

Kostrzewa M, Głowacka E, Stetkiewicz T, et al. Is serum anti-Müllerian hormone (AMH) assay a satisfactory measure for ovarian reserve estimation? A comparison of serum and peritoneal fluid AMH levels. *Adv Clin Exp Med.* 2020;29(7):853–856. doi:10.17219/acem/121010

## DOI

10.17219/acem/121010

## Copyright

© 2020 by Wrocław Medical University  
This is an article distributed under the terms of the Creative Commons Attribution 3.0 Unported (CC BY 3.0) (<https://creativecommons.org/licenses/by/3.0/>)

## Abstract

**Background.** Clinical cases have been reported with women who got pregnant with confirmed low serum anti-Müllerian hormone (AMH) concentrations, thus demonstrating that low serum AMH concentration cut-points could be fairly specific for poor ovarian response (POR) to gonadotrophin stimulation, but not for pregnancy. That observation prompted the question whether serum AMH concentration accurately corresponded to the whole amount of AMH secreted by granulosa cells.

**Objectives.** To measure AMH levels in peritoneal fluid and their correlations with serum AMH concentrations.

**Material and methods.** The reported study involved 48 female patients, aged 18–40 years, diagnosed with benign ovarian cysts and qualified for a laparoscopic cystectomy. Prior to surgery, the ovarian reserve was assessed using serum AMH concentration assay. The peritoneal fluid was also collected during the laparoscopy and AMH concentrations in peritoneal fluid were measured.

**Results.** The AMH present in the peritoneal fluid strongly correlated with AMH levels in blood serum ( $r = 0.54$ ;  $p < 0.001$ ) and higher serum AMH concentrations corresponded to higher AMH concentrations in the peritoneal fluid. There was also a significant correlation between AMH levels in serum and in peritoneal fluid, collected from patients with endometrioma and other benign cysts ( $r = 0.61$ ;  $p = 0.001$  vs  $r = 0.43$ ;  $p = 0.03$ ).

**Conclusions.** The AMH is present in the peritoneal fluid and its concentrations significantly correlate with AMH levels in serum. The assessment of AMH concentration in the peritoneal fluid may be a valuable complement to the evaluation of ovarian reserve and the diagnosis of infertility after adnexal surgery.

**Key words:** anti-Müllerian hormone, peritoneal fluid, ovarian reserve, endometrioma, fertility

## Introduction

The anti-Müllerian Hormone (AMH) is produced in granulosa cells and its highest concentration is present in the granulosa cells of the secondary, preantral and small antral follicles.<sup>1</sup> It exerts an inhibitory effect on primordial follicle recruitment and may also inhibit, through its paracrine action, the follicle-stimulating, hormone-dependent selection of follicles for dominance.<sup>2</sup> It is secreted into the blood, which makes it possible to measure it in blood serum. The AMH concentration in serum reflects the pool of ovarian follicles, while a reduced amount of antral follicles may result in a decreased serum AMH level. That is why AMH concentration in serum seems to be a reliable marker in the evaluation of ovarian reserve.<sup>1–3</sup>

According to the opinions of both the American Society for Reproductive Medicine and the American College of Obstetricians and Gynecologists, no test of ovarian reserve is likely to be precise enough for an accurate evaluation of the chances for spontaneous conception. On the other hand, there is a prevailing opinion that AMH and the antral follicle count (AFC) are promising predictive markers, especially in the cases of poor ovarian reserve (POR), which corresponds to women in the reproductive age and with regular menses whose response to ovarian stimulation or fecundity is reduced compared to other women in a comparable age.<sup>3–6</sup> The studies revealed that AMH concentrations between 0.2 ng/mL and 0.7 ng/mL had been highly sensitive (40–97%) and specific (78–92%) to discriminate a diminished ovarian reserve (<3 follicles or 2–4 retrieved oocytes) or a poor response to gonadotrophin stimulation in a population of women qualified to in vitro fertilization (IVF); however, those cut-points were neither sensitive nor specific enough to precisely predict the chances for pregnancy.<sup>3,7,8</sup> The average AMH levels, which corresponded to normal ovarian reserve, ranged between 2.5 ng/mL and 2.7 ng/mL. Regarding those values, the AMH test demonstrated sensitivity and specificity to clinical pregnancy with 83% and 82% accuracy, respectively, with the positive predictive value of 67–77%, and the negative predictive value of 61–87%, respectively.<sup>9</sup>

As we can see, measuring serum AMH concentrations to estimate chances for clinical pregnancy at very low or even hardly detectable values does not always validate the actual status. There have been a few clinical cases of women who responded to gonadotrophin stimulation or got pregnant, regardless of very low AMH concentrations – below 1.1 ng/mL.<sup>3</sup>

Those findings prompted the question of whether serum AMH concentrations accurately reflect the amount of AMH secreted by granulosa cells, thereby corresponding to the woman's reproductive potential. In order to answer this question and assuming that ovarian follicles release their contents (including AMH) into the peritoneal cavity, a comparison juxtaposing AMH concentration levels in serum with those in the peritoneal fluid seemed necessary.

The aim of the study was to determine the presence of AMH in the peritoneal fluid and compare its concentration with that of blood serum.

## Material and methods

The study was carried out at the Department of Operative Gynecology and Gynecological Oncology at the Polish Mother's Memorial Hospital Research Institute, Łódź, Poland, during the years 2014–2016. Peritoneal fluid samples were collected from female patients at the age of 18–40 years to assess AMH concentration levels. All those patients were qualified for a laparoscopic cystectomy for benign unilateral ovarian cysts. The exclusion criteria eliminated women at the age below 18 or above 40.

During laparoscopy, when a camera and 2 trocars were inserted, a volume of 5 mL of peritoneal fluid was aspirated from the Douglas cavity. The fluid samples were collected before the onset of cystectomy procedure and the cyst sac opening, to avoid contamination with either blood or cyst secretions. Prior to the operation, each patient provided 5 mL of blood for serum AMH concentration assay. The collected peritoneal fluid was centrifuged and serum was separated from the whole blood, transferred to sterile polypropylene tubes and stored at –20°C until assay. Serum AMH concentrations were measured using a Beckman Coulter Gen II enzyme immunoassay kit (Beckman Coulter Poland, Warszawa, Poland; www.beckman.com), according to its manufacturer's instructions. A total of 48 patients were recruited, out of whom 24 were diagnosed with endometrioma and 24 with ovarian cysts other than endometrioma.

The study was approved by the Ethics Committee of the Medical University of Lodz, Poland, and informed consent forms were obtained from all the included patients.

## Statistical analysis

All the data was analyzed using STATISTICA v. 12 software package (StatSoft, Inc., Tulsa, USA). The Mann–Whitney U test was applied instead of Student's t test, when variables did not pass the normality test. Spearman's correlation coefficient and the simple regression test were used to reveal relations among variables. P-value <0.05 was considered statistically significant.

## Results

Table 1 presents clinical characteristics of the recruited patients, including their obstetric and gynecological history, histopathological evaluation of operated cysts and the clinical stage of endometriosis observed during laparoscopy. The mean age of the recruited patients was 30.3 ±5.2 years.

Table 1. Characteristic of the study group

Age [years] mean SD	30.3 ±5.2	
Previous pregnancies	n	%
Intrauterine *childbirth	18	37.5
*miscariages	3	6.2
ectopic pregnancy	0	0
Primary infertility	5	10.4
Secondary infertility	4	8.3
Previous abdominal surgery	5	10.4
Adnexitis in medical history	0	0
Histopathological diagnosis of the operated cysts: *endometriomas	24	50.0
*Other than endometrioma: simple cysts	7	14.6
mature teratoma	12	25.0
other	5	10.4

The study confirmed the presence of AMH in the peritoneal fluid samples with a concentration range of  $4.69 \pm 3.14$  ng/mL. The concentration of AMH in the peritoneal fluid did not differ significantly from that in blood serum, assayed before the laparoscopic cystectomy ( $4.69 \pm 3.14$  ng/mL vs  $4.58 \pm 3.54$  ng/mL,  $p = 0.58$ ). A strong and statistically significant correlation was thus established between serum AMH concentrations before surgery and AMH concentrations in the peritoneal fluid ( $r = 0.54$ ,  $p < 0.001$ ) (Fig. 1). The higher was serum AMH concentration, the higher was the concentration of AMH in the peritoneal fluid.

When the study group was divided into patients with endometrial cysts and with cysts other than endometrioma, no significant difference was found between the mean AMH concentrations in serum and in the peritoneal fluid ( $4.12 \pm 2.7$  ng/mL vs  $5.56 \pm 3.4$  ng/mL,  $p = 0.3$ ; and  $4.05 \pm 2.71$  ng/mL vs  $5.55 \pm 3.26$  ng/mL,  $p = 0.12$ ). A significant correlation was found in both groups between serum and peritoneal fluid AMH concentrations. However, the correlation strength was definitely higher in the endometrial cyst group, in comparison to the group of patients with conditions other than endometrioma ( $r = 0.61$ ,  $p = 0.001$  vs  $0.43$ ,  $p = 0.03$ ).

Regarding the Bologna criteria, in which POR is defined as AMH  $< 1.1$  ng/mL, there were only 3 such patients in our

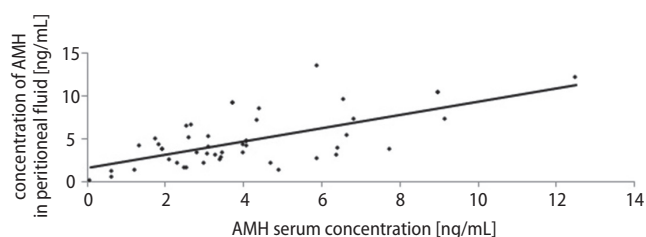


Fig. 1. Correlation of AMH concentration in peritoneal fluid with serum concentration before surgery

study group.<sup>10</sup> In only 1 patient was the concentration of AMH in the peritoneal fluid significantly higher than that in serum (1.22 ng/mL vs 0.6 ng/mL, respectively).

## Discussion

In practice, the procedures related to assistive reproductive technology (ART) require a reliable marker to evaluate the quality of obtained oocytes. Consequently, a concept was developed to determine AMH concentration in the secretion of ovarian follicles. The secretions from smaller follicles provided a 3 times higher AMH titer, compared to larger follicles, which proved a reduced AMH secretion during ovarian follicle maturation. In addition, the AMH levels from follicular secretion correlated strongly with the number of AFC observed in the early first phase of the menstrual cycle. The high levels of AMH in the follicular secretion correlated strongly with the number of clinically observed pregnancies. However, the quality of obtained embryos did not significantly differ in the group with low and high AMH levels in follicular secretions. Such reports gave the authors the basis for a hypothesis about certain importance of AMH as a qualitative marker in the assessment of ovarian reserve.<sup>4,11–14</sup>

Evaluating only AMH in blood serum seems incomplete when trying to assess the ovarian reserve. For example, young girls may have a high ovarian reserve, but their serum AMH concentrations are low. Therefore, it may be suspected that the concentration of AMH in blood serum may not entirely reflect the produced AMH volume. Hence, an idea occurred to assess the presence and concentration of AMH in peritoneal fluid. In fact, we found only 1 report in the available medical literature, evaluating the concentration of AMH in peritoneal fluid, but it was published after we started the collecting of samples. Our findings are confirmed in that study, carried out by Hipp et al. The authors compared AMH concentrations in plasma and in peritoneal fluid from women, operated for endometriosis and from a control group. They did not observe any significant differences in plasma or peritoneal fluid AMH concentrations in women with endometriosis compared to the controls. Moreover, they also found a significant correlation between AMH concentrations in plasma and in peritoneal fluid.<sup>15</sup> In addition, the authors claim that AMH concentrations in plasma may be a marker for peritoneal AMH in studies evaluating the local effects of AMH, especially in endometriosis.<sup>15</sup> Our results confirm that statement with the observed strong correlation between AMH concentrations in serum and in peritoneal fluid in our group of patients with endometriomas.

Except for 1 study, all the other found reports described assessments of AMH levels in ovarian follicles. The first study in which the concentration of AMH was measured in follicular secretion, was the work of Fallat et al. from 1997.<sup>16</sup> In their study, only polycystic ovaries syndrome (PCOS) and endometrial cysts were evaluated and

a higher concentration of AMH in the follicular secretion in women with PCOS was found, compared to women with endometrial cysts. The authors did not, however, compare the concentrations of AMH in follicles and in blood serum.

Currently, a report can be found in which AMH was assayed in secretion from the ovarian follicles during qualification for ART.<sup>4,11–13</sup> As mentioned above, those studies showed a decrease in AMH secretion during ovarian follicular maturation and a strong correlation of AMH concentration with the number of antral follicles in the early first phase of the menstrual cycle.<sup>4,11–13</sup> However, the follicular secretion of AMH was not compared either with AMH concentration in serum or peritoneal fluid.

The results of our study did not show any significant difference between AMH concentrations in serum and in the peritoneal fluid. On the other hand, a strong and statistically significant correlation was found between serum AMH concentration before surgery and the concentration of AMH in peritoneal fluid. The higher was the concentration of AMH in the peritoneal fluid, the higher was the concentration of AMH in blood serum. These results prove that the amount of AMH secreted to peritoneal fluid corresponds to AMH concentration in serum, which means that serum AMH concentration correctly reflects the secretion of AMH by granulosa cells and, therefore, the ovarian reserve.

Our results also suggest that our patient, whose AMH concentration levels in peritoneal fluid significantly differed from those in serum AMH concentration before surgery, may have had an abnormal secretion of AMH into blood serum. We thus believe that peritoneal fluid collection during laparoscopic cystectomy for AMH assay may be a valuable complement to ovarian reserve evaluation and a fairly reliable prognosis of fertility after surgery, especially in patients with low serum AMH values (<1.1 ng/mL) prior to surgery and in patients with endometriomas, in whom the surgery may potentially diminish the ovarian reserve. However, this hypothesis requires further research.

The weakness of our study was the rather small number of patients with low AMH in whom the difference between serum and peritoneal fluid AMH levels was evident. The strength of the study was the measurement of AMH in peritoneal fluid and its comparative juxtaposition with serum AMH levels in a very homogeneous group of patients.

## Conclusions

The AMH is present in the peritoneal fluid and its concentrations significantly strongly correlate with AMH levels in blood serum. The assay of AMH levels in peritoneal fluid may then be a valuable complement to ovarian reserve evaluation and a valuable marker for the prognosis of infertility after adnexal surgery.

## ORCID iDs

Marta Kostrzewa  <https://orcid.org/0000-0001-9078-5814>  
 Ewa Głowacka  <https://orcid.org/0000-0003-1688-6523>  
 Tomasz Stetkiewicz  <https://orcid.org/0000-0002-4477-6340>  
 Mariusz Grzesiak  <https://orcid.org/0000-0002-6900-4347>  
 Krzysztof Szyłło  <https://orcid.org/0000-0001-7198-4957>  
 Grzegorz Stachowiak  <https://orcid.org/0000-0003-0463-3676>  
 Jacek Radosław Wilczyński  <https://orcid.org/0000-0002-2072-6533>

## References

- Weenen C, Laven JS, von Bergh AR, et al. Anti-Müllerian hormone expression pattern in the human ovary: Potential implications for initial and cyclic follicle recruitment. *Mol Hum Reprod.* 2004;10(2):77–83.
- Themmen AP. Anti-Müllerian hormone: Its role in follicular growth initiation and survival and as an ovarian reserve marker. *J Natl Cancer Inst Monogr.* 2005;34:18–21.
- Practice Committee of the American Society for Reproductive Medicine. Testing and interpreting measures of ovarian reserve: A Committee opinion. *Fertil Steril.* 2015;103(3):e9–e17.
- La Marca A, Giulini S, Tirelli A, et al. Anti-Müllerian hormone measurement on any day of the menstrual cycle strongly predicts ovarian response in assisted reproductive technology. *Hum Reprod.* 2007;22(3):766–777.
- American College of Obstetricians and Gynecologists (ACOG). Committee opinion: Ovarian reserve testing. *Fertil Steril.* 2015;103(3):9–17.
- Bancsi LF, Broekmans FJ, Eijkemans MJ, de Jong FH, Habbema JD, te Velde ER. Predictors of poor ovarian response in in vitro fertilization: A prospective study comparing basal markers of ovarian reserve. *Fertil Steril.* 2002;77(2):328–336.
- Gnoth C, Schuring AN, Friol K, Tigges J, Mallmann P, Godehardt E. Relevance of anti-Müllerian hormone measurement in a routine IVF program. *Hum Reprod.* 2008;23(6):1359–1365.
- Penarrubia J, Fabregues F, Manau D, et al. Basal and stimulation day 5 anti-Müllerian hormone serum concentrations as predictors of ovarian response and pregnancy in assisted reproductive technology cycles stimulated with gonadotropin-releasing hormone agonist-gonadotropin treatment. *Hum Reprod.* 2005;20(4):915–922.
- Elgindy EA, El-Haieg DO, El-Sebaey A. Anti-Müllerian hormone: Correlation of early follicular, ovulatory and midluteal levels with ovarian response and cycle outcome in intracytoplasmic sperm injection patients. *Fertil Steril.* 2007;89(9):1670–1676.
- Ferraretti AP, La Marca A, Fauser BC, Tarlatzis B, Nargund G, Gianaroli L.ESHRE consensus on the definition of “poor response” to ovarian stimulation for in vitro fertilization: The Bologna criteria. *Hum Reprod.* 2011;26(7):1616–1624.
- Fanchin R, Louafi N, Mendez Lozano DH, Frydman N, Frydman R, Taieb J. Per-follicle measurements indicate that anti-Müllerian hormone secretion is modulated by the extent of follicular development and luteinization and may reflect qualitatively the ovarian follicular status. *Fertil Steril.* 2005;84(1):167–173.
- Fanchin R, Taieb J, Lozano DH, Ducot B, Frydman R, Bouyer J. High reproducibility of serum anti-Müllerian hormone measurements suggests a multi-staged follicular secretion and strengthens its role in the assessment of ovarian follicular status. *Hum Reprod.* 2005;20(4):923–927.
- Fanchin R, Mendez Lozano DH, Frydman N, et al. Anti-Müllerian hormone concentrations in the follicular fluid of the pre-ovulatory follicle are predictive of the implantation potential of the ensuing embryo obtained by in vitro fertilization. *J Clin Endocrinol Metab.* 2007;92(5):1796–1802.
- Lekamge DN, Barry M, Kolo M, Lane M, Gilchrist RB, Tremellen KP. Anti-Müllerian hormone as a predictor of IVF outcome. *Reprod Biomed Online.* 2007;14(5):602–610.
- Hipp H, Loucks TL, Nezhat C, Sidell N, Session DR. Anti-Müllerian hormone in peritoneal fluid and plasma from women with and without endometriosis. *Reprod Sci.* 2015;22(9):1129–1133.
- Fallat ME, Siow Y, Marra M, Cook C, Carrillo C. Müllerian-inhibiting substance in follicular fluid and serum: A comparison of patients with tubal factor infertility, polycystic ovary syndrome, and endometriosis. *Fertil Steril.* 1997;67(5):962–965.

# Health-related quality of life is not related to laparoscopic or robotic technique in radical cystectomy

\*Kajetan Juszcak<sup>1,A,C-F</sup>, \*Agata Gastecka<sup>1,A-D</sup>, Jan Adamowicz<sup>1,B-D</sup>, Przemysław Adamczyk<sup>2,B-D</sup>, Marta Pokrywczyńska<sup>3,E,F</sup>, Tomasz Drewa<sup>1,2,E,F</sup>

<sup>1</sup> Department of General and Oncologic Urology, Collegium Medicum, Nicolaus Copernicus University, Bydgoszcz, Poland

<sup>2</sup> Department of General and Oncological Urology, Nicolaus Copernicus Hospital, Toruń, Poland

<sup>3</sup> Department of Regenerative Medicine Cell and Tissue Bank, Department of Urology, Collegium Medicum, Nicolaus Copernicus University, Bydgoszcz, Poland

A – research concept and design; B – collection and/or assembly of data; C – data analysis and interpretation;

D – writing the article; E – critical revision of the article; F – final approval of the article

Advances in Clinical and Experimental Medicine, ISSN 1899–5276 (print), ISSN 2451–2680 (online)

Adv Clin Exp Med. 2020;29(7):857–863

## Address for correspondence

Agata Gastecka

E-mail: agata.gastecka@gmail.com

## Funding sources

The work was partly financed by the National Centre for Research and Development under the STRATEGMED I program “Prevention and Treatment of Lifestyle Diseases” project entitled “Innovative urine draining prosthesis for patients with urinary bladder cancer treated with minimum invasive urinary bladder oncological surgeries” (STRATEGMED1/235368/8/NCBR/2014 (Smart AUCI)).

## Conflict of interest

None declared

## Acknowledgements

The authors would like to thank the National Centre for Research and Development for their support.

\* Kajetan Juszcak and Agata Gastecka contributed equally to this work.

Received on March 30, 2020

Reviewed on April 15, 2020

Accepted on May 1, 2020

Published online on July 28, 2020

## Cite as

Juszcak K, Gastecka A, Adamowicz J, Adamczyk P, Pokrywczyńska M, Drewa T. Health-related quality of life is not related to laparoscopic or robotic technique in radical cystectomy. *Adv Clin Exp Med.* 2020;29(7):857–863. doi:10.17219/acem/121937

## DOI

10.17219/acem/121937

## Copyright

© 2020 by Wrocław Medical University

This is an article distributed under the terms of the Creative Commons Attribution 3.0 Unported (CC BY 3.0) (<https://creativecommons.org/licenses/by/3.0/>)

## Abstract

**Background.** Evaluating health-related quality of life (HR-QoL) is important in urological oncology.

**Objectives.** To evaluate the impact of minimally invasive radical cystectomy (RC) on the patients' QoL depending on the surgical strategy (laparoscopic compared to robotic).

**Material and methods.** The study involved 110 patients divided into 2 groups: group 1 (n = 65), qualified for robotic-assisted RC (RARC), and group 2 (n = 45), qualified for laparoscopic RC (LRC). A prospective analysis of QoL was performed. In the study, we used sociodemographic data taken from the patients' medical records, and data from standardized questionnaires of QoL surveys entitled Functional Assessment of Cancer Therapy – General (FACT-G) and Functional Assessment of Cancer Therapy for Bladder Cancer (FACT-BI).

**Results.** In the patients who had undergone LRC, a statistically significant difference in HR-QoL was noted only for the subjective well-being (SWB) domain regarding family and social life: The patients had higher SWB values before surgery than after it. In the patients who had undergone RARC, statistically significant differences in HR-QoL were noted in 3 domains: 1) SWB – family and social life, 2) FACT-BI assessment and 3) FACT-G assessment. Both before and after surgery, no statistically significant differences were found between the 2 groups for any of the HR-QoL domains.

**Conclusions.** The surgical technique of minimally invasive endoscopic RC used (laparoscopic or robotic) does not affect HR-QoL domains.

**Key words:** radical cystectomy, quality of life, urinary diversion, laparoscopic, robotic-assisted

## Introduction

In modern urological oncology, more and more emphasis is being placed nowadays on evaluating patients' health-related quality of life (HR-QoL). In general, the research largely focuses on patients with urinary bladder cancer who have been qualified for radical cystectomy (RC).<sup>1,2</sup> The RC is the standard treatment for localized muscle-invasive bladder cancer. An integral part of RC is the creation of a urinary diversion after the cystectomy. Currently, 2 types of urinary diversion are commonly used: abdominal diversion (ureterocutaneostomy or ileal conduit) and urethral diversion (orthotopic bladder substitution).<sup>3</sup> Urinary diversion rather than urinary bladder removal seems to have a significant impact on the patients' QoL, necessitating lifestyle changes and often causing stress to the patient.

The ultimate goal of HR-QoL assessment is to examine the impact of the type of treatment on the patient's health, taking into account their physical and emotional condition as well as social and functional domains. There are several instruments for HR-QoL assessment in patients with urinary bladder cancer. These tools are characterized by different development and validation phases and different contexts of use, depending on the depth of tumor infiltration, the applied therapeutic method or the urinary diversion technique after RC. Initial assessments of HR-QoL use basic tools designed to assess the overall QoL in patients with cancer: the European Organization for the Research and Treatment of Cancer Quality of Life Questionnaire (EORTC QLQ-C30) and the Functional Assessment of Cancer Therapy – General (FACT-G) questionnaire.<sup>4,5</sup>

The aim of the current study was to evaluate the impact of minimally invasive RC on the HR-QoL of patients depending on the surgical strategy used: laparoscopic compared to robotic.

## Material and methods

### Study groups

Out of 156 consecutive patients with muscle-invasive urinary bladder cancer, 110 were included in the study. The patients were divided into 2 groups according to the minimally invasive surgical technique used during RC. Group 1 consisted of 65 patients qualified for robotic-assisted RC (RARC); group 2 encompassed 45 patients qualified for laparoscopic RC (LRC). In each of the main groups, the patients were divided into subgroups depending on whether or not they had postoperative complications during their planned hospitalization. The division of the patients into these subgroups was based on the Clavien–Dindo classification.

The study was approved by the Ethics Committee of the Collegium Medicum, Nicolaus Copernicus University (Bydgoszcz, Poland; approval No. 60/2016 dated January 26, 2016, and the annex dated March 21, 2017).

## Inclusion and exclusion criteria

The inclusion criteria for the study were: 1) urinary bladder cancer qualified for RC; and 2) voluntary informed written consent to participate in the study. The exclusion criteria were: 1) RC due to neuromuscular urinary bladder dysfunction, prostate cancer or a primary tumor of an organ other than the urinary bladder; 2) changing the operating technique from LRC or RARC to open surgery, 3) senile dementia and/or the presence of a mental illness preventing an informed and voluntary decision regarding participation in the study; 4) confirmed homelessness; and 5) refusal to participate in the study for subjective reasons.

On the basis of the exclusion criteria, 46 patients out of 156 were not enrolled in the study, including 20 who underwent LRC and 26 who underwent RARC. Twelve patients from the LRC group did not agree to participate in the study, and the remaining 8 patients did not meet the inclusion criteria. In the non-included RARC group, 13 refused to participate and 13 were excluded.

## HR-QoL assessment

A prospective analysis of QoL of the patients qualified for RC was performed. In order to find out the QoL of patients undergoing RC, depending on the surgical technique used and long-term complications noted, the diagnostic survey method was used. In the study, we used sociodemographic data taken from medical records of patients and data from standardized questionnaires of QoL surveys: FACT-G, used to assess the physical condition, family and social life, emotional state and functioning in everyday life in patients with any type of cancer, and the Functional Assessment of Cancer Therapy – Bladder (FACT-BI) to assess complaints and treatment related directly to urinary bladder cancer.

The FACT-BI is a reliable, approved and flexible questionnaire used in many types and stages of urinary bladder cancer treatment developed by the Functional Assessment of Chronic Illness Therapy (FACIT) group.<sup>6</sup> It differs from EORTC instruments in that it has been validated and designed to compare HR-QoL between patients with muscle-invasive bladder cancer (MIBC) and those with non-muscle-invasive bladder cancer (NMIBC). The form consists of 27 questions from the general version of the FACT-G questionnaire, divided into 4 domains – physical, social/family, emotional, and functional – accompanied by 12 questions specific to urinary bladder cancer. These questions relate to urine function, bowel function, sexual function, body image, appetite and stoma care, and are rated on a scale of 0 to 4. The bladder-specific answers are added together and added to the FACT-G result. A high number of points indicates better HR-QoL. All the questions in the survey relate to the patient's HR-QoL over the previous week.

On the basis of the FACT-G form, a questionnaire entitled Functional Assessment of Cancer Therapy – Bladder Cystectomy (FACT-BI) formerly known as the Venderbilt

Cystectomy Index (FACT-VCI), was also developed. It is a validated tool designed for HR-QoL measurement in patients undergoing radical cystectomy. The questionnaire reserved for patients with urinary bladder cancer focuses mainly on clinical symptoms related to urinary bladder, gastro-intestinal and sexual dysfunction after radical cystectomy.<sup>6–9</sup>

The FACIT group approved the use of the FACT-G and FACT-BI questionnaires in Polish. The prospective measurements were taken twice: before surgery and within a period of  $\leq 12$  months after surgery. Before surgery, the patients completed the questionnaires given to them in the hospital by a researcher. The 2<sup>nd</sup> measurement was done using the postal survey method or with the Computer-Assisted Telephone Interviewing (CATI) method.

## Statistical analysis

The results are expressed as means  $\pm$  standard deviation (SD). To check the significance of differences in the level of the QoL before and after the procedures, a parametric Student's t-test for dependent samples (when the condition of difference distribution normality was met) and a non-parametric Wilcoxon pair order test (when there was non-normal distribution) were used. Statistical significance was set at  $p \leq 0.05$  for all the tests. The statistical calculations were performed using STATISTICA v. 10 PL software (StatSoft Polska, Kraków, Poland).

## Results

### Group characteristics

The results showed that the baseline health status of the patients in group 1 (RARC) was worse than in the patients in group 2 (LRC). In group 2, 53% of the patients were at the pT<sub>a</sub>-pT<sub>2</sub> stage of cancer progression according to the TNM scale; group 1 included a 4% lower rate of patients at this stage of the disease (49%). A higher percentage of patients at the advanced pT<sub>3</sub>-pT<sub>4</sub> stage of cancer was observed in group 1 (51%) than in group 2 (47%). The patients in group 1 were characterized by a more frequent occurrence of comorbidities; the differences between the 2 groups were 6% for cardiovascular diseases and 11% for diabetes. There were no statistically significant differences between the 2 groups in terms of body mass index (BMI) or American Society of Anesthesiologists (ASA) physical status scores.

Group 1 (RARC) included 16 women and 49 men with a mean age of 70 years (range: 52–87 years). The subgroup of RARC patients who had no postoperative complications during their planned hospitalization was made up of 17 patients, including 13 men and 4 women. The subgroup of RARC patients with postoperative complications during their planned hospitalization comprised 48 cases,

including 36 men and 12 women. A total of 48 group 1 patients survived the one-year follow-up period: 20 patients with ureterocutaneostomy (42%) and 28 patients with ileal conduits (58%).

Group 2 (LRC) included 6 women and 39 men with a mean age of 66 years (range: 43–86 years). The subgroup of LRC patients who had no postoperative complications during their planned hospitalization consisted of 14 people (13 men and 1 woman). The subgroup of LRC patients who had complications during their planned hospitalization consisted of 31 patients, including 26 men and 5 women. A total of 27 group 2 patients survived the one-year follow-up period: 16 patients with ureterocutaneostomy (59%) and 11 patients with ileal conduits (41%).

### Hospitalization time

Our results revealed no significant relationship between the surgical technique used and hospitalization time. In group 1, the hospitalization time was shorter by an average of 2 days compared to group 2. The duration of hospitalization in the subgroup of patients in whom no postoperative complications were noted was the same for both analyzed groups. The greatest difference in the length of hospital stay following RC surgery was observed in the subgroups of patients with postoperative complications; the time was shorter for the RARC group (12 days) compared to the LRC group (16 days). The results obtained in this regard are consistent with the results regarding the scale of complications. Patients from the RARC group had a lower rate of Grade III–V complications (Clavien–Dindo Scale) compared to the LRC technique, resulting in a shorter hospitalization.

### Urinary diversion

In the group of patients operated on using the LRC technique, ureterocutaneostomy (71%) was most often chosen as a method of urinary diversion. In the patients operated on with the RARC technique, the urinary diversion methods used were equally divided (51% for ureterocutaneostomy compared with 49% for ileal conduit). The study showed a statistically significant difference in the method of reconstruction of the urinary tract between the LRC and RARC groups ( $p = 0.0329$ ). A higher percentage of urinary diversion procedures using an ileal fragment (49%) was noted among patients after RARC. A statistically significant relationship between the surgical technique and the urinary diversion procedure was also found in the subgroup of patients with postoperative complications ( $p = 0.0281$ ).

### HR-QoL assessment

The 48 RARC patients and 27 LRC patients who survived the one-year follow-up period were included in the postoperative HR-QoL assessment. In both groups, males,

people living in urban areas and respondents receiving retirement benefits constituted larger shares. The average age in the LRC group was 64 years (range: 54–75 years); the average age in the RARC group was 68 years (range: 52–87 years).

The results regarding the clinical data of the patients included in the QoL assessment after RC surgery did not show any significant differences between the 2 groups. In the LRC group, 59% of the patients underwent ureterocutaneostomy (n = 16) and 41% ileal conduits (n = 11). In the RARC group, 42% of the patients underwent ureterocutaneostomy (n = 20) and 58% ileal conduits (n = 28). Among the respondents who assessed their HR-QoL after

RC surgery, 40% of those in the RARC group and 30% in the LRC group had pT3-pT4 level cancer. Patients from the RARC group who survived the one-year follow-up were characterized by higher rates of comorbidities than the patients who had undergone LRC.

In the patients who had undergone LRC, a statistically significant difference in HR-QoL occurred only for the subjective well-being (SWB) domain regarding family and social life (p = 0.0487). All of these patients had higher SWB values before surgery than after surgery. For other QoL domains, no statistically significant differences were found between the results before and after surgery (p > 0.05) (Table 1).

**Table 1.** Comparison of HR-QoL domains in patients before and after minimally invasive RC

Minimally invasive RC					
HR-QoL domains	time	n	mean	SD	p-value
PWB Physical well-being domain	before LRC	27	20.4	5.8	0.8699
	after LRC		20.1	5.4	
	before RARC	48	19.4	6.8	0.6248
	after RARC		18.9	5.2	
SWB Family-social well-being domain	before LRC	27	22.1	4.7	0.0487
	after LRC		19.6	3.8	
	before RARC	48	23.0	3.5	0.0001 <sup>a</sup>
	after RARC		19.0	5.4	
EWB Emotional well-being domain	before LRC	27	13.8	5.4	0.3648
	after LRC		14.8	4.7	
	before RARC	48	13.3	5.1	0.7536
	after RARC		13.6	5.2	
FWB Functional well-being domain	before LRC	27	18.1	6.0	0.8847
	after LRC		18.3	4.7	
	before RARC	48	17.9	5.9	0.2379
	after RARC		16.6	5.5	
BI Other ailments related to urinary bladder cancer	before LRC	27	30.3	6.6	0.0962 <sup>a</sup>
	after LRC		32.1	6.2	
	before RARC	48	29.1	6.7	0.0333
	after RARC		31.9	6.9	
TOI Trial Outcome Index	before LRC	27	68.8	14.6	0.6721
	after LRC		70.7	14.3	
	before RARC	48	66.5	15.3	0.8944
	after RARC		66.9	15.8	
FACT-G Functional Assessment of Cancer Therapy – General	before LRC	27	74.4	15.6	0.7163
	after LRC		72.8	15.7	
	before RARC	48	73.7	14.4	0.0468
	after RARC		68.1	16.5	
FACT-BI Functional Assessment of Cancer Therapy – Bladder	before LRC	27	104.8	19.6	0.9322
	after LRC		104.3	20.3	
	before RARC	48	103.1	19.3	0.3563
	after RARC		99.6	22.6	

<sup>a</sup>Wilcoxon pair order test result; HR-QoL – health-related quality of life; RC – radical cystectomy; LRC – laparoscopic radical cystectomy; RARC – robotic-assisted radical cystectomy; SD – standard deviation; n – number of patients.

In the patients who had undergone RARC, statistically significant differences in the HR-QoL were found for the following domains: 1) the SWB domain concerning family and social life ( $p < 0.0001$ ), where the patients had higher SWB values before surgery than after surgery; 2) FACT-BI ( $p = 0.0333$ ), where the patients had higher values after the procedure than before the procedure; and 3) FACT-G ( $p = 0.0468$ ), where the patients had higher values before surgery than after it. For the remaining QoL domains, no statistically significant differences were found between the results before and after surgery ( $p > 0.05$ ) (Table 1).

Both before and after surgery, no statistically significant differences were found between the RARC patients and the LRC patients for any of the HR-QoL domains ( $p > 0.05$ ). The HR-QoL of the patients in both groups was assessed at a similar level before RC surgery (Table 2).

## Discussion

Health-related QoL assessment plays a significant role in the treatment of oncological diseases. In addition to ascertaining whether and how patients benefit from

**Table 2.** Comparison of HR-QoL domains in patients before and after minimally invasive radical cystectomy (LRC compared with RARC)

Minimally invasive radical cystectomy					
HR-QoL domains	time	n	mean	SD	p-value
PWB Physical well-being domain	before LRC	27	20.4	5.8	0.6662 <sup>(a)</sup>
	before RARC	48	19.4	6.8	
	after LRC	27	20.1	5.4	0.3414
	after RARC	48	18.9	5.2	
SWB Family-social well-being domain	before LRC	27	22.1	4.7	0.3516
	before RARC	48	23.0	3.5	
	after LRC	27	19.6	3.8	0.6154 <sup>(a)</sup>
	after RARC	48	19.0	5.4	
EWB Emotional well-being domain	before LRC	27	13.8	5.4	0.6786
	before RARC	48	13.3	5.1	
	after LRC	27	14.8	4.7	0.3278
	after RARC	48	13.6	5.2	
FWB Functional well-being domain	before LRC	27	18.1	6.0	0.8926
	before RARC	48	17.9	5.9	
	after LRC	27	18.3	4.7	0.1853
	after RARC	48	16.6	5.5	
BI Other ailments related to urinary bladder cancer	before LRC	27	30.3	6.6	0.4759 <sup>(a)</sup>
	before RARC	48	29.1	6.7	
	after LRC	27	32.1	6.2	0.9298
	after RARC	48	31.9	6.9	
TOI Trial Outcome Index	before LRC	27	68.8	14.6	0.5276
	before RARC	48	66.5	15.3	
	after LRC	27	70.7	14.3	0.3078
	after RARC	48	66.9	15.8	
FACT-G Functional Assessment of Cancer Therapy – General	before LRC	27	74.4	15.6	0.8484
	before RARC	48	73.7	14.4	
	after LRC	27	72.8	15.7	0.2361
	after RARC	48	68.1	16.5	
FACT-BI Functional Assessment of Cancer Therapy – Bladder	before LRC	27	104.8	19.6	0.7192
	before RARC	48	103.1	19.3	
	after LRC	27	104.3	20.3	0.3760
	after RARC	48	99.6	22.6	

<sup>a</sup>Mann-Whitney U test result; HR-QoL – health-related quality of life; RC – radical cystectomy; LRC – laparoscopic radical cystectomy; RARC – robotic-assisted radical cystectomy; SD – standard deviation; n – number of patients.

the treatment, assessing QoL facilitates the planning and implementation of long-term care. A relationship between the clinical stage of oncological disease, the type of treatment and the patients' QoL has been observed. Patients with chronic disease adjust to the current situation faster by lowering their expectations.<sup>10</sup>

Ureterocutaneostomy is the simplest form of incontinent cutaneous diversion. Operating times, complication rates, the duration of stays in intensive care, and the length of hospital stays are lower in patients treated with ureterocutaneostomy as compared to ileal conduits.<sup>11</sup> Therefore, in older or compromised patients who need a suprapubic diversion, ureterocutaneostomy is the preferred procedure. The basic assumptions gained from previous studies are that patients with continent cutaneous or orthotopic diversions may have improved QoL compared to those with incontinent ileal conduit urinary diversions.<sup>11</sup> In a study by Gilbert et al., the QoL of patients who had undergone ileal conduit and ureterocutaneostomy procedures was assessed using the Bladder Cancer Index (BCI), which showed equal urinary bother and function scores for both groups of patients.<sup>12</sup> Others have demonstrated that in carefully selected elderly patients, all forms of wet and dry urinary diversions, including orthotopic bladder substitutions, are possible.<sup>13</sup>

Quality of life is a dynamic, multidimensional construct that changes over time and can be affected by the experience of both the patients and the healthcare providers. The HR-QoL assesses the impact of illness on the subject's life and is considered an important component of patients' attitudes to their cancer. The range of parameters assessed with an HR-QoL questionnaire includes physical function, symptoms, global judgment of health, psychological and social well-being, cognitive functioning, roles and activities, personal attitudes, and satisfaction with care.<sup>14–16</sup> Patients' acceptance of a stoma and rehabilitation in cases of ileal conduit diversion varies widely, but generally it can be said that urinary diversion is not an operation that renders the subject an invalid; psychosocial reintegration is possible, and adequate preoperative information, particularly on sexual status, is very important.<sup>17</sup> Regarding postoperative status, patients with an ileal conduit usually have the poorest self-image, defined by a decrease in sexual desire and all forms of sexual and nonsexual physical contact.<sup>17</sup> The advantages of various forms of continent urinary diversion are the presumed improvements in QoL compared with conduit diversion. However, continent urinary diversion may have some disadvantages as well. From a technical point of view, continent forms of diversion are more challenging and time-consuming, and patients leave the hospital with indwelling catheters. Once the catheters are removed, the patients must undergo a period of education in the techniques required to properly care for the reservoir or neobladder. Patients are also at a higher risk for diarrhea and vitamin B12 malabsorption. However, it is generally believed that the QoL

advantages of continent urinary diversions outweigh the potential disadvantages.<sup>18,19</sup>

Our results revealed that the patients who had undergone LRC were distinguished by slightly higher value indices for individual domains making up the overall QoL assessment than those who had undergone RARC. In the respondents who had undergone RARC, attention should be paid to the higher number of patients whose urine was drained using an ileal conduit, the higher number of patients with cancer at the pT3-pT4 level and the higher percentage of patients who were re-hospitalized due to complications than in the LRC group. The respondents who underwent RARC were on average 4 years older than the patients who had LRC. Despite the worse clinical data of the patients in the RARC group, no significant differences were found between the 2 study groups in the subjective assessments of QoL either before or after surgery. Moreover, when interpreting the results for the subjective assessment of HR-QoL, attention should be paid to the guidelines on the minimum and maximum score possible for each domain. The highest achievable result, indicating the best perceived QoL, for the HR-QoL domain for cancer (FACT-G), is 108 points, as opposed to 156 points for the domain testing HR-QoL for urinary bladder cancer (FACT-BL).

For patients from the LRC group before surgery, the FACT-G QoL was rated 31% lower than the maximum value, i.e., 33.6 points on average. After surgery, the indicator fluctuated around 33%, i.e., on average 35.2 points lower than the maximum possible. On FACT-BL, the points scored were 33% (51 points) lower than the maximum before surgery and 33% (52 points) lower after surgery. The patients in the RARC group scored 32% (34 points) below the possible maximum on FACT-G before surgery and 37% (40 points) below the maximum value after surgery. On FACT-BL, the RARC patients scored 34% (53 points) lower than the possible maximum before the procedure and 36% (56 points) lower after the procedure.

Our observations regarding the assessment of the LRC patients' QoL before and after surgery showed a significant decrease in the value of the family and social life domain ( $p = 0.0487$ ). Lower values after surgery were also noted for the domain dealing with the patient's psychological well-being. Similarly, the assessment of the RARC patients' QoL before surgery compared to the one-year follow-up showed a significant difference for the family and social life domain ( $p = 0.0001$ ). In addition, deterioration in the physical condition and functioning in everyday life of patients was observed. A significant difference was noted in the RARC patients' FACT-BL results, which were better after surgery ( $p = 0.0333$ ), and in FACT-G results, which were worse after the observation period ( $p = 0.0468$ ). Analysis of the FACT-G and FACT-BL responses shows that the patients in both study groups rated their HR-QoL not much worse after the RC procedure than before it.

There are few reports in the literature dealing with patient's QoL after RC surgery in relation to the surgical

technique used. Most authors compare assessments of QoL for continent and incontinent urinary diversions. Bochner et al. indicated that there are no significant differences in the QoL of patients who had undergone open RC and those who had had RARC, taking into account follow-up periods of 3 and 6 months.<sup>20</sup> Messer et al. reported that HR-QoL returned to the baseline 3 months after RC surgery, with no difference between open RC and RARC.<sup>21</sup>

The one-year follow-up period adopted in our study may have contributed to obtaining slightly better indicators for the QoL domains those mostly regarding emotional states. Assessing QoL a full year after RC surgery could have resulted in patients accepting their cancer and adapting to their changed body and life conditions. There were decreases in the value of domains concerning physical condition and social life in both groups of patients (LRC and RARC).

The results obtained on FACT-BI are also noteworthy: The values noted for patients from both the LRC and RARC groups were higher at the 2<sup>nd</sup> measurement, although one might expect that the necessity of living with a stoma, sexual dysfunction or scarring would significantly reduce the score. Positive adaptation to life with a stoma, and thus a better perception of QoL, largely depends on the patient's proficiency in urostomy care.<sup>22–24</sup> According to observations reported by Kristensen et al., in order to ensure a sense of self-sufficiency, urostomy care requires manual skill and adaptive in the emotional sphere.<sup>25</sup> Providing the patient with relevant information about the stoma and education in its use and care are extremely important elements of the process of improving the patients' self-sufficiency after surgery and their perception of their QoL.<sup>26,27</sup> Performing RC procedures using minimally invasive techniques does not negatively affect the patients' self-image.

## Conclusions

The results of our study indicate that the choice of minimally invasive endoscopic RC used (LRC compared to RARC) does not affect patients' HR-QoL.

### ORCID iDs

Kajetan Juszcak  <https://orcid.org/0000-0003-0354-0822>  
 Agata Gastecka  <https://orcid.org/0000-0002-3214-2287>  
 Jan Adamowicz  <https://orcid.org/0000-0003-2479-7133>  
 Przemysław Adamczyk  <https://orcid.org/0000-0002-7217-841X>  
 Marta Pokrywczyńska  <https://orcid.org/0000-0003-3259-087X>  
 Tomasz Drewa  <https://orcid.org/0000-0001-5347-4136>

### References

- Moncrief TJ, Balaji P, Lindgren BB, Weight CJ, Konety BR. Comparative evaluation of bladder-specific Health-Related Quality of Life (HRQOL) instruments for bladder cancer. *Urology*. 2017;108:76–81.
- Sosnowski R, Kulpa M, Ziętałewicz U, et al. Basic issues concerning health-related quality of life. *Cent European J Urol*. 2017;70(2):206–211.
- Stein JP, Lieskovsky G, Cote R, et al. Radical cystectomy in the treatment of invasive bladder cancer: Long-term results in 1,054 patients. *J Clin Oncol*. 2001;19(3):666–675.
- Webster K, Cella D, Yost K. The Functional Assessment of Chronic Illness Therapy (FACIT) measurement system: Properties, applications, and interpretation. *Health Qual Life Outcomes*. 2003;16(1):79.
- Danna BJ, Metcalfe MJ, Wood EL, Shah JB. Assessing symptom burden in bladder cancer: An overview of bladder cancer-specific Health-Related Quality of Life instruments. *Bladder Cancer*. 2016;2(3):329–340.
- Degboe A, Ivanescu C, Rohay JM, Turner RR, Cella D. Validity and performance of the Functional Assessment of Cancer Therapy – Bladder (FACT-BI) among advanced urothelial cancer patients. *Support Care Cancer*. 2019;27(11):4189–4198.
- Mason SJ, Downing A, Wright P, et al. Health-related quality of life after treatment for bladder cancer in England. *Br J Cancer*. 2018;118(11):1518–1528.
- Anderson CB, Feurer ID, Large MC, et al. Psychometric characteristics of a condition-specific, health-related quality-of-life survey: The FACT-Vanderbilt Cystectomy Index. *Urology*. 2012;80(1):77–83.
- Cookson MS, Dutta SC, Chang SS, Clark T, Smith JA Jr, Wells N. Health-related quality of life in patients treated with radical cystectomy and urinary diversion for urothelial carcinoma of the bladder: Development and validation of a new disease specific questionnaire. *J Urol*. 2003;170(5):1926–1930.
- Radecka B. Health-related quality of life: The role and manners of assessment in cancer patients. *Curr Gynecol Oncol*. 2015;13(3):172–179.
- Parkinson JP, Konety BR. Health-related quality of life assessments for patients with bladder cancer. *J Urol*. 2004;172(6 Pt 1):2130–2136.
- Gilbert SM, Wood DP, Dunn RL, et al. Measuring health-related quality of life outcomes in bladder cancer patients using the Bladder Cancer Index (BCI). *Cancer*. 2007;109(9):1756–1762.
- Shih C, Porter MP. Health-related quality of life after cystectomy and urinary diversion for bladder cancer. *Adv Urol*. 2011;2011:715892.
- Saber A. Urinary diversion: Historical aspect and patient's satisfaction. *Urol Nephrol Open Access J*. 2014;1(3):86–93.
- Somani BK, MacLennan SJ, N'Dow J. Quality of life with urinary diversion. *Eur Urol Suppl*. 2010;9(10):763–771.
- Varrichio CG, Ferrans CE. Quality of life assessments in clinical practice. *Semin Oncol Nurs*. 2010;26(1):12–17.
- Asgari MA, Safarinejad MR, Shakhssalim N, Soleimani M, Shahabi A, Amini E. Quality of life after radical cystectomy for bladder cancer in men with an ileal conduit or continent urinary diversion: A comparative study. *Urol Ann*. 2013;5(3):190–196.
- Saika T, Arata R, Tsumura T, et al; Okayama Urological Research Group. Health-related quality of life after radical cystectomy for bladder cancer in elderly patients with an ileal conduit, ureterocutaneousostomy, or orthotopic urinary reservoir: A comparative questionnaire survey. *Acta Med Okayama*. 2007;61(4):199–203.
- Porter MP, Penson DF. Health-related quality of life after radical cystectomy and urinary diversion for bladder cancer: A systematic review and critical analysis of the literature. *J Urol*. 2005;173(4):1318–1322.
- Bochner BH, Dalbagni G, Sjoberg DD, et al. Comparing open radical cystectomy and robot-assisted laparoscopic radical cystectomy: A randomized clinical trial. *Eur Urol*. 2015;67(6):1042–1050.
- Messer JC, Punnen S, Fitzgerald J, Svatek R, Parekh DJ. Health-related quality of life from a prospective randomized clinical trial of robot-assisted laparoscopic vs open radical cystectomy. *BJU Int*. 2014;114(6):896–902.
- Jensen BT, Kiesbye B, Soendergaard I, Jensen JB, Ammitzboell Kristensen S. Efficacy of preoperative uro-stoma education on self-efficacy after radical cystectomy: Secondary outcome of a prospective randomized controlled trial. *Eur J Oncol Nurs*. 2017;28:41–46.
- Danielsen AK, Rosenberg J. Health-related quality of life may increase when patients with a stoma attend patient education: A case-control study. *PLoS One*. 2014;9(3):e90354.
- O'Connor G. Teaching stoma-management skills: The importance of self-care. *Br J Nurs*. 2005;14(6):320–324.
- Kristensen SA, Laustsen S, Kiesbye B, Jensen BT. The Urostomy Education Scale: A reliable and valid tool to evaluate urostomy self-care skills among cystectomy patients. *J Wound Ostomy Continence Nurs*. 2013;40(6):611–617.
- Kozell K, Frecea M, Thomas JT. Preoperative ostomy education and stoma site marking. *J Wound Ostomy Continence Nurs*. 2014;41(3):206–207.
- Fujimura T. Current status and future perspective of robot-assisted radical cystectomy for invasive bladder cancer. *Int J Urol*. 2019;26(11):1033–1042.



# The assessment of phonatory and ventilatory functions in patients after microsurgery for Reinke's edema

Katarzyna Ura-Sabat<sup>1,A–D</sup>, Joanna Morawska<sup>2,C,D</sup>, Wojciech Domka<sup>1,C,D</sup>,  
Marta Gamrot-Wrzoł<sup>3,C,D</sup>, Wojciech Scierski<sup>3,A,E</sup>, Ewa Niebudek-Bogusz<sup>2,A,F</sup>

<sup>1</sup> Clinical Department of Otorhinolaryngology, Frederic Chopin Clinical Voivodeship Hospital No. 1, Rzeszów, Poland

<sup>2</sup> Nofer Institute of Occupational Medicine, Department of Audiology and Phoniatrics, Łódź, Poland

<sup>3</sup> Department of Otorhinolaryngology and Laryngological Oncology in Zabrze, Medical University of Silesia, Katowice, Poland

A – research concept and design; B – collection and/or assembly of data; C – data analysis and interpretation;

D – writing the article; E – critical revision of the article; F – final approval of the article

Advances in Clinical and Experimental Medicine, ISSN 1899–5276 (print), ISSN 2451–2680 (online)

*Adv Clin Exp Med.* 2020;29(7):865–871

## Address for correspondence

Katarzyna Ura-Sabat  
E-mail: [urka23@wp.pl](mailto:urka23@wp.pl)

## Funding sources

None declared

## Conflict of interest

None declared

Received on May 12, 2019

Reviewed on May 31, 2019

Accepted on January 21, 2020

Published online on July 3, 2020

## Abstract

**Background.** Short and long-term results of microsurgical treatment with the mini-microflap technique in patients with Reinke's edema (RE) were assessed based on the phonatory and ventilatory functions of the larynx.

**Objectives.** To assess the short and long-term results of microsurgical treatment with the mini-microflap technique in patients with RE based on the phonatory and ventilatory functions of the larynx.

**Material and methods.** Twenty patients diagnosed with advanced stage of RE confirmed with laryngo-videostroboscopy (LVS) were enrolled in the study. Phonatory function disturbances were additionally assessed on the basis of Maximum Phonation Time (MPT) measurement, Voice Handicap Index (VHI) and Voice-Related Quality of Life (V-ROQL) questionnaires. Ventilatory function was assessed using spirometry. The aforementioned complex examinations were conducted prior to surgery and 1, 6 and 9 months following the surgery.

**Results.** Good postsurgical results were obtained in subjective and objective evaluation, which assessed the phonatory function and ventilatory parameters. Post-surgery increase in MPT, VHI and VQROL was noticed in all patients in 3 check points ( $p < 0.001$ ). The results demonstrate postsurgical improvement for some LVS parameters, including assessment of glottis closure ( $p < 0.003$ ) observed 6 months after the surgery. An improvement in most of the ventilation parameters was observed also 6 months after surgery ( $p < 0.001$ ). For the spirometry flow parameter PEF, significant improvement was noted in each check point ( $p_1 < 0.004$ ,  $p_6 < 0.001$ ,  $p_9 < 0.001$ ). The study revealed a correlation between phonatory parameter – MPT and PEF observed 1 month after the procedure ( $p = 0.026$ ), confirming the interdependence of ventilatory efficiency and phonatory condition of larynx.

**Conclusions.** Mini-microflap surgery brings satisfactory clinical effect in patients with advanced stages of RE by optimization of phonatory and ventilatory functions of the larynx.

**Key words:** spirometry, voice quality, long-term outcomes, mini-microflap surgery, Reinke's edema

## Cite as

Ura-Sabat K, Morawska J, Domka W, Gamrot-Wrzoł M, Scierski W, Niebudek-Bogusz E. The assessment of phonatory and ventilatory functions in patients after microsurgery for Reinke's edema. *Adv Clin Exp Med.* 2020;29(7):865–871. doi:10.17219/acem/116755

## DOI

10.17219/acem/116755

## Copyright

© 2020 by Wrocław Medical University

This is an article distributed under the terms of the Creative Commons Attribution 3.0 Unported (CC BY 3.0) (<https://creativecommons.org/licenses/by/3.0/>)

## Introduction

Reinke's edema (RE) belongs to a group of benign masses of vocal folds (BVFM) deteriorating both phonatory and ventilatory function of the larynx.<sup>1–3</sup> Precisely, RE is classified as a disease of the lamina propria, and as its name indicates, superficial lamina propria, also referred to as Reinke's space of the vocal fold layer, is affected by this disorder.<sup>4</sup> Reinke's edema constitutes about 6–10% of all non-malignant pathologies within the glottis and is most commonly observed in middle-aged women.<sup>5,6</sup> Longlasting smoking has been found to be the most important risk factor in the etiopathogenesis of RE.<sup>1,7</sup> Four clinical stages can be distinguished, depending both on the extent of lesions on vocal folds and on glottis area narrowing caused by swollen folds.<sup>8</sup> One of the first symptoms of RE are voice disorders, most frequently manifesting themselves as persistent hoarseness and a lower than normal pitch, deteriorating the quality of voice, especially in women.<sup>9–11</sup> In more advanced stages of RE, due to the narrowing of the glottis area, ventilatory capacity can also be compromised, which is typically observed as gradually aggravating respiratory problems.<sup>12</sup> In the case of large, bilateral RE, stridor can be noticed, caused by chronic edematous hypertrophy of vocal folds obstructing the glottis, especially its posterior part responsible for the respiratory function of larynx.<sup>13</sup> Diagnosis of RE is made during a routine laryngological examination, although instrumental evaluation of the larynx by means of laryngovideostroboscopy is a valuable contribution in the diagnostic procedure.<sup>14</sup>

The management depends on the stage of the disease. At the 1<sup>st</sup> and 2<sup>nd</sup> clinical stages of RE conservative treatment is usually effective.<sup>4</sup> Microsurgery is the first treatment of choice at the 3<sup>rd</sup> and 4<sup>th</sup> stages because of the potential ventilatory function disorders. The previously used decortication technique (stripping)<sup>15,16</sup> was unsatisfactory both for the surgeon and the patient because of the poor post-surgery quality of the voice.<sup>12,15–17</sup> For this reason, the mini-microflap technique has become a more frequently used method in phonosurgical treatment of RE as a technique widening the ventilatory area of glottis and, at the same time, saving the phonatory function of the larynx.<sup>18–21</sup>

When reviewing the available literature, the authors did not find any studies that evaluated the effects of the complex microsurgical treatment of RE, including those that monitored both phonatory and respiratory functions simultaneously. The aim of the study was to comparatively assess the abovementioned functions of the larynx in patients with RE who underwent mini-microflap phonosurgery.

## Material and methods

The prospective study was carried out in 20 patients with advanced RE. The patients were qualified for phonosurgery

on the basis of laryngological examination complemented with instrumental examination – laryngovideostroboscopy (LVS). Additionally, the assessment of the phonatory and ventilatory function of the larynx was performed before and after the surgery according to a scheme described below. The examinations after operation were conducted in 3 check points: at short-term (1 month) and long-term periods (6 and 9 months after the surgery).

## The mini-microflap technique

The applied surgical mini-microflap technique was intended to both decrease the mass of the vocal folds and broaden the glottis, as well as to maintain layered, functional composition of the vocal fold. All patients underwent laryngeal microsurgery under general anesthesia. The mini-microflap technique was applied in all cases as a one-step procedure. It is based on performing an incision of the upper edge of the vocal fold without affecting its middle part. The surgery was performed with the Kleinsasser set. The Reinke's space was opened along the superior surface of the vocal fold near the ventricle, saving the anterior commissure. Subepithelial layer was dissected to aspirate fluid accumulated in the Reinke's space. The mucous, dense content of Reinke's space was sucked out and the excess mucosa was removed minimally as necessary. The surgical site was covered with a tissue layer to form a strong bond and to hold the tissue in place to facilitate healing. Tissue glue was applied when necessary.<sup>2,4,5,7,13</sup> All the patients were hospitalized for 1 day after the surgery. The patients were instructed to follow 1 week of complete vocal rest, so as not to traumatize vocal folds and were advised to respect vocal hygiene rules, with particular emphasis put on the absolute necessity of smoking cessation. They were also informed about the terms of postoperative care and examinations scheduled in 3 check points according to the scheme described below.

## Evaluation of the phonatory function

The evaluation of the phonatory function was carried out using objective and subjective methods. The instrumental methods of voice assessment included the following:

- Laryngovideostroboscopy (LVS), in which the following parameters were examined: the quality of mucosal wave, regularity of vocal fold vibration, amplitude of vocal fold vibration, and the configuration of glottal closure. Each stroboscopic parameter was rated on a 0–2 scale, where 0 – normal, 1 – limited dysfunction, 2 – severe dysfunction, e.g., absence of mucosal wave or inability of assessment.

- Measurement of the Maximum Phonation Time (MPT), which is an objective and noninvasive measurement of aerodynamic parameter of the phonatory function of the larynx. To measure MPT, the subject was

asked to phonate a sustained /a:/ vowel at a comfortable pitch and loudness as long as possible during a single exhalation.

The subjective assessment of voice included:

- Voice Handicap Index (VHI) questionnaire – both its total value (VHI-T) and the values of each subscale, i.e., the functional state (VHI-F), physical state (VHI-P) and emotional state (VHI-E), were assessed. Total scores of VHI range from 0 to 120, with 120 indicating the most severe vocal dysfunction.

- Voice-Related Quality of Life (V-RQOL) survey is a 10-point self-rating scale, which is more focused on the quality of life than on a handicap itself. A higher V-RQOL score points to a better V-RQOL reported by patients.

### Assessment of ventilatory function

The ventilatory performance was assessed in an objective way using spirometry. The following respiratory parameters were taken into account: Forced Vital Capacity (FVC), Forced Expiratory Volume in the first second (FEV1), Maximum Expiratory Flow (MEF 25, 50, 75), Peak Expiratory Flow (PEF), Tiffeneau index (FEV1/FVC), and Forced Expiratory Flow (FEV 25, 50, 75).<sup>22</sup>

### Statistical analysis

IBM SPSS Statistics v. 24 software (IBM Corp., Armonk, USA) was used to analyze the obtained results. All the parameters were statistically described and referred to the measures of central tendency and dispersion. Spearman's rank correlation coefficient (Spearman's rho) was used to identify a correlation among aggregated coefficients. Statistical significance of the treatment effects was verified with the Wilcoxon test. The value of  $p < 0.05$  proved that there were significant differences in the data: p1 – before surgery compared to 1 month after the surgery, p6 – before compared to 6 months after the surgery, p9 – before compared to 9 months after the surgery. The key results of the analytical process are presented in box-whisker plots.

## Results

### Demographical data and clinical presentation

The study included 31 subjects operated on in the Clinical Department of Otorhinolaryngology (Katowice, Poland). The final study group included 20 patients who completed a full cycle of post-surgery check-ups in 3 time check points: 1, 6 and 9 months after the surgery. There were 16 women (80%) and 4 men (20%) in the study group. Mean age was 53.2 years. Depending on the clinical advancement of RE, the patients were divided into a group of 3<sup>rd</sup> clinical advancement stage according to Bart (15 subjects) and 4<sup>th</sup> clinical advancement stage (5 subjects). In subjects with RE stage 4, the main reason for reporting for surgery was dyspnea and in subjects with RE stage 3 (Fig. 1), the main symptoms were breathing disorders, hoarseness of voice and lowering of voice in women.

All the examined patients were active smokers. They were physical workers with no occupational vocal loading. The patients were qualified for mini-microflap surgery after preliminary examination including laryngological examination with LVS and assessment of phonatory and ventilatory function.

### Comparison of pre- and post-surgery assessment of the phonatory function

Most of the results of the objective and subjective evaluation of the phonatory function indicated post-surgery improvement in comparison to the pre-surgery values. In the analysis of the results of LVS, which is the gold standard of imaging examinations of the function of the larynx, the improvement of the phonatory function was observed in the 6<sup>th</sup> month after the surgery, with an increase in the trend lasting up until the 9<sup>th</sup> month after the surgery. These results concerned all the assessed parameters in LVS: regularity of vocal fold vibration ( $p_6 < 0.014$ ,  $p_9 < 0.001$ ), amplitude of vocal fold vibration ( $p_6 < 0.004$ ,  $p_9 < 0.001$ ), the presence of mucosal wave ( $p_6 < 0.001$ ,  $p_9 < 0.001$ ), and the configuration of glottal closure ( $p_6 < 0.003$ ,  $p_9 < 0.001$ ).

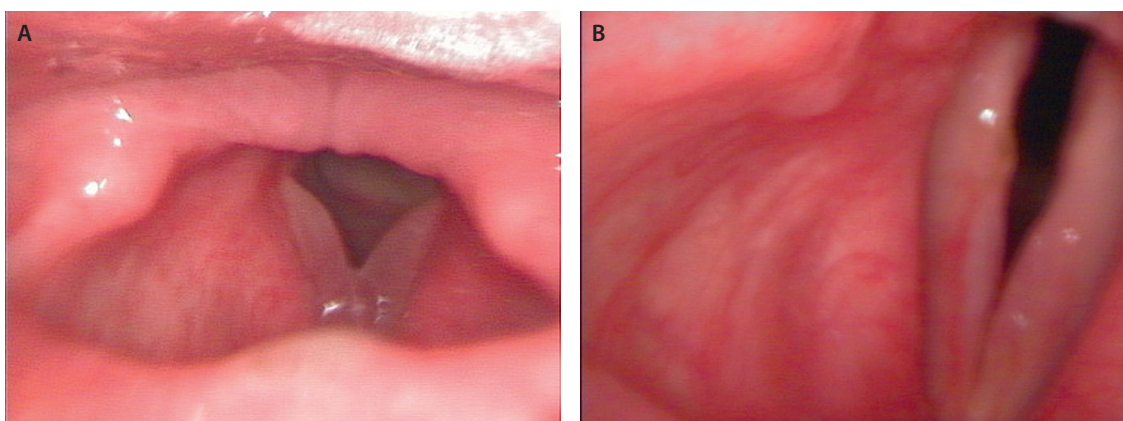


**Fig. 1.** Image of larynx in laryngovideoscopy of a patient with Reinke's edema stage 3  
A – before surgery;  
B – 9 months after mini-microflap surgery

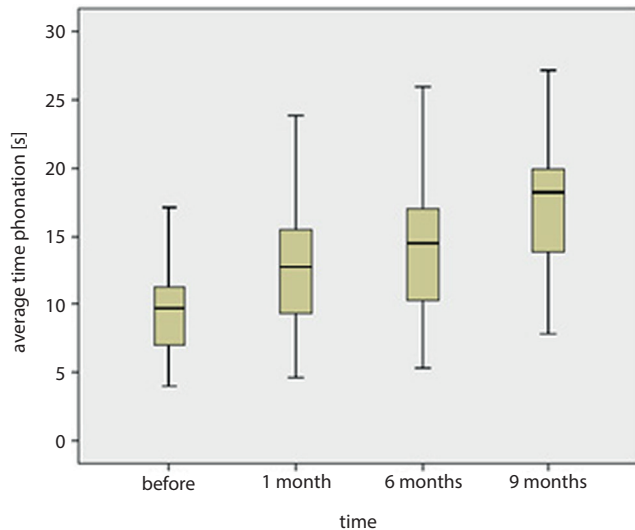


Fig. 2. The comparison of Maximum Phonation Time before and 1, 6 and 9 months after mini-microflap surgery

The study also indicated an improvement in the MPT, which is an objective aerodynamic indicator of the respiratory performance during phonation. Postsurgical increase in MPT was noticed in all patients. The research demonstrated a statistically significant improvement in the aerodynamic parameter (MPT) already 1 month after the surgery, with the rising trend persisting in the long-term observation. On average, there was an increase of 3.72 s during the 1-month observation after the surgery ( $p_1 < 0.001$ ), 4.79 s in the 6-month observation ( $p_6 < 0.001$ ) and 7.88 s in the 9-month observation ( $p_9 < 0.001$ ) (Fig. 2).

A self-assessment of the voice by means of VHI and V-RQOL revealed the post-surgery improvement of the voice from the patient's point of view. The total score of the Voice Handicap Index (VHI-T) dropped in all the patients, giving an average decrease of 26 points in 1 month ( $p_1 < 0.001$ ), 34 points in 6 months ( $p_6 < 0.001$ ) and 47 points in 9 months ( $p_9 < 0.001$ ) after the surgery (Fig. 3). Analogically, significant improvement concerned all the subscales of the VHI: physical – VHI-P, emotional – VHI-E and functional: – VHI-F, with  $p_1 < 0.001$  significance. Improvement in V-ROOL scores was observed in 18 patients in 9 month, after the procedure. V-RQOL values increased moderately after the surgery by 8 ( $p_1 < 0.001$ ), 10 ( $p_6 < 0.001$ ) and 13 points ( $p_9 < 0.001$ ) in 1, 6 and 9 months, respectively (Fig. 4).

### Comparison of pre- and post-surgery assessment of the ventilatory function

In the assessment of the ventilatory function, the most significant changes were noticed in the majority of patients after the surgery for the following parameters: Peak Expiratory Flow (PEF), Maximum Expiratory Flow (MEF 25% and 75%) and Forced Expiratory Flow (FEF 25% and 75%). The improvement in some ventilatory parameters was observed

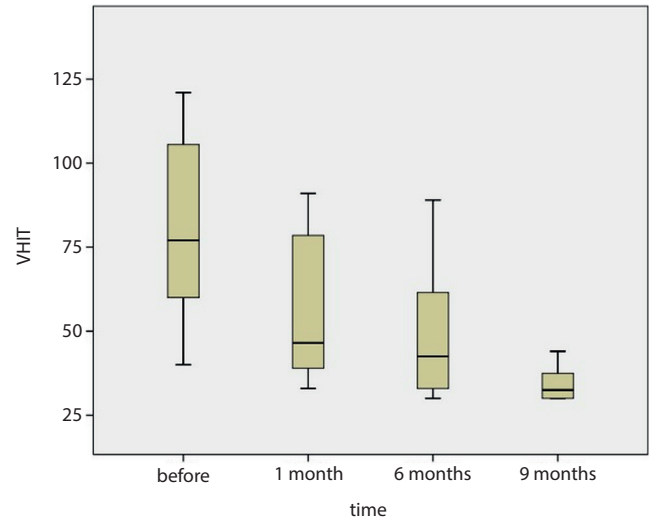


Fig. 3. The comparison of Voice Handicap Index Total before and after 1, 6 and 9 months after mini-microflap surgery

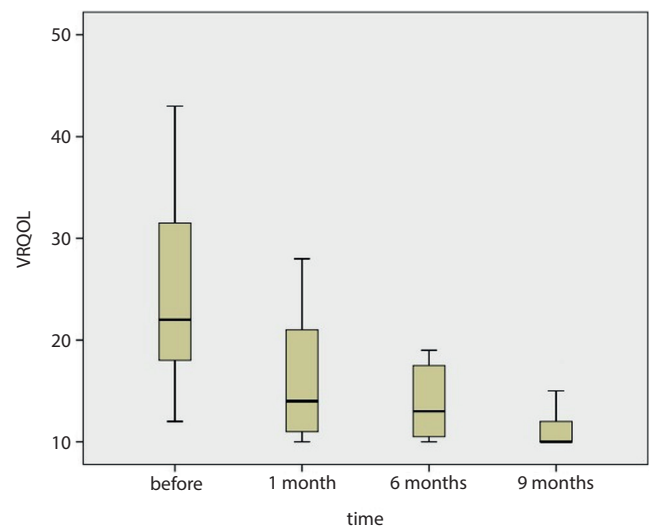


Fig. 4. The comparison of Voice-Related Quality of Life before and 1, 6 and 9 months after mini-microflap surgery

already 1 month after the surgery. The improvement concerned the following parameters: PEF ( $p_1 = 0.001$ ), Forced Expiratory Volume in the first second (FEV1) ( $p_1 = 0.024$ ), Maximum Expiratory Flow MEF 25% ( $p_1 = 0.025$ ) and MEF 75% ( $p_1 = 0.002$ ), and FEF 75% ( $p_1 = 0.025$ ).

In the assessment of the ventilatory function, a significant improvement was observed for most ventilatory parameters 9 months after the surgery: PEF ( $p_9 < 0.001$ ), FEV1 ( $p_9 = 0.024$ ), MEF 25% ( $p_9 < 0.001$ ), MEF 75% ( $p_9 < 0.001$ ), FEF 25% ( $p_9 < 0.001$ ), and FEF75% ( $p_9 < 0.001$ ). It should be underlined that the value of PEF parameter, which is described in literature as an important parameter monitoring the effectiveness of procedures widening the glottis, increased significantly already in the first month post-surgery. The increase persisted in 6 and 9 months post-surgery ( $p_6 < 0.001$ ,  $p_9 < 0.001$ ) (Fig. 5).

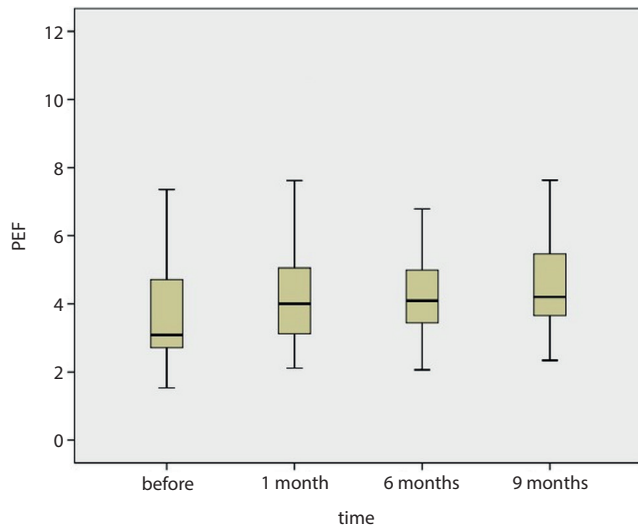


Fig. 5. The comparison of Peak Expiratory Flow before and after 1, 6 and 9 months after mini-microflap surgery

### Correlations between the parameters of phonatory and ventilatory function

Analyzing the relation between the objective and subjective parameters assessing the phonatory function of larynx, the most significant correlation was observed 9 months after surgery for aerodynamic parameter MPT and Physical subscale of Voice Handicap Index (VHI-P):  $r = -0.449$ ,  $p = 0.047$  (Fig. 6). Analogically, the study showed a correlation between MPT and V-ROOL 6 months after surgery ( $r = -0.511$ ,  $p < 0.05$ ) (Fig. 7). The longer MPT indicated that the patient experienced less difficulty in the physical aspect of voice projection. Analyzing the values of the phonation and ventilation indexes, we found the correlation between the MPT and PEF parameter in 1 month after the surgery, giving a statistically significant result of  $p = 0.026$  (Fig. 8). The results indicate that conducting the mini-microflap technique in the 3<sup>rd</sup> or 4<sup>th</sup> stage of RE broadens the glottal area, increases MPT and decreases the PEF index, thus improving the respiratory efficiency of the glottis.

### Discussion

An important aspect in the surgical management of BVFM, including RE, is the preservation of the surrounding normal tissue with as little disruption as possible; this is crucial to ensure optimal laryngeal functions postoperatively. It is advisable for surgeons operating on BVFM to use microsurgery techniques in order to prevent vocal fold damage and to preserve voice production. For this reason, the mini-microflap technique has become a more frequently used for the treatment of RE, as the functional structure of the vocal folds is maintained by preserving their epithelium intact, especially at the vibrating margin.<sup>23</sup>

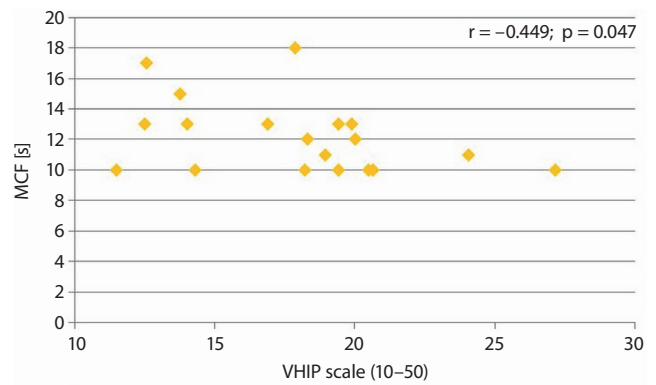


Fig. 6. Correlation between Maximum Phonation Time and Voice Handicap Index-P – physical scale

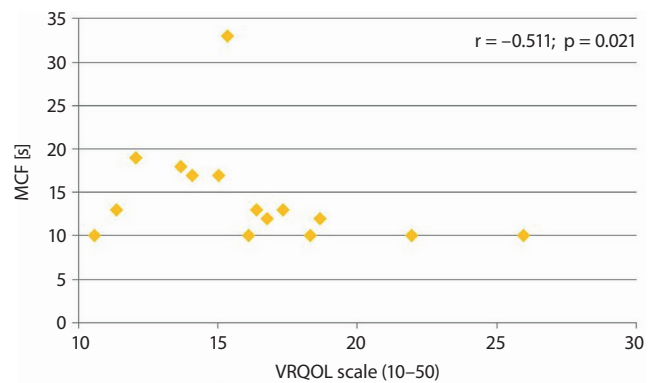


Fig. 7. Correlation between Maximum Phonation Time and Voice-Related Quality of Life

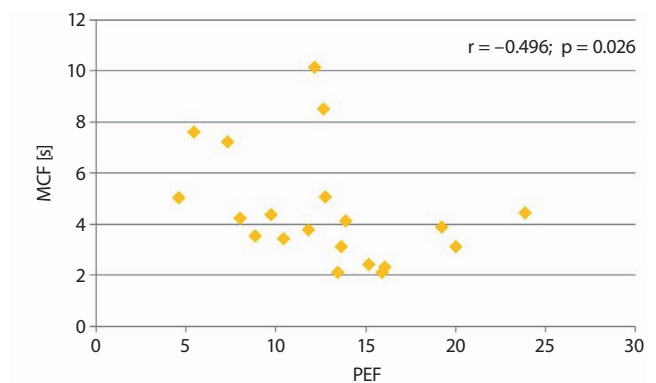


Fig. 8. Correlation between Maximum Phonation Time and Peak Expiratory Flow

The study presented the postoperative results in patients with advanced stages (3<sup>rd</sup> and 4<sup>th</sup>) of RE who underwent mini-microflap surgery. Patients with obstructive RE suffer from deterioration in their overall quality of life due to progressive voice change and respiratory symptoms.<sup>24</sup> Therefore, the examination involved a complex (objective and subjective) assessment of voice and spirometry, which were performed prior to surgery and 1, 6 and 9 months postoperatively.

The results of the study demonstrated postoperative improvement in both phonatory and ventilatory function.

Our research indicates objective improvement of voice function evaluated by means the LVS examination, which still remains a gold standard in the diagnosis of laryngeal pathology.<sup>18,19</sup> The significant improvement of LVS parameters was observed after 6 and 9 months after the surgery, particularly those indicating improvement of glottal closure ( $p_6 = 0.003$ ,  $p_9 < 0.001$ ). These good long-term postsurgical results were also observed for the other assessed parameters in LVS, e.g., regularity of vocal fold vibration ( $p_6 = 0.014$ ,  $p_9 < 0.001$ ), and amplitude of vocal fold vibration ( $p_6 = 0.004$ ,  $p_9 < 0.001$ ). Furthermore, the research demonstrated a statistically significant improvement of the aerodynamic parameter (MPT) already 1 month after the surgery, with the rising trend persisting in the long-term observation ( $p < 0.001$ ). The study confirmed the results of Lim et al., who, in a study concerning 23 patients with RE treated by means of mini micro-flap technique, reported an improvement in MPT 2 months after surgery.<sup>24</sup> These observations are of clinical value, given that considerable changes in the Reinke's area of the vocal fold affect the time of vocal fold vibration, shortening it, which in turn decreases the effectiveness of the expiration during phonation. Maximum Phonation Time, as an aerodynamic parameter, is an important element of the vocal function assessment, which indicates phonatory inefficiency of the larynx and respiratory-phonatory coordination disorder.

Given that recently an important role has been attached to the quality of life, the results of self-assessment of quality of voice were an important contribution to the study. The analysis of postsurgical results shows improvement of the VHI and V-ROOL in all time intervals – 1, 6 and 9 months after the mini-microflap surgery ( $p < 0.001$ ). These results are in line with the study concerning subjects with RE presented by Bassel et al. on the VHI-10 questionnaire 9 months after the surgery<sup>25</sup> and Soner on the Voice Performance Questionnaire (VPQ) 6 months after the surgery.<sup>23</sup> These observations, which are in accordance with our research, demonstrate that applying the mini micro-flap surgery technique in RE patients results in improvement of vibratory function of vocal folds, making them thinner and more suitable for vibratory maneuvers, which, in turn improves voice quality after the surgery.

In the assessment of ventilatory function, a significant improvement was observed for most ventilatory parameters 9 months after the surgery: PEF ( $p_9 < 0.001$ ), FEV1 ( $p_9 = 0.024$ ), MEF 25% ( $p_9 < 0.001$ ), MEF 75% ( $p_9 < 0.001$ ), FEF 25% ( $p_9 < 0.001$ ), FEF 75% ( $p_9 < 0.001$ ). It should be underlined that the value of PEF parameter, which is described in the literature as an important parameter monitoring the effectiveness of procedures widening the glottis, increased significantly already in the first month after the surgery. The increase persisted in 6 and 9 months

after the surgery ( $p_6 < 0.001$ ,  $p_9 < 0.001$ ). The results were in agreement with the studies of other authors, confirming the improvement of airflow stability and effectiveness of respiration after mini-microflap surgery.<sup>26–30</sup>

This research is the first Polish study showing a comparative analysis of the phonatory and ventilatory function after phonosurgery in patients with RE. A correlation between the MPT-aerodynamic phonatory parameter and the PEF parameter found 1 month after the procedure ( $p = 0.026$ ) may prove that reducing the mass of the vocal folds with mini-microflap surgery and widening of the glottis area improves the conditions of phonation.

Moreover, the satisfactory long-term post-surgery results of phonatory parameters assessed by means of LVS and voice self-assessment questionnaires revealed that the main goal of phonosurgery technique, i.e., maintaining the layered, functional composition of the vocal fold, was fulfilled.

It should be emphasized that our research has shown a postoperative improvement in the phonatory and ventilatory function of patients with RE, which persists for 9 months after the surgery for most of the examined parameters. The available literature on the subject presents the results of the mini-microflap surgery either 2 or 6 months after the surgery.<sup>23,24</sup> Our study indicates that, in order to obtain adequate postoperative results after surgical intervention, it is crucial to provide long-term postoperative management, including vocal hygiene guidance. Therefore, the progress of the patient after phonosurgery must be monitored with a re-examination by means of subjective and objective methods not only in short-term (1 month), but also in long-term intervals (e.g., 6 and 9 months).

## Conclusions

The study indicates that treatment with the mini-microflap technique in patients with advanced RE (3<sup>rd</sup> and 4<sup>th</sup> stage) decreases the mass of the vocal folds and widens the glottis, thereby improving the aerodynamic conditions of phonation. Moreover, the study confirmed that the abovementioned microsurgery technique improves the quality of phonatory movements of the vocal folds, as it maintains their layered, functional structure. The applied instrumental and subjective methods of voice assessment enhanced the patients' overall well-being, including their V-ROOL.

### ORCID iDs

Katarzyna Ura-Sabat  <https://orcid.org/0000-0001-6825-5788>

Joanna Morawska  <https://orcid.org/0000-0002-9431-673X>

Wojciech Domka  <https://orcid.org/0000-0003-4429-7638>

Marta Gamrot-Wrzoł  <https://orcid.org/0000-0003-0892-6935>

Wojciech Scierski  <https://orcid.org/0000-0003-3242-8047>

Ewa Niebudek-Bogusz  <https://orcid.org/0000-0002-5389-578X>

## References

- Rubin JS, Sataloff RT, Korovin GS. *Diagnosis and Treatment of Voice Disorders*. 4<sup>th</sup> ed. San Diego, CA: Plural Publishing Inc; 2014:95–105.
- Yonekawa H. A clinical study of Reinke's edema. *Auris Nasus Larynx*. 1988;15(1):57–58.
- Tan M, Bryson P, Pitts C, Woo P, Benninger MP. Clinical grading of Reinke's edema. *Laryngoscope*. 2017 Oct;127(10):2310–2313.
- Yonekawa H, Ohta F, Hirose H. Clinical classification of Reinke's edema. *Folia Phoniat Logoped*. 1992;44:92.
- Siupsinskiene N, Skumaniene M. Phonatory characteristics following different endolaryngeal microsurgical techniques in Reinke's disease [in Lithuanian]. *Medicina (Kaunas)*. 2002;38(10):982–989.
- Kravos A, Hocevar-Boltezar I, Gersak K. Serum levels of sex hormones in males with Reinke's edema. *Eur Arch Otorhinolaryngol*. 2013;270(1):233–238.
- Niemczyk K, ed. *Otolaryngologia kliniczna*. Warszawa, Poland: Medipage; 2015:1547–1549.
- Szyfter W. *Laryngologia*. Poznań, Poland: Termedia; 2016:329–335.
- Obrębowksi A. *Narząd głosu i jego znaczenie w komunikacji społecznej*. Poznań, Poland: Wydawnictwo Naukowe Uniwersytetu Medycznego w Poznaniu; 2008:15–18.
- Misiołek M, Niebudek-Bogusz E, Morawska J, Orecka B, Ścierański W, Lisowska G. Gender-related voice problems in transsexuals: Therapeutic demands. *Endokrynol Pol*. 2016;67(4):452–455.
- Martins RH, do Amaral HA, Tavares EL, Martins MG, Gonçalves TM, Dias NH. Voice disorders: Etiology and diagnosis. *J Voice*. 2016;30(6):761.e1-761.e9.
- Colton RH, Casper JK, Leonard R. *Understanding Voice Problem: A Physiological Perspective for Diagnosis and Treatment*. 4<sup>th</sup> ed. Philadelphia: Wolters Kluwer Health Adis (ESP); 2011:494.
- Yonekawa H, Nimii S, Hirose H. A follow up study of Reinke's edema after surgery. In: Dejonckere PH, Peters HFM, eds. *Communication and its Disorders: A Science in Progress*. Proceedings of the 24<sup>th</sup> Congress IALP Amsterdam, 1998, Nijmegen, the Netherlands: Nijmegen University Press; 1999:375–377.
- Dejonckere PH. Assessment of voice and respiratory function. In: Remacle M, Eckel H, eds. *Surgery of Larynx and Trachea*; 2<sup>nd</sup> ed. Berlin, Germany: Springer-Verlag; 2009:11–26.
- Tan NC, Pittore B, Puxeddu R. The 'M' shadep microflap for treatment of complex Reinke's space edema of the vocal cords. *Acta Otorhinolaryngol Ital*. 2010;30(5):259–263.
- Druck G, Mauri M. Use of the microdebrider for Reinke's edema surgery. *Laryngoscope*. 2000;110(12):2114–2116.
- Sommer C, Schults-Coulon HJ. Long-term results after microlaryngoscopic removal of Reinke's edema [in German]. *HNO*. 2007;55(5):365–374.
- Rzepakowska A, Sielska-Badurek E, Osuch-Wojcikiewicz E, Niemczyk K. Multiparametric assessment of voice quality and quality of life in patients undergoing microlaryngeal surgery: Correlation between subjective and objective methods. *J Voice*. 2018;32(2):257.e21–257.e30
- Niebudek-Bogusz E, Kopczyński B, Strumillo P, Morawska J, Wiktorowicz J, Sliwinska-Kowalska M. Quantitative assessment of videolaryngostroboscopic images in patients with glottic pathologies. *Logoped Phoniatr Vocol*. 2017;42(2):73–83.
- Caffier P, Schmidt B, Gross M, et al. A comparison of white light laryngostroboscopy versus autofluorescence endoscopy in the evaluation of vocal fold pathology. *Laryngoscope*. 2013;123(7):1729–1734.
- Young VN, Mallur PS, Wong AW, et al. Analysis of potassium titanyl phosphate laser settings and voice outcomes in the treatment of Reinke's edema. *Otol Rhinol Laryngol*. 2015;124(3):216–220.
- Miller MR, Hankinson J, Brusasco V, et al; ATS/ERS Task Force. Standardisation of spirometry. *Eur Respir J*. 2005;26(2):319–338.
- Soner T, Melek KG, Ercan K, et al. The effect of surgical treatment on voice quality in Reinke's edema: An evaluation with vocal performance questionnaire and acoustic voice analysis. *J Med Updates*. 2013;3(2):56–61.
- Lim JY, Choi JN, Kim KM, Choi HS. Voice analysis of patients with diverse types of Reinke's edema and clinical use of electroglottographic measurements. *Acta Otolaryngol*. 2006;126(1):62–69.
- Bassel H, Olivier F, Teiga PS, Bouayed S, von Wihl S, Sandu K. Subjective voice assessment after endoscopic surgery for an obstructive Reinke edema using voice handicap index. *Adv in Otolaryngol*. 2015;2015:207085. doi:10.1155/2015/207085
- Misiołek M, Namysłowski G, Warmuziński K, Ziara D, Czecior E. Efficacy of laser arytenoidectomy in bilateral vocal cord paralysis. The review of the contemporary surgical procedures. *Chir Pol*. 2003; (5)2:91–96.
- Orecka B, Misiołek H, Namysłowski G, et al. Functional results after the treatment of laryngeal stenosis [in Polish]. *Otolaryngol Pol*. 2007; 61(5):872–876.
- Harnisch W, Brosch S, Schmidt M, Hagen R. Breathing and voice quality after surgical treatment for bilateral vocal cord paralysis. *Arch Otolaryngol Head Neck Surg*. 2008;134(3):278–284.
- Swain SK, Sahu MC. Management of laryngeal airway in Reinke's edema: An anesthetic overview. *Int J Otorhinolaryngol Clin*. 2017;9(1): 35–37.
- Salmen T, Ermakova T, Schindler A, et al. Efficacy of microsurgery in Reinke's edema evaluated by traditional voice assessment integrated with the Vocal Extent Measure (VEM). *Acta Otorhinolaryngol Ital*. 2018;38(3):194–203.



# Experimental studies on the protective effects of the overexpression of lentivirus-mediated sirtuin 6 on radiation-induced lung injury

Jiying Wang<sup>1,A–F</sup>, Yong Cai<sup>2,A,E,F</sup>, Zhaoying Sheng<sup>2,B–D,F</sup>

<sup>1</sup> Department of Oncology, Shanghai Pulmonary Hospital, Tongji University School of Medicine, China

<sup>2</sup> Department of Radiation Oncology, Shanghai Pulmonary Hospital, Tongji University School of Medicine, China

A – research concept and design; B – collection and/or assembly of data; C – data analysis and interpretation; D – writing the article; E – critical revision of the article; F – final approval of the article

Advances in Clinical and Experimental Medicine, ISSN 1899–5276 (print), ISSN 2451–2680 (online)

Adv Clin Exp Med. 2020;29(7):873–877

## Address for correspondence

Yong Cai

E-mail: quetezvmxr75@163.com

## Funding sources

The research was sponsored by the Natural Science Foundation of Shanghai, China (grant No. 15ZR1434300).

## Conflict of interest

None declared

Received on January 31, 2018

Reviewed on October 17, 2018

Accepted on January 30, 2020

Published online on July 28, 2020

## Abstract

**Background.** Sirtuin 6 (*SIRT6*) can increase the radiosensitivity of non-small cell lung cancer and exert protective effects on radiation-induced lung injury.

**Objectives.** To investigate protective effects of *SIRT6* overexpression on radiation-induced lung injury in rats.

**Material and methods.** Male Wistar rats ( $n = 72$ ) were randomly divided into 3 groups. Models were made by radiating both lungs with a 6MV X linear accelerator. Each group was injected through the tail vein with normal saline (the control group and radiation group) and lentivirus carrying overexpressed *SIRT6* (the Lent-*SIRT6* group) on the same day as the modeling. Routine blood indexes (white blood cells (WBC), red blood cells (RBC), neutrophils and lymphocytes) were recorded; the rats were sacrificed and their lung tissues taken; pathological changes in the lungs were evaluated using hematoxylin and eosin (H&E) staining; and tumor necrosis factor  $\alpha$  (TNF- $\alpha$ ), interleukin 6 (IL-6) and interleukin 1 $\beta$  (IL-1 $\beta$ ) were detected with enzyme-linked immunosorbent assay (ELISA) 8 weeks after radiotherapy.

**Results.** The lung structure including alveolar walls and interstitium in the control group was normal, but the alveolar walls in the radiation group were obviously thickened and a large amount of hyperplastic fibrous tissue was found in the alveolar interstitium. The thickness and interstitial fibrosis of the alveolar walls were more alleviated in the Lent-*SIRT6* group than in the radiation group. Compared with those in the control group, the respiratory rates, levels of TNF- $\alpha$  and IL-6 in serum, neutrophils and levels of TNF- $\alpha$ , IL-6 and IL-1 $\beta$  in the liver all were increased, while WBCs and lymphocytes were decreased in the radiation group. The respiratory rates, levels of TNF- $\alpha$  and IL-6 in serum, neutrophils and levels of TNF- $\alpha$ , IL-6 and IL-1 $\beta$  in the liver were all decreased, and WBCs and lymphocytes were increased after injection with lentivirus carrying overexpressed *SIRT6*.

**Conclusions.** Sirtuin 6 inhibits inflammation and alleviates radioactive pneumonia and lung injury. Therefore, *SIRT6* can exert certain protective effects on lung injury.

**Key words:** inflammation, lung injury, sirtuin 6, radioactive pneumonia

## Cite as

Wang J, Cai Y, Sheng Z. Experimental studies on the protective effects of the overexpression of lentivirus-mediated sirtuin 6 on radiation-induced lung injury. *Adv Clin Exp Med.* 2020;29(7):873–877. doi:10.17219/acem/117685

## DOI

10.17219/acem/117685

## Copyright

© 2020 by Wrocław Medical University

This is an article distributed under the terms of the Creative Commons Attribution 3.0 Unported (CC BY 3.0) (<https://creativecommons.org/licenses/by/3.0/>)

## Introduction

At present, lung cancer has become one of the common malignant diseases with the highest incidence and mortality worldwide. The global annual death toll of cancer is up to 1.2 million, and radiotherapy is the main treatment for late-stage or postoperatively recurring lung cancer. Radiation-induced lung injury not only affects lung functions but sharply reduces the patients' quality of life, which is a common complication of lung cancer after radiotherapy. It is of great significance to protect the lungs of patients undergoing radiotherapy from damage. Sirtuin is a NAD<sup>+</sup>-dependent histone deacetylase that can alter the activity of the target protein by lysine deacetylation.<sup>1</sup>

The 7 widely expressed sirtuin subtypes (*SIRT1*–*SIRT7*) encoded in mammalian genomes play an important role in various physiological processes, including cell growth and apoptosis.<sup>2</sup> Several studies have reported that *SIRT1* exerts protective effects on lung injury of different types<sup>3,4</sup> and plays a crucial role in this process.<sup>5</sup> Our previous study found that *SIRT6* could increase the radiosensitivity of non-small cell lung cancer, and that it exerts protective effects on radiation-induced lung injury.<sup>6</sup>

Pulmonary inflammation plays a crucial role in the occurrence and development of radiation-induced lung injury, and various inflammation factors are involved in this process, such as tumor necrosis factor  $\alpha$  (TNF- $\alpha$ ) and interleukin 6 (IL-6). The aim of this study was to transfect lentiviral vectors of overexpressed *SIRT6* in models of rats with radiation-induced lung injury and observe the protective effects of *SIRT6* on radiation-induced lung injury. In the present study, lung injury was induced by routine radiation of the thoracic cavity, and changes in lung pathologies, plasma and pulmonary inflammation were compared randomly between 2 groups: 1 with overexpressed *SIRT6* lentivirus and 1 with no treatment.

## Material and methods

### Main reagents

The overexpressed lentivirus vector construction of *SIRT6* was completed by the Shanghai Genechem Company Ltd. (Shanghai, China); the enzyme-linked immunosorbent assay (ELISA) kits for IL-6 and interleukin 1 $\beta$  (IL-1 $\beta$ ) were purchased from the R&D Systems Inc. (Minneapolis, USA); and ELISA kits for TNF- $\alpha$  were purchased from the Nanjing Jiancheng Bioengineering Institute (Nanjing, China).

### Animals and grouping

Male 150–200-gram specific pathogen-free (SPF)-grade Wistar rats ( $n = 72$ ) were purchased from the Beijing Vital River Laboratory Animal Technology Co., Ltd. (Beijing,

China). They were given national-standard rodent food ad libitum. We randomly chose 48 of the rats to be radiated with a 6MV X linear accelerator for the lung models. The radiated rats were randomly divided into 2 groups of 24: the radiation group and the Lent-*SIRT6* group. The rats in the Lent-*SIRT6* group were injected with  $5 \times 10^7$  TU overexpressed *SIRT6* lentivirus through the tail vein, while those in the radiation group received the same volume (100  $\mu$ L) of normal saline. The other 24 animals were only injected with the same volume of normal saline, without X-ray radiation.

### Establishment of models of radiation-induced lung injury

The rats were intraperitoneally injected with pentobarbital sodium and then placed on the radiating table in a supine position after full anesthesia. The radiation field, adjusted according to the location of both lungs, was up to  $5 \times 4$  cm, from armpit midpoint of the forelimbs down to the xiphoid process. A 6MV X linear accelerator was used to perform a single round of chest radiation with a total dose of 20 Gy at 300 cGy/min. The rats in the control group were placed on the radiating table without being subjected to radiation. All these procedures were performed in the Department of Radiotherapy of the Affiliated Shanghai Pulmonary Hospital of Tongji University (Shanghai, China).

### Specimen collection and processing

Six rats were selected at every time point 1, 2, 4, and 8 weeks after radiation. Respiratory rates and weights were recorded, followed by intraperitoneal injection of pentobarbital sodium according to their weight. Their hearts were opened in a supine position and their right auricles were cut for 5 mL of blood. Eight weeks after radiation, 6 rats were selected and fixed with blood pincers for ligation of the lungs. After removal, the left lungs were fixed with 4% formaldehyde solution and stained with hematoxylin and eosin (H&E) for observation of pathological changes in the lungs, while the right lungs were preserved with liquid nitrogen to detect the levels of pulmonary inflammation factors.

### Detection indexes

Changes in respiratory rates, body weight and levels of TNF- $\alpha$  and IL-6 in serum were measured at 1, 2, 4, and 8 weeks after radiation, respectively. Blood routine indexes (white blood cells (WBC), red blood cells (RBC), neutrophils, and lymphocytes) were recorded at 8 weeks after radiation. The rats were sacrificed with their lung tissues taken and pathological changes of lungs were evaluated using H&E staining; the levels of TNF- $\alpha$ , IL-6 and IL-1 $\beta$  were detected using ELISA at 8 weeks after radiation.

## Statistical analysis

All statistical analyses were performed with the IBM SPSS Statistics for Windows software v. 20.0 (IBM Corp., Armonk, USA). Data in this study was expressed as  $X \pm$  standard deviation (SD). The t-test was used for comparisons between every 2 groups, and univariate analysis for comparisons among various groups;  $\alpha = 0.05$ . The threshold of statistical significance was  $p < 0.05$ .

## Results

### Pathological changes in lung tissues of different groups of rats

The lung structure, including the alveolar walls and interstitium, were normal in the control group, but the alveolar walls in the radiation group were obviously thickened and a large amount of hyperplastic fibrous tissues were found in the alveolar interstitium. The thickness and interstitial fibrosis of the alveolar walls were more alleviated in the Lent-*SIRT6* group than in the radiation group, but were still more seriously affected than those in the control group.

### Comparison of respiratory rates in different groups of rats after routine radiation

Compared with the control group without radiation and the Lent-*SIRT6* transfected rats, the respiratory rates of the rats in the radiation group increased 1 week after radiation; reached their highest value at 2 weeks after radiation; and remained high from 4 to 8 weeks after radiation. As shown in Table 1, the differences among the groups were statistically significant at each time point ( $p < 0.05$ ). The respiratory rates of the rats in the Lent-*SIRT6* group were lower than those in the radiation group, and the differences were statistically significant ( $p < 0.05$ ). As shown in Table 1, the respiratory rates in the radiation group were higher than those in the control group ( $p < 0.05$ ), except at 8 weeks after radiation.

Table 1. Respiratory rates of the 3 groups of rats at different time points

Group	1 week	2 weeks	4 weeks	8 weeks
Control group	115 ± 12	117 ± 13	121 ± 11	118 ± 12
Radiation group	143 ± 15 <sup>a</sup>	152 ± 17 <sup>a</sup>	147 ± 18 <sup>a</sup>	136 ± 16 <sup>a</sup>
Lent- <i>SIRT6</i> group	127 ± 0.18 <sup>ab</sup>	131 ± 16 <sup>ab</sup>	132 ± 15 <sup>ab</sup>	124 ± 14 <sup>a</sup>

Compared with the control group: <sup>a</sup>  $p < 0.05$ ; compared with the radiation group; <sup>b</sup>  $p < 0.05$ .

### Changes in the body weight of different groups of rats after routine radiation

As shown in Table 2, changes in body weight among the 3 groups at 1, 2, 4, and 8 weeks after radiation were in the normal range, and the differences among groups were not statistically significant ( $p > 0.05$ ).

Table 2. The body weight [g] of the 3 groups of rats after routine radiation (3 min)

Group	1 week	2 weeks	4 weeks	8 weeks
Control group	62 ± 17	89 ± 15	141 ± 13	169 ± 23
Radiation group	71 ± 16	87 ± 21	136 ± 20	172 ± 19
Lent- <i>SIRT6</i> group	65 ± 11	94 ± 18	139 ± 17	165 ± 21

### Comparison of serum TNF- $\alpha$ levels in different groups of rats after routine radiation

As shown in Table 3, compared with the control group without routine radiation and the Lent-*SIRT6* transfected rats, the serum TNF- $\alpha$  levels in the radiation group increased at 1, 2, 4, and 8 weeks after radiation. The differences were statistically significant ( $p < 0.05$ ). The serum TNF- $\alpha$  levels in the Lent-*SIRT6* group were lower than those in the radiation group, and the differences were statistically significant ( $p < 0.05$ ). The serum TNF- $\alpha$  levels in the Lent-*SIRT6* group were higher than those in the radiation group, and these differences were also statistically significant ( $p < 0.05$ ).

Table 3. Comparison of serum TNF- $\alpha$  levels in the 3 groups after routine radiation [ng/L]

Group	1 week	2 weeks	4 weeks	8 weeks
Control group	41.25 ± 5.47	39.50 ± 6.39	40.77 ± 5.83	43.14 ± 5.02
Radiation group	53.64 ± 6.29 <sup>a</sup>	66.28 ± 6.11 <sup>a</sup>	69.03 ± 7.34 <sup>a</sup>	79.75 ± 8.46 <sup>a</sup>
Lent- <i>SIRT6</i> group	57.31 ± 5.48 <sup>ab</sup>	55.41 ± 7.36 <sup>ab</sup>	51.43 ± 6.15 <sup>ab</sup>	49.26 ± 6.93 <sup>ab</sup>

Compared with the control group: <sup>a</sup>  $p < 0.05$ ; compared with the radiation group; <sup>b</sup>  $p < 0.05$ .

### Comparison of serum IL-6 levels in different groups of rats after routine radiation

As shown in Table 4, compared with the control group without routine radiation and the Lent-*SIRT6* transfected rats, the serum IL-6 levels in the radiation group increased at 1, 2, 4, and 8 weeks after radiation. The differences were

**Table 4.** Comparison of serum IL-6 levels in the 3 groups of rats after routine radiation [ng/L]

Group	1 week	2 weeks	4 weeks	8 weeks
Control group	0.91 ±0.35	1.03 ±0.44	0.98 ±0.36	1.15 ±0.37
Radiation group	1.45 ±0.62 <sup>a</sup>	1.66 ±0.77 <sup>a</sup>	1.87 ±0.71 <sup>a</sup>	1.72 ±0.84 <sup>a</sup>
Lent- <i>SIRT6</i> group	1.32 ±0.49 <sup>ab</sup>	1.24 ±0.52 <sup>ab</sup>	1.36 ±0.75 <sup>ab</sup>	1.29 ±0.55 <sup>ab</sup>

Compared with the control group: <sup>a</sup>  $p < 0.05$ ; compared with the radiation group; <sup>b</sup>  $p < 0.05$ .

statistically significant ( $p < 0.05$ ). The serum IL-6 levels in the Lent-*SIRT6* group were lower than those in the radiation group, and the differences were statistically significant ( $p < 0.05$ ). The serum IL-6 levels in the Lent-*SIRT6* group were higher than those in the control group, and these differences were also statistically significant ( $p < 0.05$ ).

### Comparison of blood routine indexes of different groups of rats at 8 weeks after routine radiation

As shown in Table 5, compared with the control group without routine radiation and the Lent-*SIRT6* transfected rats, the number of lymphocytes in the radiation group decreased, while the number of neutrophils increased. The differences were statistically significant ( $p < 0.05$ ). The number of lymphocytes in the Lent-*SIRT6* group was higher than that in the radiation group, while the number of neutrophils was higher than in the radiation group. These differences were also statistically significant ( $p < 0.05$ ). The differences in the number of neutrophils and lymphocytes between the Lent-*SIRT6* group and the control group were also statistically significant ( $p > 0.05$ ). The differences in RBCs among the 3 groups were statistically significant as well.

**Table 5.** Comparison of blood routine indexes of the 3 groups at 8 weeks after routine radiation [ $\times 10^9/L$ ]

Group	RBC	Neutrophil	Lymphocyte
Control group	6.72 ±0.85	0.61 ±0.36	4.39 ±0.37
Radiation group	6.34 ±0.91	1.28 ±0.54 <sup>a</sup>	1.65 ±0.84 <sup>a</sup>
Lent- <i>SIRT6</i> group	6.80 ±0.79	0.93 ±0.47 <sup>ab</sup>	1.29 ±0.61 <sup>ab</sup>

Compared with the control group: <sup>a</sup>  $p < 0.05$ ; compared with the radiation group; <sup>b</sup>  $p < 0.05$ .

### Comparison of levels of pulmonary inflammation factors in different groups of rats at 8 weeks after routine radiation

As shown in Table 6, compared with the control group without routine radiation and the Lent-*SIRT6* transfected rats, the IL-6 and IL-1 $\beta$  levels in the radiation group

**Table 6.** Comparison of levels of pulmonary inflammation factors in the 3 groups after routine radiation [pg/mg]

Group	TNF- $\alpha$	IL-6	IL-1 $\beta$
Control group	19.44 ±4.52	59.13 ±6.78	41.92 ±5.06
Radiation group	46.36 ±7.16 <sup>a</sup>	82.49 ±8.63 <sup>a</sup>	60.37 ±8.42 <sup>a</sup>
Lent- <i>SIRT6</i> group	27.58 ±6.24 <sup>ab</sup>	67.80 ±5.92 <sup>ab</sup>	43.63 ±0.47 <sup>b</sup>

Compared with the control group: <sup>a</sup>  $p < 0.05$ ; compared with the radiation group; <sup>b</sup>  $p < 0.05$ .

increased after radiation. The differences were statistically significant ( $p < 0.05$ ). The IL-6 and IL-1 $\beta$  levels in the Lent-*SIRT6* group were lower than those in the radiation group, and higher than those in the control group; these differences were all statistically significant ( $p < 0.05$ ).

## Discussion

The therapeutic effect of radiotherapy for lung cancer is dose-dependent. High-dose radiotherapy can improve the remission rate and local control rate of tumors, but at the same time can bring about serious side effects.<sup>7</sup> The incidence of radiation-induced lung injury is 6–20%. It has been found that gene activation during radiotherapy leads to early lung injury, including tissue and cellular dysfunction, increased vascular permeability and radiation-induced inflammation which may be caused by cytokines secreted in macrophages and leukocytes.<sup>8,9</sup> As a stimulus, inflammatory responses in radiation-induced lung injury can promote the initiation of collagen genes and stimulate fibroblast hyperplasia.<sup>10</sup>

In this study, we found that the respiratory rates in the radiation group increased after X-ray radiation. The most obvious increase occurred at 2 weeks after radiation, which was consistent with the results of related studies.<sup>11</sup> However, the increase in the respiratory rates of rats receiving overexpressed Lent-*SIRT6* were a little lower and tended to become slower. These results suggested that the rats in the radiation group had significant lung injury, whereas rats in the overexpressed Lent-*SIRT6* group could alleviate the dyspnea caused by radiation-induced lung injury.

Pathological changes in the lungs are the most direct evidence for evaluating lung injury.<sup>12</sup> In this study, H&E staining showed that the rats in the radiation group had obvious lung injury compared with the control group; it was mainly manifested by thickened alveolar walls and fibrosis, and a large amount of hyperplastic fibrous tissues in the alveolar interstitium. In the group administered with overexpressed Lent-*SIRT6*, these pathological changes were improved, which provided direct evidence for the protective effects of *SIRT6* against lung injury.

The TNF- $\alpha$  can promote inflammatory responses, while IL-6 can induce lung fibrosis by preventing the apoptosis of lung fibroblasts.<sup>13</sup> Therefore, this study analyzed changes in both the process of radiation-induced lung

injury and the overexpression of *SIRT6*. The results showed that the levels of TNF- $\alpha$  and IL-6 increased at 1 week after radiation, and could last through 8 weeks after radiation, which indicated that inflammatory responses were sustained throughout the entire process of lung injury. However, in the group of animals administered with overexpressed Lent-*SIRT6*, the levels of TNF- $\alpha$  and IL-6 decreased and had protective effects on pulmonary inflammation during the process of lung injury. In our experiments, increased Lent-*SIRT6* levels also decreased the levels of pulmonary inflammation factors. Blood tests also suggested that overexpressed Lent-*SIRT6* could improve radiation-induced neutrophils, decrease the content of lymphocytes, and exert certain effects on inflammation, which was one of the possible ways to improve the pathological changes in lung injury.

## Conclusions

In summary, *SIRT6* could effectively inhibit inflammatory responses and alleviate radiation-induced lung injury, exerting certain protective effects on lung injury. However, the mechanisms and pathways of this process call for further study.

## References

1. Finkel T, Deng CX, Mostoslavsky R. Recent progress in the biology and physiology of sirtuins. *Nature*. 2009;460(7255):587.
2. Yao T, Quan L. Research progress of MMP-9, HIF-1 and SIRT1 in acute lung injury. *Chin J Emerg Med*. 2016;25(3):384–388.
3. Imanishi S, Hayashi R, Ichikawa T, et al. SRT1720, a SIRT1 activator, aggravates bleomycin-induced lung injury in mice. *Food Nutr Sci*. 2012;3(2):157–163.
4. Li T, Zhang J, Feng J, et al. Resveratrol reduces acute lung injury in a LPS-induced sepsis mouse model via activation of Sirt1. *Mol Med Rep*. 2013;7(6):1889–1895.
5. Smith LM, Wells JD, Vachharajani VT, Yoza BK, McCall CE, Hoth JJ. SIRT1 mediates a primed response to immune challenge after traumatic lung injury. *J Trauma Acute Care Surg*. 2015;78(5):1034–1038.
6. Cai Y, Sheng ZY, Liang SX. Radiosensitization effect of overexpression of adenovirus-mediated *SIRT6* on A549 non-small cell lung cancer cells. *Asian Pac J Cancer Prev*. 2014;15(17):7297–7301.
7. Luhua W, Xiaolong F, Ming C, et al. Diagnosis and treatment of radiation-induced lung injury. *Chin J Rad Oncol*. 2015;24(1):4–9.
8. Zhixi Y, Chuanxi C. Analysis of clinical characteristics of radiation-induced lung injury in patients with non-small cell lung cancer. *Chin J Clin Oncol Rehabil*. 2015;22(1):7–8.
9. Jing J, Bingsheng W. Research progress of cytokines in radiation-induced lung injury. *J Mod Oncol*. 2016;24(3):488–491.
10. Cuiying Z, Hong S, Yanyang W, et al. Relationship among expression of TGF $\beta$ 1,  $\alpha$ -SMA, Col1a1 and FN mRNA in lung tissues of mice with radiation-induced lung injury. *J Ningxia Univ*. 2015;6(5):33–36.
11. Xin M, Qian Z, Yingmei L, et al. Experimental study on the protective effects of amifostine on radiation-induced lung injury in rats. *Chin Oncol*. 2013;23(1):1–9.
12. Weihua Y, Chunhua N, Hongmei X, et al. Experimental study on the effect of thalidomide on radiation-induced lung injury. *J Mod Oncol*. 2016;24(19):3012–3016.
13. Tingzhen X, Qichu Y, Jiaojiao A. Effect of polygonum cuspidate on plasma levels of TGF- $\beta$  IL-6 and ACE in rats with radiation-induced lung injury. *Chin J Trad Med Sci Technol*. 2016;23(1):32–36.



# The prognostic value and non-invasive predictors of splenomegaly in cirrhotic patients with hepatocellular carcinoma following curative resection

Li Zhou<sup>A-F</sup>, Shao-Bin Wang<sup>B</sup>, Shu-Guang Chen<sup>B</sup>, Qiang Qu<sup>C</sup>, Jing-An Rui<sup>C-E</sup>

Department of General Surgery, Peking Union Medical College Hospital, Beijing, China

A – research concept and design; B – collection and/or assembly of data; C – data analysis and interpretation; D – writing the article; E – critical revision of the article; F – final approval of the article

Advances in Clinical and Experimental Medicine, ISSN 1899–5276 (print), ISSN 2451–2680 (online)

*Adv Clin Exp Med.* 2020;29(7):879–886

## Address for correspondence

Li Zhou  
E-mail: lizhou02@hotmail.com

## Funding sources

None declared

## Conflict of interest

None declared

Received on September 8, 2017  
Reviewed on December 7, 2017  
Accepted on January 6, 2018

Published online on August 3, 2020

## Cite as

Zhou L, Wang S-B, Chen S-G, Qu Q, Rui J-A. The prognostic value and non-invasive predictors of splenomegaly in cirrhotic patients with hepatocellular carcinoma following curative resection. *Adv Clin Exp Med.* 2020;29(7):879–886. doi:10.17219/acem/81935

## DOI

10.17219/acem/81935

## Copyright

© 2020 by Wrocław Medical University  
This is an article distributed under the terms of the  
Creative Commons Attribution Non-Commercial License  
(<http://creativecommons.org/licenses/by-nc-nd/4.0/>)

## Abstract

**Background.** The prognostic value and non-invasive predictors of splenomegaly in cirrhotic patients with hepatocellular carcinoma (HCC) after curative resection remain unknown.

**Objectives.** To investigate the prognostic value and non-invasive predictors of splenomegaly in cirrhotic patients with HCC after curative resection.

**Material and methods.** The medical records of 78 patients with HCC and liver cirrhosis who underwent curative resection were retrospectively reviewed. The influence of spleen size, measured with clinically routine ultrasonography (USG), on overall and disease-free survival was evaluated using univariate and multivariate analyses. The efficiency of some frequently used blood-derived liver function parameters and non-invasive fibrosis markers to predict splenomegaly was also assessed.

**Results.** It was shown that tumor size >5 cm, the presence of microvascular invasion, tumor-node metastasis (TNM) stage III–IVA of the tumor, spleen size >11.45 cm, and age ≤52 years were associated with poor overall survival and/or disease-free survival in univariate analyses (all  $p < 0.05$ ). In multivariate analyses, spleen size was identified as an independent predictor for both overall and disease-free survival ( $p < 0.001$  and  $p = 0.012$ , respectively). On the other hand, platelet count, aspartate aminotransferase (AST) to platelet ratio index (APRI) and Fibrosis-4 index (FIB-4) scores were significantly different between small and large spleen groups ( $p = 0.026$ ,  $0.003$  and  $0.003$ , respectively), while statistical differences for albumin, alanine aminotransferase (ALT), AST, total bilirubin, AST to ALT ratio (AAR), and age-platelet index (API) were not found. Using receiver operating characteristic (ROC) curves, high powers of platelet count, APRI and FIB-4 in splenomegaly prediction were confirmed.

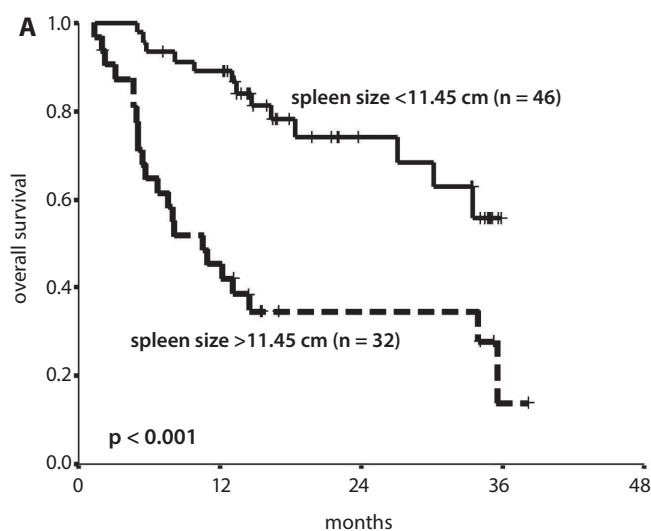
**Conclusions.** Splenomegaly, which can be predicted by some non-invasive variables, serves as a strong determinant for postresectional prognoses of cirrhotic patients with HCC.

**Key words:** splenomegaly, prognosis, hepatocellular carcinoma, non-invasive markers

## Introduction

Hepatocellular carcinoma (HCC) is well-known as a malignant neoplasm with high incidence and mortality worldwide.<sup>1</sup> According to recent epidemiological data from China, population growth and ageing led to large and rising number of new cases of HCC in 2015, despite its declining rate.<sup>2</sup> In addition, the overall long-term prognosis of HCC remains disappointing, although surgical therapies, including curative resection and liver transplantation, produce the best results in highly selected patients.<sup>1</sup> Therefore, factors associated with the outcome of HCC have long been of interest. Previous studies have identified many clinical and pathologic variables as prognosticators of HCC patients who had undergone hepatectomies.<sup>3–7</sup> The majority of them were tumor-related, such as microvascular invasion (MVI), serum  $\alpha$ -fetoprotein (AFP) level, histological grade, tumor-node-metastasis (TNM) stage, portal vein tumor thrombus, as well as tumor size and number.<sup>3–7</sup> However, it is important to note that some authors found that liver cirrhosis correlated with post-resectional survival of HCC patients, indicating that the prognosis of HCC was determined not only by the tumor itself, but also by the background liver status.<sup>3,6</sup>

Splenomegaly is one of the common clinical signs of portal hypertension that is often ascribed to liver cirrhosis. Although portal hypertension has been shown to be prognostic in patients following hepatectomy, counterexamples have also been reported.<sup>6,8–13</sup> In addition, whether splenomegaly influences the long-term prognosis of patients with resected HCC remains unclear. The present study was designed to elucidate the impact of splenomegaly on the long-term prognosis of cirrhotic patients with HCC who had undergone curative resections. The efficiency of some frequently used blood-derived liver function parameters and non-invasive fibrosis markers to predict splenomegaly in this subgroup of HCC was also assessed.



## Material and methods

### Patients and variables

The study involved 78 patients with HCC and liver cirrhosis who had undergone curative resection. Twelve factors, including the patient's general situation (age and gender) and liver background status (hepatitis B surface antigen (HBsAg), spleen size and clinically significant portal hypertension (CSPH)) as well as tumor-related factors (serum AFP value, capsule completeness, MVI, TNM stage, histological grade, as well as tumor size and number) were included in survival analyses. Clinically significant portal hypertension was diagnosed using the standard surrogate criteria, i.e., the presence of gastroesophageal varices or splenomegaly >12 cm with a platelet count <100/mm<sup>2</sup>.<sup>10</sup> Tumor-node-metastasis stages were based on the 7<sup>th</sup> edition of the American Joint Committee on Cancer (AJCC) Staging Manual for HCC.<sup>14</sup> The Edmondson–Steiner

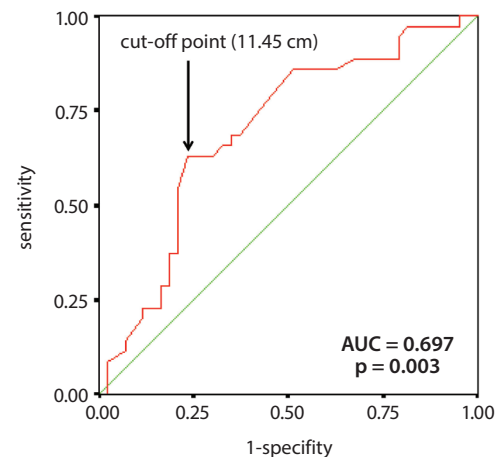


Fig. 1. Determination of the cut-off value of spleen size for overall survival based on the receiver operating characteristic (ROC) curve; AUC – area under curve

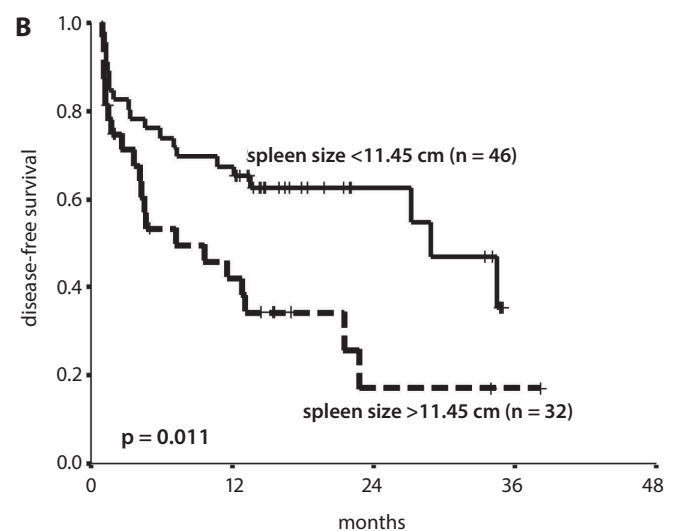


Fig. 2. Prognostic value of splenomegaly (>11.45 cm) in cirrhotic patients with hepatocellular carcinoma (HCC) following curative resection: A. overall survival; B. disease-free survival

criteria were used for tumor histological grading.<sup>15</sup> In addition, 5 blood-based liver function parameters, including albumin, alanine aminotransferase (ALT), aspartate aminotransferase (AST), total bilirubin, and platelet count, and 4 non-invasive liver fibrosis markers, including AST to ALT ratio (AAR), age-platelet index (API), AST to platelet ratio index (APRI), and Fibrosis-4 index (FIB-4) scores, were applied to predict splenomegaly.<sup>16–19</sup> The acquisition of clinicopathologic and follow-up data was approved by the institutional Ethics Committee of Peking Union Medical College Hospital (Beijing, China).

### Determination of spleen size, blood-derived liver function parameters and non-invasive fibrosis markers

Spleen size was routinely measured using ultrasonography (USG) and defined as the greatest dimension of the spleen. Serum liver function parameters, albumin, ALT, AST, and total bilirubin were detected preoperatively using

the Beckman Coulter AU5800 chemistry analyzer (Beckman Coulter Inc., Brea, USA), while the preoperative platelet number was counted using the Sysmex XE-5000 automated hematology analyzer (Sysmex Corporation, Kobe, Japan). On the basis of those results, the abovementioned non-invasive fibrosis markers were calculated according to their respective formulae.<sup>16–19</sup>

### Follow-up

All the patients underwent follow-up, mainly by serum AFP level and imaging examinations, including USG, angiography, computed tomography (CT), and magnetic resonance imaging (MRI). The follow-up period ranged from 1.4 to 38.2 months (median: 14.5 months).

### Statistical analyses

The cut-off value of spleen size was determined with the receiver operating characteristic (ROC) curve for survival

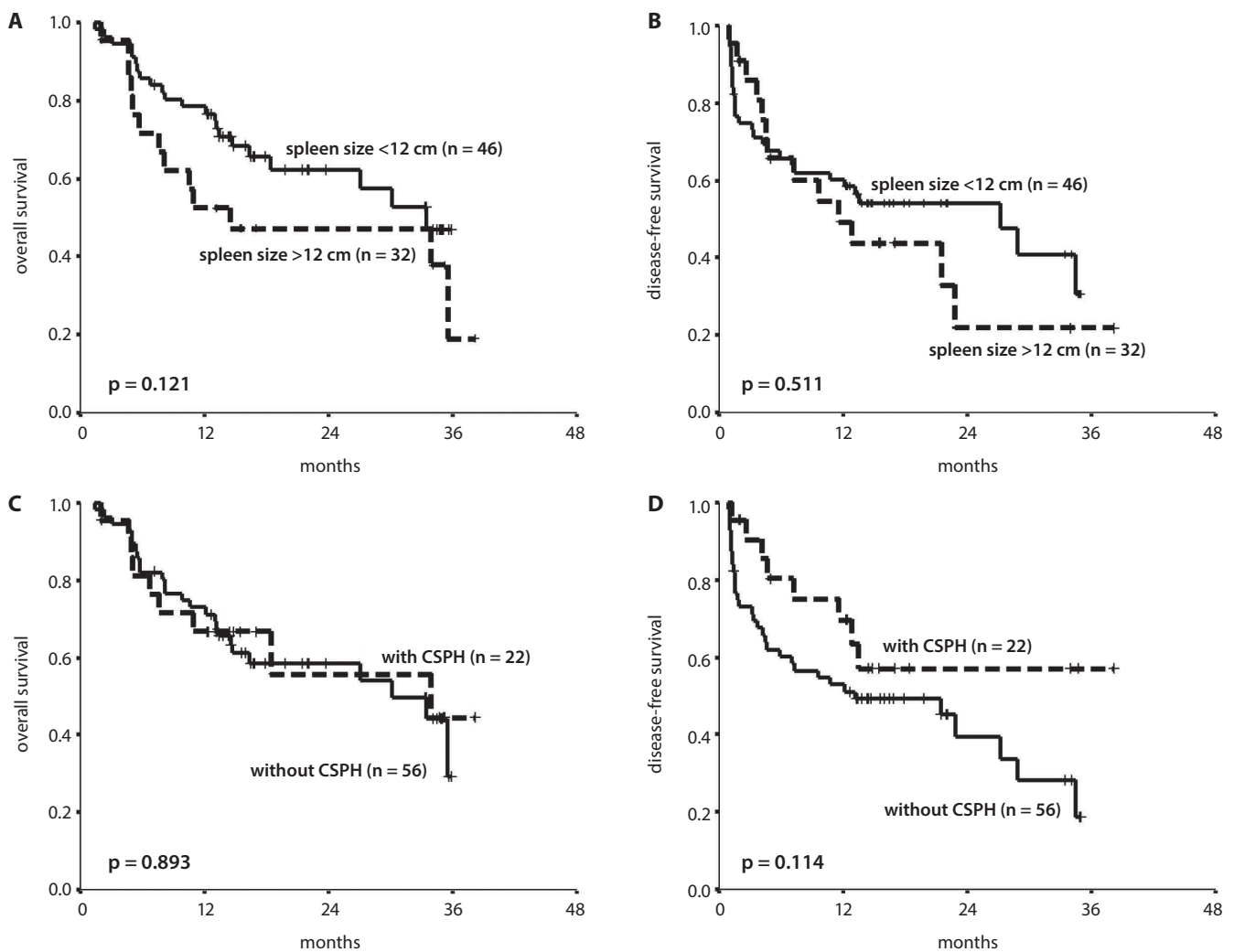


**Fig. 3.** Prognostic value of splenomegaly (>12 cm) and clinically significant portal hypertension (CSPH) in cirrhotic patients with hepatocellular carcinoma (HCC) following curative resection: A. splenomegaly (>12 cm) for overall survival; B. splenomegaly (>12 cm) for disease-free survival; C. CSPH for overall survival; D. CSPH for disease-free survival

**Table 1.** Univariate and multivariate analyses for the overall survival of cirrhotic patients with HCC following curative resection

Variables	n	Univariate			Multivariate		
		HR	95% CI	p-value	HR	95% CI	p-value
Age							
>52 years	40	0.561	0.284–1.106	0.095	N/A	N/A	N/A
≤52 years	38	1					
Gender				0.294			
male	65	1			N/A	N/A	N/A
female	13	0.653	0.295–1.447				
HBsAg				0.344			
positive	71	2.624	0.356–19.312		N/A	N/A	N/A
negative	7	1					
Tumor size				<b>0.017</b>			<b>0.059</b>
>5 cm	40	2.342	1.164–4.713		2.025	0.974–4.208	
≤5 cm	38	1			1	N/A	
Tumor number				0.054			
solitary	54	1.960	0.989–3.883		N/A	N/A	N/A
multiple	24	1					
Capsule				0.567			
complete	15	1			N/A	N/A	N/A
incomplete	63	1.261	0.570–2.785				
MVI				<b>0.011</b>			0.447
present	35	2.411	1.223–4.751		0.695	0.272–1.776	
absent	43	1			1		
TNM stage				<b>&lt;0.001</b>			<b>0.001</b>
I–II	37	1			1		
III–IVA	41	4.232	1.967–9.102		6.131	2.079–18.084	
Edmondson–Steiner grade				0.269			
II	27	1			N/A	N/A	N/A
III–IV	51	1.513	0.726–3.155				
AFP				0.339			
>20 ng/mL	58	1.504	0.652–3.467		N/A	N/A	N/A
≤20 ng/mL	20	1					
Spleen size				<b>&lt;0.001</b>			<b>&lt;0.001</b>
>11.45 cm	32	3.779	1.890–7.553		4.601	2.235–9.475	
≤11.45 cm	46	1			1		
Spleen size				0.126			
>12 cm	22	1.717	0.859–3.428		N/A	N/A	N/A
≤12 cm	56	1					
CSPH				0.894			
present	22	0.949	0.444–2.030		N/A	N/A	N/A
absent	56	1					

HCC – hepatocellular carcinoma; HR – hazard ratio; CI – confidence interval; HBsAg – hepatitis B surface antigen; MVI – microvascular invasion; TNM – tumor-node-metastasis; AFP –  $\alpha$ -fetoprotein; CSPH – clinically significant portal hypertension; values in bold are statistically significant.

and Youden's index (YI). Survival curves of patients in the small and large spleen groups were generated using the Kaplan–Meier method and compared using the log-rank test. Univariate and multivariate Cox regression analyses (proportional hazard model) were used to identify prognostic factors. The values of the blood-derived liver function parameters and non-invasive fibrosis markers in the 2 groups were compared using the Mann–Whitney U test. The predictive accuracies of the variables for splenomegaly, evaluated with the area under the curve (AUC), were shown using ROC curves. SPSS statistical software package v. 11.5 (SPSS Inc., Chicago, USA) was used for all the analyses. Statistical significance was defined as  $p < 0.05$ .

## Results

### Patient characteristics

The study group comprised 65 male (83.3%) and 13 female patients (16.7%). The patients' median age was 52 years (range: 31–74 years). There were 71 patients (91.0%) with positive hepatitis B surface antigen (HBsAg). Clinically significant portal hypertension was present in 22 patients (28.2%) and absent in 56 (71.8%). The median tumor size was 5.2 cm (range: 0.3–17 cm). Solitary tumors were found in 54 patients (69.2%), whereas 15 patients (19.2%) carried tumors with complete capsules. Microvascular invasion developed in 35 patients (44.9%).

**Table 2.** Univariate and multivariate analyses for the disease-free survival of cirrhotic patients with HCC following curative resection

Variables	n	Univariate			Multivariate		
		HR	95% CI	p-value	HR	95% CI	p-value
Age				<b>0.017</b>			<b>0.027</b>
>52 years	40	0.463	0.246–0.871		0.476	0.247–0.919	
≤52 years	38	1	N/A		1		
Gender				0.788			
male	65	1			N/A	N/A	N/A
female	13	0.894	0.394–2.026				
HbsAg				0.205			
positive	71	3.622	0.496–26.461		N/A	N/A	N/A
negative	7	1					
Tumor size				<b>0.003</b>			<b>0.015</b>
>5 cm	40	2.677	1.396–5.132		2.330	1.181–4.600	
≤5 cm	38	1			1		
Tumor number				0.170			
solitary	54	1.581	0.822–3.042		N/A	N/A	N/A
multiple	24	1					
Capsule				0.133			
complete	15	1			N/A	N/A	N/A
incomplete	63	1.736	0.845–3.567				
MVI				<b>0.014</b>			0.345
present	35	2.184	1.172–4.070		0.640	0.253–1.616	
absent	43	1			1		
TNM stage				<b>&lt;0.001</b>			<b>0.008</b>
I–II	37	1			1		
III–IV <sub>A</sub>	41	3.404	1.736–6.677		3.806	1.408–10.286	
Edmondson–Steiner grade				0.573			
II	27	1			N/A	N/A	N/A
III–IV	51	1.206	0.629–2.314				
AFP				0.337			
>20 ng/mL	58	1.446	0.681–3.072		N/A	N/A	N/A
≤20 ng/mL	20	1					
Spleen size				<b>0.013</b>			<b>0.012</b>
>11.45 cm	32	2.181	1.176–4.047		2.280	1.197–4.345	
≤11.45 cm	46	1			1		
Spleen size				0.513			
>12 cm	22	1.247	0.644–2.412		N/A	N/A	N/A
≤12 cm	56	1					
CSPH				0.121			
present	22	0.542	0.250–1.175		N/A	N/A	N/A
absent	56	1					

HCC – hepatocellular carcinoma; HR – hazard ratio; CI – confidence interval; HbsAg – hepatitis B surface antigen; MVI – microvascular invasion; TNM – tumor-node-metastasis; AFP – α-fetoprotein; CSPH – clinically significant portal hypertension; values in bold are statistically significant.

Serum AFP level was higher than 20 ng/mL in 58 patients (74.4%). Stage I, II, III, and IV<sub>A</sub> tumors were found in 13, 24, 35, and 6 patients (16.7%, 30.7%, 44.9%, and 7.7%), respectively, while 27, 48 and 3 patients (34.6%, 61.5% and 3.9%) had Edmondson–Steiner grade II, III and IV tumors, respectively.

### The prognostic value of splenomegaly in cirrhotic patients with hepatocellular carcinoma following curative resection

Using the ROC curve (Fig. 1), the point (11.45 cm) with the highest YI of spleen size for survival was defined as the cut-off value. The patients with large spleen size

had significantly poorer overall and disease-free survival than those with small spleen size ( $p < 0.001$  and  $p = 0.011$ , Fig. 2). However, when 12 cm (which is included in the standard surrogate criteria) was used as the cut-off value, spleen size was not prognostic ( $p = 0.121$  and  $0.511$ , Fig. 3A,B). Furthermore, CSPH was not a significant marker for either overall or disease-free survival ( $p = 0.893$  and  $0.114$ , Fig. 3C,D). The univariate Cox regression model identified tumor size, MVI, TNM stage, spleen size, and age as predictors for overall and/or disease-free survival (all  $p < 0.05$ , Table 1,2). In the multivariate analyses, spleen size was an independent predictor for both overall and disease-free survival (hazard ratio (HR) = 4.601, 95% confidence interval

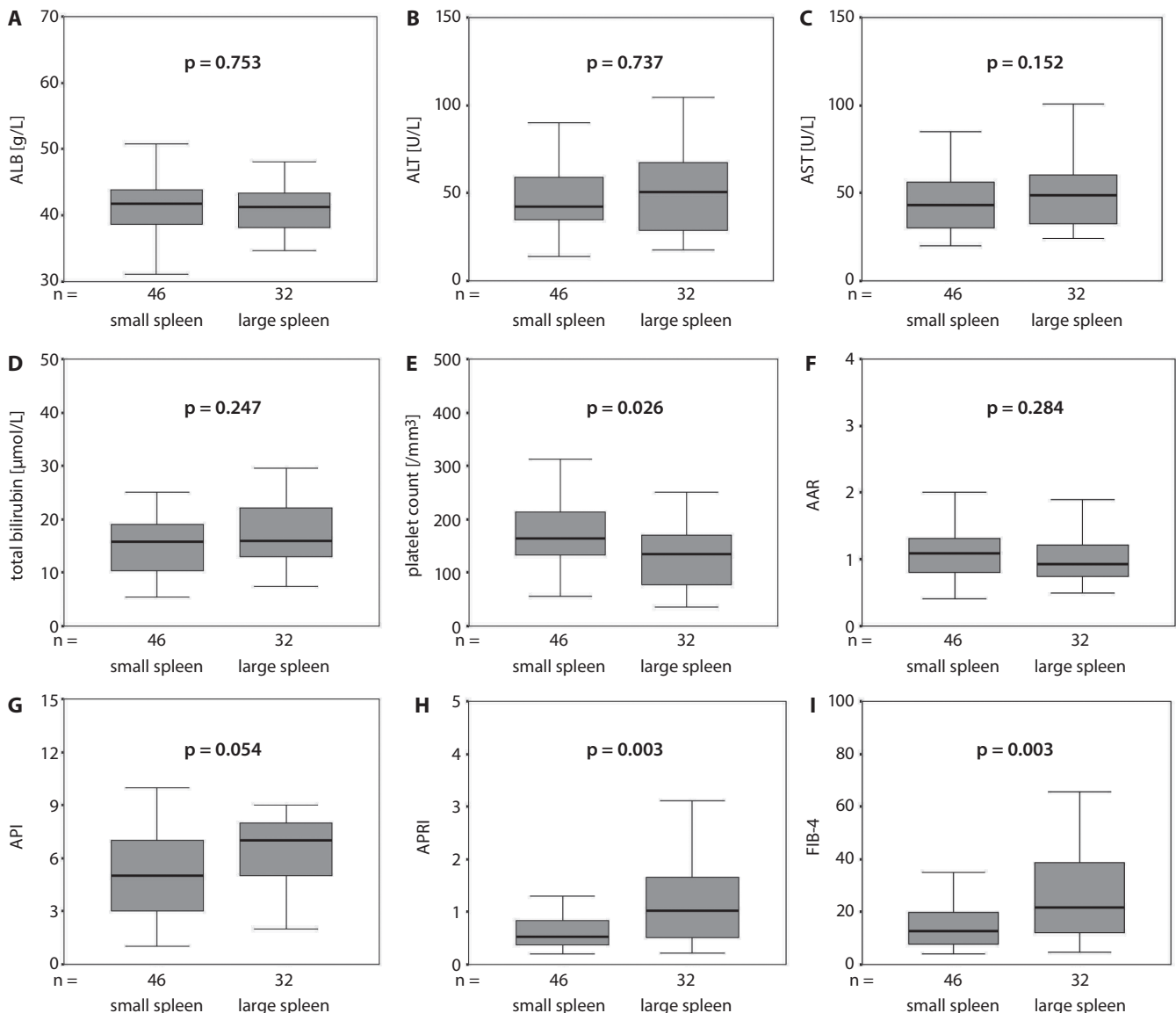


**Fig. 4.** Comparison of liver function parameters and non-invasive fibrosis markers between small ( $\leq 11.45$  cm) and large ( $> 11.45$  cm) spleen groups: A. albumin (ALB); B. alanine aminotransferase (ALT); C. aspartate aminotransferase (AST); D. total bilirubin; E. platelet count; F. AST to ALT ratio (AAR); G. age-platelet index (API); H. AST to platelet ratio index (APRI); I. Fibrosis-4 index (FIB-4)

(95% CI) = 2.235–9.475,  $p < 0.001$  for overall survival; HR = 2.280, 95% CI = 1.197–4.345,  $p = 0.012$  for disease-free survival; Tables 1 and 2), along with TNM stage, tumor size and age (all  $p < 0.05$ , Table 1,2).

### Predictive efficiency of blood-derived liver function parameters and non-invasive fibrosis markers for splenomegaly

It was revealed that there were significant differences in platelet count, APRI and FIB-4 between the small and large spleen groups ( $p = 0.026$ ,  $0.003$  and  $0.003$ , respectively, Fig. 4E,H,I), whereas the differences for albumin, ALT, AST, total bilirubin, AAR, and API were not statistically significant (Fig. 4A–D,F,G). The ROC curves demonstrated that platelet count, APRI and FIB-4 had high accuracy in predicting splenomegaly (AUC = 0.649,

$0.702$  and  $0.698$ , respectively,  $p < 0.05$ , Fig. 5E,H,I), while the other parameters were not of significance ( $p > 0.05$ , Fig. 5A–D,F,G).

### Discussion

Splenomegaly has long been well-known as an obvious sign of portal hypertension that is frequently induced by liver cirrhosis in clinical practice. It is listed as 1 of 3 factors in the standard surrogate criteria of CSPH.<sup>10</sup> It has previously been suggested that splenomegaly has a negative impact on the overall survival of patients with HCC treated with radiofrequency ablation; however, its prognostic significance in curatively resected HCC has not been elucidated.<sup>20</sup> The current study showed that splenomegaly, using the cut-off value derived from the ROC curve (11.45 cm),

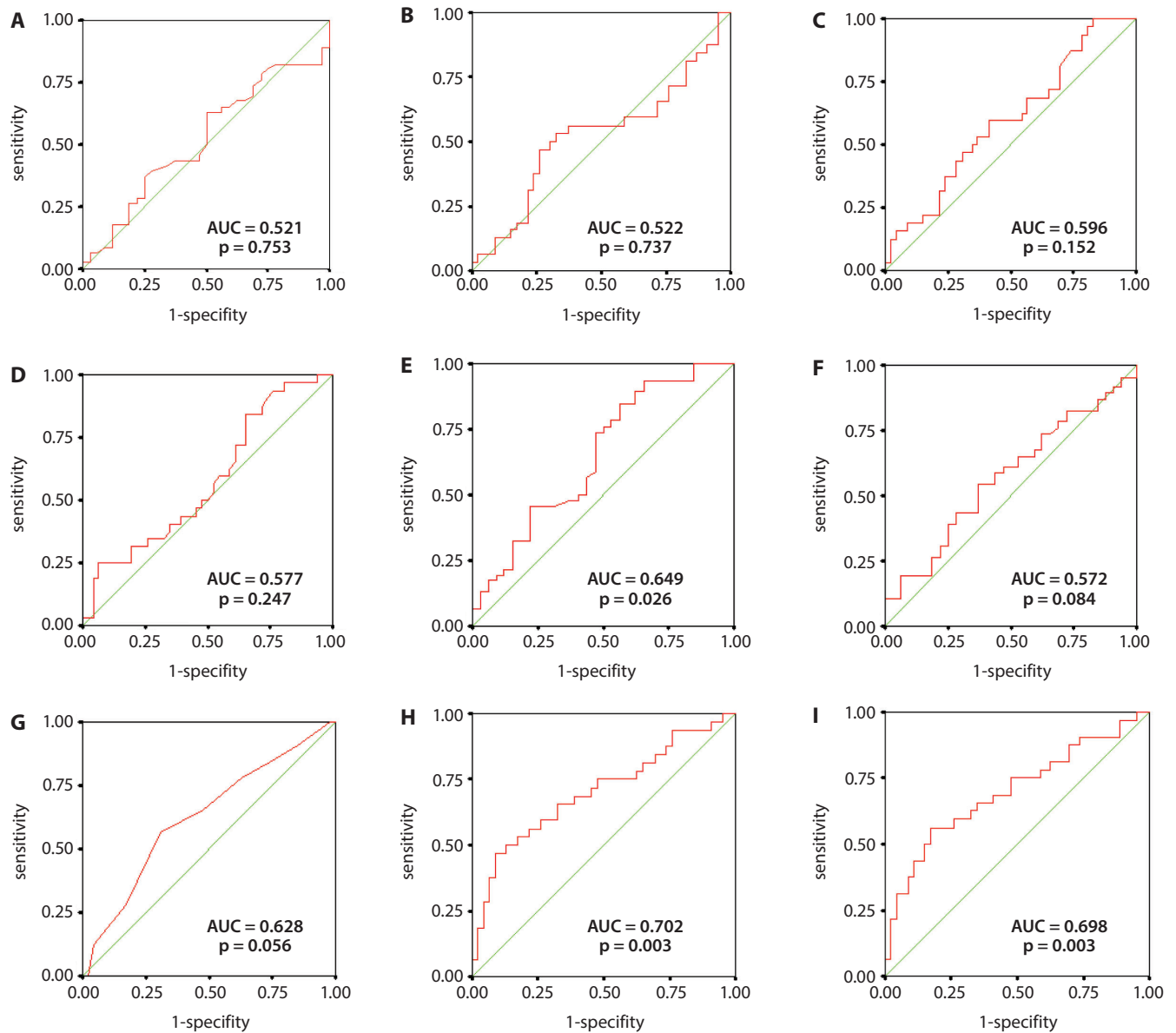


Fig. 5. Predictive accuracies of liver function parameters and non-invasive fibrosis markers for splenomegaly (>11.45 cm): A. albumin (ALB); B. alanine aminotransferase (ALT); C. aspartate aminotransferase (AST); D. total bilirubin; E. platelet count; F. AST to ALT ratio (AAR); G. age-platelet index (API); H. AST to platelet ratio index (APRI); I. Fibrosis-4 index (FIB-4); AUC – area under curve

was identified as a powerful predictor for a poor prognosis using 3 statistical tools (the log-rank test, as well as univariate and multivariate Cox regression models). These results might indicate that splenomegaly can be a promising and reliable independent prognostic marker of HCC before surgery. It should be emphasized that this variable was not only associated with overall survival, as previously found, but also with disease-free survival in HCC patients who had undergone curative resection.<sup>20</sup> Thus, this study is the first to indicate the role of splenomegaly in postsurgical recurrence of HCC. However, splenomegaly (>12 cm) was not significant to either overall or disease-free survival, indicating that this cut-off point might not be suitable for outcome prediction after resection for HCC, although it is included in the standard surrogate criteria for CSPH.<sup>10</sup>

We also found that CSPH, determined using the standard surrogate criteria, was also not prognostic in curatively resected HCC, which supports some previous investigations, including 1 from China.<sup>11–13</sup> It has already been demonstrated that liver cirrhosis/fibrosis-related peritumoral ductular reaction contributes to aggressive tumor behaviors, recurrence and poor survival, and to molecular alterations, such as nuclear translocation of  $\beta$ -catenin and upregulated *pSmad2* expression, in HCC.<sup>21,22</sup> Therefore, the inconsistent results concerning the prognostic role of CSPH suggest an urgent need for further validation of the standard surrogate criteria, because measurement of the hepatic venous pressure gradient (HVPG), regarded as the gold diagnostic criterion for CSPH, is not routinely used in clinical practice due to its invasiveness. On the

other hand, in comparison to total splenic volume calculations based on 3D reconstructions of spleen CT data, measurements of spleen size using USG might be simpler, more convenient and easier to apply in clinical practice.<sup>20</sup> Recently, it was shown that HVPG could be precisely predicted by the CT-based liver/spleen volume ratio.<sup>23</sup> In the future, determining whether USG could be used to predict HVPG might be of interest.

In addition, it was believed that the accuracy of USG-based spleen assessment could be significantly influenced by the examiner's experience, especially due to irregular contours of the spleen and overlapping with bone, kidney or bowel gas.<sup>24</sup> For inexperienced examiners or under difficult conditions, variables to aid in assessments might be of particular significance. Thus far, many non-invasive markers for predicting liver fibrosis and cirrhosis, such as AAR, API, APRI, and FIB-4, have been developed, based mainly on platelet number, liver biochemical parameters and age, and have been shown to have strong predictive power.<sup>16–19</sup> However, a counterexample was also shown.<sup>25</sup> Previously, API, APRI, FIB-4, and the platelet number were found to be effectively predictive for splenomegaly in HCC patients who underwent radiofrequency ablation.<sup>20</sup> The present study is the first validation of the efficiency of those parameters and routine liver function tests for splenomegaly in curatively resected HCC. Like Wu et al., we suggested that platelet number, APRI and FIB-4, unlike AAR, are significant variables, while albumin, ALT, AST, and total bilirubin are not of significance.<sup>20</sup> However, the predictive power of API in resected HCC deserves to be further confirmed, because its p-values were very close to the statistical limit in both direct comparison and the ROC curve.

## Conclusions

Our data indicated that splenomegaly (>11.45 cm), which can be predicted by some non-invasive variables, serves as a powerful determinant for postresectional prognoses of cirrhotic patients with HCC. However, the present work might be limited by its retrospective design and relatively small sample size. The unsatisfactory AUCs of significant parameters (around 0.7) might be associated with the latter. In the future, further large-scale prospective studies that address these issues are expected.

## References

1. El-Serag HB. Hepatocellular carcinoma. *N Engl J Med*. 2011;365(12):1118–1127.
2. Chen W, Zheng R, Baade PD, et al. Cancer statistics in China, 2015. *CA Cancer J Clin*. 2016;66(2):115–132.
3. Kluger MD, Salceda JA, Laurent A, et al. Liver resection for hepatocellular carcinoma in 313 Western patients: Tumor biology and underlying liver rather than tumor size drive prognosis. *J Hepatol*. 2015;62(5):1131–1140.
4. Chen HW, Shan L, Wan-Yee L, et al. Prognostic impact of hepatic resection for hepatocellular carcinoma. The role of the surgeon in achieving R0 resection: A retrospective cohort study. *Int J Surg*. 2015;13:297–301.
5. Xu XS, Chen W, Miao RC, et al. Survival analysis of hepatocellular carcinoma: A comparison between young patients and aged patients. *Chin Med J (Engl)*. 2015;128(13):1793–1800.
6. Goh BK, Teo JY, Chan CY, et al. Importance of tumor size as a prognostic factor after partial liver resection for solitary hepatocellular carcinoma: Implications on the current AJCC staging system. *J Surg Oncol*. 2016;113(1):89–93.
7. Liu W, Wang K, Bao Q, Sun Y, Xing BC. Hepatic resection provided long-term survival for patients with intermediate and advanced-stage resectable hepatocellular carcinoma. *World J Surg Oncol*. 2016;14:62.
8. Ishizawa T, Hasegawa K, Aoki T, et al. Neither multiple tumors nor portal hypertension are surgical contraindications for hepatocellular carcinoma. *Gastroenterology*. 2008;134(7):1908–1916.
9. Tang YH, Zhu WJ, Wen TF. Influence of clinically significant portal hypertension on hepatectomy for hepatocellular carcinoma: A meta-analysis. *Asian Pac J Cancer Prev*. 2014;15(4):1649–1654.
10. Berzigotti A, Reig M, Abraldes JG, Bosch J, Bruix J. Portal hypertension and the outcome of surgery for hepatocellular carcinoma in compensated cirrhosis: A systematic review and meta-analysis. *Hepatology*. 2015;61(2):526–536.
11. Cucchetti A, Ercolani G, Vivarelli M, et al. Is portal hypertension a contraindication to hepatic resection? *Ann Surg*. 2009;250(6):922–928.
12. Santambrogio R, Kluger MD, Costa M, et al. Hepatic resection for hepatocellular carcinoma in patients with Child–Pugh's A cirrhosis: Is clinical evidence of portal hypertension a contraindication? *HPB (Oxford)*. 2013;15(1):78–84.
13. He W, Zeng Q, Zheng Y, et al. The role of clinically significant portal hypertension in hepatic resection for hepatocellular carcinoma patients: A propensity score-matching analysis. *BMC Cancer*. 2015;15:263.
14. Cheng CH, Lee CF, Wu TH, et al. Evaluation of the new AJCC staging system for resectable hepatocellular carcinoma. *World J Surg Oncol*. 2011;9:114.
15. Edmondson HA, Steiner PE. Primary carcinoma of the liver: A study of 100 cases among 48,900 necropsies. *Cancer*. 1954;7(3):462–503.
16. Su CW, Chan CC, Hung HH, et al. Predictive value of aspartate aminotransferase to alanine aminotransferase ratio for hepatic fibrosis and clinical adverse outcomes in patients with primary biliary cirrhosis. *J Clin Gastroenterol*. 2009;43(9):876–883.
17. Poynard T, Bedossa P. Age and platelet count: A simple index for predicting the presence of histological lesions in patients with antibodies to hepatitis C virus. METAVIR and CLINIVIR Cooperative Study Groups. *J Viral Hepat*. 1997;4(3):199–208.
18. Wai CT, Greenson JK, Fontana RJ, et al. A simple noninvasive index can predict both significant fibrosis and cirrhosis in patients with chronic hepatitis C. *Hepatology*. 2003;38(2):518–526.
19. Vallet-Pichard A, Mallet V, Nalpas B, et al. FIB-4, an inexpensive and accurate marker of fibrosis in HCV infection: Comparison with liver biopsy and fibrotest. *Hepatology*. 2007;46(1):32–36.
20. Wu WC, Chiou YY, Hung HH, et al. Prognostic significance of computed tomography scan-derived splenic volume in hepatocellular carcinoma treated with radiofrequency ablation. *J Clin Gastroenterol*. 2012;46(9):789–795.
21. Xu M, Xie F, Qian G, et al. Peritumoral ductular reaction: A poor postoperative prognostic factor for hepatocellular carcinoma. *BMC Cancer*. 2014;14:65.
22. Cai X, Li F, Zhang Q, et al. Peritumoral ductular reaction is related to nuclear translocation of  $\beta$ -catenin in hepatocellular carcinoma. *Biomed Pharmacother*. 2015;76:11–16.
23. Iranmanesh P, Vazquez O, Terraz S, et al. Accurate computed tomography-based portal pressure assessment in patients with hepatocellular carcinoma. *J Hepatol*. 2014;60(5):969–974.
24. Ishibashi H, Higuchi N, Shimamura R, Hirata Y, Kudo J, Niho Y. Sonographic assessment and grading of spleen size. *J Clin Ultrasound*. 1991;19(1):21–25.
25. Eminler AT, Ayyildiz T, Irak K, et al. AST/ALT ratio is not useful in predicting the degree of fibrosis in chronic viral hepatitis patients. *Eur J Gastroenterol Hepatol*. 2015;27(12):1361–1366.

# Risk factors of recurrence and poor survival in curatively resected hepatocellular carcinoma with microvascular invasion

Li Zhou<sup>A-F</sup>, Shao-Bin Wang<sup>B</sup>, Shu-Guang Chen<sup>B</sup>, Qiang Qu<sup>C</sup>, Jing-An Rui<sup>C-E</sup>

Department of General Surgery, Chinese Academy of Medical Sciences/Peking Union Medical College, Beijing, China

A – research concept and design; B – collection and/or assembly of data; C – data analysis and interpretation; D – writing the article; E – critical revision of the article; F – final approval of the article

Advances in Clinical and Experimental Medicine, ISSN 1899–5276 (print), ISSN 2451–2680 (online)

*Adv Clin Exp Med.* 2020;29(7):887–892

## Address for correspondence

Li Zhou  
E-mail: lizhou02@hotmail.com

## Funding sources

None declared

## Conflict of interest

None declared

Received on April 18, 2017  
Reviewed on August 16, 2017  
Accepted on September 1, 2017

Published online on August 4, 2020

## Abstract

**Background.** Microvascular invasion (MVI) is a significant sign of the invasive property and a strong predictor of poor prognosis in hepatocellular carcinoma (HCC), a life-threatening malignancy. However, recurrence-associated and post-surgical long-term prognosis-associated factors in HCC with MVI remain unknown.

**Objectives.** To address the abovementioned issues, based on a Chinese patient cohort with HCC after curative hepatic resection.

**Material and methods.** The patient cohort consisted of 62 consecutive patients with HCC and MVI who underwent curative hepatic resection. The associations between clinicopathologic variables and recurrence, as well as patient overall/disease-free survival, were uni- and multivariately evaluated.

**Results.** Univariate  $\chi^2$  test identified hepatitis B surface antigen (HBsAg) positivity, high Edmondson–Steiner grade and male gender as risk factors of recurrence, whereas Edmondson–Steiner grade and HBsAg positivity were significant or marginally significant in the multivariate stepwise logistic regression analysis. Subsequently, univariate log-rank test showed that Edmondson–Steiner grade, HBsAg positivity and Child–Pugh grade were associated with overall and/or disease-free survival. Among them, the independent prognostic impact of Edmondson–Steiner grade and HBsAg positivity for both overall and disease-free survival were proven in the multivariate Cox regression analysis.

**Conclusions.** Our data suggested that Edmondson–Steiner grade and HBsAg positivity might serve as useful indicators of recurrence and pessimistic prognosis in HCC with MVI.

**Key words:** prognostic factor, recurrence, survival, hepatocellular carcinoma, hepatic resection

## Cite as

Zhou L, Wang SB, Chen SG, Qu Q, Rui JA. Risk factors of recurrence and poor survival in curatively resected hepatocellular carcinoma with microvascular invasion. *Adv Clin Exp Med.* 2020;29(7):887–892. doi:10.17219/acem/76750

## DOI

10.17219/acem/76750

## Copyright

© 2020 by Wrocław Medical University  
This is an article distributed under the terms of the  
Creative Commons Attribution Non-Commercial License  
(<http://creativecommons.org/licenses/by-nc-nd/4.0/>)

## Introduction

Hepatocellular carcinoma (HCC) is well-recognized as a malignant tumor with high incidence and mortality worldwide.<sup>1–3</sup> Therefore, identification of prognostic markers of HCC became a research hotspot. Except for some clinical and pathological variables, such as portal vein tumor thrombosis (PVTT), tumor size, alpha-fetoprotein (AFP), and Child–Pugh grade, that were previously summarized as the most robust predictors of death, microvascular invasion (MVI), one of signs of unfavorable histological features of HCC (especially the invasive property), was also revealed to be of strong predictive potential for poor prognosis in HCC after several treatment methods, such as resection, transplantation and ablation.<sup>4–14</sup> However, it was also reported that some patients who carried HCC with MVI acquired actual ten-year survival.<sup>15</sup> Therefore, there is an urgent need and particular interest for the identification of prognostic determinants in this highly invasive subtype of HCC.

The current investigation aimed to address the issues through identification of factors that were associated with recurrence and long-term survival in this subtype of HCC.

## Material and methods

### Patients

In total, 62 patients undergoing curative hepatic resection for HCC with MVI were included in the study. Their age ranged from 24 to 76 years (mean  $\pm$  standard deviation (M  $\pm$ SD) 56.8  $\pm$ 12.5 years). Tumor sizes, regarding the largest dimensions, ranged from 2 cm to 26 cm (M  $\pm$ SD 8.5  $\pm$ 4.9 cm). Microvascular invasion was diagnosed through the postoperative routine pathological examinations. Portal vein tumor thrombosis was defined as tumor involvement in the main branches of portal vein. Satellite nodules were macroscopic. Histological grading was given based on Edmondson–Steiner criteria.<sup>16</sup> The baseline characteristics of patients are shown in Table 1. The acquisition of clinicopathologic and follow-up data was approved by the institutional Ethics Committee of Peking Union Medical College Hospital, Beijing, China.

### Evaluated variables and endpoints

Twelve variables related to general situation of the patient (age and gender), hepatic background (hepatitis B surface antigen (HBsAg), hepatitis C virus (HCV), liver cirrhosis, and Child–Pugh grade) and tumor phenotypes (serum AFP value, tumor size, tumor number, PVTT, satellite nodule, and Edmondson–Steiner grade) were chosen for analyses. Post-surgical recurrence, as well as overall and disease-free survival, served as the endpoints. Disease-free survival was defined as the patient survival interval from surgery to recurrence or distant metastasis occurrence.

**Table 1.** Baseline characteristics of patients with hepatocellular carcinoma (HCC) and microvascular invasion (MVI)

Variables	n (%)
Age	M $\pm$ SD: 56.8 $\pm$ 12.5 years; range: 24–76 years
Gender	
male	53 (85.5)
female	9 (14.5)
HBsAg	
positive	52 (83.9)
negative	10 (16.1)
HCV	
positive	5 (8.1)
negative	57 (91.9)
Cirrhosis	
present	51 (82.3)
absent	11 (17.7)
Child–Pugh grade	
grade A	58 (93.5)
grade B	4 (6.5)
Tumor size	M $\pm$ SD: 8.5 $\pm$ 4.9 cm; range: 2–26 cm
PVTT	
present	19 (30.6)
absent	43 (69.4)
Satellite nodule	
present	9 (14.5)
absent	53 (85.5)
Tumor number	
solitary	55 (88.7)
multiple	7 (11.3)
AFP level	
>20 ng/mL	49 (79.0)
$\leq$ 20 ng/mL	13 (21.0)
Edmondson–Steiner grade	
I	3 (4.8)
II	14 (22.6)
III	29 (46.8)
IV	16 (25.8)

M – mean; SD – standard deviation; HBsAg – hepatitis B surface antigen; HCV – hepatitis C virus; PVTT – portal vein tumor thrombosis; AFP – alpha-fetoprotein.

### Follow-up

The follow-up for all patients, ranging from 3 to 108 (Me: 14) months, was performed through imaging examinations and serum AFP level detection, as previously reported.<sup>17,18</sup> Follow-up intervals ranged from 1 to 3 months.

### Statistical analyses

The uni- and multivariate risk factors of recurrence were identified using  $\chi^2$  and stepwise logistic regression tests. Survival analyses were adopted using Kaplan–Meier method and log-rank test. Cox regression (proportional hazard model) was used for multivariate analysis of prognostic factors. Statistical software package SPSS v. 11.5 (SPSS Inc., Chicago, USA) was applied for all the analyses. Statistical significance was indicated when a p-value was less than 0.05.

## Results

### Risk factors of recurrence in patients with hepatocellular carcinoma and microvascular invasion after curative hepatic resection

Using univariate  $\chi^2$  test, gender, HBsAg and Edmondson–Steiner grade were associated with postoperative recurrence ( $p < 0.05$ ; Table 2), but other parameters were not of significance ( $p > 0.05$ ; Table 2). Multivariate stepwise logistic regression showed that Edmondson–Steiner grade was the single independent risk factor of recurrence (hazard ratio (HR) = 6.374, 95% confidence interval (95% CI) = 1.196–33.963,  $p = 0.030$ ; Table 2), while HBsAg positivity was of marginal significance (HR = 4.933, 95% CI = 0.789–30.833,  $p = 0.088$ ; Table 2).

### Prognostic factors in patients with hepatocellular carcinoma and microvascular invasion after curative hepatic resection

Univariate log-rank test revealed that HBsAg and Edmondson–Steiner grade were significantly associated with overall survival ( $p < 0.05$ ; Fig. 1 and Table 3), whereas Edmondson–Steiner grade, HBsAg and Child–Pugh grade were significant for disease-free survival ( $p < 0.05$ ; Fig. 2 and Table 3). In multivariate Cox regression analyses, Edmondson–Steiner grade and HBsAg were identified as independent prognostic indicators for both overall and disease-free survival (HR = 2.905 and 2.942, 95% CI = 1.263–6.683 and 1.021–8.474,  $p = 0.012$  and 0.046 for overall survival, respectively; HR = 3.407 and 2.944, 95% CI = 1.577–7.360 and 1.124–7.710,  $p = 0.002$  and 0.028 for disease-free survival, respectively; Table 4).

Table 2. Univariate and multivariate factors associated with recurrence in HCC with MVI

Variables	n	Univariate analysis			Multivariate analysis		
		with recurrence	without recurrence	p-value	HR	95% CI	p-value
Age				0.147			
≥65 years	19	14	5		N/A	N/A	N/A
<65 years	43	38	5				
Gender				<b>0.045<sup>#</sup></b>			0.118
male	53	47	6		4.780	0.671–34.066	
female	9	5	4		1		
HBsAg				<b>0.001</b>			0.088
positive	52	47	5		4.933	0.789–30.833	
negative	10	5	5		1		
HCV				1.000 <sup>#</sup>			
positive	5	4	1		N/A	N/A	N/A
negative	57	48	9				
Cirrhosis				0.119 <sup>#</sup>			
present	51	45	6		N/A	N/A	N/A
absent	11	7	4				
Child–Pugh grade				0.838 <sup>#</sup>			
grade A	58	48	10		N/A	N/A	N/A
grade B	4	4	0				
Tumor size				0.962 <sup>#</sup>			
≥5 cm	53	45	8		N/A	N/A	N/A
<5cm	9	7	2				
PVTT				0.672 <sup>#</sup>			
present	19	17	2		N/A	N/A	N/A
absent	43	35	8				
Satellite nodule				1.000 <sup>#</sup>			
present	9	8	1		N/A	N/A	N/A
absent	53	44	9				
Tumor number				0.493 <sup>#</sup>			
solitary	55	45	10		N/A	N/A	N/A
multiple	7	7	0				
AFP level				0.732 <sup>#</sup>			
>20 ng/mL	49	42	7		N/A	N/A	N/A
≤20 ng/mL	13	10	3				
Edmondson–Steiner grade				<b>0.004<sup>#</sup></b>			<b>0.030</b>
I–II	17	10	7		1		
III–IV	45	42	3		6.374	1.196–33.963	

HR – hazard ratio; 95% CI – 95% confidence interval; N/A – not applicable; <sup>#</sup>  $\chi^2$  test with continuity correction; values in bold indicate statistically significant differences.

**Table 3.** Univariate analysis for overall and disease-free survival of HCC with MVI patients

Variables	n	Overall survival			Disease-free survival		
		M ±SE	95% CI	p-value	M ±SE	95% CI	p-value
Age				0.408			0.250
≥65 years	19	40 ±10	20–60		34 ±10	14–53	
<65 years	43	24 ±3	18–30		16 ±2	12–19	
Gender				0.772			0.213
male	53	28 ±5	19–37		19 ±4	12–27	
female	9	22 ±4	14–30		22 ±5	13–31	
HBsAg				<b>0.006</b>			<b>0.002</b>
positive	52	22 ±3	16–27		14 ±2	11–17	
negative	10	69 ±15	40–97		59 ±15	29–89	
HCV				0.063			0.167
positive	5	12 ±3	6–18		9 ±2	4–14	
negative	57	30 ±5	20–39		22 ±4	14–30	
Cirrhosis				0.286			0.080
present	51	27 ±5	18–36		18 ±3	11–24	
absent	11	27 ±4	19–36		22 ±4	14–30	
Child–Pugh grade				0.058			<b>0.017</b>
grade A	58	30 ±5	20–39		22 ±4	14–31	
grade B	4	11 ±5	1–21		7 ±3	1–12	
Tumor size				0.101			0.147
≥5 cm	53	27 ±5	18–37		21 ±4	12–29	
<5cm	37	74 ±8	58–90		21 ±3	15–27	
PVTT				0.095			0.095
present	19	20 ±5	11–30		13 ±3	7–19	
absent	43	34 ±6	21–46		26 ±5	16–37	
Satellite nodule				0.051			0.142
present	9	16 ±5	7–25		11 ±3	5–18	
absent	53	31 ±5	21–41		23 ±4	12–32	
Tumor number				0.203			0.337
solitary	55	31 ±5	20–41		23 ±4	14–32	
multiple	7	17 ±5	7–28		12 ±4	5–20	
AFP level				0.517			0.260
>20 ng/mL	49	26 ±4	17–34		19 ±4	11–26	
≤20 ng/mL	13	31 ±8	16–46		22 ±5	12–32	
Edmondson–Steiner grade				<b>0.001</b>			<b>&lt;0.001</b>
I–II	17	56 ±13	31–80		46 ±12	24–69	
III–IV	45	19 ±2	15–23		12 ±1	10–14	

M – mean; SE – standard error; values in bold indicate statistically significant differences.

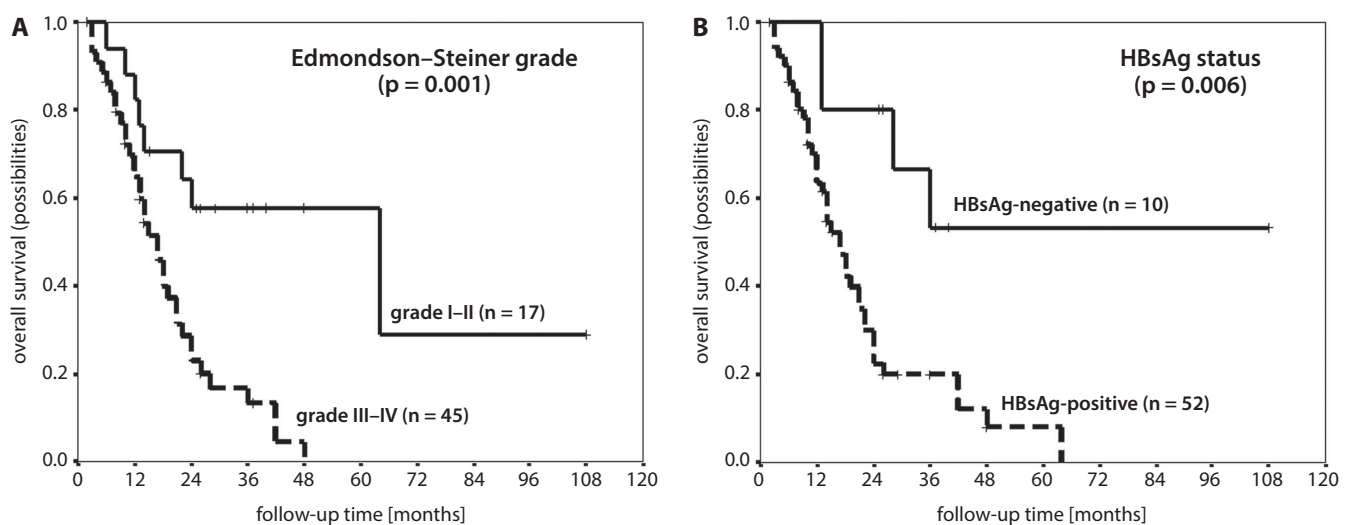


**Fig. 1.** The significant influence of the variables on overall survival of patients with HCC and MVI after curative hepatic resection. A. Edmondson–Steiner grade (solid line – grade I–II, n = 17; dashed line – grade III–IV, n = 45; p = 0.001); B. HBsAg positivity (solid line – negative, n = 10; dashed line – positive, n = 52; p = 0.006)

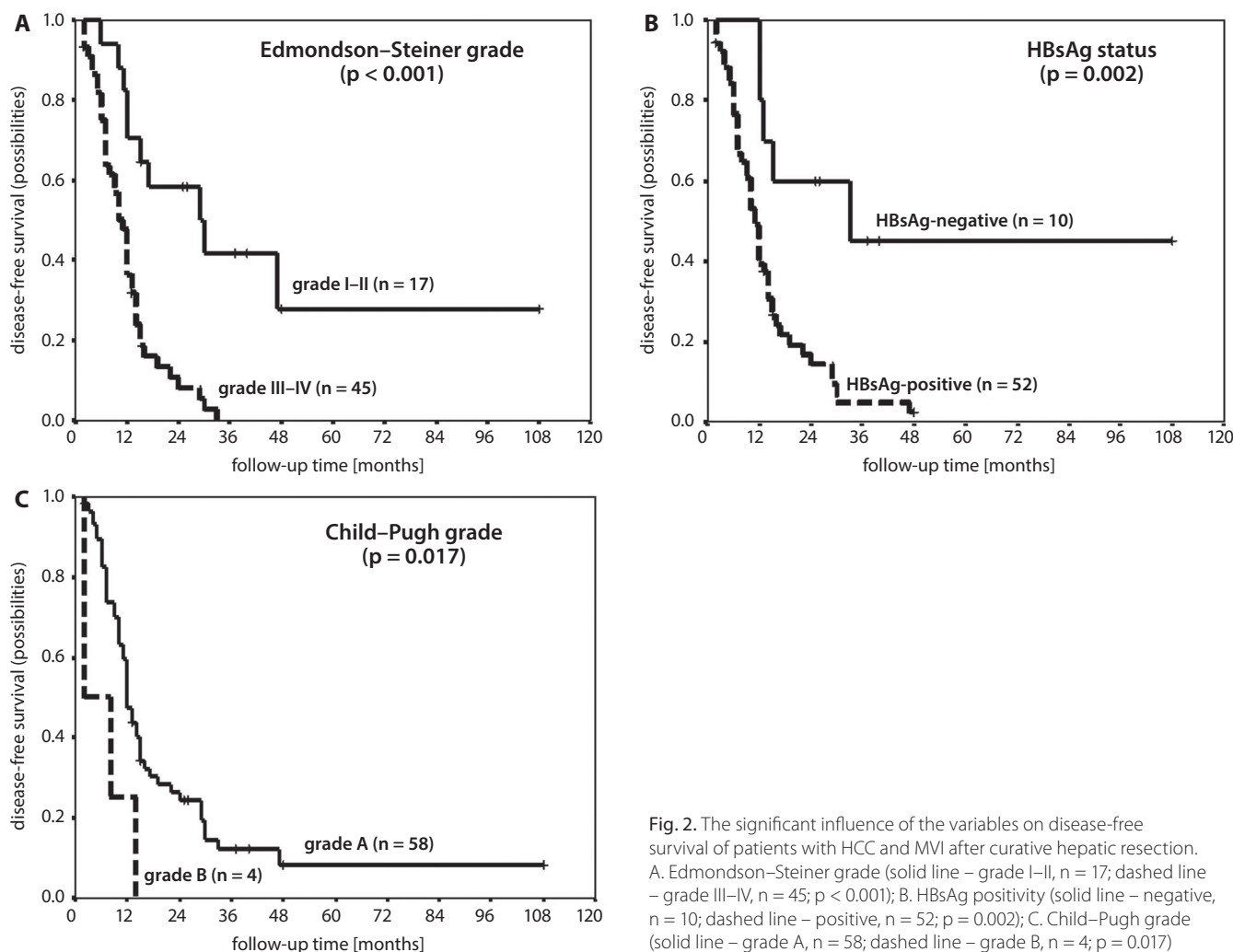


Fig. 2. The significant influence of the variables on disease-free survival of patients with HCC and MVI after curative hepatic resection. A. Edmondson–Steiner grade (solid line – grade I–II, n = 17; dashed line – grade III–IV, n = 45; p < 0.001); B. HBsAg positivity (solid line – negative, n = 10; dashed line – positive, n = 52; p = 0.002); C. Child–Pugh grade (solid line – grade A, n = 58; dashed line – grade B, n = 4; p = 0.017)

Table 4. Multivariate analysis for overall and disease-free survival of HCC with MVI

Variables	Overall survival			Disease-free survival		
	HR	95% CI	p-value	HR	95% CI	p-value
Edmondson–Steiner grade	2.905	1.263–6.683	<b>0.012</b>	3.407	1.577–7.360	<b>0.002</b>
HBsAg	2.942	1.021–8.474	<b>0.046</b>	2.944	1.124–7.710	<b>0.028</b>
Child–Pugh grade	N/A	N/A	N/A	2.043	0.718–5.813	0.181

N/A – not applicable; values in bold indicate statistically significant differences.

## Discussion

Microvascular invasion, as a marker of the invasive growth, remarkably influences prognosis of HCC in patients who underwent curative treatments, liver resection and transplantation, when recurrence and/or overall as well as disease-free survival served as endpoints.<sup>5–14</sup> However, prognostic factors of HCC with MVI remain to be explored. In the present study, factors associated with tumor recurrence were first identified. It was found that gender, Edmondson–Steiner grade and HBsAg were of statistical significance in univariate  $\chi^2$  test, while these 3 variables were significant or marginally significant

in multivariate logistic regression, respectively. Previously, gender and Edmondson–Steiner grade, along with MVI, were suggested to be correlated with post-surgical recurrence of HCC.<sup>19,20</sup> This study first showed their roles in HCC with MVI. Moreover, the more important finding of this work is to define HBsAg as a potential risk factor of recurrence in HCC with MVI, based on univariate and multivariate analyses. It was shown that high hepatitis B viral load predicted the recurrence of small HCC after curative resection.<sup>20,21</sup> We provided 2 novel predictors, HBsAg, which is routinely detected, and gender that was not predictive for recurrence in MVI-absent HCC, in addition to Edmondson–Steiner grade.<sup>22</sup> Some authors found

the association between HBsAg positivity and high AFP level, whereas AFP is reported to be involved in many malignant phenotypes of hepatoma cells, even in the activity of dendritic cells, through different mechanisms.<sup>23–25</sup> Furthermore, the finding that knockdown of HBsAg expression inhibits HCC growth provides the direct evidence for the role of HBsAg.<sup>26</sup> Therefore, our results about HBsAg and tumor recurrence might have a molecular basis.

On the other hand, it is well-known that HCC carries unsatisfactory prognosis. Thus far, its prognostic indicators, including MVI, have been identified.<sup>4–14</sup> However, prognostic indicators in HCC with MVI remain unclear and need in-depth exploration, because different survival status was also found in patients who carried HCC with MVI.<sup>15</sup> Our results showed that HBsAg and Edmondson–Steiner grade univariately and multivariately predicted both overall and disease-free survival, in consistence with reports on other types of HCC.<sup>27,28</sup> Considering the fact that these variables were independent or marginally independent risk factors for recurrence, their impact on patient survival of HCC with MVI might be understandable. Previously, the impact of HBsAg positivity on prognosis of HCC after radical or palliative therapies was also suggested.<sup>27</sup> This study first links HBsAg and HCC with MVI. Here, the authors preliminarily speculate on the possible route of its action in this subtype of HCC, as this protein stimulates tumor growth, then facilitates recurrence, and finally causes worse prognosis. Of course, this hypothesis needs to be extensively validated.

## Conclusions

Our data suggests that Edmondson–Steiner grade and HBsAg positivity might function as significant predictors for recurrence and poor prognosis in HCC with MVI after curative resection.

## References

- Pisani P, Parkin DM, Bray F, Ferlay J. Estimating the world cancer burden: Globocan 2000. *Int J Cancer*. 2001;94(2):153–156.
- Parkin DM, Bray F, Ferlay J, Pisani P. Global cancer statistics (2002). *CA Cancer J Clin*. 2005;55(2):74–108.
- Chen W, Zheng R, Baade PD, et al. Cancer statistics in China (2015). *CA Cancer J Clin*. 2016;66(2):115–132.
- Tandon P, Garcia-Tsao G. Prognostic indicators in hepatocellular carcinoma: A systematic review of 72 studies. *Liver Int*. 2009;29(4):502–510.
- Ng KM, Yan TD, Black D, Chu FC, Morris DL. Prognostic determinants for survival after resection/ablation of a large hepatocellular carcinoma. *HPB (Oxford)*. 2009;11(4):311–320.
- Belli G, Fantini C, Belli A, Limongelli P. Laparoscopic liver resection for hepatocellular carcinoma in cirrhosis: Long-term outcomes. *Dig Surg*. 2011;28(2):134–140.
- Bertuzzo VR, Cescon M, Ravaioli M, et al. Analysis of factors affecting recurrence of hepatocellular carcinoma after liver transplantation with a special focus on inflammation markers. *Transplantation*. 2011;91(11):1279–1285.
- Lim KC, Chow PK, Allen JC, et al. Microvascular invasion is a better predictor of tumor recurrence and overall survival following surgical resection for hepatocellular carcinoma compared to the Milan criteria. *Ann Surg*. 2011;254(1):108–113.
- Fan ST, Poon RT, Yeung C, et al. Outcome after partial hepatectomy for hepatocellular cancer within the Milan criteria. *Br J Surg*. 2011;98(9):1292–1300.
- Adam R, Bhangui P, Vibert E, et al. Resection or transplantation for early hepatocellular carcinoma in a cirrhotic liver: Does size define the best oncological strategy? *Ann Surg*. 2012;256(6):883–891.
- Shindoh J, Hasegawa K, Inoue Y, et al. Risk factors of post-operative recurrence and adequate surgical approach to improve long-term outcomes of hepatocellular carcinoma. *HPB (Oxford)*. 2013;15(1):31–39.
- Abdel-Wahab M, Sultan AM, Fathy OM, et al. Factors affecting recurrence and survival after living donor liver transplantation for hepatocellular carcinoma. *Hepatogastroenterology*. 2013;60(128):1847–1853.
- Li SH, Wei W, Guo RP, et al. Long-term outcomes after curative resection for patients with macroscopically solitary hepatocellular carcinoma without macrovascular invasion and an analysis of prognostic factors. *Med Oncol*. 2013;30(4):696.
- Zhao H, Chen C, Fu X, et al. Prognostic value of a novel risk classification of microvascular invasion in patients with hepatocellular carcinoma after resection. *Oncotarget*. 2017;8(3):5474–5486.
- Zheng J, Kuk D, Gönen M, et al. Actual 10-year survivors after resection of hepatocellular carcinoma. *Ann Surg Oncol*. 2017;24(5):1358–1366.
- Edmondson HA, Steiner PE. Primary carcinoma of the liver: A study of 100 cases among 48,900 necropsies. *Cancer*. 1954;7(3):462–503.
- Zhou L, Rui JA, Wang SB, Chen SG, Qu Q. The significance of serum AFP cut-off values, 20 and 400 ng/ml in curatively resected patients with hepatocellular carcinoma and cirrhosis might be of difference. *Hepatogastroenterology*. 2012;59(115):840–843.
- Zhou L, Rui JA, Wang SB, Chen SG, Qu Q. Risk factors of poor prognosis and portal vein tumor thrombosis after curative resection of solitary hepatocellular carcinoma. *Hepatobiliary Pancreat Dis Int*. 2013;12(1):68–73.
- Jeng KS, Sheen IS, Tsai YC. Circulating messenger RNA of alpha-fetoprotein: A possible risk factor of recurrence after resection of hepatocellular carcinoma. *Arch Surg*. 2004;139(10):1055–1060.
- Qu LS, Jin F, Huang XW, Shen XZ. High hepatitis B viral load predicts recurrence of small hepatocellular carcinoma after curative resection. *J Gastrointest Surg*. 2010;14(7):1111–1120.
- Xia F, Lai EC, Lau WY, et al. High serum hyaluronic acid and HBV viral load are main prognostic factors of local recurrence after complete radiofrequency ablation of hepatitis B-related small hepatocellular carcinoma. *Ann Surg Oncol*. 2012;19(4):1284–1291.
- Zhou L, Rui JA, Zhou WX, Wang SB, Chen SG, Qu Q. Edmondson–Steiner grade: A crucial predictor of recurrence and survival in hepatocellular carcinoma without microvascular invasion. *Pathol Res Pract*. 2017;213(7):824–830.
- Peng SY, Chen WJ, Lai PL, Jeng YM, Sheu JC, Hsu HC. High alpha-fetoprotein level correlates with high stage, early recurrence and poor prognosis of hepatocellular carcinoma: Significance of hepatitis virus infection, age, p53 and beta-catenin mutations. *Int J Cancer*. 2004;112(1):44–50.
- Pardee AD, Shi J, Butterfield LH. Tumor-derived alpha-fetoprotein impairs the differentiation and T cell stimulatory activity of human dendritic cells. *J Immunol*. 2014;193(11):5723–5732.
- Lu Y, Zhu M, Li W, et al. Alpha fetoprotein plays a critical role in promoting metastasis of hepatocellular carcinoma cells. *J Cell Mol Med*. 2016;20(3):549–558.
- Xiangji L, Feng X, Qingbao C, et al. Knockdown of HBV surface antigen gene expression by a lentiviral microRNA-based system inhibits HBV replication and HCC growth. *J Viral Hepat*. 2011;18(9):653–660.
- Peng ZW, Chen MS, Liang HH, et al. A case-control study comparing percutaneous radiofrequency ablation alone or combined with transcatheter arterial chemoembolization for hepatocellular carcinoma. *Eur J Surg Oncol*. 2010;36:257–263.
- Liu XY, Xu JF. Liver resection for young patients with large hepatocellular carcinoma: A single center experience from China. *World J Surg Oncol*. 2014;12:175.

# Association between heparin-binding hemagglutinin and tuberculosis

\*Feifei Pu<sup>A,B</sup>, \*Jing Feng<sup>D,E</sup>, Ping Xia<sup>E,F</sup>

Department of Orthopedics, Wuhan No. 1 Hospital (Wuhan Integrated TCM & Western Medicine Hospital), Tongji Medical College, Huazhong University of Science and Technology, China

A – research concept and design; B – collection and/or assembly of data; C – data analysis and interpretation;  
D – writing the article; E – critical revision of the article; F – final approval of the article

Advances in Clinical and Experimental Medicine, ISSN 1899–5276 (print), ISSN 2451–2680 (online)

*Adv Clin Exp Med.* 2020;29(7):893–897

## Address for correspondence

Ping Xia  
E-mail: xiapingfm@163.com

## Funding sources

This work was supported by a research project of the Hubei Health and Family Planning Commission (grant No. WJ2017Z022), a research project of the Hubei Science and Technology Department (grant No. 2016CFB666), a research project of the Wu Jieping Medical Foundation (grant No. 320.6750.17566), a research project of the Wuhan Health and Family Planning Commission (grants No. WZ18Q05 and No. WX18Z20), and a research project of Wuhan No. 1 Hospital (Wuhan Integrated TCM & Western Medicine Hospital) (grant No. 2017Y01).

## Conflict of interest

None declared

\* Feifei Pu and Jing Feng have made equal contributions to this work.

Received on December 24, 2018

Reviewed on April 24, 2020

Accepted on April 24, 2020

Published online on July 31, 2020

## Cite as

Pu F, Feng J, Xia P. Association between heparin-binding hemagglutinin and tuberculosis. *Adv Clin Exp Med.* 2020;29(7):893–897. doi:10.17219/acem/121011

## DOI

10.17219/acem/121011

## Copyright

© 2020 by Wrocław Medical University

This is an article distributed under the terms of the Creative Commons Attribution 3.0 Unported (CC BY 3.0) (<https://creativecommons.org/licenses/by/3.0/>)

## Abstract

The current global burden of tuberculosis (TB) is one of the greatest challenges to public health, particularly in developing countries, and thus effective diagnostic methods and treatment options for TB remain a central topic in basic and clinical research. Heparin-binding hemagglutinin (HBHA)-specific immune responses have been linked to protection against TB. The binding of HBHA-coated beads to epithelial and endothelial cell layers may trigger transcytosis of the beads, which is the basis for extrapulmonary dissemination. In addition, HBHA has been confirmed as a potential diagnostic marker for TB, and it is important in developing new TB vaccines and anti-TB drugs. Recently, basic research on HBHA has been intensified. The HBHA application in the field of prevention and treatment should be further explored. In addition, the existing research achievements have shown its broad application prospects. Currently, there are no relevant specialized products, and research should be accelerated. These products may contribute to the application of HBHA in the diagnosis, prevention and treatment of TB.

**Key words:** heparin-binding hemagglutinin, tuberculosis, diagnosis, treatment

## Introduction

Tuberculosis (TB), an infectious disease caused by *Mycobacterium tuberculosis* (Mtb), remains a global health problem, with an estimated 10.4 million incident cases of active TB (aTB) in 2015.<sup>1</sup> It is a major infectious disease that kills almost two million people every year, mostly in developing countries, where it poses a major health, social and economic burden.<sup>2</sup> The development of improved, clinically sensitive, rapid, and economical diagnostic tests may provide a powerful tool to better control the epidemic. Recently, polymerase chain reaction (PCR)-based methods and automatic culture systems have been made available, and these methods are in extensive regular use in laboratories in developed countries.<sup>3</sup> However, these diagnostic systems are not suitable for field use. The idea to develop a test for TB diagnosis through a serological assay has been pursued for many decades, but the results so far have been poor. Many of the antigens which have been tested did not possess adequate sensitivity or specificity, and these assays could not properly distinguish between individuals vaccinated with the *Mycobacterium bovis* bacillus Calmette–Guérin (BCG) vaccine or testing positive for purified protein derivative (PPD) and those with aTB.<sup>4</sup>

Recently, it has been demonstrated that several mycobacterial proteins undergo a process of post-translational modification in mycobacteria, providing important immunological properties. Among these proteins is heparin-binding hemagglutinin (HBHA), which is methylated in lysine residues present at the C-terminus.<sup>5,6</sup> Since the recombinant proteins produced in *Escherichia coli* cannot be properly processed, the use of these antigens in serological assays is precluded by the cumbersome procedures required to purify the native antigens. Recently, a rapid and effective system for the purification of methylated HBHA (mHBHA) has been developed, and the use of these proteins in such assays is now feasible.<sup>7</sup> The HBHA plays an important role during infection, especially during extrapulmonary dissemination to other systems in the human host. It has also been investigated as a potential diagnostic tool for latent TB, as a possible vaccine and as a booster of BCG immunity, probably by inducing cytokines that may contribute to the generation of T helper 1 (Th1) effector memory lymphocytes. The HBHA is known to bind to heparin.

The HBHA of Mtb, a dissemination factor that has been identified as an immunodominant antigen able to induce interferon gamma (IFN $\gamma$ ), is associated with protection against TB.<sup>8</sup> This surface protein interacts with non-phagocytic cells, attaches to sulfated glycoconjugates, and has the ability to agglutinate red blood cells.<sup>9,10</sup> The specific methylation of the antigen has been shown to be important in mounting an immune response against this antigen, and it has been suggested that HBHA can be used in IFN $\gamma$  release assays (IGRAs) to diagnose Mtb infection

or to discriminate between the active and latent forms of the disease. Current preclinical strategies involve administering the HBHA vaccine as a booster following vaccination with BCG.<sup>11</sup>

## Material and methods

A systematic search of electronic databases, including PubMed, EMBASE and Google Scholar, was performed in order to identify relevant articles (published until November 21, 2018) characterizing the role of HBHA in TB. To maximize the number of eligible articles, the following keywords were used in combination: [HEPARIN-BINDING HEMAGGLUTININ], [HBHA] and [TUBERCULOSIS]. Additional studies were sought from the references of all the articles retrieved; only studies examining HBHA in TB were included, while non-English language studies and review articles were excluded.

Two independent reviewers screened all the titles and abstracts, and disagreements related to inclusion or exclusion of a particular study were resolved through consensus. Once the study was selected for inclusion based on its title and abstract, the full text was further screened by 2 independent reviewers. A total of 88 articles were identified.

## Discussion

### Biochemical characteristics of HBHA

The encoding gene of *hbha* is approx. 600 bp long, and the corresponding protein is composed of 199 amino acids. The molecular mass is about 28,000 Da. The HBHA contains 3 domains: a transmembrane domain composed of 18 amino acid residues at the N-terminus, a helical region containing 81 amino acid residues of curly helical type, and it can be modified by methylation after translation into the C-terminal junction.<sup>12,13</sup> The N-terminal transmembrane region was inserted into the surface membrane to fix HBHA to the lipid membrane of the surface of the bacteria, thereby enhancing virulence, while the C-terminal domain plays an important role in mediating combination and sulfating the polysaccharide receptor.<sup>9,10</sup>

The HBHA can form a homodimer or polymer. The molecular weight of HBHA was measured using force microscopy.<sup>14</sup> Peaks represent HBHA forming dimers or polymers. At the same time, it is also found that similar effects exist in viable bacteria that produce HBHA. This phenomenon was not found in the *hbha* gene deletion mutant. Combined with the fact that HBHA mediates bacterial agglutination, it is speculated that a dimer or a polymer is formed through the interaction of the source HBHA and body agglutination. Methylation prevents the hydrolysis of HBHA protein.<sup>15</sup>

## Expression of HBHA in different carriers

Although it is generally accepted that the interaction of Mtb with alveolar macrophages is a key step in the pathogenesis of TB, interactions with other cell types, especially epithelial cells, may also be important.<sup>16</sup> In this study, we characterized the molecular properties of mycobacterial HBHA, a protein that functions as an adhesin for epithelial cells.<sup>17</sup> The gene was cloned from Mtb and *M. bovis* BCG, and the sequence was found to be identical between the 2 species. The calculated result was smaller than the finding from SDS/PAGE analysis; this difference may be due to the Lys/Pro-rich repeats of the C-terminal end of the protein and to a putative carbohydrate moiety. Glycosylation of HBHA appears to protect the protein from proteolytic degradation, which results in the removal of the C-terminal Lys/Pro-rich region responsible for binding HBHA to sulfated carbohydrates.<sup>18</sup> Evidence suggests that glycosylation is also important for HBHA-mediated hemagglutination and for certain immunological properties of the protein. Finally, the absence of a signal peptide in the coding region of HBHA raises the possibility that this protein is not secreted through the general secretory pathway.

The Mtb and *M. bovis* BCG HBHA is required for extrapulmonary dissemination, and laminin-binding protein (LBP) is involved in cytoadherence through laminin recognition.<sup>19,20</sup> These adhesins bear post-translational modifications that are not present when the proteins are produced in a recombinant (r) form in *E. coli*. Mass spectrometry analysis of HBHA reveals that the post-translational modifications are borne by the C-terminal moiety, which comprises the heparin-binding domain consisting of repeated lysine-rich motifs. Amino acid sequencing showed that these modifications consist of mono- and dimethyllysines within these motifs. The methyllysine-containing repeats were recognized by mAb 4057D2 and were also detected in LBP, which is also recognized by mAb 4057D2. This antibody does not recognize the recombinant forms of these proteins. However, when recombinant HBHA (rHBHA) and rLBP were subjected to NaOH and formalin treatment to induce lysine methylation, reactivity with mAb 4057D2 was recovered. Methylated rHBHA displayed enhanced resistance to proteolysis compared with unmethylated rHBHA, as previously observed for native HBHA. S-adenosylmethionine-dependent HBHA methyltransferase activity was detected in the cell-wall fractions of *M. bovis* BCG and of *Mycobacterium smegmatis*, a species that produces LBP but naturally lacks HBHA, suggesting that the same enzyme methylates both LBP and HBHA. This hypothesis was confirmed by the fact that HBHA produced by recombinant *M. smegmatis* was also methylated. These results show that mycobacteria use enzymatic methylation of lysines to ensure greater stability of their adhesins.

A recombinant *M. smegmatis* strain that overexpressed HBHA under the control of a strong *furA* promoter was constructed to discriminate IGRAs between aTB and latent tuberculosis infection (LTBI). The methylated activity of the purified protein was verified using hybridization with anti-methylated Lys antibody, and mHBHA was further evaluated for antigen-specific IFN $\gamma$  responses in a BCG-vaccinated Chinese population. Taken together, evaluation of the immune response to mHBHA can discriminate between healthy LTBI cases and aTB patients.

## Infection and pathogenesis of HBHA and *M. tuberculosis*

By virtue of their position at the crossroads between the innate and adaptive immune response, macrophages play an essential role in the control of bacterial infections. Paradoxically, macrophages serve as the natural habitat of Mtb. The Mtb subverts the macrophage's mechanisms of intracellular killing and antigen presentation, ultimately leading to the development of TB. The HBHA, a virulence factor involved in extrapulmonary dissemination and a strong diagnostic antigen for TB, is both surface-associated and secreted. Disruption of the *hbha* gene led to the restoration of impairment in infected macrophages, resulting in reduced apoptosis. Taken together, the data suggests that HBHA may act as a strong pathogenic factor to cause apoptosis of professional phagocytes infected with Mtb.<sup>21</sup> A recent study suggested that HBHA induces cytosolic [Ca(2+)]<sub>i</sub>, which influences the generation of reactive oxygen species (ROS) associated with the production of pro-inflammatory cytokines. These concerted and complex cellular responses induce endoplasmic reticulum stress-associated apoptosis during HBHA stimulation in macrophages. These results indicate that the endoplasmic reticulum stress pathway contributes significantly to HBHA-induced apoptosis during mycobacterial infection.<sup>22</sup>

Importantly, in vitro studies have demonstrated that the Mtb *hbha* and *esxA* gene products HBHA and ESAT6 directly or indirectly influence alveolar epithelial cell survival.<sup>23</sup> In vitro assays with the recombinant histone-like protein and HBHA, which are considered to be major mycobacterial adhesins, confirmed their function of promoting bacterial attachment to epithelial cells. In addition, these experiments suggested that the airway epithelium may act as a reservoir and/or portal of entry for *Mycobacterium leprae* in humans.<sup>24</sup> A previous study used immunoblotting to examine the humoral immune responses of aTB patients against triton-soluble proteins extracted from Mtb. Of interest, the pooled sera from TB patients that contained anti-HBHA IgM antibodies neutralized the entry of Mtb into epithelial cells. These findings suggest that IgM antibodies against HBHA may help protect against extrapulmonary dissemination.<sup>25</sup>

## Detection of HBHA in tuberculosis immunology

In recent years, T-cell-based IGRAs have been developed for immunodiagnosis of Mtb infection. Currently, these assays do not discriminate between disease and latency. Therefore, more promising antigens and diagnostic tools are continuously being searched for TB immunodiagnostics. The HBHA is a surface protein of Mtb, which promotes bacterial aggregation and adhesion to non-phagocytic cells. It has been previously assumed that the native, methylated form of this protein would be a promising antigen to discriminate between latent and active infection. A pilot investigation was performed to study the humoral and T-cell-mediated immunological responses to recombinant HBHA produced in *M. smegmatis* and to synthetic peptides in patients with recent or past TB, with atypical mycobacteriosis, and in healthy, vaccinated individuals. T-cell reactivity to HBHA was compared to the respective reactivity toward PPD and 2 surface-secreted proteins, i.e., early secretory antigen target-6 (ESAT-6) and culture filtrate protein-10 (CFP-10).<sup>26</sup> The preliminary results indicate that methylated rHBHA induced a strong T-cell-mediated immune response and the production of IgG and IgM-class antibodies in all patient groups, most surprisingly in young Finnish vaccinees. They observed a positive correlation between the reactivity to HBHA and non-specific PPD among the entire study population. As expected, ESAT-6 and CFP-10 were the most powerful antigens to distinguish between disease and immunity caused by vaccination.<sup>27</sup> On the basis of this exploratory investigation, we raise concerns that in countries like Finland, where BCG vaccination was routinely used, HBHA may not be sufficient for diagnostics because of the inability to explicitly discriminate between TB infection and immunoreactivity caused by previous BCG vaccination.<sup>28</sup>

The IGRAs based on region of difference 1 (RD1) antigens have improved the diagnosis of Mtb infection. However, IGRAs of these antigens cannot distinguish between aTB and LTBI. The Mtb HBHA induces relatively high IFN $\gamma$  responses in LTBI individuals and low responses in aTB patients, but purification of the native methylated HBHA from Mtb cultures for immunological tests is complex and time-consuming. The study showed that T-cell responses against mHBHA were always lower in aTB patients than in LTBI individuals, regardless of the site of infection or the results of bacteriological tests. This allowed for a high discrimination between these 2 groups of Mtb-infected individuals, even in the BCG-vaccinated and high-TB-incidence setting of China. Additionally, the combination of mHBHA and RD 1 antigens in an IGRA enhanced the diagnostic efficacy for aTB cases. Taken together, inclusion of the immune response to mHBHA can differentiate between healthy LTBI cases and aTB patients.<sup>15</sup>

In a recent study, 165 outpatients and 133 healthy volunteers were included in an investigation of the role of HBHA

in TB diagnosis, including serodiagnostic tests and IGRAs. None of the healthy volunteers had been BCG-vaccinated, including 73 individuals with PPD (–) and 60 with PPD (+) (i.e., P–B– and P+B–). Of all 165 outpatients, 77 had pulmonary tuberculosis (PTB) and 88 had extrapulmonary tuberculosis (EPTB). The HBHA protein was used for serodiagnostic tests and IGRAs in peripheral blood mononuclear cells. They found that HBHA serodiagnostic tests with IGRAs had a limited potential for use as auxiliary tools for the differential diagnosis of PTB and EPTB, because both methods showed low sensitivity and specificity.<sup>29</sup>

## Conclusions and future prospects

Tuberculosis is one of the greatest challenges to public health, particularly in developing countries, and thus effective diagnostic methods and treatment options for TB remain a central topic in basic and clinical research. The HBHA-specific immune responses have been linked to protection against TB. Lately, the investigation of HBHA in basic research has been intensified. The HBHA application in the field of prevention and treatment should be further explored. In addition, recent findings have shown its broad application prospects. Currently, there are no relevant specialized products, and research should be accelerated. These products may contribute to the application of HBHA in the diagnosis, prevention and treatment of TB.

### ORCID iDs

Feifei Pu  <https://orcid.org/0000-0002-9174-8780>

Jing Feng  <https://orcid.org/0000-0001-9895-6534>

Ping Xia  <https://orcid.org/0000-0002-5544-3082>

### References

1. Wang Y, Wang Q, Zhu R, et al. Trends of spinal tuberculosis research (1994–2015): A bibliometric study. *Medicine (Baltimore)*. 2016;95(38):e4923.
2. Kumar K. Spinal tuberculosis: Natural history of disease, classifications and principles of management with historical perspective. *Eur J Orthop Surg Traumatol*. 2016;26(6):551–558.
3. Chen CH, Chen YM, Lee CW, Chang YJ, Cheng CY, Hung JK. Early diagnosis of spinal tuberculosis. *J Formos Med Assoc*. 2016;115(10):825–836.
4. Nagashima H, Tanishima S, Tanida A. Diagnosis and management of spinal infections. *J Orthop Sci*. 2018;23(1):8–13.
5. De Maio F, Squeglia F, Goletti D, Delogu G. The mycobacterial HBHA protein: A promising biomarker for tuberculosis. *Curr Med Chem*. 2018;26(11):2051–2060. doi:10.2174/0929867325666181029165805
6. Raze D, Verwaerde C, Deloison G, et al. Heparin-binding hemagglutinin adhesin (HBHA) is involved in intracytosolic lipid inclusions formation in *Mycobacteria*. *Front Microbiol*. 2018;9:2258.
7. Sali M, Buonsenso D, D'Alfonso P, et al. Combined use of Quantiferon and HBHA-based IGRA supports tuberculosis diagnosis and therapy management in children. *J Infect*. 2018;77(6):526–533.
8. Loxton AG, Black GF, Stanley K, Walzl G. Heparin-binding hemagglutinin induces IFN- $\gamma$ (+) IL-2(+) IL-17(+) multifunctional CD4(+) T cells during latent but not active tuberculosis disease. *Clin Vaccine Immunol*. 2012;19(5):746–751.
9. Lanfranconi MP, Alvarez HM. Functional divergence of HBHA from *Mycobacterium tuberculosis* and its evolutionary relationship with Tada from *Rhodococcus opacus*. *Biochimie*. 2016;127:241–248.

10. Huang TY, Irene D, Zulueta MM, et al. Structure of the complex between a heparan sulfate octasaccharide and mycobacterial heparin-binding hemagglutinin. *Angew Chem Int Ed Engl*. 2017;56(15):4192–4196.
11. Segura-Cerda CA, Aceves-Sánchez MJ, Marquina-Castillo B, et al. Immune response elicited by two rBCG strains devoid of genes involved in c-di-GMP metabolism affect protection versus challenge with *M. tuberculosis* strains of different virulence. *Vaccine*. 2018;36(16):2069–2078.
12. Delogu G, Brennan MJ. Functional domains present in the mycobacterial hemagglutinin, HBHA. *J Bacteriol*. 1999;181(24):7464–7469.
13. Biet F, de Melo Marques MA, Grayon M, et al. *Mycobacterium smegmatis* produces an HBHA homologue which is not involved in epithelial adherence. *Microbes Infect*. 2007;9(2):175–182.
14. Esposito C, Cantisani M, D'Auria G, et al. Mapping key interactions in the dimerization process of HBHA from *Mycobacterium tuberculosis*, insights into bacterial agglutination. *FEBS Lett*. 2012;586(6):659–667.
15. Wen HL, Li CL, Li G, et al. Involvement of methylated HBHA expressed from *Mycobacterium smegmatis* in an IFN- $\gamma$  release assay to aid discrimination between latent infection and active tuberculosis in BCG-vaccinated populations. *Eur J Clin Microbiol Infect Dis*. 2017;36(8):1415–1423.
16. Raze D, Verwaerde C, Deloison G, Berisio R. A structural overview of mycobacterial adhesins: Key biomarkers for diagnostics and therapeutics. *Protein Sci*. 2018;27(2):369–380.
17. Silva CA, Danelishvili L, McNamara M, et al. Interaction of *Mycobacterium leprae* with human airway epithelial cells: Adherence, entry, survival, and identification of potential adhesins by surface proteome analysis. *Infect Immun*. 2013;81(7):2645–2659.
18. Lefrançois LH, Bodier CC, Lecher S, et al. Purification of native HBHA from *Mycobacterium avium* subsp. *paratuberculosis*. *BMC Res Notes*. 2013;6:55.
19. Pethe K, Bifani P, Drobecq H, et al. Mycobacterial heparin-binding hemagglutinin and laminin-binding protein share antigenic methyllysines that confer resistance to proteolysis. *Proc Natl Acad Sci U S A*. 2002;99(16):10759–10764.
20. Pethe K, Puech V, Daffé M, et al. *Mycobacterium smegmatis* laminin-binding glycoprotein shares epitopes with *Mycobacterium tuberculosis* heparin-binding haemagglutinin. *Mol Microbiol*. 2001;39(1):89–99.
21. Sohn H, Kim JS, Shin SJ, et al. Targeting of *Mycobacterium tuberculosis* heparin-binding hemagglutinin to mitochondria in macrophages. *PLoS Pathog*. 2011;7(12):e1002435.
22. Choi JA, Lim YJ, Cho SN, et al. Mycobacterial HBHA induces endoplasmic reticulum stress-mediated apoptosis through the generation of reactive oxygen species and cytosolic Ca<sup>2+</sup> in murine macrophage RAW 264.7 cells. *Cell Death Dis*. 2013;4(12):e957.
23. Pavlicek RL, Fine-Coulson K, Gupta T, et al. Rv 3351c, a *Mycobacterium tuberculosis* gene that affects bacterial growth and alveolar epithelial cell viability. *Can J Microbiol*. 2015;61(12):938–947.
24. Silva CA, Danelishvili L, McNamara M, et al. Interaction of *Mycobacterium leprae* with human airway epithelial cells: Adherence, entry, survival, and identification of potential adhesins by surface proteome analysis. *Infect Immun*. 2013;81(7):2645–2659.
25. Shin AR, Lee KS, Lee JS, et al. *Mycobacterium tuberculosis* HBHA protein reacts strongly with the serum immunoglobulin M of tuberculosis patients. *Clin Vaccine Immunol*. 2006;13(8):869–875.
26. Dirix V, Schepers K, Massinga-Loembe M, et al. Added value of long-term cytokine release assays to detect *Mycobacterium tuberculosis* infection in HIV-infected subjects in Uganda. *J Acquir Immune Defic Syndr*. 2016;72(3):344–352.
27. Hutchinson P, Barkham TM, Tang W, Kemeny DM, Bin-Eng Chee C, Wang YT. Measurement of phenotype and absolute number of circulating heparin-binding hemagglutinin, ESAT-6 and CFP-10, and purified protein derivative antigen-specific CD4 T cells can discriminate active from latent tuberculosis infection. *Clin Vaccine Immunol*. 2015;22(2):200–212.
28. Savolainen L, Pusa L, Kim HJ, Sillanpää H, Seppälä I, Tuuminen T. Pilot study of diagnostic potential of the *Mycobacterium tuberculosis* recombinant HBHA protein in a vaccinated population in Finland. *PLoS One*. 2008;9(9):e3272.
29. Sun Z, Nie L, Zhang X, Li Y, Li C. Mycobacterial heparin-binding hemagglutinin adhesion-induced interferon  $\gamma$  and antibody for detection of tuberculosis. *Indian J Med Res*. 2011;133(4):421–425.

